Organisation of Sterol-Rich Membranes in Cell Polarisation

Dissertation

zur

Erlangung der naturwissenschaftlichen Doktorwürde

(Dr. sc. nat.)

vorgelegt der

Mathematisch-naturwissenschaftlichen Fakultät

der

Universität Zürich

von

Adam Rafal Kijowski

aus

Polen

Promotionskomitee

Prof. Dr. Damian Brunner (Leitung der Dissertation)

Dr. Robin Klemm

Prof. Dr. Lucas Pelkmans

Prof. Dr. Kai Simons

Prof. Dr. Gisou van der Goot

Zürich 2016

Organisation of Sterol-Rich Membranes in Cell Polarisation

It is the cells which create and maintain in us,
during the span of our lives,
our will to live and survive, to search
and experiment, and to struggle.

Albert Claude, 1974

Contents

Acknowledgments

First and foremost, I would like to express my most sincere gratitude to my PhD supervisor Prof. Damian Brunner. I am thankful that you introduced me to the fascinating life of Biology and People, which allowed me to experience the most fruitful and exciting time of my life. I am immensely grateful for your constant support, motivation, and vast knowledge.

Aside from my supervisor, I would like to extend my gratitude to the members of my Thesis Committee: Prof. Lucas Pelkmans, Prof. Gisou van der Goot, Prof. Kai Simons, and Dr. Robin Klemm. I would especially like to acknowledge Dr. Robin Klemm for your presence at all my progress reports. I will always be grateful for your time, insightful advice, and continuous support.

Special thanks to all the former and present members of the Brunner Lab. Thank you for offering a great scientific atmosphere for brainstorming ideas. I am grateful for all the amazing lab retreats, precious support in the good and bad moments and the fun we had these past 5 years.

Special thanks to Maria Barbara Heimlicher, with whom I shared a lab desk. You were always conscious of my project, and a great support base day in day out. I just do not know how to express my gratitude that I got to share these past 5 years with you.

My sincere gratitude to Dr. Stephen Huisman, for introducing me to the lab environment and microbiology technics. I am grateful for all the help you granted me, the intelligent discussions we held, and the never-ending support.

I would also like to thank Michèle Grüner, for all the lab fun, and perceptive discussions about SRMs, yeast, and life. Thank you very much for agreeing to join the project and collaborate on it in the future. Your precious work is revolutionary.

I would also like to thank David Dreher for his excitement to develop the software that I used to analyse data in this thesis. It was a very fruitful and rewarding experience collaborating with the physicist. Also, I would like to give thanks to Werner Boll for all your help regarding lab facilities, Dr. Erich Frei, and Oleg Georgiev for ensuring a great working atmosphere.

Last but not least, I would like to thank all my family and friends for their understanding, constant support and confidence in me during these 5 years. Thank you very much!

Abbreviations

BFA	Brefeldin A
ER	Endoplasmic reticulum
ER-PM	Connections between the cortical ER and the PM
Exocyst	Octameric protein complex involved in membrane tethering
Filipin	Fluorescent binding dye of oxysterols
GFP-tna1p	Transmembrane fluorescent protein and live marker of SRMs
Gma12p	GFP epitope- tagged -1,2 galactosyl-transferase
LatB	Latrunculin B
LTPs	Lipid transfer proteins
MCSs	Membrane contact sites
MTs	Microtubules
OSBP	Mammalian oxysterol-binding protein
Oshes	Oxysterol-binding proteins
P1	SRM formation during SE
P2	SRM polarisation during SE
P3	Fast growth initiation from a single growth site during SE
P4	Fast growth initiation from the secondary end during SE
PI(4)P	Phosphatidylinositol 4-phosphate
PIP2	Phosphatidylinositol 4,5-bisphosphate
PM	Plasma membrane

SE	Starvation exit
SRM	Sterol-rich membrane

Summary

Cell polarisation, the act of breaking symmetry, is essential for polarised growth and the generation of distinct cell morphology. In the cylindrical fission yeast cells, specialised, sterol-rich membranes (SRMs) form defined domains in the plasma membrane (PM) at the growing cell poles. During *de novo* cell polarisation, biosynthesis of sterols is fundamental for the formation of SRMs and subsequently polarised growth initiation. SRM domains serve as platforms on which the growth and polarity machinery assemble. Also, SRM stabilisation at cell poles is controlled by microtubule-delivered tea1p. To identify components mediating the formation and tea1-dependent sorting of SRMs, we studied presumptive mutants of factors involved in sterol trafficking. Surprisingly, the initial cell polarisation occurs independent of most of the components of the classical vesicle transport pathways. In contrast, two components of the non-vesicular transport of lipids (oxysterol-binding proteins - oshes) are involved in the formation and polarisation of SRMs. It is known that the signalling lipid PI(4)P physically and genetically interacts with oshes and mediates non-vesicular transport of lipids. Accordingly, we found that PI(4)P synthesis is essential for the SRM formation and cell polarisation. We hypothesise that during cell polarisation of fission yeast, these components act together at the membrane contact sites, between the endoplasmic reticulum (ER) and the PM. In support of this hypothesis, we observed that the two oshes accumulate at similar regions of the cortical ER. In addition, we found that connections between the ER and the PM are involved in SRM formation and cell polarisation. To our knowledge, it is the first time that non-vesicular transport of sterols is correlated with *de novo* cell polarisation. How tea1p controls all these components remains to be shown. In summary, this thesis presents a new concept of cell polarisation, involving conserved factors that drive the formation and polar localisation of SRM domains, which in turn sets the basis for polarised growth.

Zusammenfassung

Zellpolarisation, der Vorgang der die Symmetrie bricht, ist essentiell für das polarisierte Wachstum und die Erzeugung von eindeutiger Zellmorphologie. An den wachsenden Zellpolen von zylindrischen Spalthefe-Zellen formen spezialisierte, sterol-reiche Membranen (SRMs) definierte Abschnitte in der Plasmamembran (PM). Während der *de novo* Zellpolarisation ist die Biosynthese von Sterolen fundamental für die Entstehung von SRMs und anschliessender Initiierung des polarisierten Wachstums. SRM-Abschnitte dienen dabei als Plattformen, an denen sich die Wachstums- und Polarisations-Maschinerie zusammensetzt. Ausserdem wird die Stabilisierung von SRMs an den Zellpolen von tea1p gesteuert, welches durch Mikrotubuli herantransportiert wird. Wir untersuchten Mutanten, um Komponenten zu identifizieren, welche die Bildung und die tea1p-abhängige Sortierung von SRMs vermitteln. Diese Mutanten umfassten mutmassliche Faktoren, die in den Transport von Sterolen involviert sein könnten. Überraschenderweise findet die Erst-Zellpolarisation unabhängig von den meisten der Komponenten des klassischen Vesikel-Transportweges statt. Im Gegensatz dazu sind zwei Komponenten des nicht-vesikulären Transportweges von Lipiden (Oxysterol-bindende Proteine - oshes) an der Bildung und Polarisation von SRMs beteiligt. Es ist bekannt, dass das Signallipid PI(4)P physisch und genetisch mit den oshes interagiert und den nicht-vesikulären Transport von Lipiden vermittelt. Dementsprechend fanden wir heraus, dass die PI(4)P-Synthese essentiell für die SRM-Bildung und die Zellpolarisation ist. Wir stellen die Hypothese auf, dass diese Komponenten während der Zellpolarisation der Spalthefe an Membrankontaktstellen zusammenarbeiten - zwischen dem Endoplasmatischen Retikulum (ER) und der PM. Unsere Beobachtungen unterstützen diese Hypothese, da die zwei oshes in ähnlichen Regionen des kortikalen ER akkumulieren. Zusätzlich fanden wir heraus, dass Verbindungen zwischen ER und PM an der Bildung von SRMs und der Polarisation der Zellen beteiligt sind. Unseres Wissens nach ist dies das erste Mal, dass nicht-vesikulärer Transport von Sterolen mit der *de novo* Zellpolarisation in Zusammenhang gebracht

wird. Es bleibt offen, wie tea1p all diese Komponenten steuert. Zusammengefasst gesagt, praäsentiert diese Doktorarbeit ein neues Konzept der Zellpolarisation. Dieses beinhaltet konservierte Faktoren, die Bildung und polarisierte Lokalisierung von SRM-Abschnitten antreiben. Dies wiederum bildet die Grundlage für polarisiertes Wachstum.

List of Figures

List of Tables

1 Introduction

1.1 Principles of cell polarisation

Cell polarisation is an act of breaking symmetry, which leads to cell polarity [Alberts et al., 2014]. All cell types polarise, at least temporarily [Etienne-Manneville, 2004]. Cellular polarisation is essential for morphogenesis, proliferation and differentiation in uni- and multicellular organisms [Sohrmann, 2003]. Thus, a detailed understanding of how cells generate polarity is important both from the perspective of fundamental science and for medical applications [Siegrist, Doe, 2007]. Cell polarisation is manifested by distinct cellular morphologies, which are the result of confinement of their growth activity to specific regions [Huisman, Brunner, 2011]. However, cell polarity can also be manifested at the level of signalling molecules, without any detectable morphological polarisation [Sohrmann, 2003].

Several mathematical models have been developed to describe how an initially symmetric structure can be transformed into an asymmetric, polarised one [Turing, 1952], [Gierer, Meinhardt, 1972], [Meinhardt, Gierer, 2000]. These models propse the role of autocatalytic feedback loops, combined with inhibitory interactions [Meinhardt, Gierer, 2000]. Convincing experiments in various developmental systems, have confirmed the importance of these feedback loops and inhibitory interactions. A polarised pattern can spontaneously emerge from an initially symmetric but unstable system, in the absence of an asymmetric cue [Wedlich-Soldner, 2003]. These observations suggest that the final asymmetric pattern can be entirely self-organising [Sohrmann, 2003], [Wedlich-Soldner, 2003], [Bendezú et al., 2015].

Established polarity is a result of asymmetric distribution of proteins, lipids, mRNAs and/or organelles [Siegrist, Doe, 2007]. This asymmetry can be further stabilised by rearrangements of the cytoskeleton, enabling the cell to assume an asymmetric shape [Sohrmann, 2003].

Although, cell polarisation is established in accordance to diverse functional contexts, its broad features are thought to be general and conserved [Etienne-Manneville, 2004].

Cdc42p in eukaryotic organisms, was shown to play a central role in cell polarisation in many functional contexts [Etienne-Manneville, 2004]. Although, cdc42p is not identified in prokaryotes, GTPase-dependent mechanisms of cell polarity control exist [Treuner-Lange, Søgaard-Andersen, 2014]. Cdc42p belongs to the Rho family of GTPases. It uses a molecular switch (conformational change) to hydrolyse GTP to GDP, in order to balance its activity from on (GTP bound) to off (GDP bound) state [Etienne-Manneville, Hall, 2002]. Rho proteins are implicated in controlling plethora of signal transduction pathways in multicellular and uni-cellular eukaryotes [Etienne-Manneville, Hall, 2002]. Activity of cdc42p and other Rho-GTPases need to be controlled temporally and spatially to achieve correct polarisation [Caviston et al., 2002], [Etienne-Manneville, 2004].

It is important to understand if the mechanisms of cell polarisation pathways are conserved in different cell types, how these pathways are wired, and how defined cell morphologies translate into cellular functions.

1.2 Fission yeast and cell morphogenesis

Schizosaccharomyces pombe (fission yeast) is an unicellular eukaryotic organism that belongs to ascomycetous fungi [Wixon, 2002]. Their cells have cylindrical shape, which normally measure 7-14 μm in length and 3-4 μm in width [Hayles, Nurse, 2001] (**Figure 1.1**). Their regular shape and genetic amenability have made them a useful model for studying cell polarity control [Hayles, Nurse, 2001]. Fission yeast cells were isolated from the African millet beer in 1893 by P. Lidner and pombe means beer in Swahilii [Wixon, 2002]. In 1950s Urs Leupold and Murdoch Mitchison introduced fission yeast as a model organism to study the cell cycle and yeast genetics [Yanagida, 2002]. In 2001 Paul Nurse received a Nobel Prize in Physiology or Medicine for the work on cell cycle regulation in fission yeast [Yanagida, 2002]. In 2002 the sequence of fission yeast genome was published as the sixth eukaryotic model organism [Wood et al., 2002]. The *S. pombe* genome contains 14.1 Mbs, which encode for 4970 proteins located on 3 chromosomes [Wixon, 2002], [Wilhelm et al., 2008].

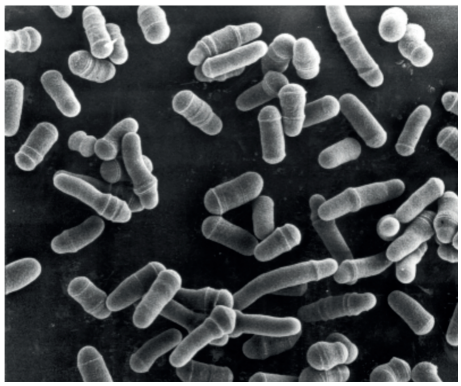

Figure 1.1: **Scanning electron micrograph of the *S. pombe* culture (adapted from [Hayles, Nurse, 2001])**

1.2.1 Life cycle of fission yeast cells

Vegetatively growing fission yeast cells are rod shaped and grow exclusively by extension of their cell poles [Mitchison, Nurse, 1985]. They always divide in the middle, in order to generate two daughter cells of equal size [Mitchison, Nurse, 1985]. Their growth is regulated by several transitions, during the cell cycle [Chang, Martin, 2009]. After cell division cells growth only from the cell end, which was inherited from the previous cell cycle [Chang, Martin, 2009]. During that time, the new and the old ends differ in their morphology [Atilgan et al., 2015]. After cell division, growth at the new end (the end which was created after septation) initiates [Chang, Martin, 2009]. This process is called NETO (new-end take-off). Bi-polar growth is maintained at both cell ends. Cells grow straight, maintaining their width and growth zones dimensions [Chang, Huang, 2014]. After reaching a critical size (13-14μm), they divide again by the central fission [Mitchison, Nurse, 1985]. (**Figure 1.2**)

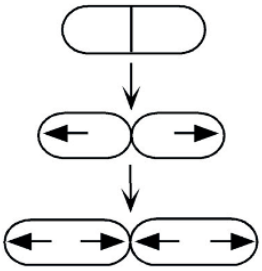

Figure 1.2: **Growth pattern of wild-type fission yeast cells**

Arrows represent the directions of growth in pairs of daughter cells. Figure adapted from [Feierbach, Chang, 2001].

1.2.2 The architecture of fission yeast cells - a simplified model

S. pombe cells are encased by a rigid cell wall, which is essential to maintain their shape [OSUMI, 1998], [Hayles, Nurse, 2001]. Bi-layered plasma membrane (PM) enables the contact between the outer and inner space of the cell. Inside the cell, there are several sub-cellular compartments that are surrounded by the highly dynamic cytoplasm [Alberts et al., 2014], [Munder et al., 2016]. The cytoplasm is crisscrossed by a system of protein filaments, which build the cytoskeleton [Alberts et al., 2014]. In fission yeast, the cytoskeleton is composed mainly of the actin and microtubule networks. The actin network is organised into actin patches - (involved mainly in endocytosis) and actin cables - (generally required for polarised membrane traffic). The microtubule network is very dynamic and is organised into bundles, which are oriented parallel to the main cell axis. Microtubules (MTs) are important to ensure that after cell division growth can reinitiate from the cell poles [Huisman, Brunner, 2011], [Martin, Arkowitz, 2014]. In addition, growing MTs are attached to the nucleus, where they are involved in positioning the nucleus in the cell centre. In mitosis, MTs build the mitotic spindle, which ensures the equal distribution of DNA into the two daughter cells during cell division [Neumann, Nurse, 2007], [Höög et al., 2007].

The nuclear DNA is surrounded by the nuclear envelope, which consists of inner and outer membranes [Zhang, Oliferenko, 2013]. The latter is continues with the endoplasmic

reticulum (ER), suggesting a close relationship between the NE and ER dynamics [Zhang, Oliferenko, 2013]. The ER is the manufacturing centre for lipids, and also many proteins, due to the binding to ribosomes. It forms an interconnected network of cisterns and tubules [Zhang et al., 2012], which contains regions of the rough ER (ribosome connected) and smooth ER (without connected ribosomes) [Herevard, 1974]. The ER connects to the PM, which, in addition to MTs, ensures the proper positioning of the nucleus [Zhang et al., 2010], [Zhang et al., 2016], [Alberts et al., 2014]. The ER-PM connection depends on two VAP proteins scs2p and scs22p, which physically link the ER with the PM [Zhang et al., 2012]. Moreover, lipid storage organelles - lipid droplets, originate at the ER [Meyers et al., 2016]. The Golgi apparatus, is a stack of closely-apposed and flattened cisterns, which are regulated by the presence of microtubule bundles [Ayscough et al., 1993a]. Proteins and lipids are often processed in the ER, and subsequently transported to the Golgi apparatus (where they are modified and probably sorted). Cargos are subsequently transported to the post-Golgi vesicles, which are delivered mainly via the actin cables to the PM (but also to other destinations) [Martin, Arkowitz, 2014], [Alberts et al., 2014]. Fission yeast contain different size vesicles, however the functional significance of this is not yet known [Höög et al., 2007]. Defined endosomal compartments are not described in fission yeast, however it is believed that the Golgi apparatus and endosomes form a so called Golgi-endosomal compartment [Yu et al., 2012].

Mitochondria, which are generally involved in ATP production, in fission yeast are organised as a large, branched network that shrinks and grows with the MTs [Das et al., 2010], [Yaffe et al., 2011]. They are distributed by the MTs in a motor-independent manner [Höög et al., 2007], [Li et al., 2015]. In addition, membrane surrounded peroxisomes most probably originate at the ER. They are intimately associated with, and move along, mitochondria [Jourdain et al., 2008]. Moreover, fission yeast cells contain several small vacuoles, which are implicated in protein turnover and play additional functions [Iwaki et al., 2003].

(**Figure 1.3**)

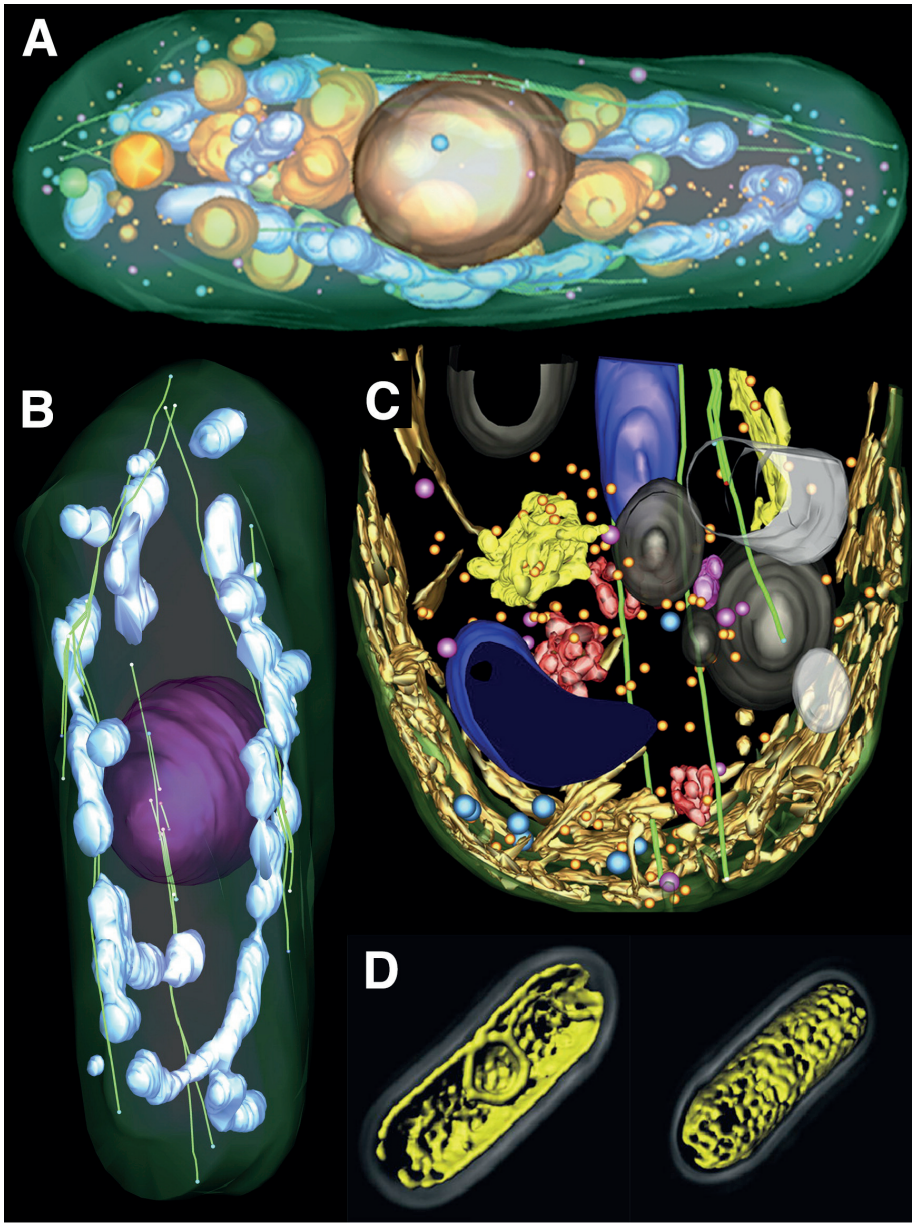

Figure 1.3: **The architecture of fission yeast cells - examples**

A - Model of electron tomogram of an entire cell volume (there are present mitochondria, the nucleus, microtubules and different membrane structures). **B** - Model of electron tomogram (MTs bundles (green) splaying around mitochondria (blue)). **C** - Cellular architecture at fission yeast cell pole (The Golgi apparatus (yellow), vesicles (grey), membrane clusters (red), vacuoles (white), ER (dark yellow), PM (dark green). **D** - expression of the the ER marker protein (GFP-AHDL) - 3D-rendered views based on confocal scanning micrographs (cell center on the left, cell cortex on the right).
Subfigures A, B and C are adapted from [Höög et al., 2007]. Subfigure D is adapted from [Zhang et al., 2012].

1.2.3 Maintenance of fission yeast cell polarity

1.2.3.1 Defining and shaping growth zones

The cylindrical shape of fission yeast cells is a consequence of the maintenance of growth sites at the cell ends. Fission yeast expresses six Rho-family GTPases that are involved in polarised growth control [Pérez, Rincón, 2010]. The most heavily studied GTPase, cdc42p, specifies growth sites [Pérez, Rincón, 2010]. Knockdown of *cdc42* results in small and round cells [Miller, Johnson, 1994], while a full deletion is lethal. The activity and localisation of cdc42p is regulated by its activating guanine nucleotide exchange factor - GEFs (gef1p and scd1p) and deactivating GTPase-activating protein - GAPs (rga4p and rga6p) [Pérez, Rincón, 2010], [Hirota, 2003], [Coll, 2002], [Revilla-Guarinos et al., 2016]. GEFs ensure activation of the cdc42p at the cell poles and GAPs deactivate cdc42p at the cell sites, restricting cdc42p activity away from the cell ends [Revilla-Guarinos et al., 2016]. A series of the upstream regulators (orb6p, orb3p, scd1p, ras1p, efc25p) and downstream effectors (orb2p, the exocyst complex components generally involved in membrane tethering at the PM) and the actin cable nucleating formin - for3p, are implicated in the cdc42p-dependent cell polarity maintenance [Das et al., 2009], [Wang et al., 1991], [Onken et al., 2006], [Fukui et al., 1986]. Moreover, it has been suggested that modulation of cdc42p activity, by its oscillatory activation between the two cell poles, could be involved in controlling growth zone dimensions [Das et al., 2012], [Bendezú et al., 2012], [Martin, Arkowitz, 2014].

Other Rho GTPases in fission yeast are also involved in polarised growth control. Removal of rho1p leads to round cells [Nakano et al., 1997]. Moreover, rho1p is an activator of one of synthetases, involved in cell wall formation [Qadota et al., 1996]. In addition, rho2p GTPase regulation is implicated in width maintenance, therefore also influencing growth zone dimensions [Villar-Tajadura et al., 2008]. For additional review see, [Huisman, Brunner, 2011] and [Martin, Arkowitz, 2014].

The size of the growth zone and its width are controlled by the activation of Rho GTPases [Martin, Arkowitz, 2014], although models suggest that neither cdc42p, nor

its dependent cell wall synthesis regulators are reliable predictors for growth domain geometry [Abenza et al., 2015]. The model proposed that growth geometry is mainly regulated by exocytic factors and the membrane fusion machinery, which induce shape changes in growth domains [Abenza et al., 2015]. Interestingly, the width of the cell can be altered after perturbation of the actin cable-mediated membrane transport [Feierbach, Chang, 2001], [Win et al., 2000], [Motegi et al., 2001], and after manipulation of the actin cytoskeleton by a low-dose of Latrunculin A (LatA) [Kelly, Nurse, 2011a], which leads to wider cells. However, the role of these factors in determining the overall pattern of vesicle fusion with the PM, and consequently in the establishment and maintenance of proper cell geometry, is not yet clear [Abenza et al., 2015].

1.2.3.2 Positioning of polarised growth sites

Mechanisms of growth site selection in fission yeast are not completely understood [Huisman, Brunner, 2011]. A number of morphogenetic mutants, growing bent or branched, have been isolated [Verde, 1995]. These cells are highly polarised, but exhibit ectopic growth site positioning [Verde, 1995]. Interestingly, it has been reported that growth site positioning depends on MTs [Laporte et al., 2015].

MTs of fission yeast form antiparallel bundles that align along the long cell axis. MTs are polarised. Their minus ends overlap in the center and the nucleus is attached to this overlap region [Höög et al., 2007]. In contrast, the MTs plus ends grow towards the cell poles [Sawin, Nurse, 1998], [Höög et al., 2013]. After reaching the cell ends, they switch from growth to shrinkage (an event called catastrophy) [Höög et al., 2013]. During interphase, microtubules have two functions. First, the deposition of the cell end marker proteins at the cell poles to ensure the initiation of growth from cell poles after cell division). Second, to keep the nucleus in the center of the cell. This is achieved by pushing forces exerted by growing MTs plus ends at cell poles. Role of MTs-dependent growth site positioning is regulated by +TIP proteins and pushing forces at the cell poles [Sawin, Tran, 2006]. Vice versa, the MT dynamics is controlled by constraints imposed

by cell shape [Terenna et al., 2008], [Minc et al., 2009].

Cells need to restrict microtubule catastrophes to the cell poles, to ensure the correct deposition of the cell end marker tea1p and its effector tea4p. *tea1*Δ and *tea4*Δ mutant cells are bent or branched. They also fail to perform NETO (switch from mono-polar to bi-polar growth). A similar phenotype is showed for the +TIP protein mutant *tip1*Δ (mutant exhibit short MTs), due to the tea1p mis-positioning. However, it is not clear how tea1p/tea4p module executes its function, although several connections are proposed [Huisman, Brunner, 2011]. In particular, tea4p was shown to interact with pom1p [Martin, Arkowitz, 2014]. *pom1*Δ cells exhibit growth site positioning defects, similar to *tea1*Δ and *tea4*Δ mutants [Bähler, Pringle, 1998]. Another role of tea4p is to bind dis2p via its SH3 domain and RVxF motif [Alvarez-Tabares et al., 2007]. This binding plays a role in pom1p localisation at the cell poles [Alvarez-Tabares et al., 2007], [Alvarez-Tabares et al., 2007]. In addition, pom1p was proposed to regulate the cell size control by forming a gradient, which starts from cell poles towards cell middle [Padte et al., 2006], [Hachet et al., 2011], however this property is under debate [Wood, Nurse, 2013]. Moreover, pom1p negatively regulates the inhibitor of cdc42p activity, the GAP rga4p. However, *rga4*Δ mutants do now exhibit major morphological phenotypes. Recently, rga6p was identified as a second cdc42p GAP [Revilla-Guarinos et al., 2016]. The double mutant *rga4*Δ*rga6*Δ is not able to maintain cell polarity [Revilla-Guarinos et al., 2016]. It is interesting if tea4p/pom1p also negatively regulate this second GAP.

tea1p/tea4p also binds the actin nucleator formin for3p. The functional connection between tea1p/tea4p and for3p is unclear, since *for3*Δ cells do not exhibit similar phenotypes as *tea1*Δ and *tea4*Δ mutants [Feierbach, Chang, 2001], [Kokkoris et al., 2014], [Makushok et al., 2016b]. In addition, it is known that tea1p forms 50-100nm protein clusters at cell poles, where it temporarily binds to the membrane anchored mod5p and tea3p that localises to the new cell pole [Arellano et al., 2002], [Snaith et al., 2005], [Bicho et al., 2010], [Dodgson et al., 2013]. Role of these clusters is not clear.

Another aspect of polarity positioning, which involves tea1p/tea4p is NETO, switch from mono-polar to bi-polar growth. *tea1*Δ and *tea4*Δ cells cannot activate growth at

the new born end after cell division. A number of mutants exhibit the same phenotype as *tea1*Δ/*tea4*Δ or only activate the newly born end. In addition, these mutants also differ in the inheritance of the growth site activation pattern, where new born cells activate both of cell poles at the same time or their progeny show variability in the end activation pattern. This mix of phenotypes arises from different aspects of the NETO control. Cells need to appropriately advance in the cell cycle, control that only one end is activated, activate appropriate end; they need to make sure they can support the second growth site and finally activate growth at the second end. The range of different phenotypes, and the high number of components playing role in NETO, make it difficult to dissect the exact mechanism of this process [Huisman, Brunner, 2011].

(**Figure 1.4**)

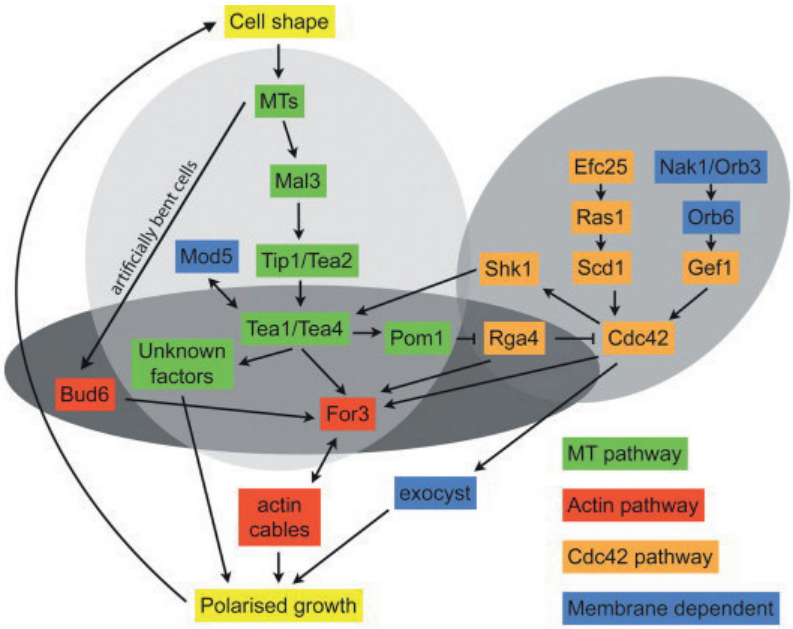

Figure 1.4: **Schematic representation of cell polarity network in fission yeast**

The light grey colour presents the protein module involved in growth site confinement, the medium grey colour shows the protein module involved in growth site positioning, and the dark colour oval presents the protein module involved in NETO control. Figure adapted from [Huisman, Brunner, 2011].

1.2.4 Polarised growth and the secretory machinery in fission yeast

Polarised growth of fission yeast depends on the force resulting from the turgor pressure [Slaughter, Li, 2006]. This force is counterbalanced by stiffness of the cell wall regulated by enzymes delivered via exocytosis. Exocytosis is also required for the delivery of the previously mentioned Rho-GTPases (for example cdc42p), which are associated with the membranes and are involved in polarised growth. It is a fundamental ability of the cell to define specific locations for exocytosis (places where membrane is delivered) but also locations for endocytosis (places where membrane is recovered). This ability is critical for growth of defined geometries [Martin, Arkowitz, 2014].

Here, we will briefly describe the basic steps of exocytic trafficking from the ER to the PM of membrane-encapsulated cargos and we will briefly describe the principles of endocytosis in fission yeast.

1.2.4.1 The early secretory pathway in fission yeast

The delivery of different cargos from the ER to the PM depends predominantly on the function of the vesicular secretory pathway, which involves intermediate compartments [Mellman, Warren, 2000], [Nickel, 2003]. Protein cargoes exiting from the ER in different model organisms are packaged into membranous vesicles [Watson, Stephens, 2005]. The formation of vesicles occurs in specialised regions of the ER, the so called ER exit sites, also known as transitional ER (tER) [Saito, Katada, 2015] In fission yeast, the vesicular marker sec24p, a COPII vesicle coat protein, is released from the tER. sec24p-GFP localises to punctate structures of various sizes, which exhibit the ER localisation [Vjestica et al., 2007]. Protein cargos to be secreted are folded and often glycosylated in the endoplasmic reticulum (ER) [Alberts et al., 2014]. The ER is also the major site of the lipid synthesis, including most of the lipids, which are known to form secretory vesicles in different model organisms [Nakase et al., 2010]. In fission yeast, several enzymes from different lipid biosynthesis pathways are localised to the ER [Matsuyama et al., 2006].

It is believed that in fission yeast, similar to other model organisms, vesicles, budding from the ER are destined to the Golgi apparatus. Similar to mammalian cells and in contrast to budding yeast the fission yeast Golgi apparatus is composed of a system of stacked Golgi cisterns, which most probably originate from the vesicles derived from the ER [Ayscough et al., 1993b], [Vjestica et al., 2007], [Suda, Nakano, 2011], [Day et al., 2013]. It is accepted that the Golgi apparatus consists of the cis, medial and trans compartments [Day et al., 2013], [Alberts et al., 2014]. Individual stacks have a different set of enzymes, used for processing of cargo proteins during their transport from the cis to the trans Golgi face [Alberts et al., 2014]. Cis compartments in fission yeast are marked by anp1p-mcherry, which is homolog of the Golgi mannosyltransferase complex [Vjestica et al., 2007]. It localises to several particles, distributed throughout the cell interior. Similar localisation is known for the marker of the trans-Golgi compartment sec72p-GFP. Cis and trans Golgi markers partially colocalise with each other, suggesting they might temporarily serve as the separate organelles, similar to other model organisms [Vjestica et al., 2007]. The Golgi cisternal stacking depends on MTs [Ayscough et al., 1993b], [Ayscough, Warren, 1994], [Brazer et al., 2000], however loss of MTs does not result in exocytic defects and there is no apparent physical association between MTs and the Golgi apparatus [Ayscough et al., 1993b], [Höög et al., 2007].

1.2.4.2 The post-Golgi membrane trafficking in fission yeast cells

The secretory vesicles, carrying membrane and protein cargos from the Golgi apparatus, are transported along formin-nucleated actin cables via myosin V motors [Wang et al., 2016]. In fission yeast, the main formin for3p drives actin cable assembly [Feierbach, Chang, 2001], [Nakano, 2002]. Myosin V motor - myo52p, is responsible for transporting cell wall-dependant synthetase - bgs1p and other cargos [Mulvihill et al., 2006], [Estravís et al., 2011]. It is known that myo52p does not only use actin cables to transport cargos but can also actively shape actin cables. During membrane trafficking, myo52p promotes the extension of cables and therefore their distribution throughout the

cellular space [Lo Presti et al., 2012].

The yeast exocytic pathway is regulated by a series of Rab GTPases [Ling et al., 2014]. In budding yeast the two redundant Rabs - ypt31p and ypt32p act redundantly in controlling the exit of vesicles from the Golgi [Benli et al., 1996], [Jedd et al., 1997]. They are required for the interaction between myo52p and post-Golgi vesicles [Casavola et al., 2008], [Lipatova et al., 2008], [Santiago-Tirado et al., 2011]. In fission yeast, the ypt3p homolog of ypt31p/ypt32p, which is also the homolog of the mammalian rab11p, localises to the cell poles and sites of cytokinesis [Cheng et al., 2002]. It co-immunoprecipitates and partially colocalises with the myo52p. Its localisation is dependent on both myo52p and the for3p. It has been shown that ypt3p can act as a cargo receptor for myo52p [Lo Presti, Martin, 2011]. In agreement, ypt3p in fission yeast is required at multiple steps of the exocytic pathway, including post-Golgi trafficking [Cheng et al., 2002] and is redundant with the ryh1p (rab6p homolog from mammalian cells), which is also implicated in membrane trafficking [He et al., 2006]. In budding yeast yp31p/ypt32 localise to late-Golgi cisterns and secretory vesicles in the signalling cascade to activate sec4p (ypt2p is a homolog of sec4p in fission yeast and rab8p homolog in mammalian cells) [Craighead et al., 1993], [Ortiz et al., 2002], [Jin et al., 2011], [Wang et al., 2016]. yp31p/ypt32 from budding yeast are involved in the signalling cascade, leading to the activation of sec4p by its GEF activating protein sec2p. In addition this cascade involves a role of PI(4)P and osh4p (kes1p homolog from fission yeast) and presumably the non-vesicular transport of lipids at the Golgi [Ling et al., 2014]. These interactions have not been studied so far in fission yeast, however it is known that ypt2p and ypt3p puncta colocalise in 48%, mainly at cell poles and at the division site [Wang et al., 2016]. It was suggested that they might act in a similar signalling cascade on the secretory vesicles as in budding yeast [Wang et al., 2016]. The *ypt2VN* mutant rapidly stop growing at restrictive temperature and accumulates large number of secretory vesicles in the cytoplasm [Craighead et al., 1993].

It addition, it is revealed that in fission yeast, the Golgi dependent trafficking of GPI-anchored protein ecm33p, from the Golgi to the PM, is dependent on zinc

homeostasis, regulated by cis4p, which localises to the Golgi apparatus [Fang et al., 2008], [Jaiseng et al., 2012], [Fang et al., 2014]. Block of delivery of ecm33p to the PM can be rescued by over-expression of the ubiquitin-ribosome fusion protein ubi1p, as ubi1p removal is essential for viability [Fang et al., 2008], [Jaiseng et al., 2012]. Interestingly, it is proposed that ecm33p trafficking from the Golgi bypasses the presumptive endosomal compartment and this transition is most probably regulated by the clathrin adaptor protein apm1p [Fang et al., 2014]. Clathrin adaptor protein (AP) complexes are known to be involved in post-Golgi trafficking, by regulating the formation of transport vesicles and by selection of cargos to be delivered into different post-Golgi routes, namely endosomes, degradation compartments or the PM [Ohno, 2006]. Accordingly, mutants of the adaptor protein subunits in fission yeast play role in the Golgi dependent trafficking [Kita et al., 2004], [Ma et al., 2009], [Yu et al., 2012].

Although actin-related transport mutants of fission yeast are slightly affected in their cell shape, it is striking that polarised cell growth in most of these mutants can occur [Bendezu, Martin, 2011].

1.2.4.3 Membrane tethering and fusion at the PM in fission yeast cells

It has been proposed in budding yeast that the previously mentioned sec4p (ypt2p homolog in fission yeast) dependent cascade is linked to the membrane tethering at the PM. sec4p indirectly binds the exocyst complex subunit sec15p [Ling et al., 2014]. The octameric exocyst complex is involved in the physical attachment of vesicles over a distance to promote the fusion reaction [TerBush et al., 1996], [Alberts et al., 2014], [Wu, Guo, 2015], [Wang et al., 2016]. Such presumptive interaction of sec4p/ypt2p with the exocyst has not been evaluated in fission yeast, however it is appreciated that once vesicles reach the target membrane, different reactions initiate the vesicle-membrane fusion. They involve tethering, docking, priming, SNARE complex assembly (essential for membrane fusion), and subsequent merging of two membranes [Jahn, Fasshauer, 2012], [Alberts et al., 2014], [Wang et al., 2016]. Vesicle tethering at the PM determines

sites of vesicle incorporation to the PM [Wang et al., 2016].

Exocyst complex components in fission yeast localise to sites of active secretion on the PM [Wang et al., 2002]. sec8p, one of the exocyst complex subunits is essential for cell viability, but temperature-sensitive mutants can grow in a polarised manner during interphase until cell division. They cannot digest septas in order to separate after cell division [Wang et al., 2002]. It was suggested that their polarised growth activity could be a result of redundant polarity pathways or feedback loops [Wang et al., 2002]. Indeed, it was shown that polarised cell growth can occur independently of the cytoskeletal transport and the exocyst, however it has been proposed that these two processes act redundantly to promote polarised growth. They are individually dispensable, but together they are essential [Snaith et al., 2011], [Bendezu, Martin, 2011].

Two previously mentioned morphogenetic modules, the actin-based transport and the exocyst-mediated membrane tethering, are functionally and physically linked to the unconventional exocyst subunit sec3p [Jourdain et al., 2012], [Bendezú et al., 2012], (**Figure 1.5**). Cells without functional sec3p lack actin cables, have delocalised actin regulating components (for example for3p), are misshapen and impaired in protein secretion [Jourdain et al., 2012]. Similar to budding yeast, studies by [Bendezú et al., 2012] showed that sec3p is functionally linked to exo70p (another exocyst component) [Zhang et al., 2008]. The *sec3*Δ*exo70*Δ double mutants showed synthetic lethality. sec3p together with exo70p are proposed to act as a localisation determinant of the site of cell polarity [Bendezú et al., 2012], [Jourdain et al., 2012]. In addition, components of this complex were shown to bind to cdc42p.

Two morphogenetic modules of exocytosis are downstream effectors of the master regulator of the cell polarity - cdc42p [Bendezu, Martin, 2011], [Estravís et al., 2012]. cdc42p regulates formin activation and actin cable assembly. In addition, it is also required for the exocyst function, contributing to polarised secretion [Estravís et al., 2012]. Therefore, cdc42p participates in membrane trafficking. It was shown that cdc42p is required for the correct transport or recycling of cell wall biosynthesis enzymes to the

plasma membrane [Estravís et al., 2012]. Moreover, it has been suggested that pob1p, which is a scaffold protein of cdc42p, is responsible for executing cdc42p-dependent functions in membrane trafficking [Estravís et al., 2012]. In addition, cdc42p mutant phenotypes can be partially rescued by the over-expression of ypt2p [Estravís et al., 2011].

Another member of the Rho GTPase family in fission yeast - rho3p was found to partially suppress the exocyst mutant *sec8-1* [Martin, Arkowitz, 2014]. Over-expression of rho3p restores the exocyst localisation in cdc42p and pob1p mutants, suggesting that both rho3p and cdc42p/pob1p play a role in tethering the exocyst to the growth sites. It is not known if cdc42p and rho3p execute their function independently [Estravís et al., 2012]. Interestingly, the previously mentioned phenotypes of the adaptor complex subunit apm1p mutant (implicated in the post-Golgi trafficking) can also be rescued by rho3p [Kita et al., 2011].

Membrane buddying and fusion, are two of most fundamental processes in life. These processes are based on the merging of two membranes into one single membranous structure [Jahn et al., 2003]. They are performed by evolutionary conserved multi-protein complexes, which consist of different SNARE proteins [Bonifacino, Glick, 2004]. Several lines of evidence revealed that SNARE proteins are crucial for maintenance of the cell polarity in different model organisms [Low et al., 2000], [Mellman, Nelson, 2008], [Rodriguez-Boulan, Macara, 2014]. The pairing between the vesicle-localised v-SNARE and the PM-localised t-SNARE provides the force for the fusion between the vesicle and the membrane [Cai et al., 2007], [Jena, 2011]. The fission yeast genome encodes for 19 SNARE proteins [Wood et al., 2011], however 3 of them are homologs of the budding yeast PM-SNARE complex components: the Syntaxin 1 homolog (psy1p), Synaptobrevin (syb1p) and the SNAP25-like component (sec9p). These components are highly conserved. Psy1p and sec9p localise to the PM and syb1p is localised to Golgi-endosomal intracellular structures and the medial ring during cytokinesis [Yamaoka et al., 2013]. Syb1p is also visible at the PM, because it cycles between the cell surface and the endocytic pathway [Estravís et al., 2011].

It has been suggested that PM-SNAREs in *S. pombe* have similar functions to their mammalian equivalents [Yamaoka et al., 2013]. It has been shown that the fission yeast v-SNARE syb1p, is essential for cell morphogenesis [Yamaoka et al., 2013]. In particular, it is involved in the cell elongation and cytokinesis [Edamatsu, Toyoshima, 2003]. Psy1p function was studied during sporulation. It plays role in the forespore membrane formation and endocytosis [Maeda et al., 2014], [Kashiwazaki et al., 2011]. Over-expression of psy1p (but not the syb1p) is able to rescue polarised growth defects in the cdc42p mutant [Estravís et al., 2011]. In addition sec9p is involved in sporulation and cytokinesis [Nakamura et al., 2005].

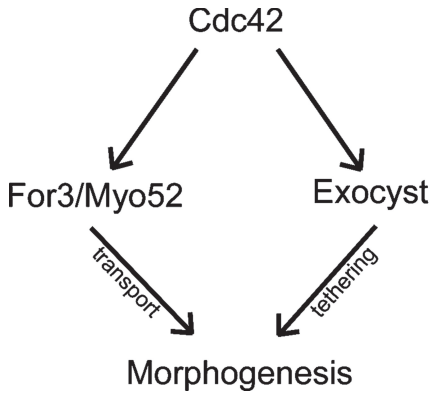

Figure 1.5: **Model of two redundant morphogenesis modules under the control of cdc42p**

Two parallel morphogenetic modules are redundant for polarised cell growth (the actin-dependent transport and the exocyst-dependent membrane tethering at the PM). Described in 1.2.4. Figure adapted from [Bendezu, Martin, 2011].

1.2.4.4 Principles of endocytosis in fission yeast

Defining specific sites of endocytosis is important for growth of defined geometries [Martin, Arkowitz, 2014]. There, actin cytoskeleton is essential. During endocytosis, cells internalize molecules from the outside of the PM but also recycle membranes and proteins localised to the PM [Alberts et al., 2014]. In fission yeast this process is precisely coordinated. Initially, the clathrin proteins (initially involved in the membrane

invagination), end4p, panlp, activators of arp2/3, wsplp, myo1p and arp2/3 complex, respectively, are recruited to the site of endocytosis. In addition, the AP-2 complex, is involved in the proper temporal and spatial dynamics of endocytic patches, most probably by modulating interaction between clathrin and membrane lipids [León de et al., 2016]. The arp2/3 complex (involved in the actin patch assembly) generates the force needed for detachment of endocytic vesicles from the PM [Sirotkin et al., 2010]. This needs actin fillament capping and cross-linking with fimbrin. After a vesicle is internalised, actin patch components detach from the vesicle [Sirotkin et al., 2010], [Basu et al., 2014].

It was shown that endocytosis and turgor pressure in fission yeast are linked. *S. pombe* cells, like other cell-walled organisms, have a high turgor pressure, enabling growth and survival. It was suggested that turgor pressure opposes invagination of the PM during endocytosis. Reducing turgor in fission yeast modulates speed of early steps of endocytosis and rescues defects in several endocytic mutants. It was suggested that endocytosis in fission yeast is regulated by homeostasis between actin-dependent forces and opposing forces created by the high turgor pressure [Basu et al., 2014].

In budding yeast, it has been shown that cdc42p regulates membrane recycling through endocytosis or regulated extraction of cdc42p from the PM. This phenomenon is crucial for the polarised localisation of cdc42p [Marco et al., 2007], [Slaughter et al., 2009]. It is possible that cdc42p is involved in similar activity in fission yeast, since it is known that cdc42p is essential for the actin-dependent transport of vesicles and localisation of cell wall synthesising enzymes [Estravís et al., 2012]. It suggests that membrane recycling through endocytosis could be the important process, involved in the maintenance of polarised growth. Indeed, several endocytic mutants lose their growth polarity [Castagnetti et al., 2005], [Codlin et al., 2008]. In addition, end4p/sla2p, which is implicated in endocytosis and cortical actin organisation, is involved in polarised growth and is proposed to be a downstream factor of tea1p, as it was previously described as required for proper positioning of growth sites [Castagnetti et al., 2005]. It is not known if localisations of endo- and exocytosis are linked with each other in fission yeast and if

this potential feature is involved in the maintenance of polarised growth.

1.2.5 Introduction to PIP2 and PI(4)P

Phosphoinositides are lipids and belong to the class of glycerophospholipids [Martin, Arkowitz, 2014]. They are characterised by the presence of an inositol group. Phosphoinositides derive from phosphatidylinositol (PI) [Balla, Balla, 2006]. They play a central role in the activity, regulation and recruitment of many signalling proteins [Balla, Balla, 2006].

Phosphatidylinositol 4,5-bisphosphate (PIP2) is generated via phosophorylation of phosphatidylinositol-4-phosphate (PI(4)P) by the Phosphatidylinositol-4-phosphate 5-kinase (PtdIns4P5K). PIP2 is implicated in many cellular functions, like transcription, cytoskeleton organisation, membrane trafficking and signal transduction [Fruman et al., 1998], [Simonsen et al., 2001], [Yin, Janmey, 2003], [Roth, 2004], [Li et al., 2013]. Although, PIP2 is a precursor of other signalling molecules, it also directly coordinates endocytosis, the organisation of the cytoskeleton and recycling of synaptic vesicles [Berridge, Irvine, 1984], [Toker, Cantley, 1997], [Takenawa, Itoh, 2001], [Audhya et al., 2004], [Li et al., 2013].

In fission yeast, the essential kinase its3p phosphorylates PI(4)P to PIP2 [Zhang et al., 2000]. Temperature-sensitive mutant *its3-1* contains low amount of PIP2 at restrictive temperature [Zhang et al., 2000]. In fission yeast PIP2 plays a role in the organisation of actin patches, cell separation [Zhang et al., 2000], membrane trafficking [Li et al., 2013], maintenance of cell polarity [Jourdain et al., 2012], cell wall integrity [Deng et al., 2005], localisation of the membrane tethering complex - exocyst, and it is suggested to play role as the spatial landmark determinant for sites of polarised growth [Bendezú et al., 2012]. In fission yeast, PIP2 is enriched at the site of cell division and at the cell cortex [Zhang et al., 2000], [Li et al., 2013].

The over-production of its3p leads to higher levels of PIP2 and cell growth defects [Zhang et al., 2000]. In addition, it causes the accumulation of abnormally localised

its3p in the cytoplasm, untypical endo-membrane structures, multimella Golgi and fragmented vacuoles [Li et al., 2013]. These phenotypes can be rescued by gyp10p, a GTPase-activation protein (GAP) that negatively regulates the previously mentioned Rab GTPases ypt3p and ryh1p that are working in the post-Golgi membrane trafficking [Li et al., 2013]. Mutants of ypt3p and ryh1p can suppress phenotypes caused by over-expression of its3p. It has been suggested that PIP2 and Rab-mediated trafficking are functionally linked [Li et al., 2013].

PI(4)P is a product of phosphorylation of phosphatidylinositol (PI) by the phosphatidylinositol 4-kinases and it is further phosphorylated to produce the previously described PIP2 [Balla, Balla, 2006]. In different cell types, PI(4)P is an essential signalling molecule at the PM and the Golgi apparatus in the regulation of membrane trafficking, cytoskeletal organization, lipid metabolism, signal transduction pathways and cytokinesis [Matteis, Godi, 2004], [Janetopoulos et al., 2005], [Strahl, Thorner, 2007], [Strahl et al., 2005], [Walch-Solimena, Novick, 1999a], [Garcia-Bustos et al., 1994], [Brill et al., 2000].

In mammalian cells and budding yeast, there are identified different pools of PI(4)P, which are synthesised by different enzymes from the PI. The two mainly studied enzymes producing PI(4)P in budding yeast are stt4p and pik1p and their functions are non-redundant. Both enzymes are essential for the yeast viability. Stt4p has been shown to be responsible for the production of the PM pool of PI(4)P and is required for the formation of the actin cytoskeleton, endosome motility and cell wall biosynthesis [Audhya et al., 2000], [Chang et al., 2005], [Balla, Balla, 2006]. Pik1p is involved in PI(4)P synthesis, functioning in the cytokinesis, protein secretion, endocytosis and maintenance of the Golgi structures [Walch-Solimena, Novick, 1999b], [Audhya et al., 2000], [Strahl et al., 2005], [Balla, Balla, 2006]. pik1p generates the Golgi and nuclear pool of PI(4)P [Balla, Balla, 2006].

Numerous *in vitro* studies on liposomes consider PI(4)P as a potential metabolic

energy source, involved in the exchange of sterol (or phosphoserine (PS)) between the closely opposing membranous structures. Therefore, it is important in the generation of important lipid gradients. PI(4)P is shown to bind to the oxysterol-binding protein family (osh proteins, oshes), which are involved in the lipid distribution and transport. Oshes compete for the PI(4)P binding with other lipids. The mechanism involves the so called counterflow transport of sterol (or PS) and PI(4)P (exchange of sterol/PS for PI(4)P) (more details in 1.3.1.3; for review [Mesmin, Antonny, 2016] and [Drin et al., 2016]).

The fission yeast genome encodes 3 putative phosphatidylinositol 4-kinases: lsb6p, stt4p and pik1p [Wood et al., 2011]. Among those *pik1* is the only essential gene [Park et al., 2009] [Wood et al., 2011]. In fixed cells, GFP-pik1p colocalises with the Golgi apparatus marker gma12-GFP [Park et al., 2009]. *pik1* sequence in fission yeast contains two functional regions: lipid kinase domain and the region for binding to cdc4p (component of the contractile ring involved in cytokinesis [McCollum, 1995]). [Park et al., 2009] revealed that the lipid kinase is the one, which is essential for pik1p function. Temperature sensitive allel of *pik1* (*pik1-td*) is impaired in membrane trafficking what leads to defects in septation and cell separation [Park et al., 2009].

As mentioned above, PI(4)P, synthesised by pik1p at the Golgi, (see, 1.2.4.2) is involved in the activation of the ypt3p/sec4p cascade in budding yeast, leading to the loading and transport of the post-Golgi membrane vesicles onto actin cables [Ling et al., 2014]. This potential role of PI(4)P in polarised secretion in fission yeast has not been studied so far.

1.3 Compartmentalisation of the PM and lipid rafts

Cells are surrounded by the plasma membrane (PM), what gives them identity and provides a boundary in between inner and outer space of the cell [Simons, Sampaio, 2011]. Amphipathic properties of lipids enable their spontaneous self-organisation into a double layer and membrane formation [Simons, Sampaio, 2011]. The PM is composed

by lipids but also by proteins, which span the layer of the PM with their transmembrane domains or are attracted to a membrane on the inside or the outside of the cell [Jacobson et al., 2007], [Engelman, 2005], [Coskun, Simons, 2009].

In the 1972 Singer and Nicolson presented the *fluid mosaic* model of the structure of the cell membranes [Singer, Nicolson, 1972]. The model is based on the thermodynamic properties of the membrane organisation and assumes that proteins and lipids are mobile within the membrane matrix. Since more than 40 years, the *fluid mosaic model* remains relevant. The PM is composed mainly by the variety of hundreds of different glycerophospholipids, sphingolipids, and also by the sterols [Simons, Sampaio, 2011]. Membrane is compartmentalised by sphingolipid-cholesterol-protein assemblies called lipid rafts [Nicolson, 2014], [Simons, Ikonen, 1997].

Since almost two decades there are increasing amount of evidence confirming existence of lipid rafts in the PM [Alberts et al., 2014]. Initially, lipids rafts have been identified as the detergent insoluble glycolipid-enriched complexes (DRM - detergent resistant membranes) [Simons, Ikonen, 1997]. Numerous lipid raft-associated proteins have been identified, which localise to DRMs [Simons, Ikonen, 1997]. Some examples are GPI-anchored proteins or Src proteins [Danielsen, 1995], [Casey, 1995]. Newly developed microscopy techniques allow to detect nanoscopic protein clusters in the PM which are believed to be lipid rafts [Simons, Gerl, 2010], [Owen et al., 2012], [Truong-Quang, Lenne, 2014].

Lipid rafts are proposed to cluster into larger, more stable raft domains - stabilised rafts. Stabilised rafts are prone to subsequently coalesce and to form micrometere raft phases, which can be seen under a fluorescence microscope [Simons, Gerl, 2010]. Lipid rafts are implicated in several basic processes like: signal transduction [Simons, Toomre, 2000], post-Golgi trafficking and sorting of cargos [Schuck, 2004], endocytosis and virus budding [Rajendran, 2005]. In addition, perturbations in the assembly of the lipid rafts are implicated in several diseases (for review, [Michel, Bakovic, 2012]).

1.3.1 Lipid rafts, sterol and cell polarity

The asymmetric distribution of membrane proteins and lipids in different cell surface domains is a common feature of all eukaryotic cells. As previously mentioned, it appears that lipid rafts are functioning in several biological processes. One of them is the control of cell polarity [Lingwood et al., 2009].

1.3.1.1 Roles of sterol in cell polarity

Sterols are enriched at the surface of the apical membrane in epithelial cells [Simons, Meer van, 1988]. Moreover, the cholesterol content is significantly different in the unpolarised epithelial cells comparing to the polarised cells [Sampaio et al., 2011]. Its synthesis is core to the formation of the apical, lipid raft-enriched membrane because it is required for delivery of several specific raft-destined proteins [Simons, Meer van, 1988], [Meer van, Simons, 1988], [Bagnat, 2000], [Simons, Sampaio, 2011].

It is appreciated that sterol has a potential to decrease the flexibility of acyl chains in a bilayer, and therefore to increase the PM thickness and impermeability [Mesmin et al., 2013a]. Its function in other cellular compartments is still elusive, however it is known that increase of sterol content in the trans-Golgi network (TGN) modifies its membrane structure. This function is essential to transport a subset of carriers from the TGN to the PM [Holthuis, Menon, 2014], [Duran et al., 2012], [Wang et al., 2000]. It has been proposed that sterol is enriched in the TGN-derived vesicles and that the sorting of raft-associated lipids is performed in this organelle [Klemm et al., 2009]. Moreover, a functional screen in budding yeast showed that sterol is required for the delivery of cargo proteins to the PM [Proszynski et al., 2005]. In addition, sterol is required for the oligomerisation and apical sorting of lipid raft-destined (GPI)-anchored proteins from the TGN to the PM [Paladino et al., 2008].

It has been reported that sterol is functional at the level of the endocytic recycling compartment (ERC). ERCs can accommodate up to 35% of the total cholesterol content of the cell [Wustner et al., 2002]. ERCs play a role as the intermediate transport

compartment between TGN and the PM but are also involved in the recycling of membranes that are endocytosed from the PM, and the retrograde transport of proteins and lipids from the PM to the TGN [Maxfield, McGraw, 2004], [Ang et al., 2004], [Taguchi, 2013]. It has been shown that cholesterol is important for the integrity of ERCs and that the ERC-dependent pool of cholesterol plays role in cholesterol homeostasis and the transport of different lipid-anchored proteins [Mukherjee et al., 1998], [Hao, 2004]. Moreover, it is known that cholesterol is involved in sorting of molecules at the ERCs, similar to sorting at the TGN [Mukherjee et al., 1999], [Gagescu et al., 2000]. Strikingly, several SNARE proteins, which are involved in the membrane fusion process and are related to the TGN and recycling endosomes, have additional sequence to recognise cholesterol, which is involved in the localisation of these SNAREs [Enrich et al., 2015], [Reverter et al., 2014].

1.3.1.2 Establishing sterol gradients

It is clear that lipid rafts are central to the cell polarity [Sampaio et al., 2011], [Simons, Gerl, 2010], however detailed mechanisms of how the sterol distribution is controlled and maintained is not well described. Cholesterol in mammalian cells and ergosterol in yeast form intracellular gradients. The ER contains less than 5% of the total sterol, while the TGN and the PM can contain up to 40% [Drin et al., 2016]. Cholesterol in mammals and ergosterol in yeast are mainly synthesised in the ER but can also derive from lipid droplets, where esterified sterols are stored. In addition, sterol can be taken up from extracellular space in higher eukaryotic organisms [Mesmin et al., 2013a].

It was suggested that sterol gradients can be regulated by the activity of the ER-localised protein ACAT. This protein converts cholesterol to cholesteryl-esters, which are localised to the lipids droplets [Mesmin et al., 2011]. In addition, several studies report tight junctions, intercellular barriers between epithelial cells [Anderson, Van Itallie, 2009], to play important roles in lipid polarity formation and

maintenance [Meder et al., 2005], [Kälin, Meer van, 2009]. A recent report excludes this possibility [Ikenouchi et al., 2012], while in addition, others propose membrane trafficking-independent routs of maintaining cell polarity [Halbsgut et al., 2011].

It is appreciated that most of the sterol transport from the ER to the PM is independent of vesicular membrane trafficking [Urbani, Simoni, 1990]. [Baumann et al., 2005b]. It is possible that the sterol gradient is maintained by the high affinity of sterol to the saturated lipids in the TGN or the PM [Holthuis, Menon, 2014]. In addition, a list of lipid transport proteins (LTPs) that can mediate vectorial sterol transport between different organelles, was identified [Drin et al., 2016]. There are several proteins known, that act as LTPs and are present at the membrane contact sites (MCSs). MCSs are regions where membranes are in close proximity [Prinz, 2014]. The ER network is the optimal organelle to form such contacts. It extends through the cytoplasm and contacts several organelles, including the TGN and the PM [Prinz, 2014], [Mesmin, Antonny, 2016]. Different proteins have been identified to mediate these connections. In budding yeast, its2p and scs2/scs22p are critical for the tethering of the ER to the PM [Manford et al., 2012]. LTPs are also involved in formation of MCSs [Prinz, 2014]. In addition, it has been reported that members of the OSBP-related proteins family (Oxysterol-binding proteins), called ORP, in mammalian cells, and oshes (OSBP homologs) in yeast are involved in lipid transfer between membranes from two distinct organelles [Olkkonen, Li, 2013]. OSBP from mammals and osh4p (kes1p) in yeast can establish a sterol gradient by lipid exchange, using PI(4)P as a driving force [Mesmin et al., 2013b], [Saint-Jean de et al., 2011a], [Filseck Moser von et al., 2015b].

1.3.1.3 Counterflow transport of sterols and PI(4)P at the membrane contact sites

Studies of oxysterol binding-proteins, osh4p (kes1p) from yeast and OSBP from mammalian cells, revealed their highly conserved property to bind PI(4)P [Saint-Jean de et al., 2011b]. They are able to bind sterol and PI(4)P in a mutually exclusive manner

[Saint-Jean de et al., 2011b], [Drin et al., 2016]. This feature gives insight into the mechanism of the regulation of the directional movement of lipids and their asymmetric distribution. Current model propose that osh4p (kes1p) and OSBP (oxysterol-binding protein) exchange sterol and PI(4)P between the ER and the trans-Golgi network [Filseck Moser von et al., 2015b], [Mesmin, Antonny, 2016].

osh4p (kes1p) has the so called ORD domain, which contains a hydrophobic cavity to bind sterol. In addition, charged residues of the ORD domain recognise PI(4)P and accommodate it via its acyl chains [Filseck von et al., 2015]. A model has been proposed, that osh4p transfers sterol from the ER to the Golgi, by exchanging it for PI(4)P, which is transported from the Golgi to the ER. In this model sterol transport is driven by the PI(4)P gradient, which is created by a pik1p kinase in the TGN, (**Figure 1.6**). After transport of PI(4)P from the Golgi to the ER, PI(4)P is hydrolysed by a sac1p phosphatase [Mesmin, Antonny, 2016], (**Figure 1.6**). These studies are based on *in vitro* experiments on liposomes [Saint-Jean de et al., 2011b], [Mesmin et al., 2013b], [Filseck von et al., 2015] and similar was shown for the mammalian OSBP. Although the role of osh4p (kes1p) in sterol transport *in vivo* was questioned [Georgiev et al., 2011], [Beh et al., 2012], osh4p (kes1p) is known to bind post-Golgi secretory vesicles in living cells, mediating interactions between several membrane trafficking regulators, and functioning in remodelling and in maturation of secretory vesicles [Alfaro et al., 2011a], [Ling et al., 2014]. It was suggested that these findings do not contradict the sterol/PI(4)P exchange model and it is proposed that osh4p can promote sterol/PI(4)P homeostasis at the Golgi to enable the maturation of the TGN [Mesmin, Antonny, 2016].

In addition, osh4p interacts genetically with the PI/Phosphatidylcholine (PC) transfer protein sec14p, which regulates the Golgi lipid composition and the formation of secretory vesicles from the TGN. It was suggested that sec14p promotes the production of PI(4)P by a pik1p kinase. In contrast, the sterol/PI4P exchange activity of osh4p is supposed to counteract pik1p and sec14p at the TGN [Mesmin, Antonny, 2016], (**Figure 1.6**), (**Figure 1.6**).

OSBP is predicted to function similar to osh4p in the counterflow transport of sterol

and PI(4)P [Mesmin et al., 2013b], [Blagoveshchenskaya et al., 2008], [Roy, Levine, 2004]. In contrast to osh4p, the sterol binding of OSBP is auto-inhibited and requires an interaction with a VAP-A protein, a homolog of scs2p/scs22p from budding and fission yeast, at the MCSs. The FFAT motif of OSBP interacts with the VAP-A. This interaction is essential for the sterol transfer. It was suggested that VAP-A is involved in building physical connections between the ER and membranes of the TGN. It induces conformational changes in OSBP, to enable sterol binding [Mesmin, Antonny, 2016]. In addition, OSBP contains a PH domain, that can bind PI(4)P and a GTP-bound arg1p. However, *in vitro* studies showed that this interaction is not essential to facilitate lipid transfer [Mesmin et al., 2013b].

In addition, *in vivo* studies of another oxysterol-binding proteins in budding yeast: osh6p, osh7p [Maeda et al., 2013], [Filseck Moser von et al., 2015a] and mammalian equivalents [Chung et al., 2015], revealed their function in transporting phosphoserine (PS) between the ER and the PM (**Figure 1.6**).

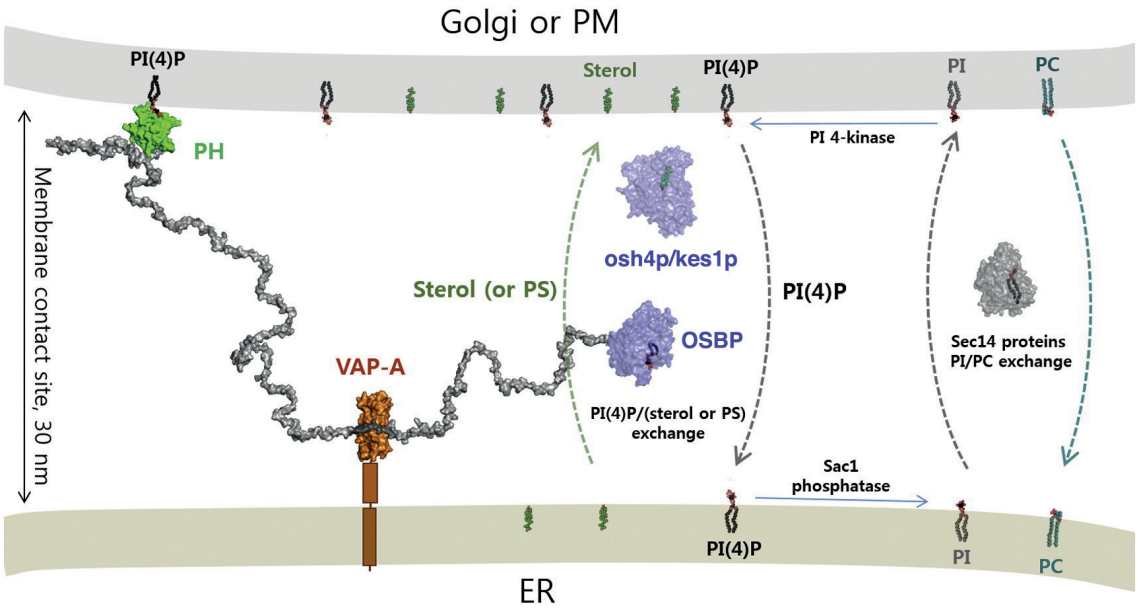

Figure 1.6: **osh4p/OSBP related structural model of lipid transport at the membrane contact sites**

Structural model of lipid/PI(4)P counter-transport, based on [Mesmin, Antonny, 2016] and additionally described in **1.3.1.3**. Figure adapted from [Tong et al., 2016].

1.3.2 Sterol-rich membrane domains

Sterol-rich membrane domains (SRMs) are thought to be analogues to lipid rafts [Klose et al., 2010], however it is not known if they are homogenous or if they contain smaller domains. SRMs are enriched in sphingolipids and sterols [Bagnat, 2000].

1.3.2.1 SRMs in Fungi

SRMs were mainly described in fungi [Wachtler et al., 2003], [Alvarez et al., 2007], [Fischer et al., 2008], [Bühler et al., 2015a], [Makushok et al., 2016a]. In these organisms, SRMs can be visualised by staining with filipin, a sterol-binding dye [Drabikowski et al., 1973]. A main sterol in fungi is ergosterol, the yeast counterpart of cholesterol. It can be detected predominantly at the polarised growth sites in different species [Alvarez et al., 2007].

In *Saccharomyces cerevisiae* (budding yeast) [Bagnat, Simons, 2002a], [Bagnat, Simons, 2002b], and *Cryptococcus neoformans* [Nichols, 2004], SRMs localise to tips of mating projections, in *Schizosaccharomyces pombe* at cell ends, the site of cytokinesis and tips of mating projections [Wachtler et al., 2003], [Takeda et al., 2004]. In *C. albicans* and *A. nidulans* at the hyphal tips and septa [Fischer et al., 2008].

In *C. albicans* and *A.nidulans* SRMs have been shown to be essential for growth directionality and localisation of cell end landmark proteins [Alvarez et al., 2007], [Takeshita et al., 2008]. This suggested a role of SRMs in the maintenance of polarised growth and in the presentation of the virulence factors, which are often SRM associated, such as GPI-anchored proteins [Alvarez et al., 2007], [Rella et al., 2016]. In *S. cerevisiae* SRMs serve as platforms for the sorting of proteins destined to the cell surface [Bagnat, Simons, 2002b], [Takeda et al., 2004], [Takeda, Chang, 2005], [Wachtler et al., 2003]. Moreover, recent studies revealed a crucial role for SRMs in fission yeast cell polarisation [Makushok et al., 2016b]. This special role will be introduced in the last subsection (see, **1.4**)

1.3.2.2 Sterol-rich membrane domains in fission yeast cells

1.3.2.2.1 Localisation control of SRMs in vegetatively growing fission yeast cells

SRMs in fission yeast predominantly localise to growing cell ends, sites of cytokinesis and tips of mating projections. SRM localisation is cell cycle dependent and involves the secretory pathway [Takeo, 1985], [Wachtler et al., 2003]. Prolonged interference with the actin cytoskeleton, for example by Latrunculin A or B, leads to ectopic SRM distribution. In contrast, the disruption of microtubules does not cause abnormal SRM localisation [Wachtler et al., 2003]. In addition, SRM localisation depends on the polarity regulator orb1p [Nurse, Snell, 1994], as *orb1-13* mutants show homogeneous filipin staining in the PM [Wachtler et al., 2003].

In exponentially growing cells, SRM localisation depends on the type I myosin myo1p, a myosin motor involved in endocytosis. Deletion of *myo1* causes homogeneous localization of SRMs along the entire PM at all stages of the cell cycle while its over-expression leads to SRM ectopic positioning [Takeda, Chang, 2005]. The homogeneous distribution of SRMs is linked to the TH1 domain of myo1p and its potential binding to acidic phospholipids [Takeda, Chang, 2005]. These results show that SRMs do not exclusively localise to growth sites and sites of cytokinesis. Strikingly, *myo1*Δ cells grow cylindrical and exhibit normal localisation of growth and polarity markers [Takeda, Chang, 2005]. Recently, Makushok et al. suggested that polar growth activity in these cells is a consequence of redundant tea1p-dependent polarity pathway confining polar growth activity to the cell poles, probably due to the growth site inheritance [Makushok et al., 2016a]. The double mutant *myo1*Δ*tea1*Δ is mostly roundish [Makushok et al., 2016a] indicating redundancy between these two systems (more information about role of myo1p in cell polarisation, (see, **1.4** and [Makushok et al., 2016a]).

In addition, the localisation of SRMs has been linked to the btn1p. Its removal causes temperature sensitivity for growth and relocation of SRMs from cell poles to the entire

PM. Btnt1p function in the distribution of SRMs is linked to F-actin patch formation and endocytosis, since conditional mutants of actin (*cps8-188*) and endocytosis (*end4*Δ) also show homogenous distribution of SRM throughout the PM [Codlin et al., 2008]. Growth site localisation of SRMs also involves a kin1p kinase, which is implicated in determining the localisation of cell wall synthesising enzymes and F-actin [La Carbona, Le Goff, 2006], [Cadou et al., 2010].

The localisation of SRMs also depends on sphingolipid synthesis. Removal of three enzymes, responsible for the production of the most abundant complex sphingolipid in fission yeast (MIPC), results in homogeneous filipin staining of the entire PM and increased sensitivity to the anti-fungal drugs [Nakase et al., 2010]. This fact correlates with previously mentioned defects in endocytosis and F-actin, leading to the similar phenotype.

SRM localisation to the cell middle is independent of contractile ring formation. It happens after contractile ring formation but before it starts to contract [Takeda et al., 2004], suggesting a specific role in this process. Positioning of SRMs at the contractile ring region depends on cdc15p. This protein localises to SRMs and is involved in proper shaping of SRMs at this position. Removal of cdc15p leads to spiral-like SRMs in the cell middle. Localisation of SRMs is also affected by over-expression of cdc15p [Takeda et al., 2004].

1.3.2.2.2 Sterol-related functions of SRMs in vegetatively growing *S. pombe*

Ergosterol biosynthesis is known to be involved in the maintenance of the PM structure and localisation of PM proteins [Iwaki et al., 2008]. Several proteins have been shown to localise to SRMs in fission yeast, like the glucan synthetase bgs4p, whose localisation to SRMs depends on SRM integrity (which can be disturbed by the prolonged incubation with filipin) [Wachtler et al., 2003]. Other examples of proteins localising to SRMs are the lipid-raft marker homolog pma1p or the MARK kinase family member kin1p [Takeda, Chang, 2005] [Cadou et al., 2010]. The main PM-t-SNARE psy1p,

regulating membrane fusion and polarised secretion, localises to SRMs at the cell surface in exponentially growing cells and during meiosis [Kashiwazaki et al., 2011]. This was biochemically confirmed by the presence of psy1p in the detergent-resistant membrane fraction, the standard assay to determine association of proteins to sterol-enriched domains [Simons, Ikonen, 1997]) [Kashiwazaki et al., 2011]. Moreover, more than 600 encoded proteins from the fission yeast genome are assigned to contain transmembrane domains, of which a substantial amount is linked to the cell division or show a localisation to growth sites [Wood et al., 2011]. It is highly possible that spatial localisation of SRMs determine locations, where these presumptive SRM-associated proteins execute their functions.

Deletion of enzymes, responsible for the early steps of ergosterol synthesis in fission yeast lead to cell death [Makushok et al., 2016a], however interference with the sterol composition, by removal of selected enzymes involved in the later steps of ergosterol synthesis, results in sensitivity to Li+, abnormal cell morphology, defects in septum formation, indicating a lower activity of the cytoskeleton, cell wall synthesising and degrading enzymes, and sporulation defects [Iwaki et al., 2008]. In addition, interference with the membrane composition, by prolonged incubation with the sterol-binding dye filipin, leads to mispositioned and misshapen actomyosin rings [Wachtler et al., 2003]. Over-expression of the C-4 sterol methyl oxidase erg25p causes similar phenotypes as incubation with filipin [Wachtler et al., 2003].

Strikingly, interference with ergosterol synthesis causes defects in timing of endocytosis of the SRM-localised protein psy1p (during sporulation and forespore membrane (FSM) formation) [Kashiwazaki et al., 2011].

1.4 *De novo* cell polarisation of fission yeast cells

Subsection is based on [Makushok et al., 2016a] which sets the basis for this thesis.

Cell polarity in fission yeast was mainly studied in cycling cells, which inherit

polarity cues after each cell division. In order to omit polarity inheritance, *de novo* generation of cell polarity was followed in cells, which were exiting glucose starvation (SE - starvation exit). Glucose starved cells lose their polar distribution of growth and polarity machineries (also observed in [Laporte et al., 2015]). Moreover, SRMs (stained by filipin, which is a sterol binding dye) are not visible in this condition. Strikingly, the authors revealed that SRM formation is core to *de novo* cell polarisation and subsequent polarised growth. SRMs serve as platforms for the assembly of growth and polarity machineries. In addition, the authors suggest that SRMs could be involved in symmetry breaking. Ergosterol biosynthesis is the first step of the *de novo* generation of polarity. Subsequently, ergosterol needs to be delivered to the PM and recruited to the cell poles. These steps are independent of cdc42p activity. SRM dynamics during SE can be followed at the single cell level due to a novel live protein marker - GFP-tnalp, which stains SRMs in all the conditions presented in [Makushok et al., 2016a].

SE is divided into 4 phases. Around 10min after glucose addition, several randomly distributed SRMs are visible in the PM (Pl). This phase is not dependent on the presence of the cytoskeleton or cell growth. Growth and polarity markers (for3p and bud6p) accumulate in the vicinity of these randomly distributed SRMs, therefore SRMs are proposed to serve as platforms for assembly of growth and polarity machineries. Each SRM is a presumptive growth site.

SRMs are subsequently polarised during P2. This phase involves the microtubule-dependent polarity factor tea1p and its effector tea4p, which are deposited at cell ends. Both cell poles are covered by SRMs and slow growth is initiated from both sites. During cell polarisation, laterally localised SRMs need to be removed. This process involves neither cdc42p activity, nor is dependent on fast growth initiation. Interestingly, SRM removal during P2 involves F-actin but not the F-actin organising polarity factors for3p and bud6p. Additionally, *tea1*Δ and *tea4*Δ mutants cannot stabilise SRMs at cell poles and any SRM from P1 can become the site of P2 initiation and subsequently become a growth site. *tea1*Δ mutants initiate P2 and fast growth (P3) at the same time, therefore the authors suggest that in those cases, cdc42p activity might be critical for

growth initiation in this condition, in contrast to wild-type cells.

Cell poles-deposited tea1p prepares for mono-polar fast growth initiation (P3) and later switching to bipolar growth (P4). During P3, cells initiate fast growth at only one of the cell ends. Fluorescence intensity of SRMs at the fast-growing end is higher than at the opposite pole. Moreover, SRMs at the fast-growing pole enlarge, and their size correlates with the growth speed of the cells. This phase is dependent on the actin cable organising formin - for3p, which is involved in SRM domain maintenance, and in achieving high growth rates. Later, only 35% of cells switch to bi-polar growth (P4). This phase involves bud6p. *bud6*Δ mutants exhibit unstable growth site positioning. Moreover, some cells can swap their fast growing end or can switch to completely mono-polar growth.

In addition, tea1p and myo1p act redundantly in controlling growth site confinement, *myo1*Δ cells have SRMs distributed throughout the PM, however they grow in cylindrical manner due to MT-dependent tea1p positioning to the cell ends. Double mutation *tea1*Δ*myo1*Δ is semi-lethal. The few germinating spores that are viable, are almost round. However, they contain SRMs enriched at the cell poles. The Authors suggest that tea1p and myo1p provide two redundant mechanisms for confining growth and that there is a third tea1p- and myo1p- independent growth and SRM domain confining system, after cells establish continuous growth and division cycles.

At the moment, it is unclear how fission yeast builds SRM domains in the first place, and how the molecular network of tea1p-related factors and F-actin removal of SRMs are coordinated.

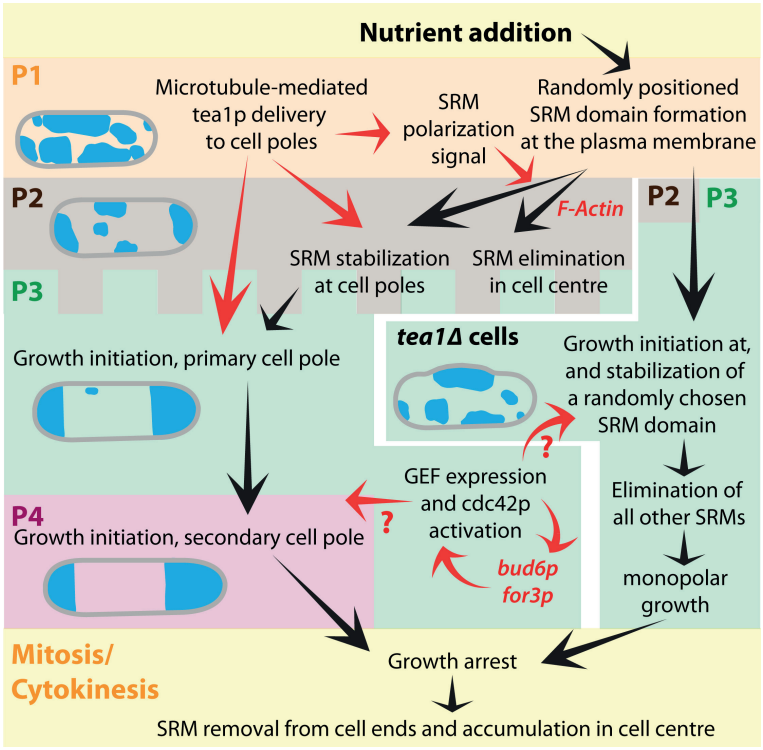

Figure 1.7: **Cell polarisation of fission yeast in SE**

The drawing summarises phases of cell polarisation in fission yeast during the first cell cycle of SE in wild-type and *tea1*Δ cells. Red arrows show instructive influence, black arrows correspond to the temporal sequence of events. Adapted from [Makushok et al., 2016a].

2 Materials and methods

2.1 Yeast strains and cell culture

Standard culturing and handling methods of *S. pombe* were implemented [Moreno et al., 1991]. All *S. pombe* strains used in this study are listed in a **Table 1**.

2.1.1 Experimental assays

2.1.1.1 Exponential growth

Exponentially growing cells were grown in the synthetic medium Edinburgh Minimal Medium (EMM2) with 2% glucose at 25 °C. EMM2 was supplemented with amino acids when indicated.

2.1.1.2 Starvation and starvation exit

Fission yeast cells were starved for glucose as described before [Zaitsevskaya-Carter, 1997]. Briefly, exponentially growing cells were shifted to low glucose medium by centrifugation for 2 min at 2200 rpm and re-suspension of the resulting pellet in EMM2 with 0.5% glucose. For strains carrying auxotrophic markers, the medium was supplemented with the according amino acids. Starvation cultures were started at OD 0.2 and grown at 25 °C for 3 days with constant shaking.

Starvation exit (SE) was triggered by addition of EMM2 medium with 2% glucose supplemented with amino-acids if required in proportion 1:4 (volume of starved culture:volume of EMM2). Temperature-sensitive mutants were pre-incubated at 36 °C for 1h with constant shaking before fresh medium, preheated to 36 °C, was added. Cells were kept at the according temperature throughout SE. If SE was performed at permissive 25 °C it is indicated in the figure legend.

For live imaging at 25 °C, cells were loaded on an imaging dish (details see, **2.2.1.2**) at room temperature. SE was started by addition of 2 ml of EMM2.

For live imaging at 36 °C, cells were loaded on an imaging dish (details see, **2.2.1.2**)

and 1ml EMM medium was added onto the cells at room temperature. Subsequently, cells were incubated for 1h at 36 °C in the imaging chamber. The medium was removed and SE was triggered by the addition of 2ml of EMM2 preheated to 36 °C.

The conditional mutant *pik1-td* carrying the episomally expressed GFP-piklp and the strain carrying the *81nmt1-kes1* construct were supplemented with thiamine, both in starvation and in SE.

2.1.1.3 Brefeldin A treatment

Brefeldin A (BFA) (from LC Laboratories) was dissolved in DMSO. Starved cells were incubated with BFA (200μm/ml final concentration) 1h before SE. EMM2 medium (pre-warmed up to 36 °C when needed) including the drug was added to initiate SE.

2.1.2 Generation of strains

2.1.2.1 GFP-tagged recombinant proteins

GFP tagged strains were constructed according to the standard protocol by homologues recombination [Bähler et al., 1998]. Plasmid DL191 (pFA6a-linker-GFP-kanMX6) was used as a template for the PCR-based approach. Proteins were tagged at their C-terminus for endogenous expression levels. All primers used are listed in a **Table 2**.

2.1.2.2 Deletion of *oshE* and repression of *kes1*

oshE (SPBC646.08c) was deleted based on the standard protocol described by [Bähler et al., 1998]. The plasmid DL50 (KS-ura4), containing ura4 cassette was used as a template.

Gene repression of *kes1* was achieved by placing it under control of the repressible *81nmt1* promoter [Maundrell, 1990]. The procedure was performed according to [Bähler et al., 1998] with a plasmid DL360 (pFA6a-natMX6-P81nmt1) as a template.

Experiments were carried by pre-culturing of the recombinant strain in EMM2 in the presence of thiamine. Subsequently, starvation and SE were performed as described in **2.1.1.2** with thiamine supplementation.

Primers for deletion of *oshE* and repression of *kes1* are listed in the **Table 2**.

2.1.2.3 Genetic crosses

Genetic crosses were performed according to standard protocols [Forsburg, Rhind, 2006].

Most of strains in this study are result of the genetic crosses between parental strains (source listed in the **Table 1**) and the wild-type. Accordingly, auxotrophic markers (ade6, leu1-32 and ura4-D18) were removed from most of the studied strains. Their removal is strongly recommended because they are known to be inhibitory for starvation exit experiments [Sajiki et al., 2009]. Only two strains were carrying auxotrophic mutations and experiments including these strains were compared to wild-types also carrying auxotrophic markers.

Strain	Genotype	Source	Sources of original strains used for crosses
558	h-	Original 972 wild-type strain	
1886	h- P3nmt1-**GFP-tna1p**::kanMX6	[Makushok et al., 2016a]	
2955	h- **anp1p-mcheery**::ura4 Pnmt1-**GFP-tna1p**::kanMX6 ura3-D18 ade6-M216	Lab collection	[Vjestica et al., 2007], [Makushok et al., 2016a]
1980	h+ P3nmt1-**mcheery-tna1p**::kanMX6 ade6-M216 ura4-D18	Lab collection	
2020	h+ P3nmt1-**tdtomato-tna1p**::kanMX6 ade6-M216 leu1-32 ura4-D18	Lab collection	
2402	h+ **anp1p-mcheery**::ura4+ ade6-M216 leu1-32 ura4-D18	[Vjestica et al., 2007]	
3701	h- **mug33p-mKate**::kanMX6 P3nmt1-**GFP-tna1p**::kanMX6	This study	[Snaith et al., 2005], [Makushok et al., 2016a]
4192	h- **gma12p-GFP**::ura4 ura4-D18	This study	[Wang et al., 2002]
3680	h- **sec8-1** P3nmt1-**GFP-tna1p**::kanMX6 ura4-D18	This study	[Wang et al., 2002], [Makushok et al., 2016a]
3677	h- **sec8-GFP**::ura4-D18 ura4-D18 leu1-32	[Wang et al., 2002]	
4864	h? **sec8-1 ypt2VN**::ura4 ura4-D18	This study	[Wang et al., 2002], [Craighead et al., 1993]
4853	h? (probably sterile) **sec8-1 for3Δ**::kanMX6	This study	[Wang et al., 2002], [Feierbach, Chang, 2001]
4885	h? **sec3-916**::HphR **exo70Δ**::kanMX6	This study	[Jourdain et al., 2012], [Kim et al., 2010]
4284	h- **psy1-S1**::ura4 ura4-D18	This study	YGRC/NBRP Japan
4288	h- leu1::**syb1-sp58 syb1Δ::ura4** ura4-D18	This study	YGRC/NBRP Japan
4193	h+ leu1::**sec9-10** sec9::ura4 ura4-D18	This study	YGRC/NBRP Japan
4883	h? **psy1-S1**::ura4 leu1::**syb1-sp58** syb1Δ::ura4 ura4-D18	This study	YGRC/NBRP Japan
3765	h+ **kes1-HL-GFP**::kanMX6 ade6-M216 leu1-32 ura4-D18	This study	
4847	h? **kes1-HL-GFP**::kanMX6	This study	
4417	h+ **kes2-HL-GFP**::kanMX6	This study	
4312	h+ **osh2-HL-GFP**::kanMX6	This study	
4415	h+ **osh3-HL-GFP**::kanMX6	This study	
4414	h+ **oshE-HL-GFP**::kanMX6	This study	
4416	h+ **osh7-HL-GFP**::kanMX6	This study	
4184	h+ **kes1**Δ::kanMX6	This study	[Kim et al., 2010]
4848	h+ **kes2**Δ::kanMX6	This study	[Kim et al., 2010]
4178	h- **osh2**Δ::kanMX6	This study	[Kim et al., 2010]
4148	h- **osh3**Δ::kanMX6	This study	
4934	h- **oshE**Δ::ura4 ura4-D18	This study	[Kim et al., 2010]
4826	h+ **osh7**Δ::kanMX6	This study	[Kim et al., 2010]
4857	h? **kes1**Δ::kanMX6 **kes2**Δ::kanMX6	This study	[Kim et al., 2010]
4854	h? **kes1**Δ::kanMX6 **osh3**Δ::kanMX6	This study	[Kim et al., 2010]
5047	h? **kes1**Δ::kanMX6 **oshE**Δ::ura4 ura4-D18	This study	[Kim et al., 2010]
4842	h- **kes1**Δ::kanMX6 **osh7**Δ::kanMX6	This study	[Kim et al., 2010]
4884	h- **81nmt1kes1**::natMX6 **osh2**Δ::kanMX6	This study	[Kim et al., 2010]
4879	h? **osh7**Δ::kanMX6 **kes2**Δ::kanMX6	This study	[Kim et al., 2010]
4860	h? **osh7**Δ::kanMX6 **osh2**Δ::kanMX6	This study	[Kim et al., 2010]
4862	h? **osh7**Δ::kanMX6 **osh3**Δ::kanMX6	This study	[Kim et al., 2010]
4966	h? **osh7**Δ::kanMX6 **oshE**Δ::ura4 ura4-D18	This study	[Kim et al., 2010]
681	h+ **tea1**Δ::ura4 ura4-D18	[Makushok et al., 2016a]	
4960	h? **kes1**Δ::kanMX6 **tea1**Δ::ura4 ura4-D18	This study	[Kim et al., 2010], [Makushok et al., 2016a]
4963	h? **osh7**Δ::kanMX6 **tea1**Δ::ura4 ura4-D18	This study	[Kim et al., 2010], [Makushok et al., 2016a]
4020	h+ **cdc42-3**::kanR	This study	[Tatebe et al., 2008]
4940	h? **kes1**Δ::kanMX6+ **cdc42-3**::kanR	This study	[Kim et al., 2010], [Tatebe et al., 2008]
4941	h? **osh7**Δ::kanMX6+ **cdc42-3**::kanR	This study	[Kim et al., 2010], [Tatebe et al., 2008]
4850	h? pik1Δ::ura4 pREP41X-Ub-R-DHFRts-pik1 (referred as **pik1-td** cells) leu1-32 ur	This study	[Park et al., 2009]
4869	h? pik1Δ::ura4 pREP41-2Xe**GFP-pik1p** leu1-32 ura4-D18	This study	[Park et al., 2009]
4253	h- **its3-1**	This study	[Zhang et al., 2000]
751	h+ ade6-M216 leu1-32 ura4-D18	Moasayuki Yamamot	
3662	h+ **scs2**Δ::ura4 **scs22**Δ::ura4 ura4-D18 leu1-32 ade6	[Zhang et al., 2012]	
3661	h- **rtn1**Δ::ura4+ **yop1**Δ::ura4+ **tts1**Δ::ura4+ ura4-D18 leu1-32 ade6	[Zhang et al., 2010]	

Table 1: **S. pombe strains used in the study**
The list is arranged in the order as presented in this thesis.

Strain	Primer	Sequence
kes1-HL-GFP::kanMX6	DPE 1070	AAGATAAAGATGAGGGCTTTGAAGAAGCTACTAAGTGT CTTAGACAGCCTGTTAAAGAAGGTTTCTGGTATTATCTT AGAATCCTTGGAGCTCCTTCAGG
	DPE 1071	TTCACTTCAACTTAACCAAAGTCGTTAATGAAAGCCAG AGAGGAAATATATCTTACCATGAACAAGCTCGTAAAAG TGAAGAATTCGAGCTCGTTTAAAC
kes2-HL-GFP::kanMX6	DPE 1315	TTGAACCAGGCTTCTGGATTTACATTGGTGACACTCATC CTTCATTGCCAGCAGGAGAACAACCTGTCAAACGGATG GAAATCCTTGGAGCTCCTTCAGG
	DPE 1316	CATAGATAATCTAAATGAAAAGTGCTGATTTCGTACTA AAAGCCAACCGTTAAAAGAACCTTTAGTAAAATCGTTG ATCGGAATTCGAGCTCGTTTAAAC
osh2-HL-GFP::kanMX6	DPE 1303	TATTGGAAAATAAGAGAGGAAGCTGGTGAAGCTCATTT GGCCGGAAAGGAATTTGAATGGCCTAATGTTGATGATA TTTTATCCTTGGAGCTCCTTCAGG
	DPE 1304	AATAAAACTAAATAAACTTTACTCAGTGTTGTTGGTCAT AGTGTGTCAAATAGTTGGATTGCCATTCCTTGCCTTTTT GCGAATTCGAGCTCGTTTAAAC
osh3-HL-GFP::kanMX6	DPE 1309	CAATTTGGCAATTAAAAAAGGAAAATAATTATTGGGAA TCTCGTGAAAACTCTACTTGGAGTTCATGTCCTAAATTA TGGATCCTTGGAGCTCCTTCAGG
	DPE 1310	AGACAAAATATATATGAAACGAAGGAAAAACCAACGA TTTATGCAGCATTAAGAAACTTAAGAGTATTTTTTTAAG GGACGAATTCGAGCTCGTTTAAAC
oshE-HL-GFP::kanMX6	DPE 1306	AGGAAGGTCGACCGACCCTTACTGAAGAAGGTAAGAA GGTCCTTGAGCAGTCCTTGTCAGATGAGTACATTCACG GAAGTATCCTTGGAGCTCCTTCAGG
	DPE 1307	CAAAGACTCATGCCATCATTTTATGAAAACACAAATCA GCATTACCAACGTTACAGAATTGAAAACTCATGAGTTA TAATGAATTCGAGCTCGTTTAAAC
osh7-HL-GFP::kanMX6	DPE 1312	CGGTTGATGAATATCATGACGCTCAACTCCCTGACCCT AATACTCTATCAAAGTTACATGAAGAACAGGATCCAGC TTTAATCCTTGGAGCTCCTTCAGG
	DPE 1313	AATAGGTTAATAGTGTATAAAGAACTAAATCCCAATTA AGGAAAAATATGGTAAATAACAACGTTGCAATTTATCT CTCTGAATTCGAGCTCGTTTAAAC
oshEΔ::ura4 ura4-D18	DPE 1279	GTGCCACCAACATTTATCAACGCAAAGATATCTCTTGA AAAGAATAGATTTTTGGTCAGTAGTAGGACCAGGACCT AAAGCGCCAGGGTTTTCCCAGTCACGAC
	DPE 1280	AAGGTAGGGAAAAAGTTCTAAATGCACGCCAATTAAA GAGTTTGTGAAAAGGGTTAAAAATTAACGTTTTATGAA AGACAAGCGGATAACAATTTCACACAGGA
81nmt1kes1::natMX6	DPE 1397	TATTGCATTTCTCAATACAATTTACGCAATATTCCAAGC CTAAATGAGCCCATTTCAATTGGTTTTACGCGTCCCACC ATGAATTCGAGCTCGTTTAAAC
	DPE 1413	AAAGCGTACTTTGTAGTAGAGCGAAGCCTTTTGTCTCCT TCGCCATCACGAGAATCATCAGAACTCGTTGTTTTACTC ATGATTTAACAAAGCGACTATAAGTC

Table 2: **Sequences of the primers**

2.2 Microscopy and image analysis

2.2.1 Imaging conditions, cells labelling and sample preparation

2.2.1.1 Cells labelling

For live cell imaging of SRM dynamics, the SRM live protein marker GFP-tna1p was used. It was shown to localise similar to filipin, a fluorescent dye to stain sterols [Drabikowski et al., 1973], [Makushok et al., 2016a]. However, we observed GFP-tna1p accumulation in sub-cellular structures (under two conditions studied) if the membrane trafficking pathway was perturbed (see, **3.1**).

Therefore, filipin (Sigma) was used for most of experiments in this study. It cannot be used for *in vivo* imaging as it disrupts the cell membrane [Bradley et al., 1980], [Souto-Padron, Souza de, 1983]. Samples from starvation and different time-points of SE were labelled separately. Filipin was used at a final concentration of 5μg/ml from a 4000x stock solution in DMSO as previously described by [Takeda et al., 2004].

The cell wall was labelled with Rhodamine Griffonia Simplicifolia-Lectin I (GFL I, BSL I), further called Rhodamine-lectin (Vector laboratories) to allow for cell segmentation and image analysis. Its final concentration was 4μg/ml.

Both dyes were pre-mixed in EMM (for labelling starved cells) or EMM2 (for labelling cells in SE) - with amino acids or thiamine when required. Concentrations of filipin and Rhodamine-lectin in the pre-mix were adjusted to match the final concentrations for filipin and for Rhodamine-lectin after mixing with cell culture on the imaging dish (details in **2.2.1.2**). The mixture was prepared 30s before its application, in the aluminium-covered Eppendorf tube. The tube was subsequently vortexed.

2.2.1.2 Sample preparation

For still imaging, 100μl of lectin (1 mg/ml in water) (purchased from Vector laboratories) was applied into wells of a sterile plastic bottom 8 well imaging dish (Ibidi). After 5min the lectin was removed and the dish was dried by evaporation.

The pre-made staining mix (described in, **2.2.1.1**) was distributed into 3 wells of the imaging dish and gently mixed with the appropriate volume of starved cells or cells in SE to a final volume of 200μl. The dish was covered by aluminium foil and centrifuged for 1 minute at 300 rpm at 25 °C. The whole procedure took ∼2min. In order to avoid potential artefacts caused by filipin [Bradley et al., 1980] samples were immediately imaged on an epifluorescence microscope (detailed in **2.2.1.3**).

For live cell imaging, a glass bottomed imaging dish (Bioswisstec) was coated with 2μl of lectin (2 mg/ml in water). 80μl of starved cell culture were added and centrifuged at 300 rpm at 25 °C. Subsequent triggering of SE in these conditions is described in **2.1.1.2**.

2.2.1.3 Microscopy conditions

2.2.1.3.1 Microscopes

Epifluorescence microscope - Axiovert 200M widefield fluorescence microscope (Zeiss) with mercury lamp. System combined with a Coolsnap HQ camera (Roper Scientific), run with MetaMorph software (Molecular Devices). Pixel size for 40x (NA 1.4 Oil) objective was 0.157μm and for 100x (NA 1.4 oil) 0.0628μm.

Zeiss Andor spinning disc confocal microscope - A Zeiss Axio Observer Z1 confocal microscope with a Yokogawa spinning disc unit, motorised piezo and LED illumination. The system was provided with an Andor Neo sCMOS camera with a pixel size of 0.065μm for the 100x NA 1.4 Oil Plan Apo objective.

Leica Andor spinning disc confocal microscope - A Leica DM microscope with a Yokogawa spinning disc unit, LED illumination, a motorised piezo and an incubation chamber was used. Images were acquired by a 63x NA 1.4 Oil Plan Apo objective connected to an Andor iXon3 EMCCD camera with a pixel size 0.11μm.

2.2.1.3.2 Imaging filipin and Rhodamine-lectin stained cells

All filipin and Rhodamine-lectin stained samples were imaged by the Epifluorescence microscope. Images used for quantifications were acquired at 40x magnification as z-stacks of 5 slices with 1μm steps. Otherwise, they were taken in the 100x magnification as z-stacks of 11 slices with 0.5μm steps.

2.2.1.3.3 Imaging tna1p dynamics and colocalisations

Fast-time resolution movies involving GFP-tna1p were acquired by the Zeiss Andor spinning disc confocal microscope. In addition, data described in **3.1.4** (comparison of timing of SE in different temperatures) required the precise maintenance of temperature. Therefore, time-lapse movies were acquired by the Leica Andor spinning disc confocal microscope, which contained an incubation chamber. As an exception GFP-tna1p mug33p-mKate strain in SE, mCherry-tna1p and tdtomato-tna1p, were imaged by the Epifluorescence microscope with the 100x magnification.

2.2.1.3.4 Brightfield imaging

Brightfield pictures from **Figure 3.9** and **Figure 3.23** were acquired on the Epifluorescence microscope (100x objective, DIC system).

2.2.1.3.5 Imaging markers of secretory machinery and non-vesicular transport components

sec8p-GFP (**Figure 3.7**) and anp1-mCherry (**Figure 3.2**) were imaged by the Epifluorescence microscope. We used 100x magnification and imaged z-stacks of 11 slices with 0.5μm steps.

gma12p-GFP (**Figure 3.3**) was imaged by the Leica Andor spinning disc confocal microscope. We used 63x magnification and imaged z-stacks of 11 slices with 0.5μm steps.

GFP-tagged oxysterol binding proteins (**Figure 3.19** and **Figure 3.22**) were imaged on the Zeiss Andor spinning disc confocal microscope. Z-stack specifications are included to figure legends. The exception was kes1-GFP (**Figure 3.19**, A), which was imaged on the Epifluorescence microscope.

2.2.2 Image analysis

Basic image processing was performed using the ImageJ software. All microscopy pictures presented in the figures are maximum projections from z-stacks (unless otherwise indicated). Deconvolution was done using Huygens software (Scientific Volume Imaging).

2.2.2.1 Generation of kymographs based on GFP-tna1p signal

Movies of cells expressing GFP-tna1p were acquired in 3min time-intervals as described before [Makushok et al., 2016b]. The stacks for all time-points were maximum projected, converted to 8bit and subjected to kymograph analysis in Image J. Briefly, a line was drawn through the major axis of the cell (**Figure 2.1**, A), long enough to cover the whole cell after elongation during SE. The width of the line was increased to cover the whole cell diameter (**Figure 2.1**, A). Subsequently, kymographs were generated with the standard kymograph plugin (**Figure 2.1**, B). Based on these kymographs, it is not possible to estimate P1 initiation. The start of this phase was estimated based on manual raw data evaluation. P2 initiation could be read from the kymographs as the moment when bright GFP-tna1p signal appears at the cell pole region. P3 starts with the moment of growth initiation from at least one of cell ends. P4 begins with growth initiation at the second pole (**Figure 2.1**, B). Details about phases of SE are described in [Makushok et al., 2016b] or introduction to this thesis (see, **1.4**).

This description corresponds to data presented in **3.1.4**.

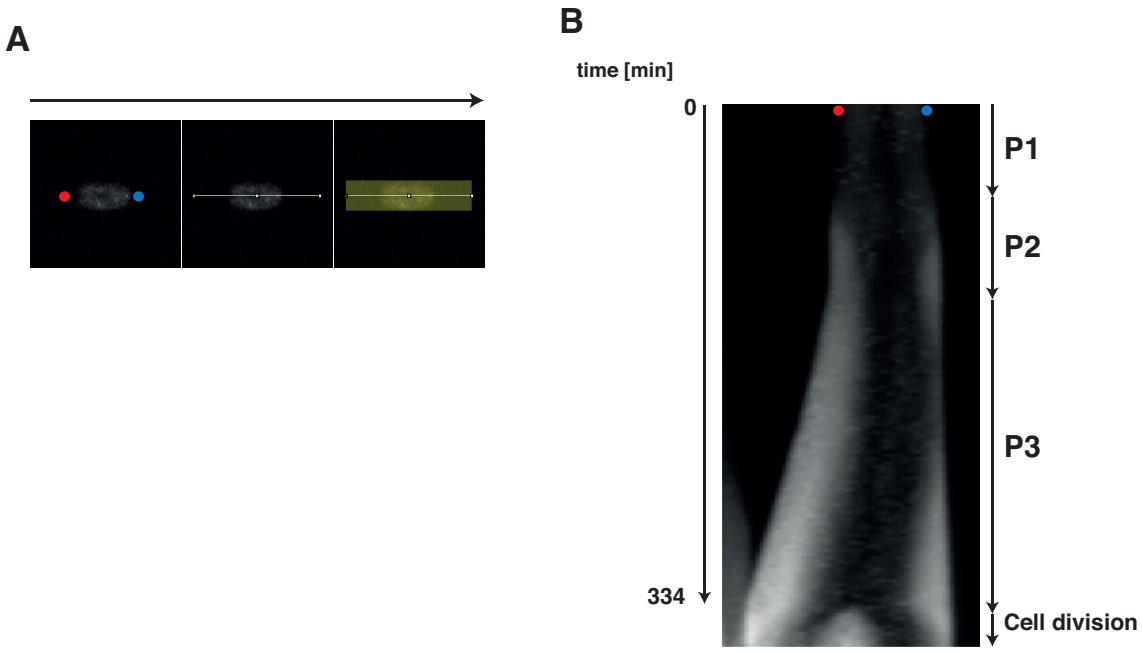

Figure 2.1: **Generation of a kymograph based on GFP-tna1p signal during SE**

A - 3 pictures, presenting the same wild-type cell in starvation at 25 °C. Panel shows how line was draw, which was used for subsequent generation of the kymograph. Arrow indicates sequence of events. **B** - Example kymograph showing event of cell polarisation (P2) and fast growth (P3) during SE. Arrows on the right side correspond to phases of SE. Arrow on the left presents time from the beginning of SE until cell division. Red and blue dots in figure B correspond to cell poles from figure A.

2.2.2.2 Analysis of filipin stained SRMs during SE

In this section the methods are described, that were used to process data used for the quantification of SRM distribution and description of phases of SE.

2.2.2.2.1 Image processing for quantification of filipin stained SRMs

Filipin - First, average projections of z-stacks were performed. Second, the images were corrected for background by using the Background subtraction tool of the MOSAICsuite plugin [Shivanandan et al., 2013].

Rhodamine lectin - First, maximum projections of z-stacks were done. Subsequently, background was corrected by the background subtractor of the

MOSAICsuite plugin [Shivanandan et al., 2013]. Images for particular imaging sets were grouped into one stack and normalised by using *Enhance contrast* tool and all pixels were saturated by 0.4%.

2.2.2.2.2 Segmentation of cells

First, we used Ilastik software [Sommer et al., 2011]. It provides a pixel classification module in order to generate objects probabilities (**Figure 2.2**, B). Rhodamine-lectin pictures were used to obtain probabilities (**Figure 2.2**, A).

Next steps of cell segmentation were done by CellProfiler 2.0 using custom made processing pipeline [Dimopoulos et al., 2014]. *SmoothKeepingEdges* method was performed to ensure better detection of primary objects. Probabilities of cell interior were segmented by using *IdentifyPrimaryObjects* module (**Figure 2.2**, D). Then, objects were filtered in order to eliminate artefacts of the image segmentation. Filtering was done based on *Solidity feature* (minimum value 0.8: maximum value - 1.0). As another step, cell boundaries were detected by using the nuclear propagation method from the *IdentifySecondaryObjects* module [Frechin et al., 2015] (**Figure 2.2**, E). There, the manual threshold was chosen (0.005).

In the nuclear propagation method, the edges of primary objects were expanded to form secondary objects. The *Distance B* option was used to allow for thresholding of the original cell outline pictures (Rhodamine-lectin). This enabled segmentation to be limited to a certain distance away from edges of the primary objects, excluding background regions (primary objects were expanded by 6 pixels). Finally, to ensure a better separation of object boundaries, they were shrunk by 1 pixel. Our method appears to be very robust, artefacts only represent a minor part of the segmented cells. (**Figure 2.2**, F, G, H)

Our measurements showed that diameters of wild-type cells were close to 4μm (**Figure 3.21**, B). This fits to previously reported measurements by using fluorescently labelled lectin [Zegman et al., 2015].

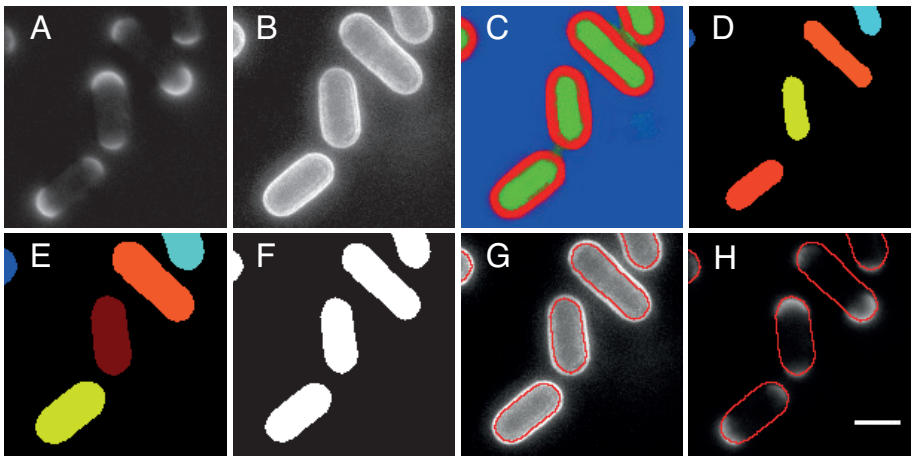

Figure 2.2: **Segmentation method**
Example of image processing during segmentation (wild-type cells 1h in SE at 25 °C) **A** - Filipin stained cells (pre-processed picture 2.2.2.2.1) **B** - Rhodamine-lectin staining (pre-processed picture 2.2.2.2.1) **C** - Probabilities of cell seeds (green), cell outlines (red) and image background (blue). **D** - Primary objects **E** - Secondary objects **F** - Final segmentation **G** - Overlaid outline of the segmentation with the Rhodamine-lectin signal **H** - Overlaid outline of the segmentation with the filipin signal. Scale bar: 5μm.

2.2.2.2.3 Detection of cell outlines and measurement of cell length and cell width

In collaboration, David Dreher (IMLS, UZH) designed a software running under the Matlab Inc. to compute the outlines of the segmented cells (see, 2.2.2.2.2). The computation is based on the rough pixel estimate of the width of the cell wall as 3 pixels. This function expects objects that can be sufficiently fitted with an ellipse and have a smooth border. Points, at which the major and minor axis cross the object outline (end points) are defined and the length and width of the object is estimated as the distance between the corresponding end points.

2.2.2.2.4 Measuring SRM width

The Matlab Inc. based software was designed by David Dreher (IMLS, UZH). Briefly, the filipin signal is filtered by the low pass filter in order to reduce noise and the images are overlaid with the corresponding segmentations. Subsequently, the signal of filipin is read along the object outline. Peaks of intensity of filipin signal along outlines of the

cells are detected based on the *Find Peaks* function (Matlab Inc). The horizontal lines are computed at a given percentage (in our case 80%) of peak value above the minimum value of the detected filipin signal (**Figure 2.3**). Measurement of SRM width depends on peak height and significant local minima of the peaks lying between the horizontal lines. (more details, Matlab documentation files - *Peak analysis*).

2.2.2.2.5 SRM classification

SRMs were classified as polar SRMs or side SRMs. Polar SRMs localised to the tip region of the cell and their width (horizontal line) had to cross the end point of the major axis length at the cell outline. All remaining SRMs were classified as side SRMs. (**Figure 2.3**)

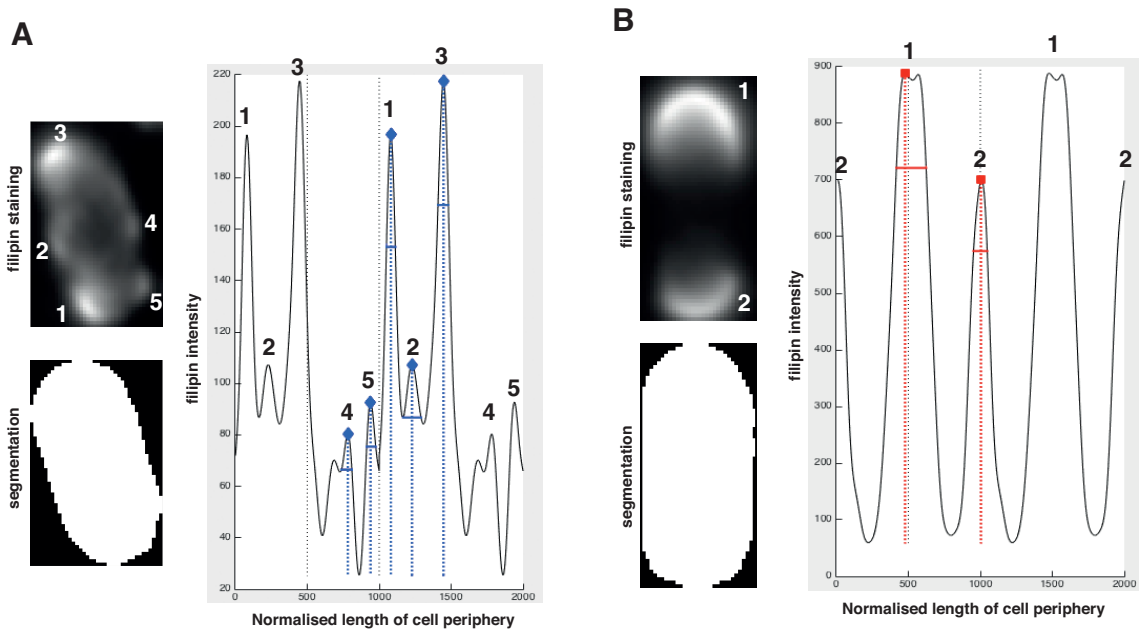

Figure 2.3: **Examples of measured SRM widths and SRM classification**

Examples of measured SRM widths and SRM classification. **A** - Filipin signal of a wild-type cell 45min in SE. **B** - Filipin signal of a wild-type cell 120min in SE.
The graphs show the filipin signal along the cell outline. The SRM domains (numbers above) and their corresponding widths (horizontal lines) and classification (blue: side, red: polar) are depicted for the corresponding pictures. The points, at which the major axis crosses the cell periphery is marked by 0 and 500 on the X axis of each graph. These points repeat at 1000, 1500 and 2000 positions at the X axis. Vertical scattered lines correspond to heights of peaks above the minimum value of the detected signal.
Images processed as described in **2.2.2.2**.

2.2.2.2.6 Ratio of polarisation

In order to compare the progress of SE between different strains, we developed a *Ratio of polarisation* (rP). First, a quantity *PolarSum* for polar SRMs is calculated. PolarSum includes absolute intensity of each SRM (PolarInt) multiplied by its width (PolarWidth). If a cell contains two polar SRMs, both values are summed up.

$$PolarSum = (PolarInt_1 * PolarWidth_1) + (PolarInt_2 * PolarWidth_2) \qquad (1)$$

The quantity *SideSum* for side SRMs is calculated the same way. However, this case, the number of possible SRMs is not limited.

$$SideSum = (SideInt_1 * SideWidth_1) + (SideInt_2 * SideWidth_2) + etc. \quad (2)$$

Finally, rP is calculated as follows:

$$rP = \frac{PolarSum}{PolarSum + SideSum} \quad (3)$$

In this case, large and/or intense polar SRMs increase the rP towards 1, while strong and/or large side SRMs reduce the rP towards 0. (**Figure 2.4**).

The same quantification of wild-type controls (for corresponding temperatures) is used as a reference to all the figures.

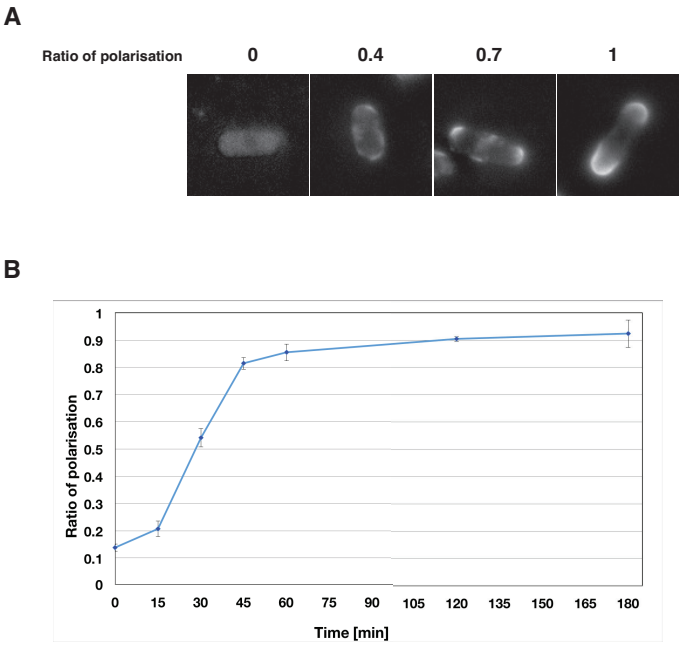

Figure 2.4: **Mean Ratio of Polarisation (rP) describes polarisation state of the fission yeast cell population during SE**

A - Pre-processed wild-type cells in SE. Values above each picture indicate the estimated rP.
B - Time course of average rP values of wild-type in SE (at 25 °C). Each average rP was measured from mean rPs from 3 experiments. Error bars represent the average standard deviation of the mean rP values.
(n>600 per time-point)

2.2.3 Tables describing phases of SE

Each subsection is summarised by a summary table to simplify our observations in SE into 5 basic categories. The phases are represented with a colour code.

Categories are as follows:

phase occurs as in wild type (or faster) - particular phase started at similar time as in wild type control.

short delay - phase initiated 30-60min later than in wild type control.

delay; small defect - phase initiated with a delay of around 30-60min or/and there was a small defect in SRM distribution, shape/size of SRMs or speed of cell elongation.

strong delay: defect - phase occurred significantly later than in wild-type and/or there was a strong phenotype in the SRM distribution or speed of growth.

phase does not occur - until 180min, in SE phase did not initiate.

Occasionally, table legend contains two additional categories:

P2 occasionally at ectopic position - until 120min in SE small subset of cells polarised from random SRM but after 180min in SE all cells stabilised defined SRMs at cell poles.

P2 at ectopic position - cells polarised from random SRM. Such phenotype is known for example for *tea1*Δ mutants ([Makushok et al., 2016b], Introduction, **1.4**).

3 Results

3.1 Vesicle trafficking and cell polarisation

Fission yeast cells exit starvation (SE) in four consecutive phases as described in [Makushok et al., 2016b]. Initially, cells exiting starvation form multiple, randomly distributed SRM domains in the plasma membrane (PM) (within 5-10 min from the start of SE). The second phase of SE (P2) starts within half an hour after nutrient addition, when SRMs reorganise and are confined to the two cell poles. This phase is controlled by polar tea1p that is deposited in a microtubule-dependent fashion, and which regulates positioning of SRMs at cell poles. As described in the Introduction (see, **1.2.3.2**) tea1p ensures that a putative site for future growth forms during P2 and is maintained throughout P3, which depicts the mono-polar growth phase. This does not require cdc42p [Makushok et al., 2016b], which was thought to be essential for the establishment of cell polarity [Martin, Arkowitz, 2014]. cdc42p activity slowly builds up and becomes detectable only after 1 hour of SE. The third phase of SE (P3 begins with a significant increase in growth speed at one cell pole, called *primary pole*. P3 starts approximately 30min after the onset of P2. The beginning of P3 of SE is defined as time at which growth speed at the primary pole exceeds more than 0.8μm/hour. The fourth phase (P4) begins when fast growth (above 0.8μm/hour) in addition is triggered at the second pole, termed *secondary pole* [Makushok et al., 2016b].

It is known that membrane delivery to the PM and membrane tethering are collectively involved in the cell polarity maintenance [Bendezu, Martin, 2011]. Since tea1p is key to the correct polarisation of SRMs, we hypothesised that tea1p regulates PM trafficking of *de novo* synthesised ergosterol, for example by positioning membrane trafficking-dependent machinery at the cell cortex.

3.1.1 Sub-cellular GFP-tna1p structures are of vesicular origin

GFP-tna1p is a live marker of SRMs in the PM of *S. pombe* [Makushok et al., 2016a], (**Figure 3.1**, A). Unlike filipin, GFP-tna1p in addition localises to dynamic cytoplasmic particles in SE and exponentially growing cells (**Figure 3.1**, B, C), [Makushok et al., 2016a]. These sub-cellular structures are likely to be of vesicular origin [Makushok et al., 2016a]. It was shown in budding yeast that SRMs and SRM-associated proteins can be transported together in higher-order vesicles [Klemm et al., 2009]. Therefore, we were interested in the nature of sub-cellular GFP-tna1p structures.

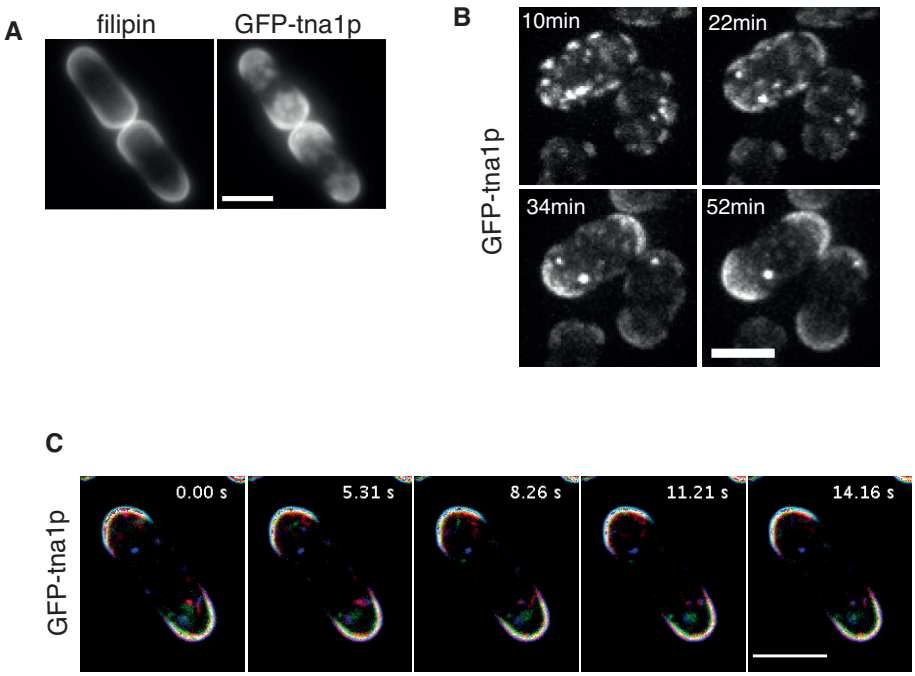

Figure 3.1: **GFP-tna1p localises to mobile particles in exponentially growing cells and in SE**

A - Exponentially growing GFP-tna1p-expressing cells stained with filipin (figure adapted from [Makushok et al., 2016a]). **B** - Time lapse sequence of GFP-tna1p-expressing cells during SE. Numbers indicate time in SE (figure adapted from [Makushok et al., 2016a]). **C** - Mobile intracellular localisation of GFP-tna1p in a cycling cell. Red colour corresponds to top peripheral section, green - middle section, blue - bottom section. Each time-point represents max-projection of 3 z-sections (acquired in 0.5μm distance).
Scale bars: 5μm.

3.1.1.1 Sub-cellular particles of GFP-tna1p colocalise with a marker of vesicular compartments in exponentially growing *S. pombe* cells

Since GFP-tna1p contains 13 transmembrane domains it should be produced in the ER and delivered to the PM via vesicular transport [Wood et al., 2011], [Alberts et al., 2014]. To test whether this involves a passage through the Golgi, we imaged cells co-expressing GFP-tna1p and anp1p-mCherry, a marker of the cis-compartment of the Golgi apparatus [Vjestica et al., 2007]. As previously reported, in exponentially growing cells anp1p-mCherry localised to particles throughout the cytoplasm, which are reminiscent of the GFP-tna1p particles (**Figure 3.2**, A). Although, in movie sequences most GFP-tna1p and anp1p-mCherry particles did not co-localise (**Figure 3.2**, A). Only occasionally we could observe what appeared to be transient co-localisation, indicating however this could just be due to random co-localisation events resulting from the mobility of the two structures (**Figure 3.2**, A).

In order to further evaluate the origin of the GFP-tna1p particles we crossed a strain carrying GFP-tna1p with another strain carrying marker for different membrane trafficking compartments - mug33p [Snaith et al., 2011]. Mug33p is a protein that was previously shown to localise to multiple sub-cellular particles. Subset of these sub-cellular particles correspond to the Golgi/endosomal compartment marked by the v-SNARE GFP-syb1p and different structures of the endocytic machinery [Snaith et al., 2011], [Kita et al., 2011]. Moreover, mug33 localises to rarely visible particles, which display occasional vectorial movements towards the PM. These rare particles are named as tubulovesicular elements (TUVs). Very rare translocations of TUVs were shown to be of vesicular origin, since they were abolished in mutants with perturbed vesicular transport [Snaith et al., 2011]. To see if mug33p and tna1p co-localise, we generated cells expressing GFP-tna1p and an mKate-tagged version of mug33p (mug33p-mKate). Fluorescence imaging of exponentially growing cells revealed that most of sub-cellular particles of both markers co-localised (**Figure 3.2**, B). Therefore, we conclude that GFP-tna1p localises to similar vesicular structures as mug33p [Snaith et al., 2011].

Since, rare translocations of mug33p (TUVs) depend on membrane trafficking, this indicates that subset of sub-cellular particles, which colocalised with TUVs, are of vesicular origin. Since most other known fluorescent markers of components of the secretory pathway in fission yeast are tagged with GFP we could not use those for co-staining with GFP-tna1p. Unfortunately, our attempts to tag any of the known GFP-tagged markers with red fluorescent proteins failed. Similarly, we could not obtain a functional red fluorescent protein-tagged tna1p: we did manage to generate haploid strains of cells expressing mCherry-tna1p and tdtomato-tna1p, but both had a delayed growth cycle (data not shown) and showed ectopic localisation of tna1p (**Figure 3.2**, C).

Nevertheless, these results provide an evidence that subset of GFP-tna1 particles in exponentially growing cells are of vesicular origin. It suggests that GFP-tna1p particles during SE are also of vesicular origin, however it remained to be shown.

3.1.1.2 Localisation of GFP-tna1p during SE dependents on the Golgi-apparatus

Since, particles of GFP-tna1p in exponentially growing *S. pombe* transiently colocalised with the marker of cis-Golgi apparatus - anp1p-mCherry and colocalised with mug33p, which marks compartments of the secretory compartments, we decided to evaluate similar colocalisations in SE. Unfortunately, during SE anp1-mCherry particles were not visible (**Figure 3.3**, A). Instead, we observed large globular structures, which filled the central part of the cytoplasm and most probably represent vacuoles (**Figure 3.2**, A), [Liu et al., 2015]). Our attempts to study GFP-tna1p and mug33p-mKate co-localisation during SE were also unsuccessful, due to the prominent vacuolar structures of mug33p-mKate (**Figure 3.2**, B). In order to evaluate potential vesicular origin of GFP-tna1p particles in SE, we decided to perturb the membrane trafficking machinery. We used an inhibitor of vesicle transport from the ER to the Golgi apparatus - Brefeldin A (BFA) [Graham et al., 2004], [Arioka et al., 1991], [Driouich,

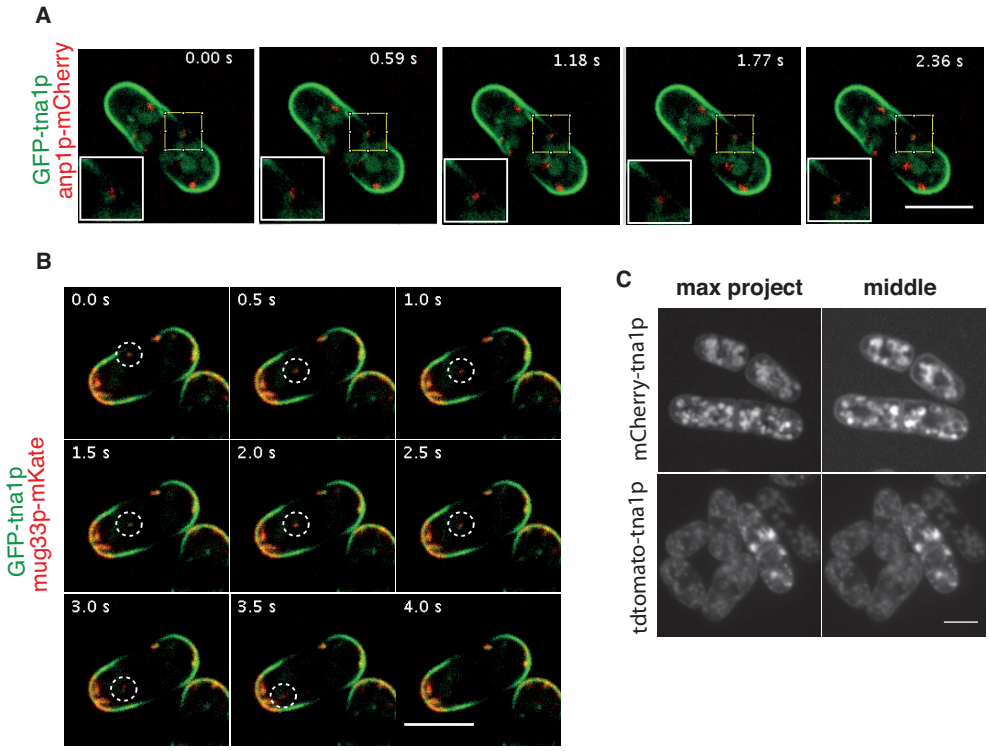

Figure 3.2: **GFP-tna1p particles in exponentially growing *S. pombe* colocalise with a marker of secretory compartments**

A - Mobility and time-restricted colocalisation between anplp-mCherry (red) and GFP-tna1p (green). Small squares represent zoom-in of regions labelled at the cell area. Each time-point represents max-projection of 3 z-sections (acquired in 0.5μm distance). **B** - Localisation of mCherry-tna1p and td-tomato-tna1p in exponentially growing *S. pombe* cells. Top row represents mCherry-tna1p. Bottom row represents td-tomato-tna1p. Max-projected pictures and a middle z-section (from a z-stack of 11 z-sections acquired in a 0.5μm distance). **C** - Colocalisation between mug33p-mKate (red channel) and GFP-tna1p (green channel) in exponentially growing *S. pombe*. Each time-point represents max-projection of 3 z-sections (acquired in 0.5μm distance). Scale bars: 5μm.

1993], [Turi et al., 2001]. This drug is known to cause redistribution of the Golgi into the ER, resulting in the failure in transportation of molecules out of this mixed ER-Golgi system in mammalian cells, and other organisms [Lippincott-Schwartz et al., 1991], [Pelham, 1991], [Wang et al., 2002]. The specific target of BFA is not known, however it has been reported that BFA inhibits essential Golgi-localised GTPases, what results in the Golgi stress and redistribution of markers of the Golgi machinery to the ER [Kowalczyk, Petersen, 2016]. Unfortunately, there is no report confirming an effect of BFA in fission yeast cells in SE.

In order to examine, effects of BFA on the Golgi during SE, we decided to observe localisation of the Golgi-apparatus marker after BFA treatment. Gma12p-GFP is a Golgi marker-protein that localises to multiple particles of various sizes in exponentially growing fission yeast cells [Brazer et al., 2000]. When such cells are treated with BFA gma12p-GFP relocates from the Golgi to the ER [Wang et al., 2002]. To test whether BFA (dissolved in DMSO) also affects ER to Golgi transport during SE we monitored localisation of GFP-gma12p in cells exiting starvation in the presence of BFA (**Figure 3.3**, C). In starvation, DMSO-treated control cells and BFA-treated cells only contained few gma12p-GFP particles (**Figure 3.3**, C, starvation). When in SE, the control cells increased the size and number of gma12p-GFP particles during the first 15min (**Figure 3.3**, C, 15min). In contrast, in BFA-treated cells the existing gma12p-GFP structures initially increased in size but their number appeared to remain constant. During subsequent time-points in SE DMSO-treated cells increased number of gma12p-GFP particles, comparing to previous time-points (**Figure 3.3**, C, 60min, 135min). After 135min in SE control cells contained many gma12p-GFP structures with a variety of sizes. In contrast, BFA-treated cells showed a gradual decrease of gma12p-GFP signal, until at 135min of SE the signal had almost completely disappeared (**Figure 3.3**, C, 135min). Wild-type cells visibly increased their length showing that they had initiated growth, however BFA-treated cells seemed to only slightly increase both their length and width, indicating lack of polarised fast growth initiation (**Figure 3.3**, C, 135min). Our data suggest that BFA affects morphology of the Golgi apparatus during SE.

We next investigated whether BFA-mediated disruption of the Golgi apparatus would affect GFP-tna1p localisation during SE. In the first 15min of SE, GFP-tna1p became visible near the plasma membrane in patches that were smaller and less defined than the membrane domains present in control cells (**Figure 3.3**, D, 15min). In addition, the bright GFP-tna1p particles were present inside the cells. Over time, the sub-cellular GFP-tna1p signal increased in distinct locations throughout the cell (**Figure 3.3**, D, 60min, 135min). At 135min it became obvious that the GFP-tna1p signal outlined

the ER (**Figure 3.3**, D, 135min). This suggests that GFP-tna1p accumulates in the ER in BFA-treated cells and further confirms the effectiveness of the BFA-treatment. Only a small portion of GFP-tna1p enriched at the cell poles (**Figure 3.3**, D, 135min). Unfortunately, our image resolution was not sufficient to distinguish whether this polar pool localised to the plasma membrane or the polar region of the ER, which closely aligns with PM in fission yeast [Zhang et al., 2012].

We conclude that localisation of GFP-tna1p dependents on the functional secretory pathway.

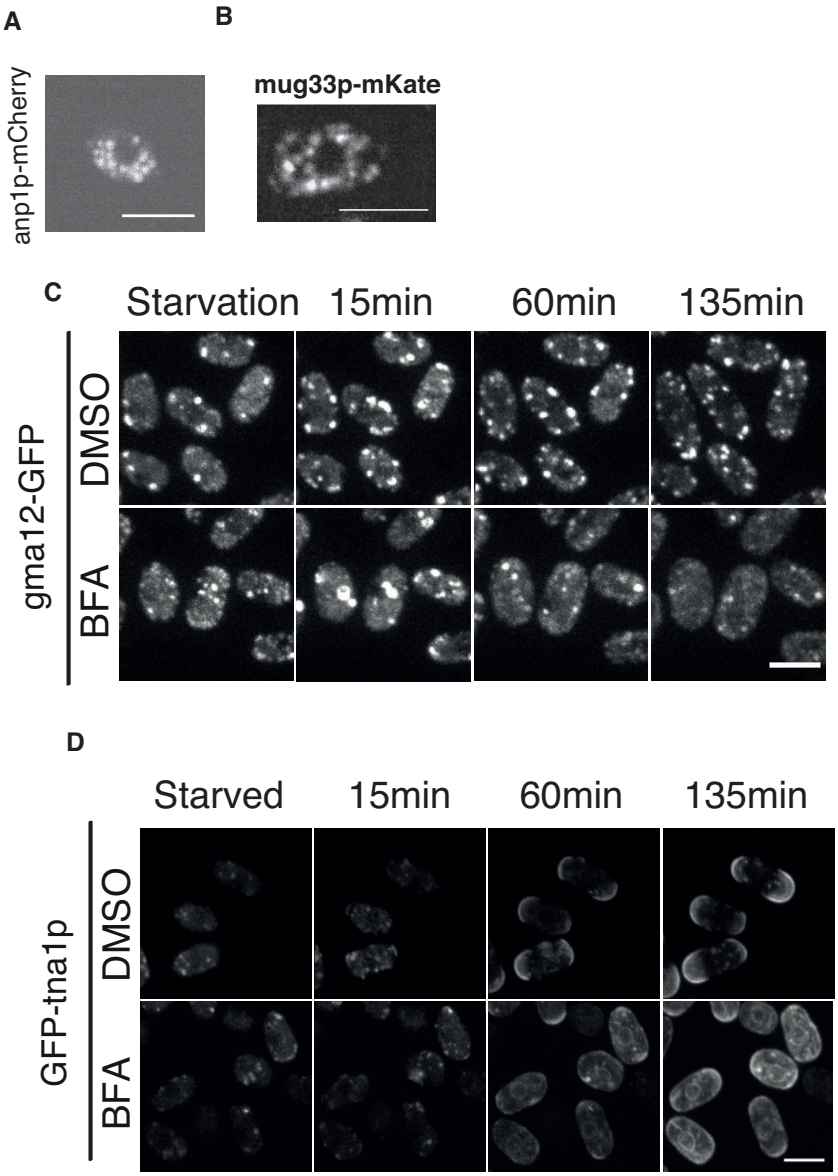

Figure 3.3: **Localisation of GFP-tna1p during SE depends on the Golgi apparatus**

A - anp1p-mCherry localisation 30min after start of SE. **B** - mug33-mKate 30min after start of SE **C** - gma12p-GFP upon DMSO (solvent) and BFA treatment in starvation and during SE. **D** - GFP-tna1p upon DMSO (solvent) and BFA treatment in starvation and during SE.
Scale bars: 5μm.

3.1.2 BFA treatment does not affect SRM polarisation

Our finding that GFP-tna1p delivery to the plasma membrane was blocked in BFA-treated cells shows that GFP-tna1p follows the secretory route via the Golgi apparatus (see, **3.1.1.2**) but this does not allow concluding that SRM formation at the plasma membrane is similarly inhibited. To follow SRMs formation in BFA-treated and DMSO-treated control cells exiting starvation we labelled them at various time points with the fluorescent dye filipin that directly binds to sterols [Drabikowski et al., 1973]. Surprisingly, BFA did not affect the formation of the randomly distributed SRMs in P1 as these appeared with proper timing and they were brightly labelled and well-defined (**Figure 3.4**, 15min). P2 in BFA treated cells also happened similar in control cells (**Figure 3.4**, 60min). As aforementioned, BFA-treated cells did not initiate P3 so cells are smaller than the control at 180min into SE (**Figure 3.4**). Taken together, our results suggest that, unlike GFP-tna1p delivery to the SRMs and unlike growth, the initial SRM formation during starvation exit and the subsequent MT/tea1p-mediated SRM polarisation do not depend on the classical ER to Golgi secretory pathway.

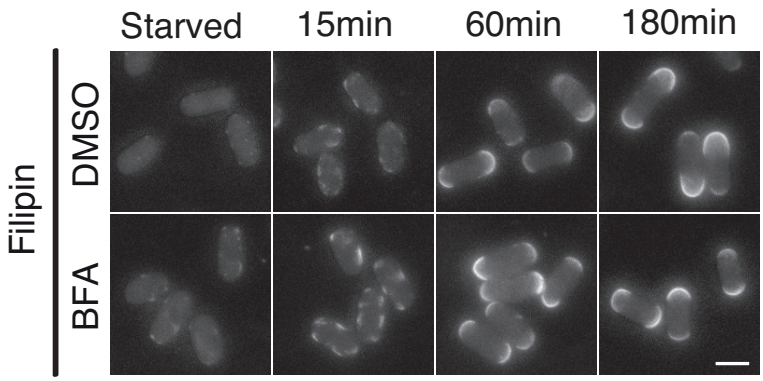

Figure 3.4: **Cell polarisation without the intact Golgi apparatus**

Filipin staining of wild type during SE. Cells were treated by DMSO (solvent) and BFA. Wild type was pre-treated by the drug for 1h in starvation and medium with a glucose was added in the presence of the drug. Scale bar represent 5μm.

3.1.3 Role of the exocyst complex component sec8p during SE

Our results on the effect of BFA during SE align with data on the effects of BFA in cultured mammalian cells. There, BFA was shown to only partially inhibit the delivery of newly synthesised cholesterol from the ER to the PM [Heino et al., 2000]. Delivery thus could go through a Golgi-independent transport pathway. To test whether this was the case for ergosterol delivery in cell polarisation during SE we tested additional secretory mutants for their requirement in this process. sec8p is a component of the exocyst complex [Wang et al., 2002] and *sec8* gene is essential for the cell viability. Sec8p plays a critical role in exocytosis in several organisms [Wu, Guo, 2015]. *sec8-1* is a point mutation allele in the *sec8* gene. *sec8-1* cells are viable at permissive temperature, however they display small defects in exocytosis. After shift to restrictive temperature *sec8-1* cells are able to perform a polarised growth, however they are specifically defective in cleavage of the division septum and cell separation [Wang et al., 2002]. This defect causes lethality. It is known that sec8p is required for efficient delivery of cell wall building enzymes to the site of cytokinesis and it additionally influences the transport of SRMs from cell poles to the PM in the cell center [Wang et al., 2002], [Wachtler et al., 2003].

3.1.3.1 The exocyst component sec8p is dispensable for SRM polarisation

To address the role of sec8p during SE, we used *sec8-1* mutant cells. Consistent with a secretion defect, we did not detect GFP-tna1p domains forming at the plasma membrane during SE at the restrictive temperature (**Figure 3.5**). Instead, we observed massive accumulation of GFP-tna1p signal inside the cells. However, when staining with filipin, we found *sec8-1* cells to form randomly distributed SRM domains similar to the wild type (**Figure 3.5**, 15min). During P2 SRM polarisation occurred normally, while GFP-tna1p remained accumulated in the cell interior (**Figure 3.5**, 60min). At 180min of SE, cells initiated P3 and started polar growth. GFP-tna1p enriched at the cell pole regions but did not form the typical polar caps seen with filipin. At this stage most

cells had a normal SRM cap at the growing cell pole, while filipin staining at the second pole was faint or not detectable (**Figure 3.5**, 180min). This suggests that these cells are growing mono-polar and cannot initiate P4. tea1p is known to be involved in cell polarisation and in stabilisation of SRM at the opposite end during P4 [Makushok et al., 2016b]. Our data show that sec8p is not essential for SRM formation and tea1-dependent SRM polarisation. However, once cells initiate growth, the tea1p-mediated stabilisation of SRMs at the secondary, non-growing pole during P3 seems to involve exocyst activity.

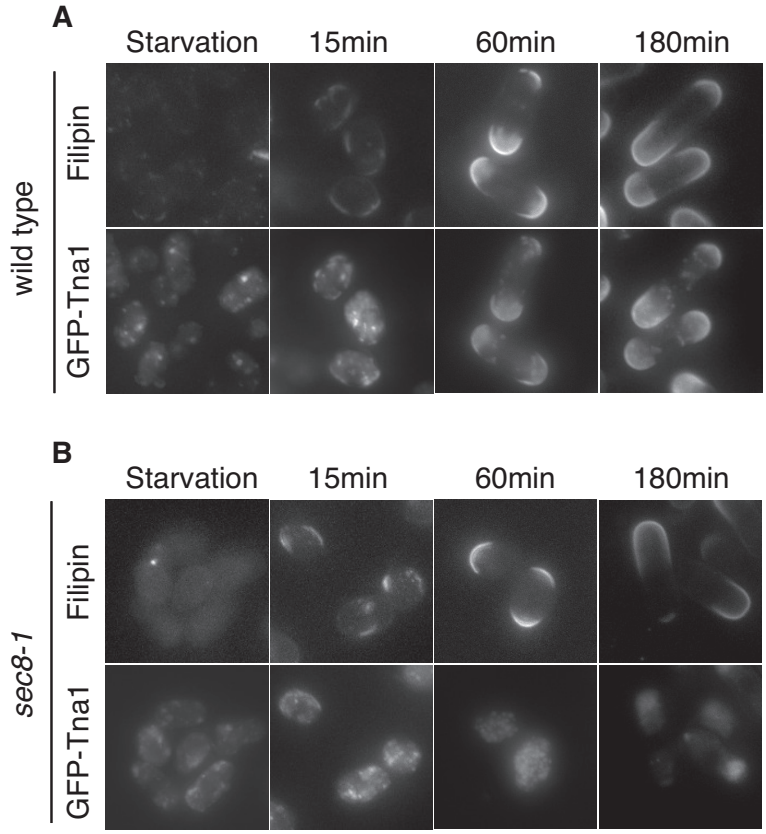

Figure 3.5: **Filipin and GFP-Tna1 localisation during SE in a *sec8-1* mutant**

A - SE of wild type cells. Top panel represents filipin staining. Bottom panel shows GFP-tna1p localisation.
B - SE of *sec8-1* mutant cells. Top panel represents filipin staining. Bottom panel shows GFP-tna1p localisation. Scale bars represent 5μm.

3.1.3.2 sec8p-GFP accumulates at SRMs during P1 and at non-growing ends during P3

Exocyst complex components localise to sites of active secretion at the PM of *S. pombe* cells [Wang et al., 2002]. In non-growing starved cells, sec8p-GFP dots distributed randomly at the cell periphery (**Figure 3.6**). During P1 of SE sec8p-GFP localised to the randomly distributed SRMs (**Figure 3.7**, 15min). After P2 and into P3, sec8-GFP dots accumulated at the cell poles, but localisation was clearly biased towards one pole in many cells (**Figure 3.7**, 60min, 180min). Co-localisation analysis of sec8p-GFP with filipin revealed that the preferred pole for sec8-GFP accumulation was the one with less filipin staining (**Figure 3.7**, 180min). This pole was previously found to correspond mostly to the non-growing cell pole [Makushok et al., 2016b]. This further supports a role for sec8p in tea1p-mediated stabilisation of SRM domains at non-growing, secondary cell poles during P3.

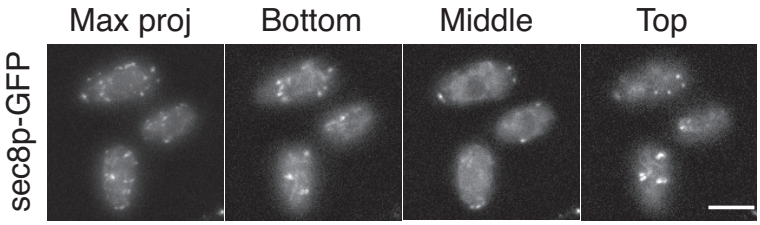

Figure 3.6: **sec8p-GFP localise to cell periphery in glucose-starved cells**

Sec8p-GFP expressing strain during glucose starvation. Panel presents maximum projection and 3 different single planes from a z-stack. Single planes represent different depths of the cell volume. Scale bar, 5μm.

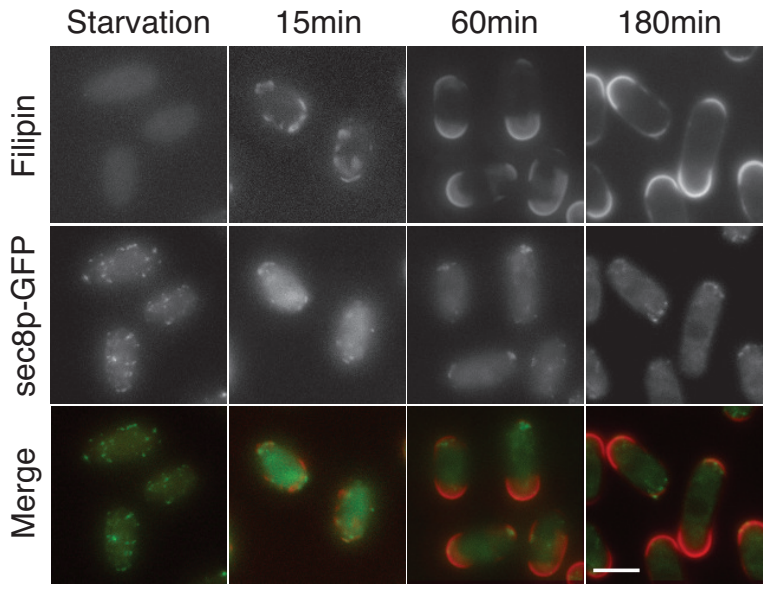

Figure 3.7: **sec8p-GFP accumulates close to SRMs during P1 and is abundant at non-growing ends during P2**

Figure shows co-localisation of filipin and sec8p-GFP during SE. Each picture is a maximum projection. Scale bar, 5μm.

3.1.4 Quantitative estimation of phases of SE at different temperatures

Our data show that GFP-tna1p does not allow following SRM formation and localisation dynamics in conditions in which secretion is affected. Therefore, the previous live imaging based way of SRM domain analysis was not applicable and we had to develop an alternative, quantitative assay to describe cell polarisation based on filipin staining. As we wanted to do this using various temperature-sensitive mutants we first had to explore the effects of temperature on SRM dynamics during SE in GFP-tna1p-expressing wild-type cells. These cells were growing at the standard permissive (25 °C) and restrictive (36 °C) temperatures.

We performed manual kymograph analysis (see Materials and Methods, **2.2.2.1**) of the GFP-tna1p signal (measured from the start of EMM2 medium addition) at 25 °C and 36 °C and compared our data to results from [Makushok et al., 2016b], which were acquired at 30 °C. Data are summarised in a **Table 3**. Kymographs did not allow to estimate initiation of P1, therefore this phase was exceptionally evaluated based on the

original data. Data revealed that when grown at 25 °C cells exiting starvation initiated P1 later than cells exiting starvation at 30 °C. In contrast, at 36 °C , cells initiated P1 similar to cells grown at 30 °C. Kymographs revealed that at this stage, no fast growth was detectable, which is in agreement with the data published in [Makushok et al., 2016b]. At 25 °C P2 initiated later than at 30 °C and 36 °C. P3 showed different initiation times at different temperatures. Briefly, at 25 °C cells initiated growth later than at 30 °C and cells at 30 °C initiated growth later than at 36 °C. P4 at 25 °C started significantly later than at both higher temperatures. Only in 25% of cells grown at 25 °C started P4 as compared to 34% reported for cells at 30 °C (see, [Makushok et al., 2016b]) and 44% at 36 °C (**Table 3**).

In summary, at the lower, permissive temperature of 25 °C P1, P2, P3 and P4 initiated later than at higher restrictive temperature 36deg. In general, initiation times of particular phases of SE at studied conditions were different than reported in [Makushok et al., 2016b]. This means that in our studies with *ts* mutants we had to consider different timing for the described phase of SE. In our analysis we thus focused on cell aliquots taken at 15min, 60min, and 180min of SE (unless stated otherwise). Thereby, 15min corresponds to P1, 60min corresponds to P2, 120 min corresponds to P3 and 180min corresponds to P4 at both 25 °C and 36 °C (Table 3).

A

	Phase	Starting time (min after the release from starvation)
25°C	P1	13 ± 7 (n = 30)
	P2	58 ± 12 (n =27)
	P3	125 ± 34 (n = 29)
	P4	281 ± 101 (n = 8)
30°C	P1	5-10min
	P2	34 ± 18 (n =269)
	P3	63 ± 33 (n = 394)
	P4	165 ± 85 (n = 40)
36°C	P1	7 ± 3 (n = 30)
	P2	34 ± 13 (n =24)
	P3	82 ± 32 (n = 29)
	P4	179 ± 80 (n = 18)

B

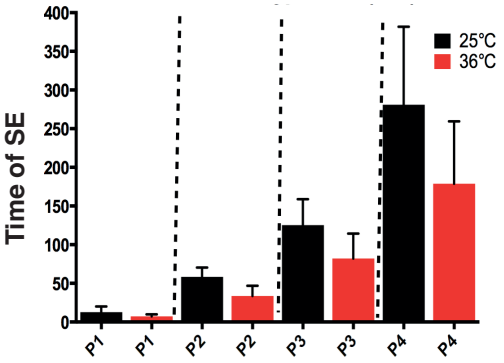

Table 3: **Timings of the four phases of SE in wild type cells at different temperatures**

A - Table presenting initiation time of 4 phases of SE at different temperatures, based on GFP-tna1p signal (method description in **2.2.2.1**). Data corresponding to 30 °C are adapted from [Makushok et al., 2016b]. **B** - Graphs presenting initiation times of phases of SE at 25 °C and at 36 °C. Data correspond to table from figure A.

3.1.5 Golgi-related membrane trafficking and membrane tethering at the PM are not critical for cell polarisation

3.1.5.1 Cell polarisation is not critically-dependent on redundant post-Golgi trafficking components

There are two complementing groups of components mediating efficient exocytosis: Group 1, includes actin delivery and actin nucleation-related components (for example myo52p and for3p) and Group 2 includes exocyst-related vesicle tethering factors (for example sec8p) [Snaith et al., 2011] [Bendezu, Martin, 2011]. Cells double mutant for components of the same group can maintain their polarised growth and are thus non-additive [Snaith et al., 2011] [Bendezu, Martin, 2011], Introduction (see, **1.2.4**).

Accordingly, it is known that in SE, member of group 1 such as for3p is not to be required for P1 and P2 of *de novo* cell polarisation during SE and *for3*Δ cells start showing a reduced growth phenotype during P3 [Makushok et al., 2016b]. For group 2

members, we have already shown that sec8p is not essential for P1, P2 and most probably for P3 of SE but functions probably in efficient establishment of P4 (**Figure 3.5**).

It is known that the two protein groups are redundant for polar growth since simultaneous mutation of a component of each group results in misshaped and spherical cells [Bendezu, Martin, 2011]. The redundancy between group 1 and 2 factors in polar growth raises the possibility that also in SE these components "rescue" each other when one is mutated. We therefore investigated the effects on *de novo* cell polarisation during SE in double mutant cells lacking the function of one member each of group 1 and group 2. For this we created a yeast strain carrying the temperature sensitive *sec8-1* mutant and a deletion of *for3* (*for3*Δ). As described in [Bendezu, Martin, 2011] and [Snaith et al., 2011] this combination caused synthetic lethality at the permissive temperature, which however could be rescued by growth on medium containing 1M sorbitol as osmotic stabiliser [Bendezu, Martin, 2011]. Surprisingly, we were able to obtain a *sec8-1 for3*Δ mutant strain, without sorbitol supplementation. The genotype of this strain was confirmed by gene sequencing and by back-crossing to wild-type cells showing the expected segregation of the two mutant genes.

Quantification of cell diameters showed that in starvation *sec8-1 for3*Δ mutant cells were smaller and wider compared to wild type cells (**Figure 3.8**). Filipin stained small and faint dots (**Figure 3.9**, B). During SE, these cells showed normal P1 and formed SRMs similar to the wild type. During P2, cells polarised their SRMs. However, the ratio of polarisation (rP) (see Materials and methods, **2.2.2.2.6**) showed that this occurred with a delay of around 30min (**Figure 3.9**, A). We think this is due to variability in P2 induction, since at 60min into SE, when wild type cells were mostly polarised, we observed a mix of polarised cells and cells still containing randomly distributed SRMs in *sec8-1 for3*Δ mutants (**Figure 3.9**, B, C). After 180min of SE mutant cells were clearly polar with a ratio of polarisation (rP) (see Materials and methods, **2.2.2.2.6**) similar to the wild-type (**Figure 3.9**, A, B). This suggests that the redundant vesicle trafficking systems are not essential for SRM formation and polarisation although they do to some extent support the polarisation step making it more synchronous.

During SE *sec8-1 for3*Δ mutants were enlarging in both length and width, however length increase was higher than width increase (**Figure 3.8**). The data showed that SRMs in *sec8-1 for3*Δ mutants only localise to a single cell-end what is similar to single *sec8-1* mutants.

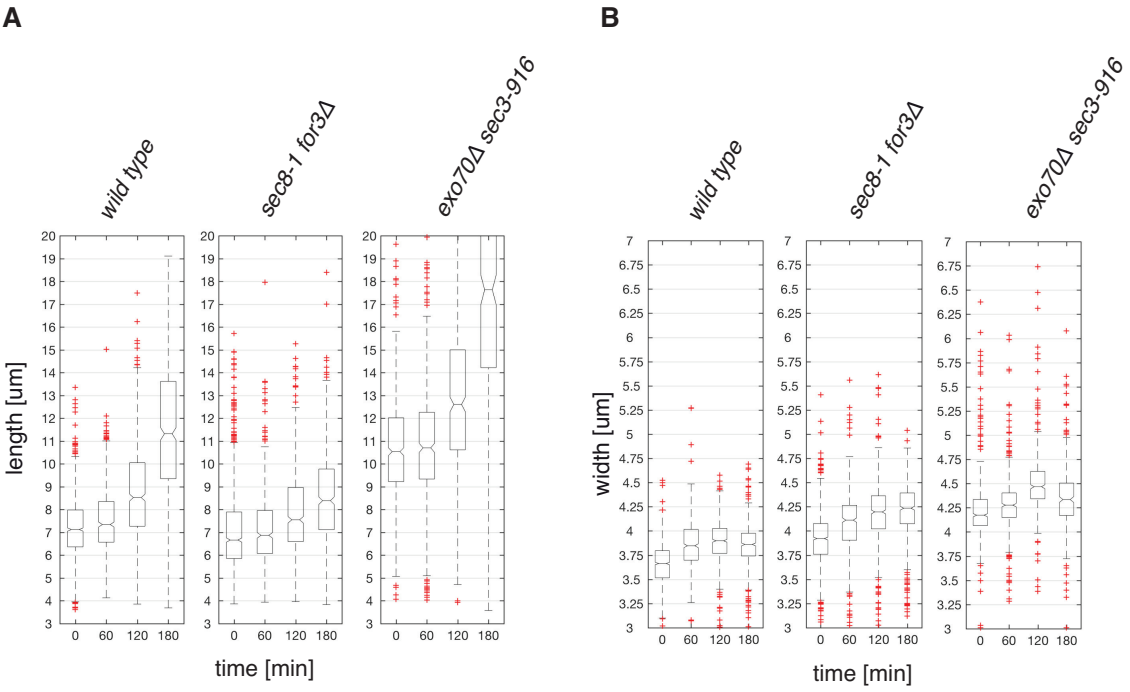

Figure 3.8: **Growth of post-Golgi trafficking double mutants**

A - Boxplots representing the distribution of measurements of cell length of wild type, *sec8-1 for3*Δ and *sec3-916 exo70*Δ. Quantification of glucose starved cells (0min) and cells during SE (n>600). Notches represent 95% confidence intervals of the median. **B** - Boxplots representing the distribution of measurements of cell width of wild type, *sec8-1 for3*Δ and *sec3-916 exo70*Δ. Quantification of glucose starved cells (0min) and cells during SE (n>600). Notches represent 95% confidence intervals of the median.

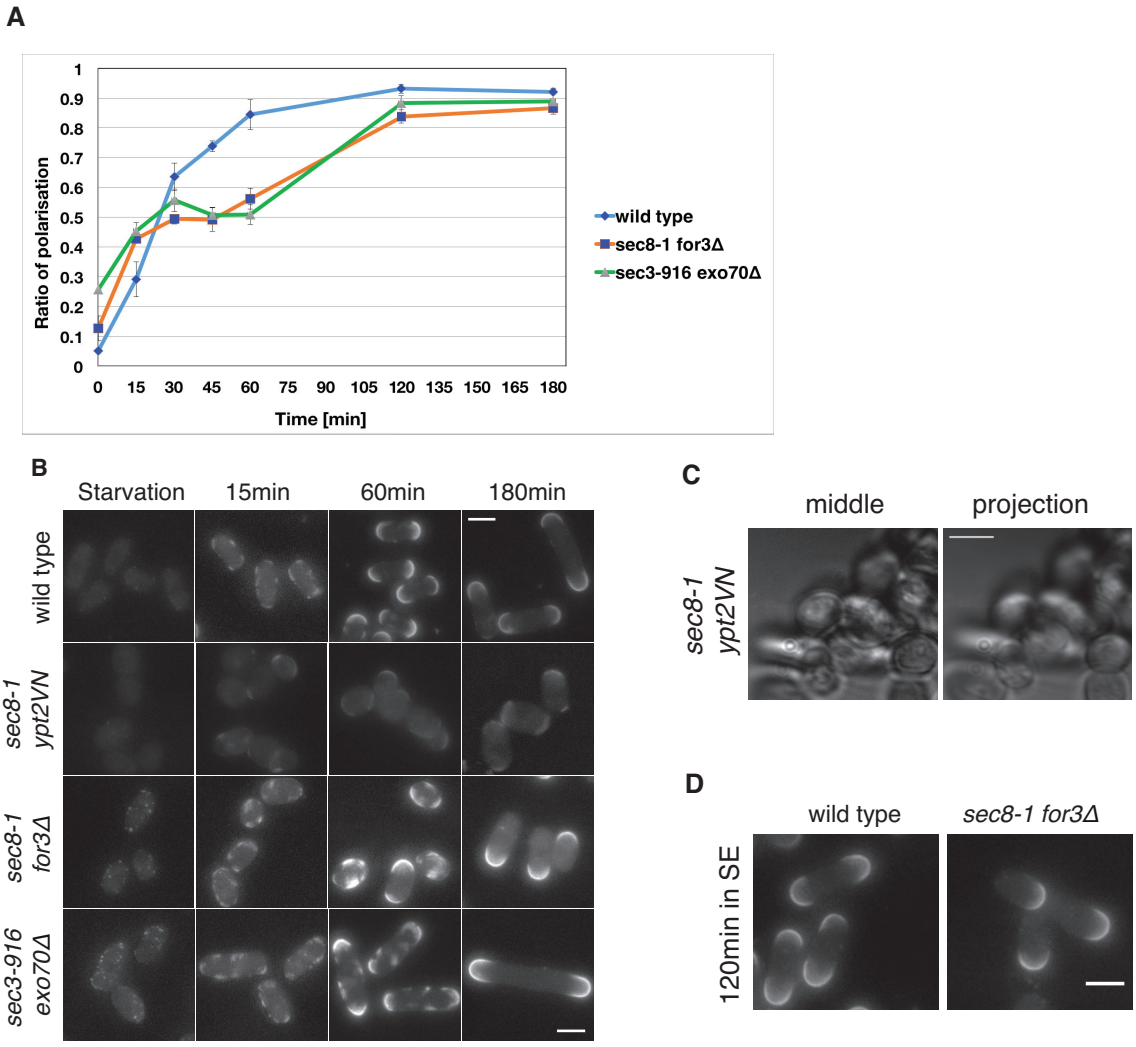

Figure 3.9: **Role of post-Golgi trafficking in cell polarisation**

A - Time course of average rP (Ratio of Polarisation) values for cells in SE. Each average rP was measured from mean rPs from 3 experiments (n>200 per experiment). Error bars represent the average standard deviations of mean rP values. Wild type, *sec8-1 for3*Δ and *sec3-916 exo70*Δ mutants were plotted. **B** - Filipin staining of wild type, *sec8-1 ypt2VN*, *sec8-1 for3*Δ and *sec3-916 exo70*Δ in starvation and during SE. Scale bar, 5μm. **C** - Brightfield pictures of *sec8-1 ypt2VN* in glucose starvation. Left - middle section. Right - average z-stack projection. Scale bar, 5μm. **D** - Filipin staining of wild type and *sec8-1 for3*Δ cells 120min in SE. Scale bar, 5μm.

It has been proposed that two complementary pathways for cell morphogenesis (actin delivery and exocyst complex) are functionally and physically linked by the exocyst component - sec3p. Cells without functional sec3p lack actin cables and components of the exocyst complex are not localised to defined regions [Jourdain et al., 2012], [Bendezú et al., 2012]. As a consequence these cells are misshapen and impaired in protein secretion [Jourdain et al., 2012]. Similarly to the budding yeast model, studies by [Bendezú et al., 2012] showed that *sec3* is genetically linked to *exo70* (one of the exocyst components) [Zhang et al., 2008]. *sec3*Δ and *exo70*Δ are redundant for cell viability.

In order to study the role of the genetically interacting components *sec3* and *exo70* we used temperature-sensitive mutants of *sec3* - *sec3-913* and *sec3-916* [Jourdain et al., 2012]. Unfortunately, we were not able to obtain a double mutant *sec3-913 exo70*Δ, however *sec3-916 exo70*Δ was viable. It is known that colonies of fission yeast carrying *sec3-916* mutation are not growing at restrictive temperature [Jourdain et al., 2012]. Cells die after defects in the cell separation (similar to *sec8-1*; described in **3.1.3**), [Jourdain et al., 2012].

We followed SE in the double mutant *sec3-916 exo70*Δ. We observed that these cells had high number of filipin dots in the PM in starvation (what was reflected by the high rP ratio (**Figure 3.9**, A, B), Materials and methods **2.2.2.2.6**). Mutants initiated P1 like wild-type cells and after 60min from the start of SE most mutant cells developed defined SRM domains at cell poles (**Figure 3.9**, A), however additional SRMs were still present at lateral positions, which is reflected in the lower rP value comparing to the wild-type control (**Figure 3.9**, A). Cells were very big and were elongating with much faster speed than wild-type cells (**Figure 3.8**). After 180min cells were clearly polar (**Figure 3.9**, A), having bipolar filipin localisation of SRMs with qualitatively similar size of both domains. We conclude that sec3p and exo70p are not required for starvation exit.

In order to strengthen our observations, we created a double mutant *sec8-1 ypt2VN*. Ypt2p is a Rab-GTPase (sec4p orthologueue from budding yeast and rab8p orthologue from mammalian cells), playing role in delivery of post-Golgi vesicles to the PM

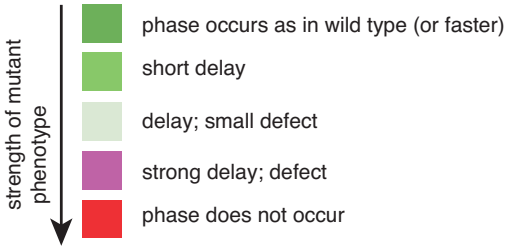

Strain name	P1	P2	P3
sec8-1 for3Δ			
sec8-1 ypt2VN		?	?
sec3-916 exo70Δ			

Table 4: **Table summarising SE in Golgi-related double mutants in SE**
Question mark indicates that we were not able to evaluate a stage of SE in unbiased way (The table summarises data until 180min in SE). (Materials and methods, **2.2.3**).

(see Introduction, **1.2.4.2**). *ypt2VN* cells rapidly arrest their growth after shift to restrictive temperature and accumulate high number of secretory vesicles in the cytoplasm [Craighead et al., 1993]. We observed that the double mutant *sec8-1 ypt2VN* was severely clumped and it was almost impossible to spot single cells (**Figure 3.9**, C). Due to this fact we were not able to segment these cells and to calculate the rP ratio (Materials and methods, **2.2.2.2.6**). An example of a few relatively not clumped cells, which were very rare to spot are presented in the **Figure 3.9**, B. Manual inspection confirmed that cells visibly entered P1, however unbiased assessment of the P2 initiation at 60min time-point was impossible. Although, we could spot several cells with two opposing SRMs at cell poles. It is possible that this double mutant behaves similarly to previously described *sec8-1 for3*Δ and *sec3-916 exo70*Δ, which were defected in the SRM removal at the onset of P2. After 180min in SE there were number of cells with a clearly polarised pattern of SRMs at the poles **(Figure 3.9**, B).

Description of phases of SE in post-Golgi double mutants are summarised in a **Table 4**. Width measurements of SRMs and their distribution, which were used for the calculation of the rP, for selected time-points during SE are included as a Supplementary figure (see, **Figure 5.1**).

3.1.5.2 BFA treatment of post-Golgi double mutants does not affect cell polarisation

The intact Golgi apparatus is not critically involved in SE (**Figure 3.4**). Moreover, classical post-Golgi components are not essential for the establishment of cell polarity (**Figure 3.9**, A, B and C). To test whether these two systems act redundantly, we decided to treat post-Golgi double mutants with BFA (drug which inhibits growth initiation during SE and affects protein secretion to the PM during SE (see, **3.1.1.2**).

We evaluated how double post-Golgi mutants (see, **3.1.5.1**) exit starvation in the presence of BFA. First, we measured rP values for consecutive time-points of SE. We observed that DMSO (as a drug solvent) slightly affected values of rP only in the mutants **(Figure 3.11**, A, B and C). However, DMSO and BFA treatments did not differ very much from each other and there was a trend in increasing rP during time of SE **(Figure 3.11**, B and C).

Filipin staining showed that all mutants treated with BFA entered P1. P2 was slightly delayed at the 60min time-point, similar to DMSO and non-treated cells **(Figure 3.12**, A). Although, the polarisation trend could be observed and after 180min in SE most cells were clearly in P2. As expected, double mutants treated with BFA did not initiate P3.

Summarising, our data suggest that the intact Golgi apparatus and classical post-Golgi trafficking are not essential for the establishment of cell polarity.

Summary information about phases of SE in post-Golgi double mutants treated with BFA are summarised in a **Table 5**. Width measurements of SRMs and their distribution, which were used for the calculation of the rP, for selected time-points during SE are included as a Supplementary figure (see, **Figure 5.2**).

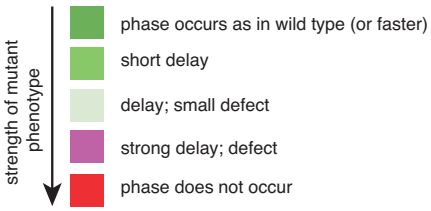

Strain name	*Treatment*	*P1*	*P2*	*P3*
Wild-type	*DMSO*			
Wild-type	*BFA*			
sec8-1 for3Δ	*DMSO*			
sec8-1 for3Δ	*BFA*			
sec8-1 ypt2VN	*DMSO*		*?*	*?*
sec8-1 ypt2VN	*BFA*		*?*	
sec3-916 exo70Δ	*DMSO*			
sec3-916 exo70Δ	*BFA*			

Table 5: **Table summarising SE after BFA treatment of the post-Golgi double mutants** The table summarises data until 180min in SE (Materials and methods, **2.2.3**).

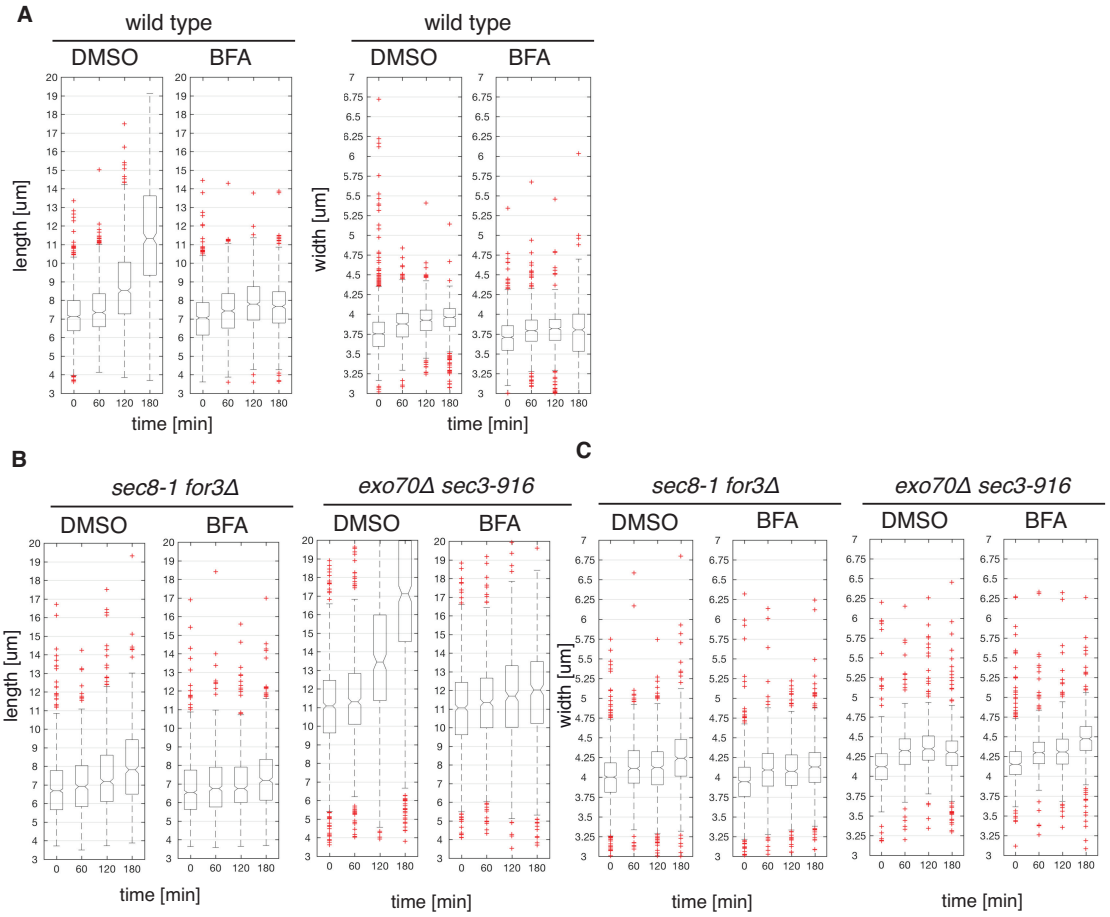

Figure 3.10: **Cell length and width in the post-Golgi double mutants treated with BFA**

A - Boxplots representing the distribution of cell length and cell width of wild type, *sec8-1 for3*Δ and *sec3-916 exo70*Δ cells starved at 25 °C for 3 days (and incubated at 36 °C for 1h before start into SE with a presence of DMSO/BFA) and during SE at 36 °C (in the presence of the drug) (n>600). Notches represent 95% confidence intervals of the median. **B** - Boxplots representing the distribution of measurements of cell length and cell width of wild type, *sec8-1 for3*Δ and *sec3-916 exo70*Δ cells. Strains were starved at 25 °C for 3 days (and incubated at 36 °C for 1h before start into SE with a presence of DMSO/BFA) and during SE at 36 °C (in the presence of the drug) (n>600). Notches represent 95% confidence intervals of the median.

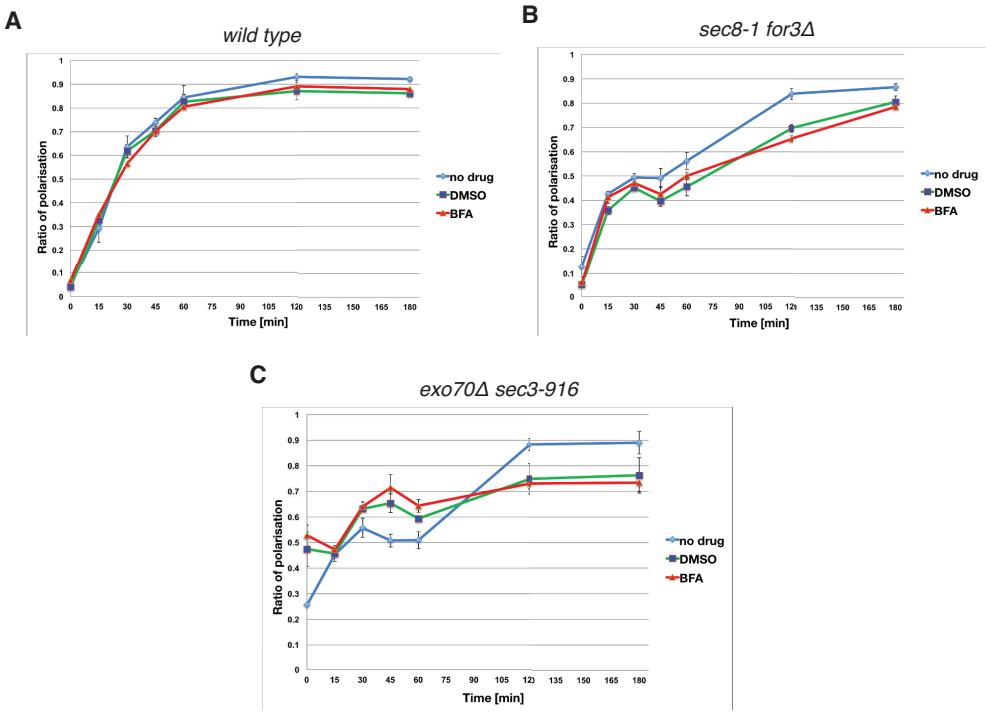

Figure 3.11: **Ratio of polarisation in the post-Golgi double mutants treated with BFA**

Time course of average rP values during SE. **A** - wild type, **B** - *sec8-1 for3*Δ, **C** -*sec3-916 exo70*Δ. Series correspond to not treated cells (no drug) - blue, DMSO - green and BFA-treated cells - red. Each average rP was measured from mean rPs from 3 experiments (n>200 per experiment). Error bars represent the average standard deviation of the mean rP values.

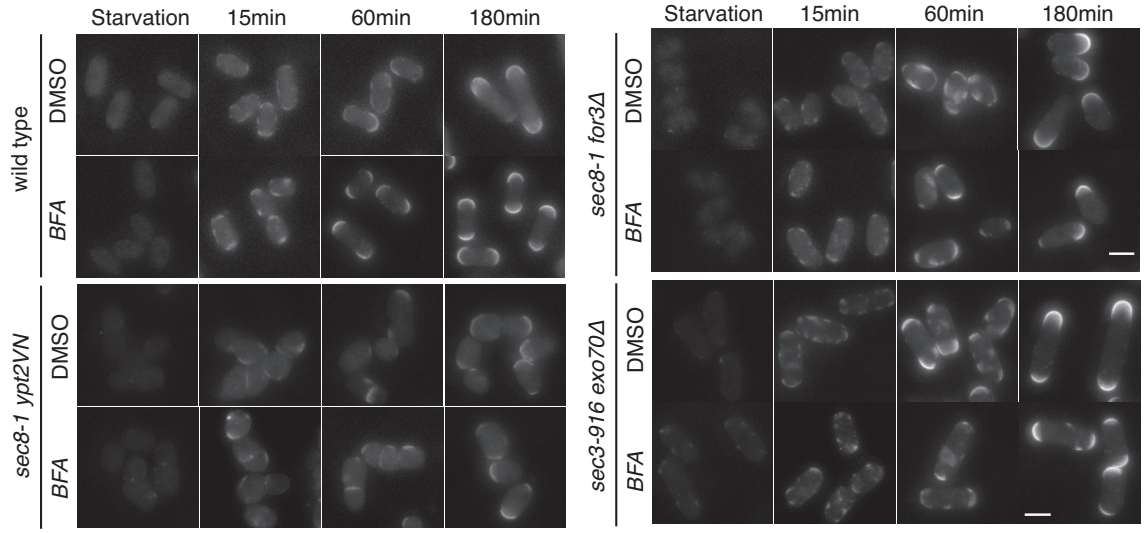

Figure 3.12: **Distribution of SRMs in the post-Golgi double mutants treated with BFA**

Filipin stainings of wild type, *sec8-1 ypt2VN*, *sec8-1 for3*Δ and *sec3-916 exo70*Δ cells in starvation and during SE. Cells treated with DMSO (solvent) and BFA. Strains were starved at 25 °C and pre-treated by the drug for 1h in starvation at 36 °C before start of SE. SE was initiated by adding DMSO and BFA with a medium containing glucose. Scale 5, μm.

3.1.6 The role of membrane fusion proteins in cell polarisation

3.1.6.1 PM-SNARE mutants can establish cell polarity

Mutants of post-Golgi trafficking suggested that cell polarisation is not driven by the vesicular membrane trafficking (see, **3.1.5.2**). We went to test this and looked at the mutants defected in the last step of membrane transport - membrane fusion. As described in Introduction (see, **1.2.4.3**) membrane fusion is mediated by the SNARE complexes [Jahn et al., 2003] and fission yeast contains 3 of PM-SNARE proteins (mammalian and budding yeast homologs): psy1p (homolog of t-SNARE) syb1p (homolog of v-SNARE), sec9p (homolog of SNAP25-like component).

To study the role of PM-SNARE complexes in SE we used individual PM-SNARE complex mutants *psy1-S1*, *syb1-sp58* and *sec9-10* [Maeda et al., 2014], [Yamaoka et al., 2013], [Nakamura et al., 2005]. All were shown to be essential for growth. *syb1*Δ mutant is essential for the maintenance of polarised shape. In addition, *psy1* is known to play role during sporulation and endocytosis and *sec9* is involved in cytokinesis [Maeda et al., 2014], [Edamatsu, Toyoshima, 2003], [Yamaoka et al., 2013], [Nakamura et al., 2005]. In addition, to strengthen our observations we have created a double mutant between *psy1-S1* and *syb1-sp58*.

All mutants entered P1 at 15min into SE. However, *psy1-S1* and the double mutant *psy1-S1 syb1-sp58* formed slightly smaller and less bright SRM domains **(Figure 3.14**, B). In addition, *sec9-10* cells contained untypical big SRMs and additional small filipin dots in between SRM domains.

Wild type and the mutants cells increased their rP ratio during SE **(Figure 3.14**, A), however all mutants showed slightly lower values of the rP (compared to the wild type) (see Materials and methods, **2.2.2.2.6**). This pattern was similar to post-Golgi mutants presented in the previous subsection (**Figure 3.9**, A). Qualitative evaluation of P2 entry showed that this phase actually occurred at 60min in SE **(Figure 3.14**, B, 60min). This fact can also be confirmed by the more abundant pool of polar SRMs at 60min, as presented in the corresponding histograms (Supplementary figure, **(Figure 5.3)**). The

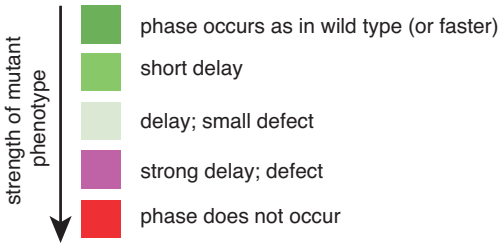

Strain name	P1	P2	P3
psy1-S1			
syb1-sp8			
sec9-10			
psy1-S1 syb1-sp8			

Table 6: **Table summarising phases of SE in PM-SNARE mutants**
The table summarises data until 180min in SE (Materials and methods, **2.2.3**).

lower rP values might reflect SRMs which were slightly offset from the major axis of the cell **(Figure 3.14**, B, 60min). After 180min in SE cells were polarised, however we think that many of them had problems in formation of SRM at the opposite end of the cell **(Figure 3.14**, B, 180min) (similarly to the *sec8-1* mutants (**Figure 3.5**, 180min).

Median growth speed of wild type and *psy1-S1* mutants increased between 120-180min in SE and reached more than 0.8μm/h, therefore we conclude that *psy1-S1* cells can enter P3. Other mutants also increased their length between 120-180min, however it was significantly lower than for wild-type and *psy1-S1* cells. It suggested that *syb1-sp58*, *sec9-10* and *psy1-S1 syb1-sp58* mutants were delayed in P3 initiation or performed slower growth (which is known for cells in P2 [Makushok et al., 2016b]).

Our data show that PM-SNARE mutants are able to enter P1 and P2, however we think they might contribute to cell polarisation by making it more synchronous. Further evaluation of functionality of the PM-SNARE complex in described mutant conditions will need to be performed.

Phenotypes of PM-SNARE mutants are summarised in a **Table 6**. Width measurements of SRMs and their distribution, which were used for the calculation of the rP, for selected time-points during SE are included as a Supplementary figure (see, **Figure 5.3**).

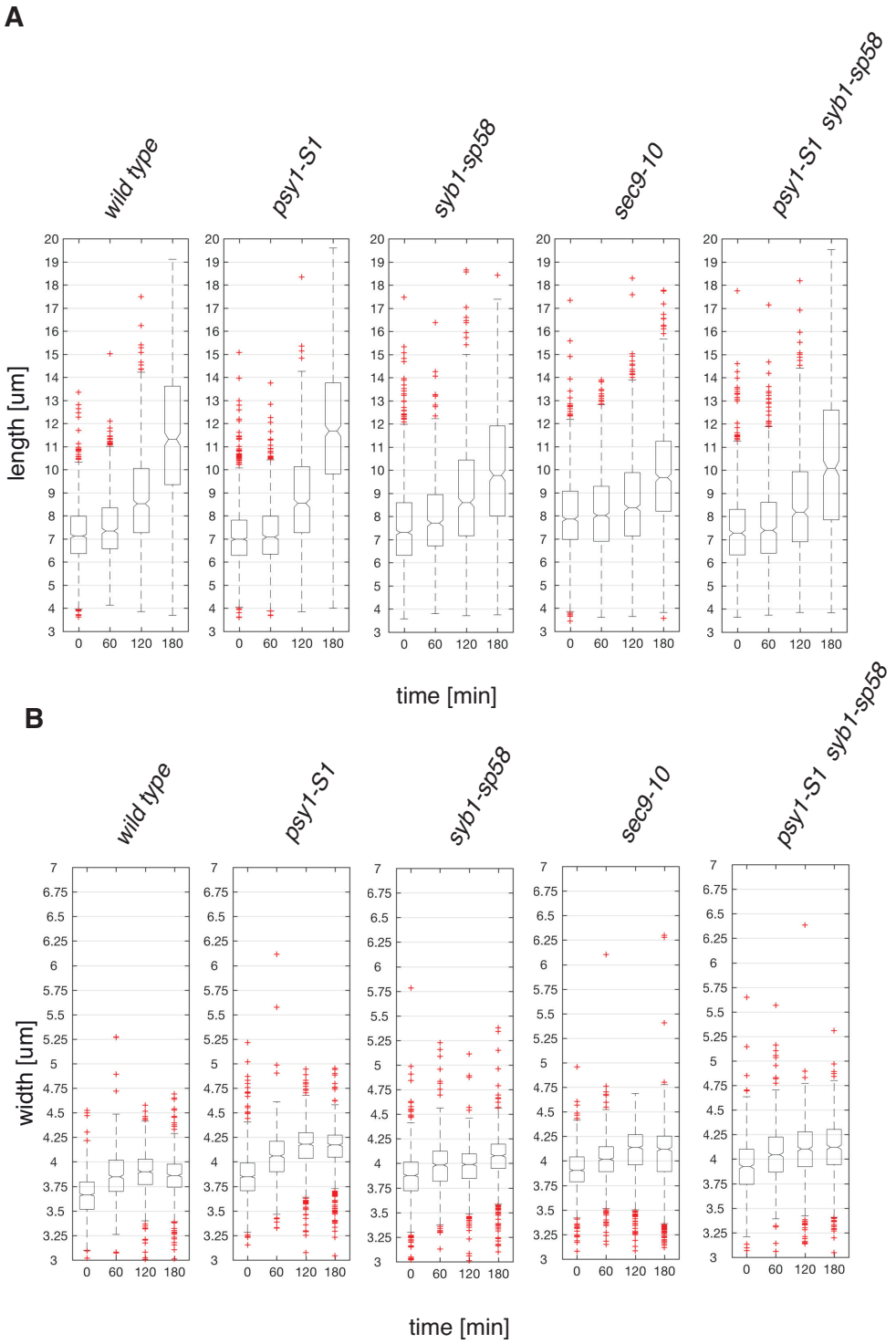

Figure 3.13: **Cell length and width of PM-SNARE mutants in S. pombe during SE**

A - Boxplots representing the distribution of measurements of cell length of wild type, *psy1-S1*, *syb1-sp58*, *sec9-10* and *psy1-S1 syb1-sp58* cells. Quantification of glucose starved cells (0min) and cells in SE (n>600). Notches represent 95% confidence intervals of the median. **B** - Boxplots representing the distribution of measurements of cell width of wild type, *psy1-S1*, *syb1-sp58*, *sec9-10* and *psy1-S1 syb1-sp58* cells. Quantification of glucose starved cells (0min) and cells in SE (n>600). Notches represent 95% confidence intervals of the median.

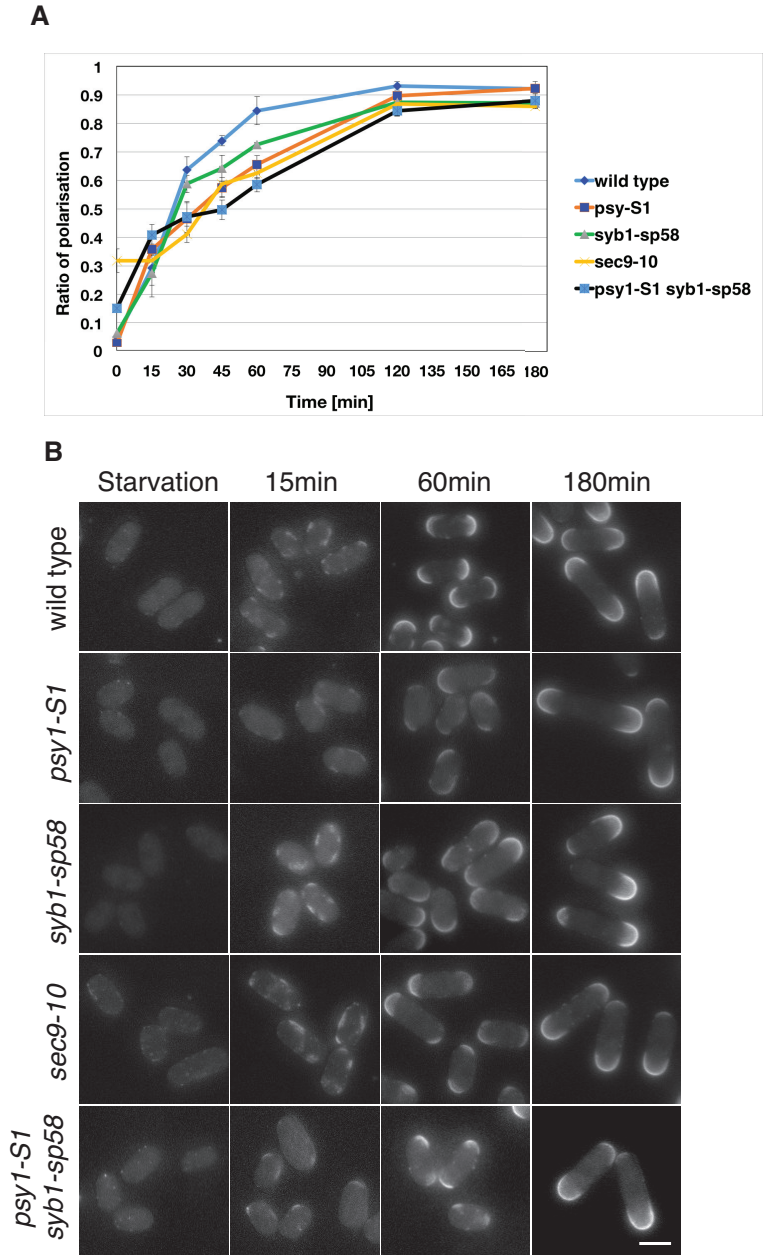

Figure 3.14: **PM-SNARE mutants are not essential for *de novo* cell polarisation**

A - Time course of average rP (Ratio of Polarisation) values for cells in SE. Each average rP was measured from mean rPs from 3 experiments (n>200 per experiment). Error bars represent the average standard deviations of mean rP values. Experiments with wild type, *psy1-S1*, *syb1-sp58*, *sec9-10* and *psy1-S1 syb1-sp58* cells were plotted. **B** - Filipin staining of wild type, *psy1-S1*, *syb1-sp58*, *sec9-10* and *psy1-S1 syb1-sp58* cells in starvation and during SE. Scale bar, 5μm.

3.1.6.2 Effects of BFA treatment on PM-SNARE mutants

Our data suggest that membrane trafficking is not required for cell polarisation. To strengthen our hypothesis and to test if PM-SNAREs are redundant with the Golgi-dependent trafficking we treated wild-type and PM-SNARE mutants with BFA (see, 3.1.1.2).

All DMSO and BFA-treated mutants entered P1, however formation of SRMs in the double mutant *psy1-S1 syb1-sp58*, treated with BFA, was significantly different. We observed few small SRMs and tiny filipin dots **(Figure 3.17**, A). We conclude that perturbing membrane fusion at the PM together with affecting the Golgi-mediated trafficking with BFA, causes an SRM formation phenotype. However, this phenotype did not prevent continues transport of sterols to the PM and its simultaneous clustering into SRMs during later time-points of SE **(Figure 3.17**, A).

The rP ratios for *syb1-sp58* and *sec9-10* mutants treated with BFA were similar to DMSO-treated control cells. In contrast, we observed that BFA-treatment decreased the rP ratio in *psy1-S1* and more so in the double mutant *psy1-S1 syb1-sp58* **(Figure 3.16**, B, E). In these mutants we observed bigger pool of SRMs at lateral positions (Supplementary figure, **(Figure 5.4)**). We think that such low rP values are a result of additional filipin dots present in the PM and SRMs at cell poles, which seemed to be more offset from the major axis, (in contrast to wild-types and other SNARE mutants **(Figure 3.17**, A). This speculation would need to be evaluated in the future. Additionally, most of observed single mutant cells treated with BFA had mono-polar pattern of SRMs.

Most significantly all studied PM-SNARE mutants treated with BFA continued increasing their rP ratio. Strikingly, the double mutant *psy1-S1 syb1-sp58* lost its polarised state after 180min in SE **(Figure 3.16**, E), **(Figure 3.17**, A).

We conclude that all SNARE mutants treated with BFA can enter P2, however *psy1-S1* and the double mutant *psy1-S1 syb1-sp58* are delayed in this process, which indicates their non-essential role in *de novo* cell polarisation. Although, at 180min in SE

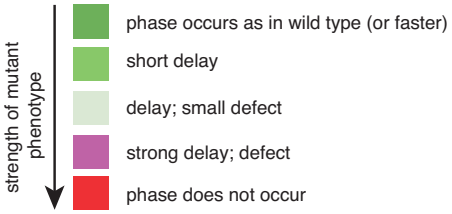

Strain name	Treatment	P1	P2	P3
Wild-type	*DMSO*			
Wild-type	*BFA*			
psy1-S1	*DMSO*			
psy1-S1	*BFA*			
syb1-sp58	*DMSO*			
syb1-s5p8	*BFA*			
sec9-10	*DMSO*			
sec9-10	*BFA*			
psy1-S1 syb1-sp8	*DMSO*			
psy1-S1 syb1-sp8	*BFA*			

Table 7: **Table summarising phases of SE after BFA treatment of the PM-SNARE mutants**

The table summarises data until 180min in SE (Materials and methods, 2.2.3).

most double mutant cells lose their polar SRM localisation and some side SRMs appear in the PM **(Figure 3.17**, A). These data suggest that the double SNARE mutant cells -treated with BFA, cannot maintain their polarised state. Moreover, we conclude that membrane fusion is involved in the formation of SRMs at opposite ends during P2. This couples to previously mentioned role of sec8p in the formation of bi-polar pattern of SRMs (**Figure 3.5)**.

Phenotypes of the PM-SNARE mutants treated with BFA are summarised in a **Table 7**. Width measurements of SRMs and their distribution, which were used for the calculation of the rP, for selected time-points during SE are included as a Supplementary figure (see, **Figure 5.4**).

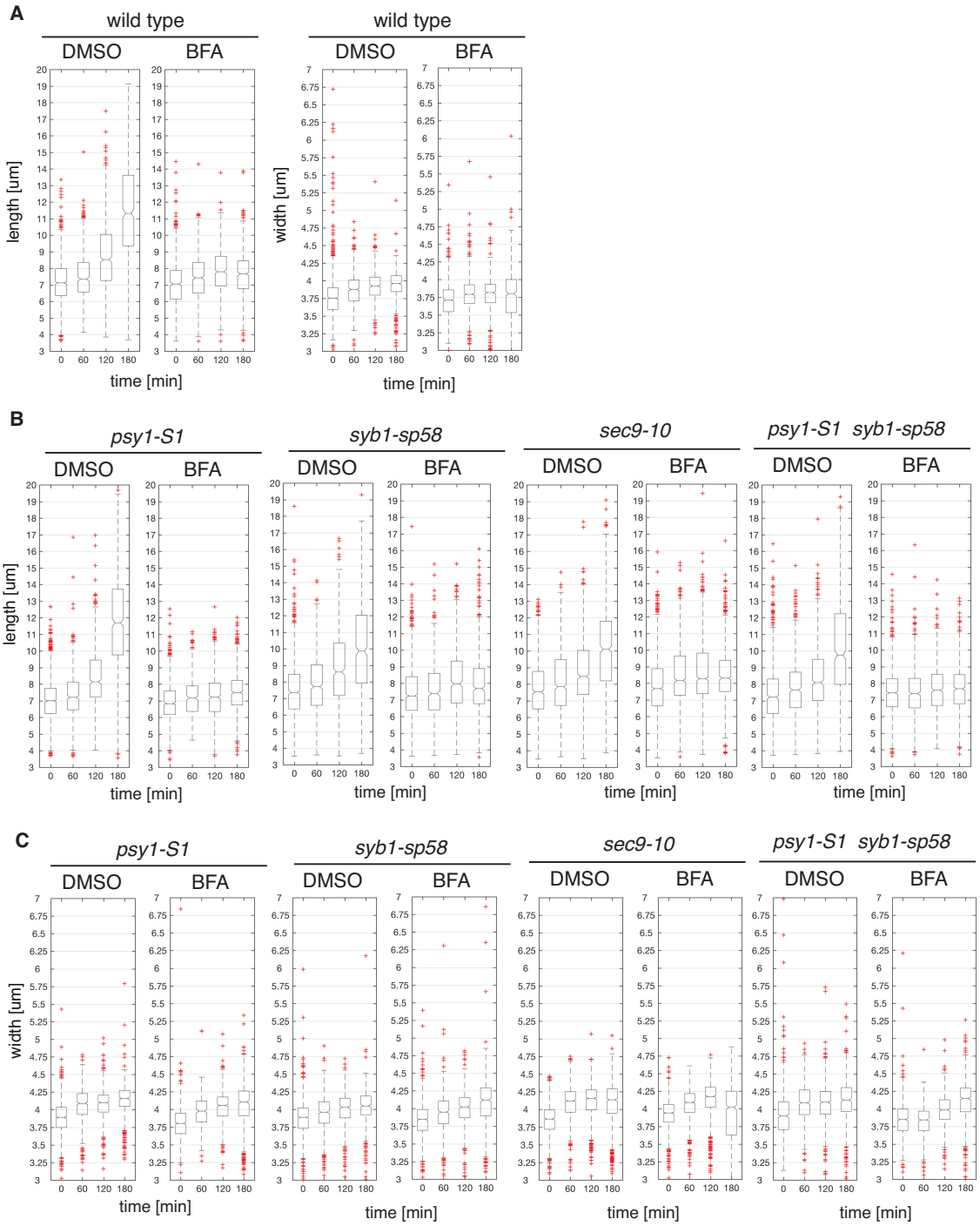

Figure 3.15: **BFA effect on cell length and width during SE of PM-SNARE mutants in *S. pombe***

A - Boxplots representing the distribution of cell length and cell width of wild type, *psy1-S1*, *syb1-sp58*, *sec9-10* and *psy1-S1 syb1-sp58* cells starved at 25 °C for 3 days (and incubated at 36deg for 1h before start into SE with a presence of DMSO/BFA) and during SE at 36 °C (in the presence of the drug) (n>600). Notches represent 95% confidence intervals of the median. **B** - Boxplots representing the distribution of measurements of cell length and cell width of wild type, *psy1-S1*, *syb1-sp58*, *sec9-10* and *psy1-S1 syb1-sp58* cells. Strains were starved at 25 °C for 3 days (and incubated at 36deg for 1h before start into SE with a presence of DMSO/BFA) and during SE at 36 °C (in the presence of the drug) (n>600). Notches represent 95% confidence intervals of the median.

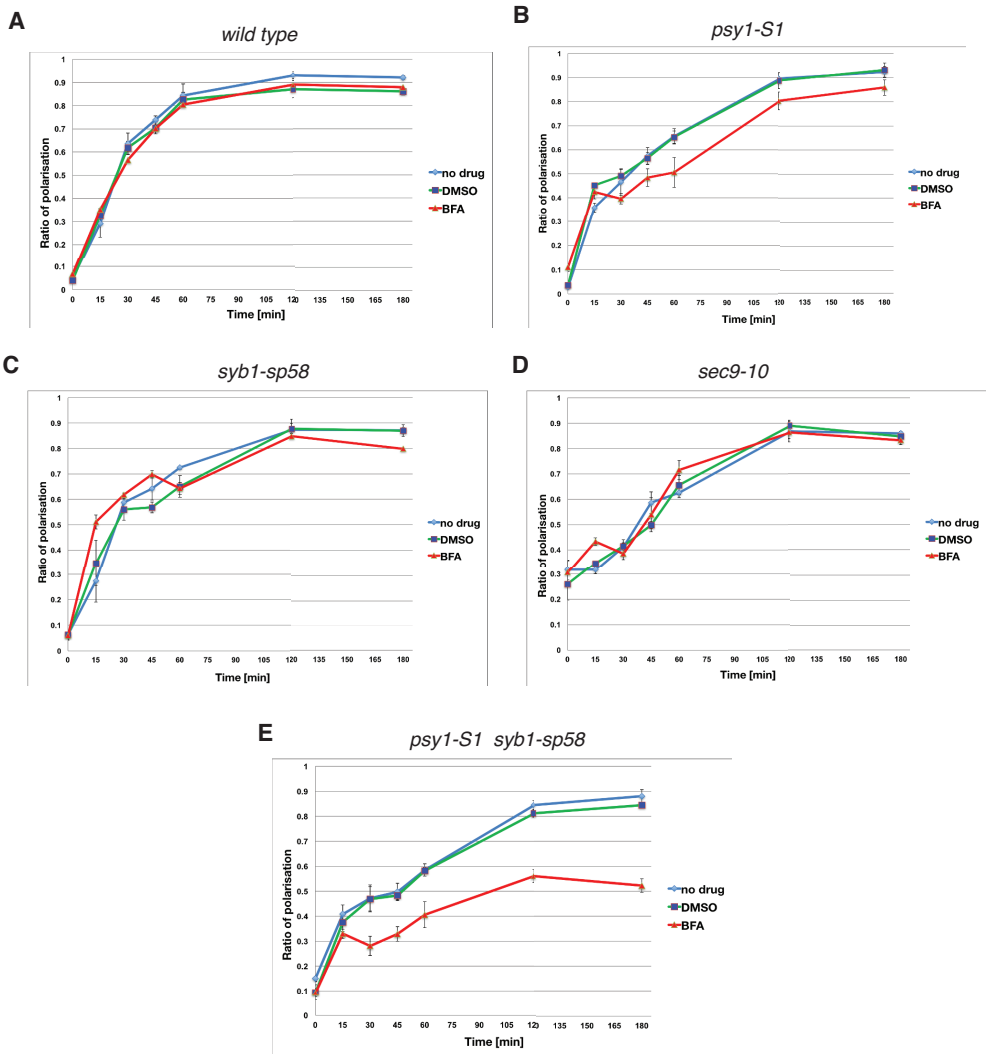

Figure 3.16: **BFA effect on Ratio of Polarisation during SE of PM-SNARE mutants in *S. pombe***

Time course of average rP values during SE. **A** - wild type, **B** - *psy1-S1*, **C** -*syb1-sp58*, **D** -*sec9-10* and **E** -*psy1-S1 syb1-sp58*. Series correspond to not treated cells (no drug) - blue, DMSO - green and BFA-treated cells - red. Each average rP was measured from mean rPs from 3 experiments (n>200 per experiment). Error bars represent the average standard deviation of the mean rP values.

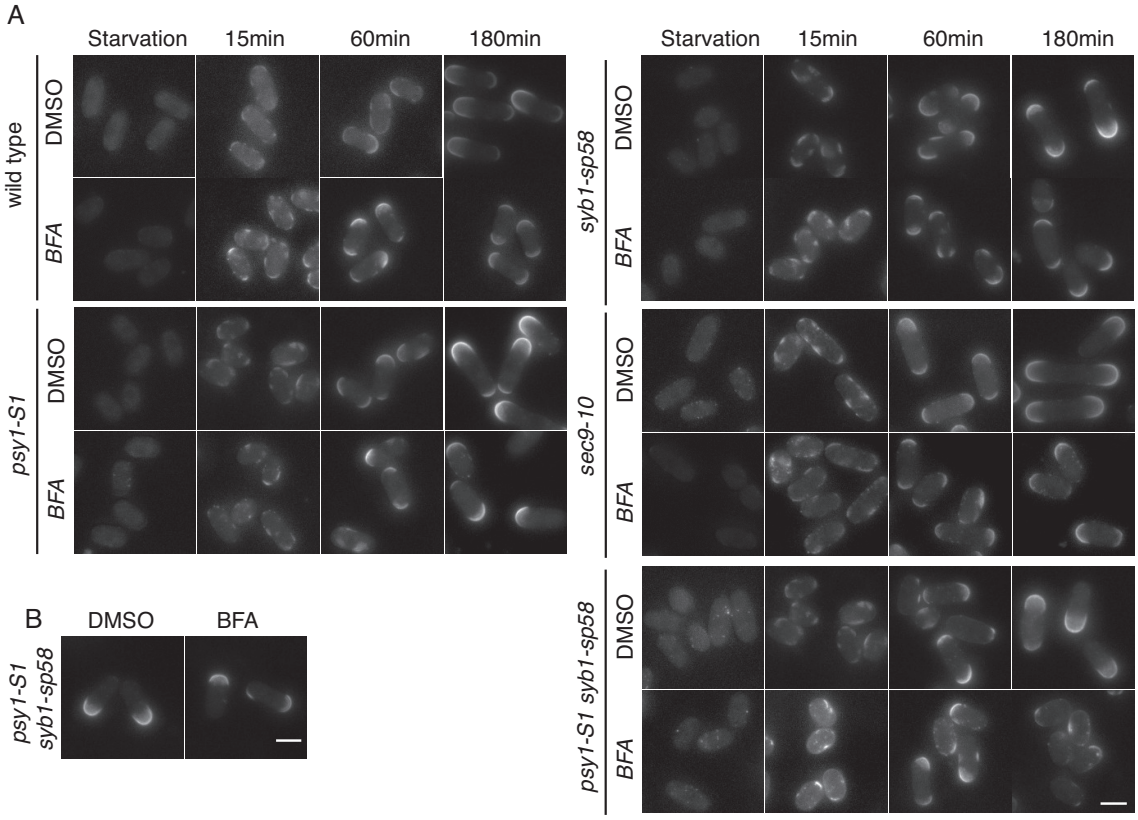

Figure 3.17: **BFA effect on SRM distribution of PM-SNARE mutants during SE in *S. pombe***

Filipin stainings of wild type, *psy1-S1*, *syb1-sp58*, *sec9-10* and *psy1-S1 syb1-sp58* cells in starvation and during SE. Cells treated with DMSO (solvent) and BFA. Strains were starved at 25 °C and pre-treated with the drug for 1h in starvation at 36 °C before start of SE. SE was initiated by adding DMSO and BFA with a medium containing glucose. Scale 5, μm.

Summarising, our data suggest that Golgi-mediated trafficking and membrane fusion are not essential for the formation (P1) and polarisation of SRM domains (P2) during SE. However, they might have additional and non-essential role in efficiency of P2 entry, the speed of growth in P3 and subsequent maintenance of polarity. Together, this brings us to the conclusion that SRM formation and tea1p-dependent polarisation might be driven by as yet not described non-vesicular modes of lipid transfer.

3.2 Non-vesicular membrane trafficking and cell polarisation

Ergosterol delivery to the PM, observed as the appearance of the filipin-stainable SRMs, is not critically-dependent on the activity of classical modes of secretion. As wrote in the Introduction (see, **1.3.1.2**) sterols in budding yeast are sorted by the main sorting and secretory organelle - the trans-Golgi-apparatus [Klemm et al., 2009]. However, studies from mammalian cells showed that Brefeldin A, a drug that inhibits protein transport from the ER to the Golgi apparatus (also described in **3.1.1.2**), decreases the transport of newly synthesised sterol to the PM by only 20% [Heino et al., 2000]. Therefore, alternative non-vesicular transport pathway of *de novo* synthesised sterol was proposed [Baumann et al., 2005a], [Maxfield, Menon, 2006]. Our results support these observations by showing that transport of *de novo* synthesised sterol during P1 of SE is not critically dependent on the Golgi-dependent exocytosis and membrane fusion (see, **3.1**). We propose that non-vesicular transport of sterol must be critical for SRM formation and cell polarisation in SE. In contrast to P1 and P2, vesicular transport of *de novo* synthesised sterol plays a role after establishment of polarity during P3 and P4.

We became interested if orthologues of known non-vesicular transporters of lipids (lipid transfer proteins - LTPs) are required for P1. Since it is known that tea1p is involved in P2, we wanted to know if mutants of LTPs also exhibit similar phenotypes as *tea1*Δ (we described general principles of non-vesicular sterol transport in the Introduction: see, **1.3.1.2** and **1.3.1.3**).

3.2.1 Oxysterol-binding protein orthologues in fission yeast cells

Oxysterol-binding proteins (osh proteins or oshes) are known LTPs involved in the sterol distribution at the PM, endocytosis, growth, and maintenance of cell polarity in yeast and in the maintenance of the PM morphology [Beh, 2004]. They are also implicated in membrane trafficking and non-vesicular transport at the Golgi [Mesmin, Antonny, 2016].

We found 6 presumptive osh proteins in fission yeast based on the *S. pombe* database [Wood et al., 2011] **(Figure 3.18)**. This is in agreement with [Bühler et al., 2015b],

fission yeast	budding yeast	*A. nidualns*
kes1p	kes1(osh4p)	oshCp
kes2p	osh4p	oshCp
osh2p	osh1p, osh2p	oshAp
osh3p	osh3p	oshBp
oshEp	-	oshEp
osh7p	osh6p, osh7p	oshDp

Table 8: **orthologues of fission yeast oxysterol-binding proteins**

where the authors also identified 6 *S. pombe* proteins of oshes. We named them based on the closest protein sequence homologs in *S. cerevisiae* and *A. nidulans* [Altschul et al., 1990]. Therefore, the names are as follows: kes1p (SPBC1271.12), kes2p (SPBC354.07c), osh2p (SPBC2F12.05c), osh3p (SPAC23H4.01c), oshEp (SPBC646.08c), and osh7p (SPCC23B6.01c) (see, **Table 14**).

Similar to budding yeast and *A. nidulans*, all oshes in fission yeast contain the oxysterol binding protein-related domain (ORD) **(Figure 3.18)**, which is responsible for binding of lipids (principles of lipid binding via this type of domain are described in the Introduction, see, **1.3.1.3**). Moreover, two oshes: osh2p and osh3p have additional N-terminal sequences, which encode lipid-interacting PH domains. In addition, osh2p has 3 ankyrin repeats (known to function in protein-protein interactions) and osh3p has a secretory-related GOLD domain **(Figure 3.18)**. kes1p and kes2p both are orthologues of kes1p from *S. cerevisiae* and oshCp from *A. nidulans*. However, kes1p from fission yeast has a higher homology to kes1p from *S. cerevisiae*, than kes2p [Altschul et al., 1990]. Moreover, kes2p from fission yeast does not contain a Coil region at its C-terminal part, in contrast to kes1p. Another identified osh is a osh7p/oshDp, which is a sequence homolog of both osh6p and osh7p from budding yeast and belongs to the same phylogenetic group as oshDp from *A. nidulans*. We were not able to find an obvious sequence homolog of oshEp in budding yeast. However, oshEp from fission yeast has sequence homology with oshEp from *A. nidulans*. In contrast to the orthologue of oshEp in *A. nidulans*, the ORD domain of oshEp in *S. pombe* is split into two parts. Moreover, it is the only osh in fission yeast cells, that does not contain the characteristic OSBP signature (a sequence

coding for the conserved pentapeptide from mammalian orthologue of oshes - OSBP).

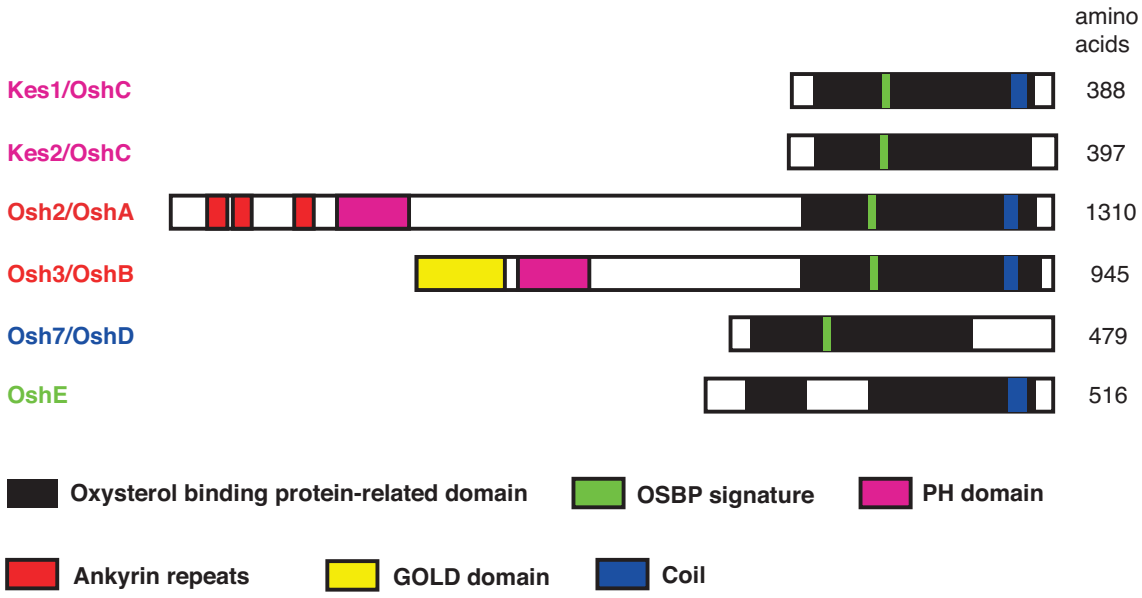

Figure 3.18: **Domain structure of oxysterol-binding protein orthologues in *S. pombe***

Domain structure of osh proteins in *S. pombe*. colours indicate: purple, pleckstrin homology (PH) domain; black, oxysterol-binding protein-related domain (ORD); green, red, ankyrin repeats; OSBP signature (a conserved pentapeptide sequence from the mammalian Oxysterol-binding protein); blue, part of a predicted coiled-coil region; yellow, Golgi dynamics (GOLD) domain The domain structure was prepared based on information from the the InterPro online resource [Mitchell et al., 2015]. Graphics adapted from [Bühler et al., 2015b].

3.2.1.1 Localisation of oxysterol-binding proteins in exponentially growing fission yeast

In order to learn more about the osh proteins in fission yeast, strains expressing GFP tagged osh proteins were generated (see Material and methods **2.1.2**). Localisations of osh proteins and their presumptive homologs in budding yeast and *A. nidulans* are summarised in supplementary table (see, **Table 14**).

Kes1p-GFP in *S. pombe* localised to the cytoplasm in growing cells and sites of cytokinesis. It also seemed to accumulate at cell poles in subset of cells. Deconvolution revealed more clearly that kes1p-GFP is concentrated at cell poles **(Figure 3.19**,

A). This pattern of localisation is similar to the images of kes1p-GFP in the *Schizosaccharomyces pombe Postgenome Database* (SPD) [Matsuyama et al., 2006]. However, in contrast to the SPD, the nuclear envelope localisation of kes1p-GFP was not visible in our studies **(Figure 3.19**, A). Interestingly, in *A. nidulans* the kes1p homologue localises to the cytoplasm but also accumulates at growing ends [Bühler et al., 2015a]. Such pattern of localisation is distinct from its *S. cerevisiae* homologue where kes1p localises to the cytoplasm, Golgi apparatus and exocytic vesicles [Li et al., 2002], [Alfaro et al., 2011b], [Bühler et al., 2015a].

In contrast to kes1p-GFP, **kes2p-GFP** localised the cytoplasm but, in addition, signal resembling the nuclear envelope was observed. We also saw pronounced particles, however as these were also seen in unlabelled cells they most likely represent autofluorescence **(Figure 3.19**, B).

Osh2p-GFP localised to the cytoplasm and to fluorescent particles of high intensity **(Figure 3.19**, B), however the osh2p orthologues in *S. cerevisiae* (osh1p and osh2p) localise to structures adjacent to the vacuole, Golgi and more diffusely to the bud and a bud neck [Levine, Munro, 2001], [Kvam, 2004]. osh2p orthologue in *A. nidulans* - GFP-oshAp was reported to transiently localise to the Golgi cisternae [Bühler et al., 2015a].

Osh3p-GFP expression was very low and the signal did not raise above background levels **(Figure 3.19**, A). The SPD localisation database presents osh3p-GFP as a cytoplasmically-localised protein [Matsuyama et al., 2006]. In contrast, osh3p-GFP in budding yeast localises to the cisternal part of the cortical ER [Stefan et al., 2011]. In *A. nidulans*, oshBp, the sequence homolog of osh3p, localises to several cortical particles, which were interpreted to be at the edge of the ER tubular structures [Bühler et al., 2015a].

OshEp-GFP localised to the cytoplasm but was concentrated at the cortex, (see the deconvolved image in **(Figure 3.19**, B) [Matsuyama et al., 2006]. In contrast, the GFP-oshEp orthologue in *A. nidulans* localises to several immobile particles, believed to be the peripheral ER [Bühler et al., 2015a].

Osh7p-GFP was concentrated in the nucleus, diffused in the cytoplasm and a concentrated signal was also seen at the cell cortex **(Figure 3.19**, B). Similarly, oshDp in *A. nidulans* has a diffuse cytoplasmic localisation with some concentration at the cortex (proposed to localise to cortical ER) [Bühler et al., 2015a]. In contrast, the *S. cerevisiae* osh7p orthologues osh6p and osh7p localise to the cytoplasm and accumulate at the cortex [Huh et al., 2003], [Wang et al., 2005] [Schulz et al., 2009].

Localisations of osh proteins and their presumptive homologs in budding yeast and *A. nidulans* are summarised in supplementary table (see, **Table 14**).

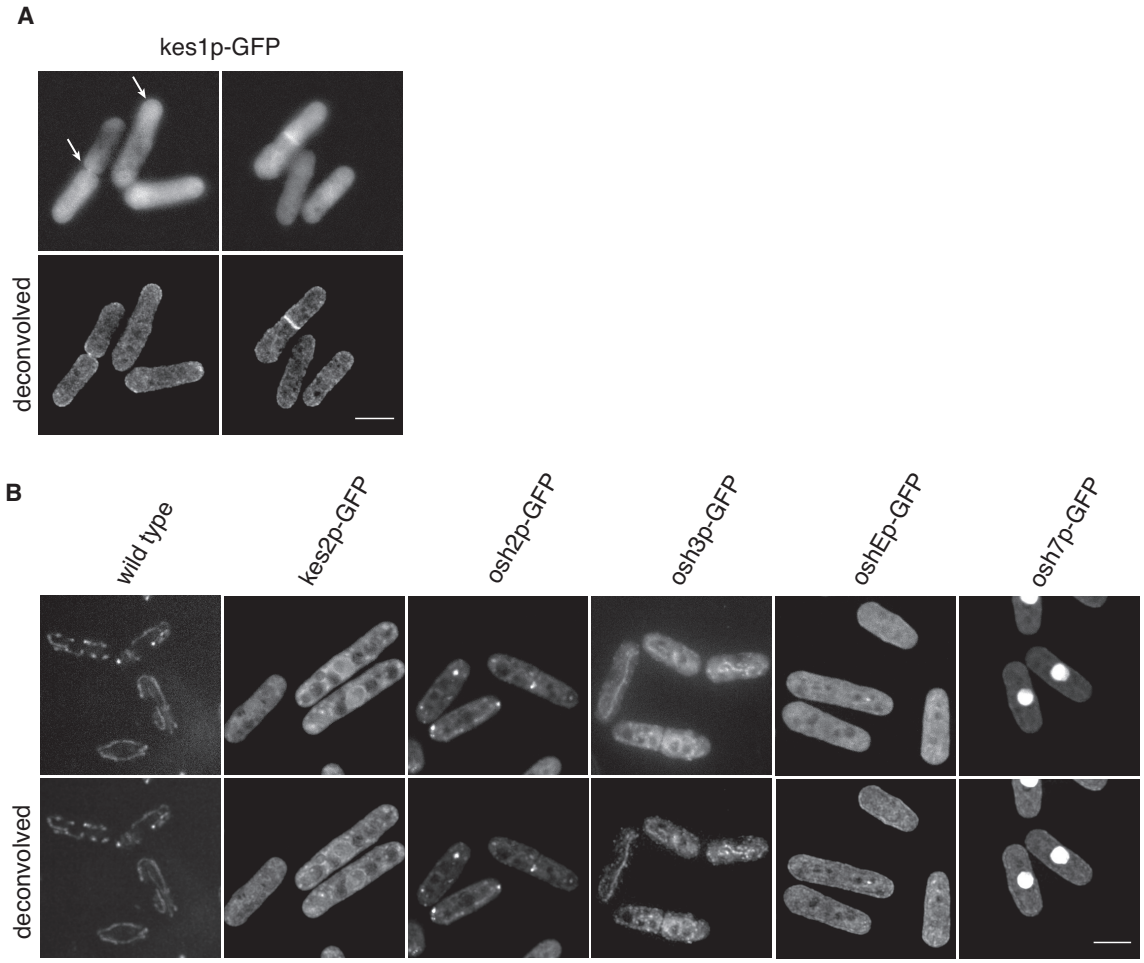

Figure 3.19: **Localisation of the GFP-tagged oxysterol-binding proteins in *S. pombe***

A - Localisation of kes1p-GFP in exponentially growing fission yeast cells. Top panel - epifluorescence microscopy pictures. Bottom - same images after deconvolution. **B** - Localisation of wild-type, kes2p-GFP, osh2p-GFP, osh3p-GFP, oshEp-GFP and osh7p-GFP in exponentially growing fission yeast cells. Top panel - spinning-disc confocal microscopy pictures. Bottom - same images after deconvolution. Max-projection of 11 z-sections (acquired at 0.5μm distance). Scale bars: 5μm.

3.2.1.2 Role of oxysterol-binding proteins in SE

As previously mentioned, *de novo* cell polarisation of fission yeast cells is not critically dependent on membrane trafficking and membrane fusion (see, **3.1**), therefore we hypothesised that lipid transfer proteins (LTPs) (working in non-vesicular transfer of lipids) might be involved in cell polarisation. Oxysterol-binding proteins (oshes) are known LTPs. Their collective removal in budding yeast causes a range of polarity phenotypes, including mis-positioning of cdc42p and membrane trafficking machineries [Kozminski et al., 2006] (see, **3.2**). Moreover, recent studies in *A. nidulans*, revealed a function for oshes in the maintenance of single growth positions [Bühler et al., 2015b]. All this suggests that oshes might play a role in the establishment of cell polarity in fission yeast cells.

We investigated *osh*Δ mutants during starvation and SE after staining with filipin. For most *osh*Δ mutants (*kes2*Δ, *osh2*Δ, *osh3*Δ and *oshE*Δ) phenotypes were mild **(Figure 3.20)**. In general, cells were slightly shorter at the 180min time-point at the end of the experiment due to reduced growth speeds in P3 and P4 **(Figure 3.21**, A). However, the two remaining osh mutants *kes1*Δ and *osh7*Δ were more severely affected in SE **(Figure 3.20)**. In starvation, *kes1*Δ and *osh7*Δ mutants retained numerous filipin-stainable punta distributed all around the cell membrane. These punctae were still present during P1 and defined shapes of SRM domains were not observed **(Figure 3.20**, B). We conclude that *kes1*Δ and *osh7*Δ have problems in the P1 entry.

After the first 60min of SE *kes1*Δ and *osh7*Δ mutants did not enter P2. Numerous dots were present; however, they were not as abundant as in the previous time-points. Additionally, SRM domains were now seen in the cell membrane **(Figure 3.20**, B, C).

Surprisingly, *kes1*Δ cells started growing between 60-120min in SE and subset of cells polarised at cell poles **(Figure 3.21**, A), **(Figure 3.20**, C). However, numerous filipin-stainable dots were present, reflected by the low rP ratio **(Figure 3.20**, A). Length increase in *osh7*Δ mutants was not statistically significant **(Figure 3.21**, A).

After 180min SE all strains including *osh7*Δ polarised their SRM domains

(Figure 3.20, B). Very small filipin-stainable dots were present in the PM of *kes1*Δ, but they were still highly abundant in *osh7*Δ **(Figure 3.20**, B). At this point *osh7*Δ cells were still barely elongating and did not increase their length by more than 0.5μm between 0 and 180min into SE **(Figure 3.21**, A). Interestingly, *osh7*Δ mutants increased their width consistently during various time-points of SE. Growth speeds changed from 0 to 0.25μm after 180min **(Figure 3.21**, B). This is similar to the observation in [Makushok et al., 2016a], where during isotropic growth of the LatB-treated cells, width was increasing by a comparable 0.2μm. Finally, we did not observe any obvious difference in the mono and bi-polar pattern of SRMs of any *osh*Δ mutant **(Figure 3.20**, B).

We conclude that the oxysterol-binding protein homologues kes1p and osh7p influence SE. kes1p and osh7p are involved in the P1 and P2 initiation. Since, there is no evidence to show that tea1p controls removal of SRM domains or their *de novo* formation, we hypothesise that osh7p and kes1p confer these functions independently from tea1p. In addition, these mutants are highly defective in P2 entry, what makes us to suggest that tea1p, in a microtubule-dependent manner, might control osh7p and kes1p in order to stabilise SRMs at cell poles. Of all the osh mutants *osh7*Δ cells show the strongest phenotypes. They cannot initiate fast growth and are barely elongating. *osh7*Δ mutants have a polarity defect because they constantly increase their width, and are growing almost isotropically. We suggest that other oshes might work on the level of secretion of cell wall components, since the only phenotypes that we detected were related to the rate of cell elongation.

Phenotypes of osh mutants are summarised in a **Table 9**. Width measurements of SRMs and their distribution, which were used for the calculation of the rP , for selected time-points during SE are included as a Supplementary figure (see, **Figure 5.6**).

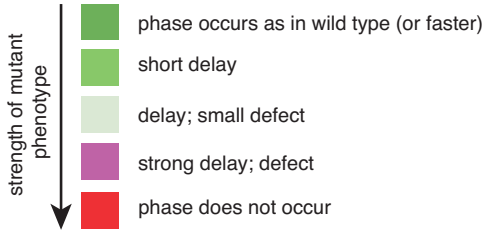

Strain name	P1	P2	P3
kes1Δ			
kes2Δ			
osh2Δ			
osh3Δ			
oshEΔ			
osh7Δ			

Table 9: **Table summarising SE after removal of oxysterol binding proteins**
The table summarises data until 180min in SE (Materials and methods, **2.2.3**).

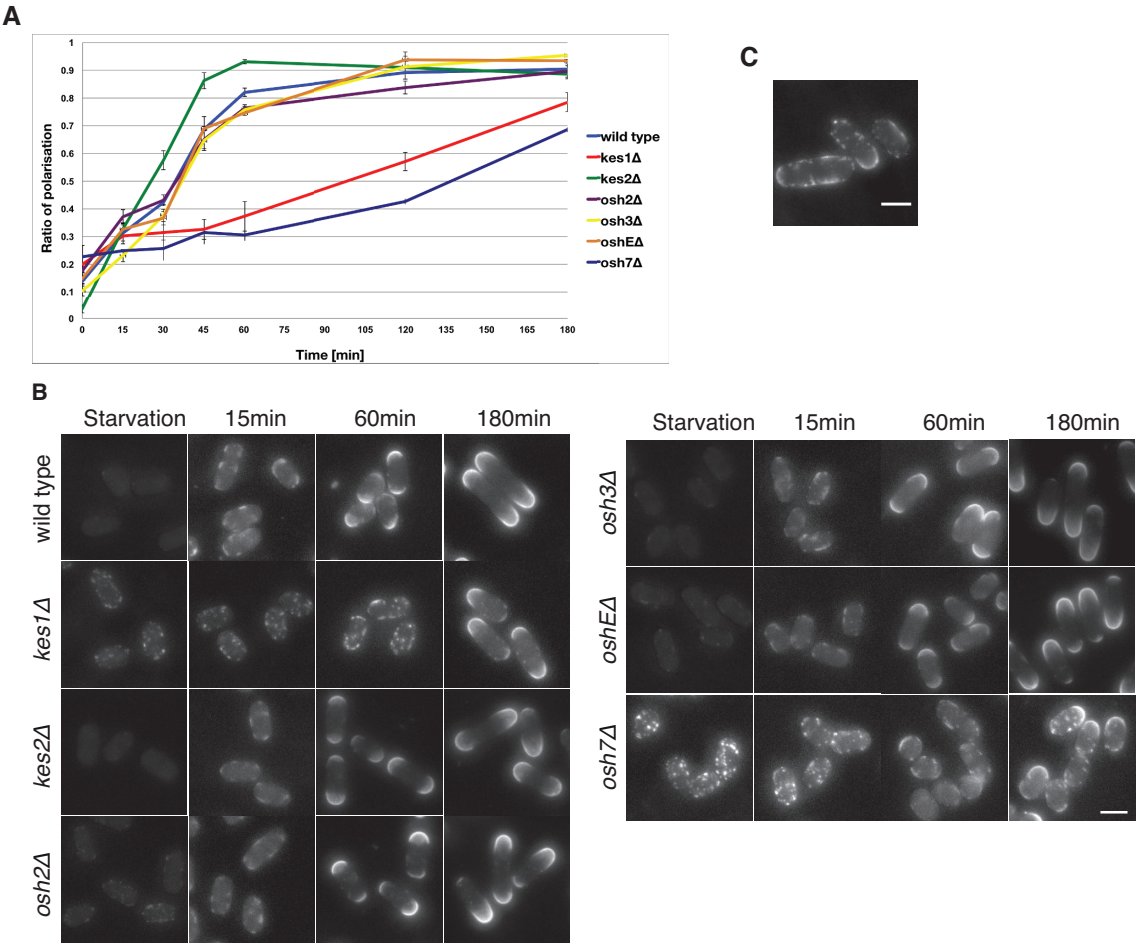

Figure 3.20: **Role of single oshes during cell polarisation**

A - Time course of average rP (Ratio of Polarisation) values for cells in SE. Each average rP was measured from mean rPs from 3 experiments (n>200 per experiment). Error bars represent the average standard deviations of mean rP values. Experiments with wild type, *kes1*Δ, *kes2*Δ, *osh2*Δ, *osh3*Δ, *oshE*Δ and *osh7*Δ were plotted. **B** - Filipin staining of wild type, *kes1*Δ, *kes2*Δ, *osh2*Δ, *osh3*Δ, *oshE*Δ and *osh7*Δ cells in starvation and during SE. Scale bar, 5μm. **C** - Filipin staining of *kes1*Δ cells 120min in starvation exit. Scale bar, 5μm.

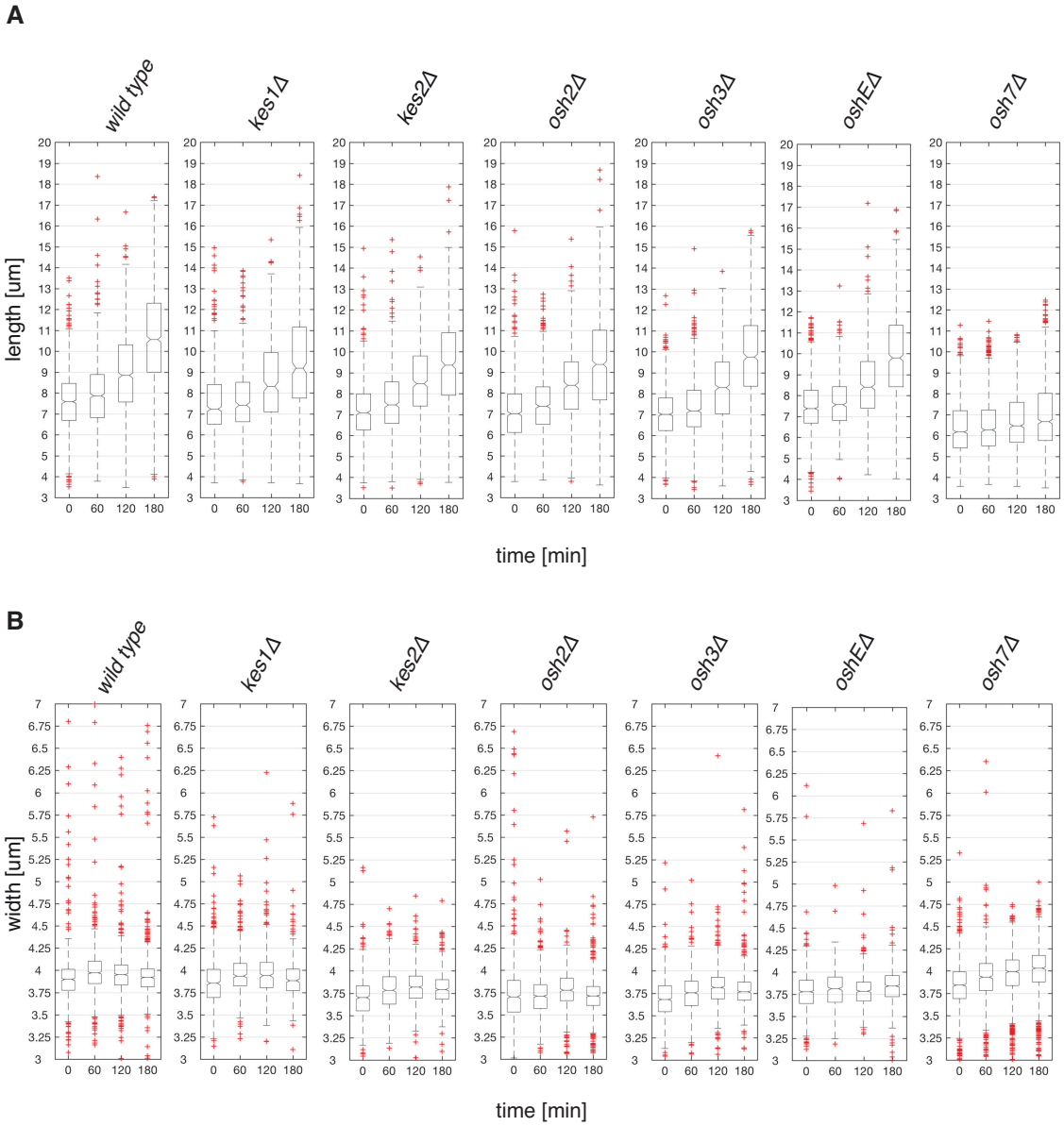

Figure 3.21: **Cell length and width of *osh*Δ mutants during SE**

A - Boxplots representing the distribution of measurements of cell length of wild type,*kes1*Δ, *kes2*Δ, *osh2*Δ, *osh3*Δ, *oshE*Δ and *osh7*Δ. Quantification of glucose starved cells (0min) and cells during SE (n>600). Notches represent 95% confidence intervals of the median. **B** - Boxplots representing the distribution of measurements of cell width of wild type,*kes1*Δ, *kes2*Δ, *osh2*Δ, *osh3*Δ, *oshE*Δ and *osh7*Δ. Quantification of glucose starved cells (0min) and cells during SE (n>600). Notches represent 95% confidence intervals of the median.

3.2.1.3 Localisation of kes1p and osh7p during SE

As described above, *kes1*Δ and *osh7*Δ mutants exhibit defects in SE (see, **3.2.1.2**). Therefore, we decided to observe their localisation during this process. In starved cells kes1p-GFP was not visible above the autofluorescence signal **(Figure 3.22**, starvation). 15min after entry into SE we observed signal at the cell cortex, which most probably represent the ER, PM or ER-PM contact sites **(Figure 3.22**). In addition, roundish structures were visible, similar to the vacuole-like structures observed in Figure 3.3. 60min into SE, the kes1p-GFP cortical signal became more pronounced and the intracellular signal was less defined and seemed to be more dispersed **(Figure 3.22**, 60min). After 180min into SE, the cortical signal of kes1p-GFP was clearly visible and, in addition, kes1p-GFP was present as a diffuse stain in the cytoplasm and the nucleus **(Figure 3.22**, 180min). In contrast to kes1p-GFP, osh7p-GFP was visible in the cell cortex in starved cells **(Figure 3.22**, starvation). We also observed a very strong signal in the cell nucleus and cytoplasmic localisation. This pattern of localisation did not visibly change for consecutive time-points of SE **(Figure 3.22)**. We conclude that both kes1p-GFP and osh7p-GFP are concentrated at the cell cortex during SE. Kes1p-GFP is not present at that region in starvation, however it appears at the cortex after entry intro SE. osh7p-GFP is present at the cortex, both during starvation and SE. Additionally, its strong signal in the nucleus might indicate a role in this organelle.

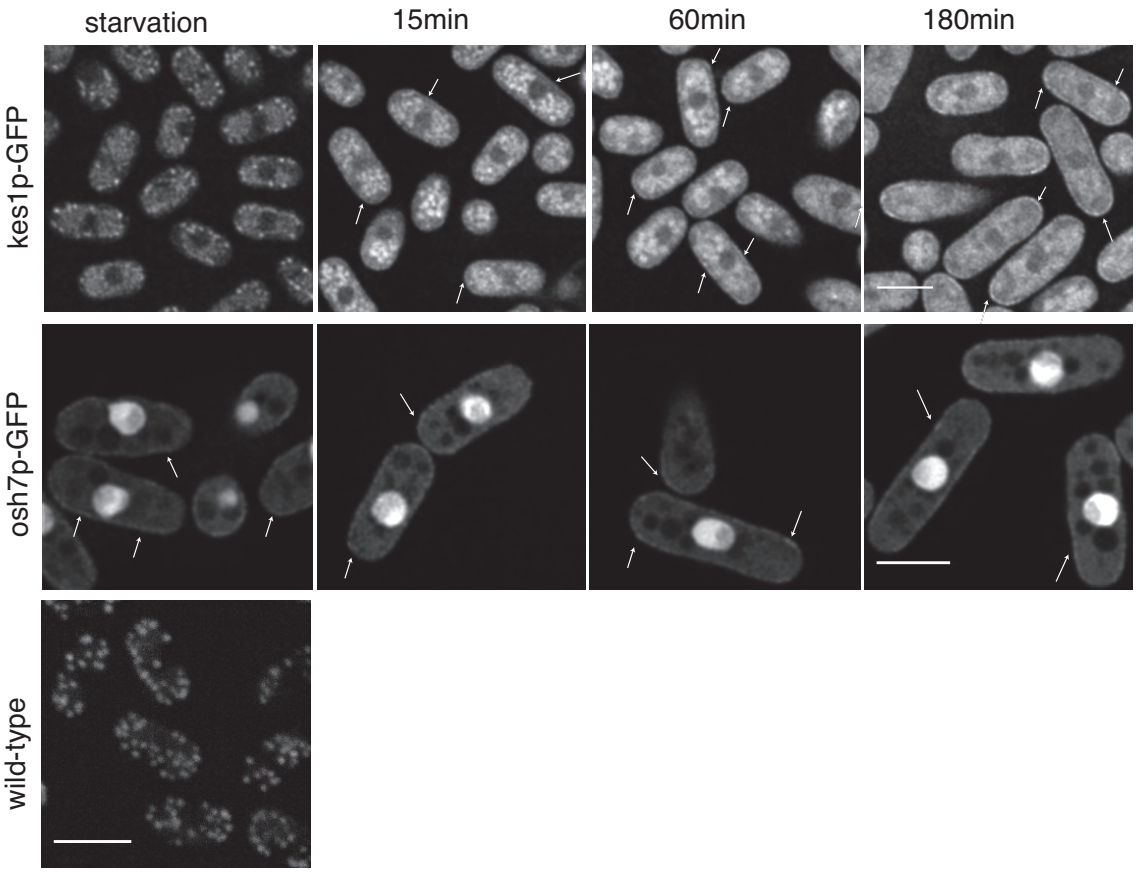

Figure 3.22: **Localisation of kes1p-GFP and osh7p-GFP during SE**

Localisation of kes1p-GFP and osh7p-GFP under their endogenous promoters during SE. Images represent deconvolved middle sections from the z-stacks. Time-scale presents time in SE. Arrows point on positions with cortical accumulation. Pictures are max-projections of 11 z-sections (acquired in 0.5μm distance). Not deconvolved data and max projections are available in Supplementary figures section (see, **Figure 5.7**). Wild-type control acquired in the same imaging conditions as kes1-GFP and osh7p-GFP. Scale bars: 5μm.

3.2.1.4 Combinatorial effects of removal of multiple oxysterol-bindings proteins

Collectively, the osh proteins in *S. cerevisiae* are involved in bud formation, endocytosis and affect intracellular sterol distribution, the maintenance of polarised growth by regulating membrane trafficking, cdc42p localisation, and septin ring polarisation and assembly [Kozminski et al., 2006]. Double mutants of *kes1* with other osh genes, showed the most severe phenotypes in budding yeast [Beh et al., 2001]. Our studies reveal that *kes1*Δ in *S. pombe* is involved in sterol removal and formation of SRM domains. Therefore, we decided to create double mutants between *kes1*Δ mutants and deletions of the other *osh* genes.

We obtained the double mutants *kes1*Δ*kes2*Δ, *kes1*Δ*osh3*Δ, *kes1*Δ*oshE*Δ and *kes1*Δ*osh7*Δ. Interestingly, we were not able to obtain *kes1*Δ*osh2*Δ. The mating between *kes1*Δ and *osh2*Δ resulted in irregular tetrads with only 1 or 2 spores **(Figure 3.23**, C). Therefore, we decided to shut-off *kes1* expression (by the thiamine-represable *81nmt1* promoter) in the background of an *osh2*Δ deletion (hereafter named *kes1-shut off osh2*Δ).

15min from the start of SE, double mutants did not form SRMs and looked similar to *kes1*Δ, except *kes1*Δ*osh3*Δ, which was able to build defined SRM domains **(Figure 3.23**, B, 15min). The double *osh* mutants were not polarised at 60min into SE **(Figure 3.23**, B, 60min), although SRM-domains started being visible in most of the strains. The exception was *kes1*Δ*osh7*Δ, where filipin dots were so numerous that we were not able to state if additional SRM domains were forming. *kes1*Δ*osh3*Δ was the only double mutant where filipin dots were not detected **(Figure 3.23**, B). The filipin signal for *kes1*Δ*osh3*Δ and *kes1*Δ*kes2*Δ became surprisingly low **(Figure 3.23**, B). Such behaviour suggests an instability in the delivery of ergosterol to the PM. The rP ratios for all the mutants were very variable until this stage **(Figure 3.23**, B), (Materials and methods, **2.2.2.2.6**).

120min into SE, most double mutants of *kes1* significantly increased their rP ratios, which suggests that they started to enter P2. The rP values for double mutants were

higher than for single *kes1*Δ, what suggests that they might enter P2 faster, or contain lower amounts of filipin dots **(Figure 3.23**, A), (Materials and methods, **2.2.2.2.6**). The exception was the rP ratio of *kes1*Δ*osh7*Δ, which did not significantly change compared to the previous time-points **(Figure 3.23**, A). We think there were no signs of polarisation in this strain.

At 180min into SE, rP ratios increased for all the mutants. As predicted the rP for *kes1*Δ*osh7*Δ did not change much and the rP ratio for *kes1*Δ*osh3*Δ was the highest among the *kes1* mutants **(Figure 3.23**, A, 180min). Most *kes1*Δ double mutants were polarised, except *kes1*Δ*osh7*Δ **(Figure 3.23**, A, B, 180min). In this mutant we observed many filipin dots in the PM and only occasionally shapes of SRM domains **(Figure 3.23**, B, 180min).

Regarding change in cell length between 120-180min, only *kes1*Δ*osh7*Δ mutants did not enter P3 **(Figure 3.24**, A). Instead they increased their width **(Figure 3.24**, B). In contrast, in *kes1*Δ*kes2*Δ and *kes1*Δ*osh3*Δ mutants, growth speeds were significantly higher between 120-180min in SE than for the single *kes1*Δ **(Figure 3.24**, A).

Interestingly, *kes1-shut off osh2*Δ had a defect in SRM formation (many filipin dots and occasionally present SRMs with abnormal shapes) at 15min in SE **(Figure 3.23**, B). Later, SRMs defined formed but the mutant was strongly delayed in cell polarisation **(Figure 3.23**, A, B) comparing to the wild-type. Even after P2 initiated, cells had defect in removal of SRMs from cell sides **(Figure 3.23**, B, 180min). This mutant did not initiate P3 until 180min in SE **(Figure 3.24**, A).

Summarising, *kes1*Δ*osh7*Δ mutants did not readily polarise and did not initiate polarised growth. In contrast, *kes1*Δ*osh3*Δ showed an almost wild-type phenotype.

The *osh7* deletion had strong defect in all the phases of SE and in combination with the *kes1*Δ mutation these defects were increased. Therefore, we decided to investigate

double mutants of *osh7*Δ with deletions of other *osh* homologs.

Combinatorial effects of double mutants between *osh7*Δ with deletions of other oshes displayed weaker or similar phenotypes than single *osh7*Δ (except *osh7*Δ*kes1*Δ, which was described before). In general, *osh7*Δ*kes2*Δ, *osh7*Δ*osh2*Δ and *osh7*Δ*osh3*Δ were more similar to wild-type strain, however *osh7*Δ*oshE*Δ looked more similar to single *osh7*Δ. These observations are reflected in the rP ratios and corresponding pictures **(Figure 3.25**, A, B).

Surprisingly, double mutants of *osh7*Δ did not have as large amount of filipin dots when compared to a single *osh7*Δ and the double mutant *kes1*Δ*osh7*Δ **(Figure 3.25**, B). These observations are summarised in the corresponding histograms, which highlight the abundance of side filipin dots in the PM of particular mutants **(Figure 5.9**, starvation). Moreover, in contrast to *osh7*Δ and *kes1*Δ*osh7*Δ other double mutants displayed more or less defined SRM domains after 15min in SE **(Figure 3.25**, B). To our surprise, *osh7*Δ*osh3*Δ mutant significantly elongated in between 0-60min **(Figure 3.26**, A). We have not observed such high growth speed at this stage of SE in any of the strains described before.

After 180min the rP ratio of all the double *osh7*Δ mutants increased. The rP of *osh7*Δ*oshE*Δ mutant was very similar to the single *osh7*Δ **(Figure 3.25**, A), (Materials and methods, **2.2.2.2.6**). This can also be noticed visually by comparing the corresponding filipin stainings **(Figure 3.25**, B). The *osh7*Δ*oshE*Δ mutant had fewer fiipin dots in the PM, explaining why the rP ratio for *osh7*Δ*oshE*Δ was marginally higher than for single *osh7*Δ mutant **(Figure 3.25**, A, B). Similar to *osh7*Δ and *osh7*Δ*kes1*Δ mutants, *osh7*Δ*oshE*Δ mutants did not initiate the fast growth. In contrast, other double mutants of *osh7*Δ entered P3 between 120-180min into SE.

Our data suggest that osh7p function opposes other osh proteins. Deletions of *oshes* (except of *kes1*Δ) can rescue single *osh7*Δ phenotypes to different extents. Deletion of *osh3* has the highest rescue potential and other deletions have lower rescue potential: *osh2*Δ, *kes2*Δ and *oshE*Δ, respectively.

We summarise that similar to budding yeast, *osh* genes in *S. pombe* share overlapping functions. We see that different *osh* genes interact with each other. *kes1* and *osh7* work together in the establishment of the cell polarity. In contrast *kes2*Δ, *osh2*Δ, *osh3*Δ and *oshE*Δ rescue the mutant phenotype of *osh7*Δ. In addition, *kes2*Δ, *osh3*Δ and *oshE*Δ rescue *kes1*Δ. Their rescue potential varies for both *osh7* and *kes1*. We speculate that mechanism of rescue involves the faster removal of filipin dots from the PM, either by not allowing for their formation during glucose starvation in the first place, or their faster removal during SE.

Combined information about phases of SE in the double mutants of *osh7*Δ and *kes1*Δ are presented as a (see, **Table 10**). Width measurements of polar and side SRMs are included as a supplementary figure (see, **Figure 5.8**).

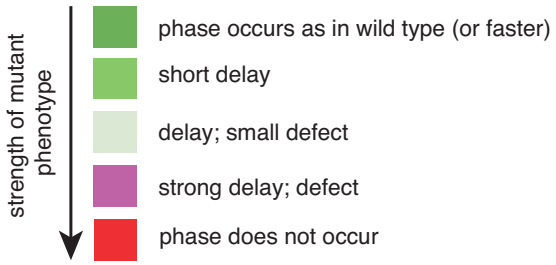

Strain name	P1	P2	P3
Deletion of oxysterol-binding proteins			
kes1Δ			
kes2Δ			
osh2Δ			
osh3Δ			
oshEΔ			
osh7Δ			
Combinations between *kes1Δ* and other *oshΔ*			
kes1Δkes2Δ			
kes1Δosh3Δ			
kes1ΔoshEΔ			
kes1Δosh7Δ			
kes1 shut-off osh2Δ			
Combinations between *osh7Δ* and other *oshΔ*			
osh7Δkes1Δ			
osh7Δkes2Δ			
osh7Δosh2Δ			
osh7Δosh3Δ			
osh7ΔoshEΔ			

Table 10: **Table summarising SE after in single and double deletions of osh proteins** The table summarises data until 180min in SE (Materials and methods, **2.2.3**).

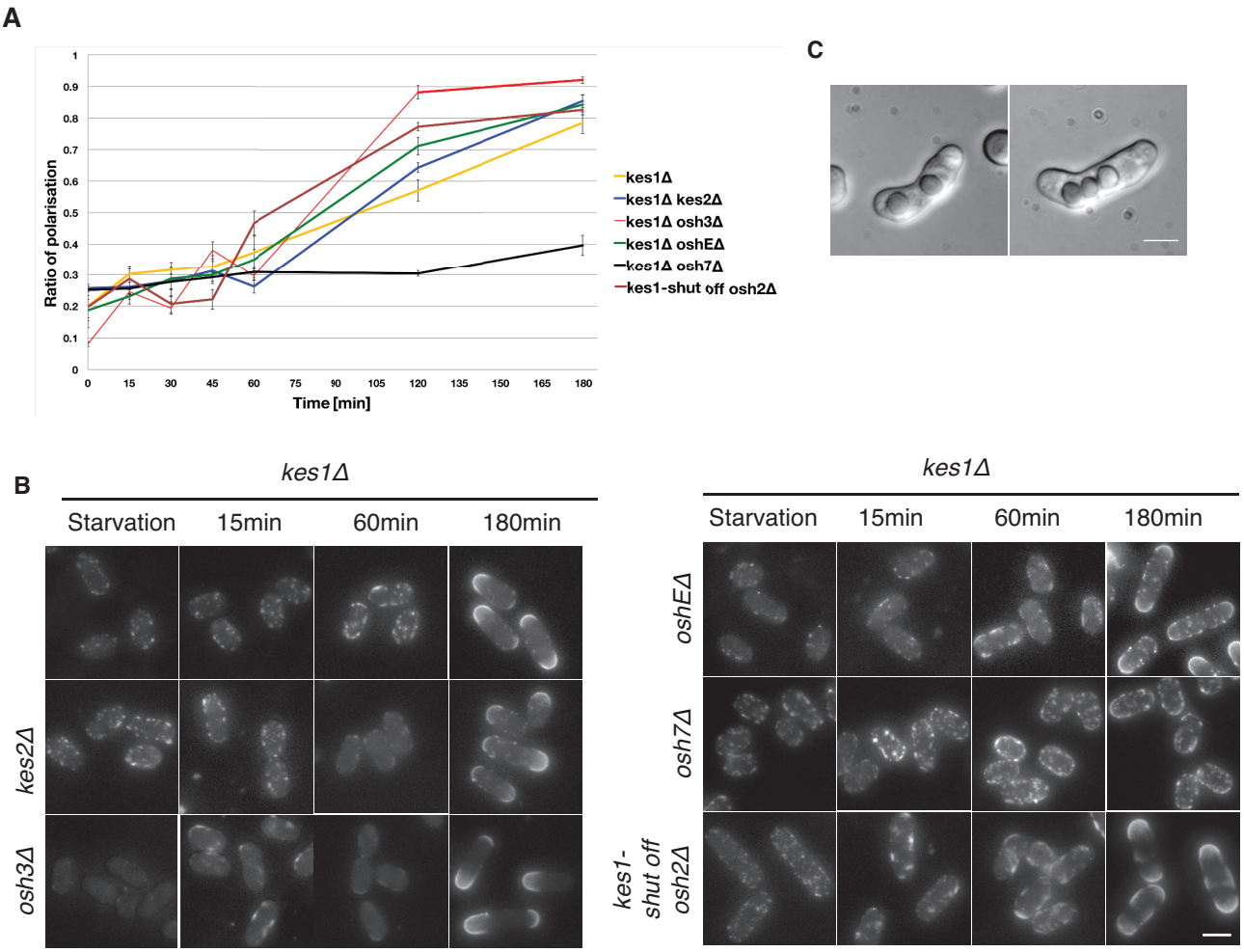

Figure 3.23: **Phenotypes of double mutants of *kes1* with other *osh* mutants in cell polarisation**

A - Time course of average rP (Ratio of Polarisation) values for cells in SE. Each average rP was measured from mean rPs from 3 experiments (n>200 per experiment). Error bars represent the average standard deviations of mean rP values. **B** - Filipin staining of double *kes1*Δ*osh*Δ mutants. Scale bar, 5μm. **C** - Sporulation after mating between *kes1* and *osh2*. DIC pictures. Average projections from 11 z-sections. Scale bar, 5μm.

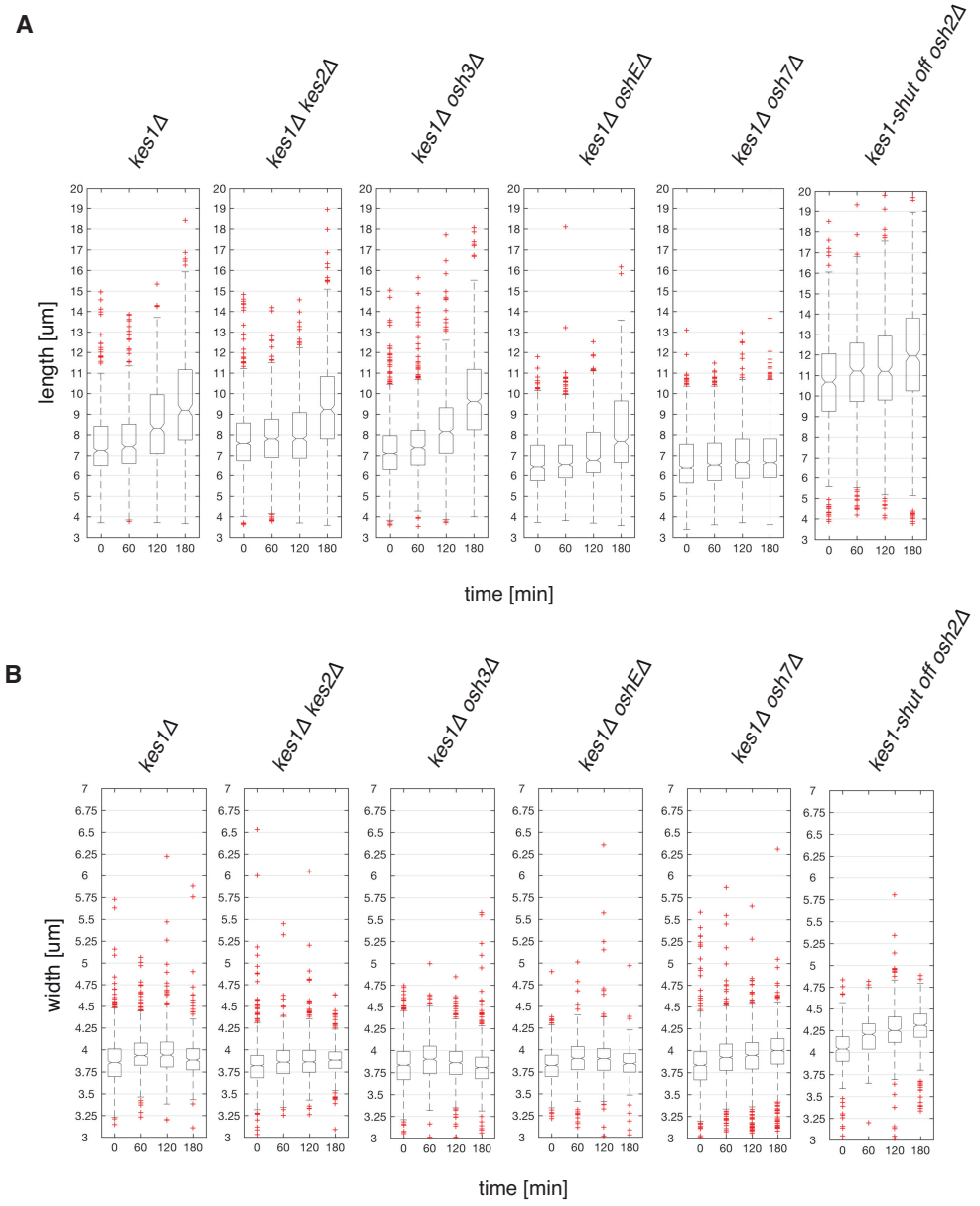

Figure 3.24: **Cell length and width during SE of double mutants of *kes1* with other *osh* mutants**

A - Boxplots representing the distribution of cell length. Quantification of glucose starved cells (0min) and cells during SE (n>600). Notches represent 95% confidence intervals of the median. **B** - Boxplots representing the distribution of cell width. Quantification of glucose starved cells (0min) and cells during SE (n>600). Notches represent 95% confidence intervals of the median.

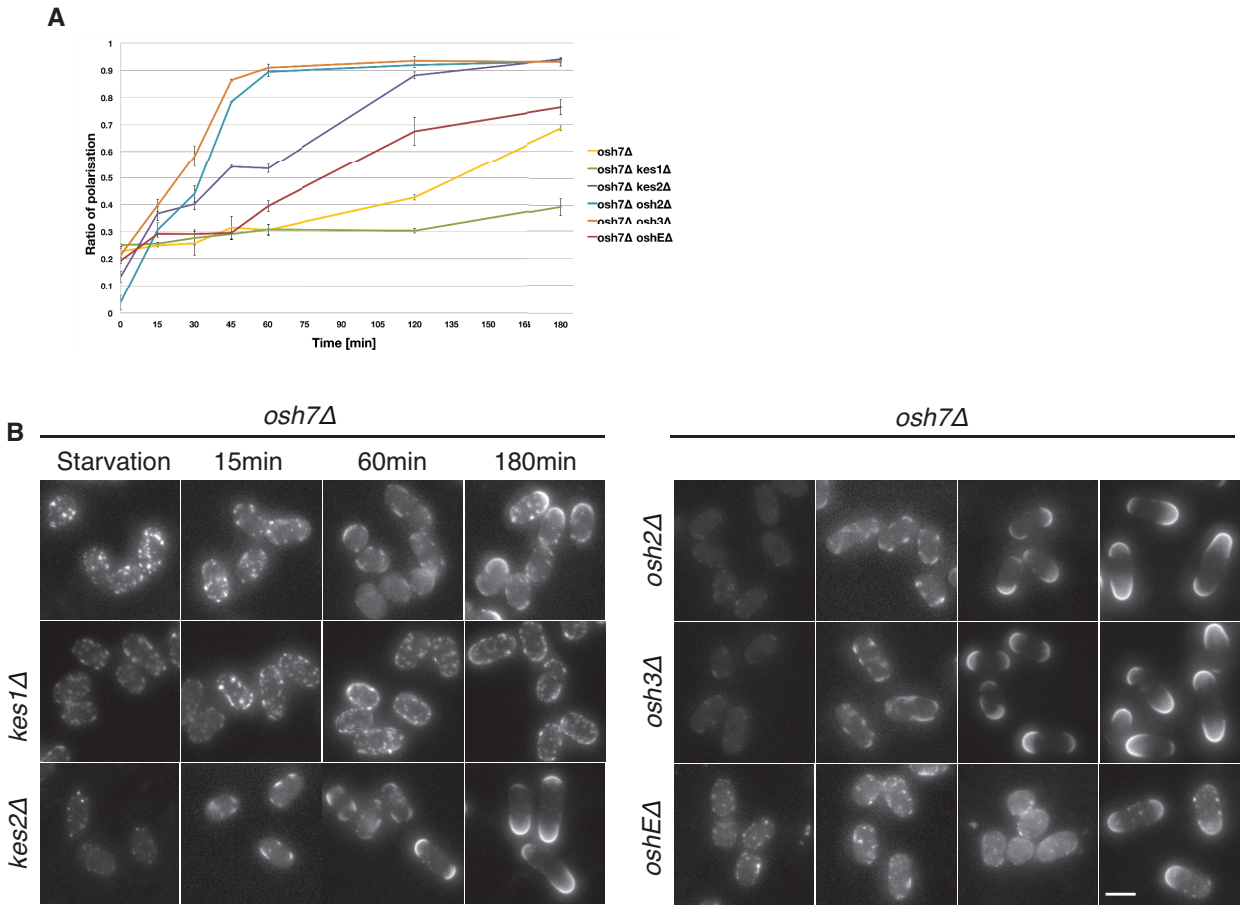

Figure 3.25: **Role of double mutants between *osh7* and other *osh* deletions in cell polarisation**

A - Time course of average rP values for cells in SE. Each average rP was measured from the mean rPs from 3 experiments (n>200 per experiment). Error bars represent the average standard deviations of the mean rP values. **B** - Filipin staining of double $osh7\Delta osh\Delta$ mutants. Scale bar, 5μm.

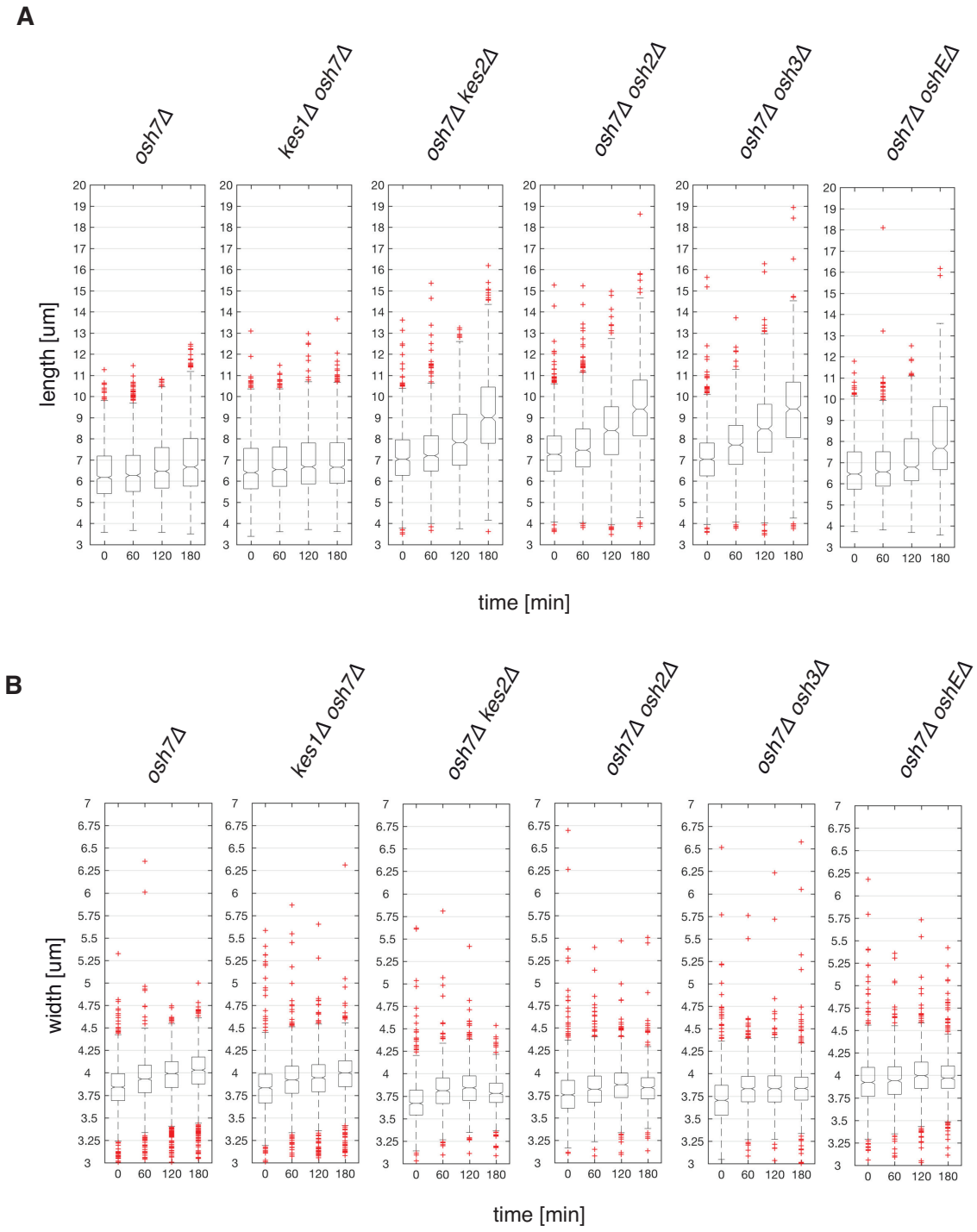

Figure 3.26: **Cell length and width increase during SE of double mutants between *osh7* and other *osh* deletions**

A - Boxplots representing the distribution of cell length. Quantification of glucose starved cells (0min) and cells during SE (n>600). Notches represent 95% confidence intervals of the median. **B** - Boxplots representing the distribution of cell widths. Quantification of glucose starved cells (0min) and cells during SE (n>600). Notches represent 95% confidence intervals of the median.

3.2.1.5 *kes1*Δ*osh7*Δ initiates polarised growth after several hours in SE

Since the *kes1*Δ*osh7*Δ double mutant was not polarised at 180min into SE, we decided to follow its behaviour during later time-points of SE. We observed that the rP ratio was constantly increasing and reached around 0.67 after 360min of SE **(Figure 3.27**, A). At this time-point most wild-type cells had already divided (**Table 3**).

After 240min in SE, filipin dots in *kes1*Δ*osh7*Δ were still present, although defined SRM domains at cell poles became brighter than the dots **(Figure 3.27**, B). After 300min in SE the pattern of filipin staining did no longer significantly changed. In addition, the pool of polar SRMs shifted towards larger widths, indicating that polar SRMs were growing **(Figure 3.27**, B, C).

We measured cell length and width and observed that between 180-240min in SE the mutant slightly increased its length and increased its speed of growth in this dimension from 0.2 to 0.45μm/h **(Figure 3.27**, D). We did not observe a significant change in its width **(Figure 3.27**, D). Between 240-300min in SE neither significant change in length, nor in width was detected. Unexpectedly, between 300-360min in SE *kes1*Δ*osh7*Δ cells initiated fast elongation (1.1μm/h). At this time-point we also detected a small change in width, most probably a consequence of still present filipin dots **(Figure 3.27**, B, D). We conclude that *kes1*Δ*osh7*Δ is able to enter P2 and P3, however these phases are strongly delayed.

Our data further suggest that kes1p and osh7p collectively contribute to the establishment of the cell polarity and both proteins are involved in SRM formation. We hypothesise that tea1p controls both proteins to ensure the proper timing of stabilisation of SRMs at the cell poles.

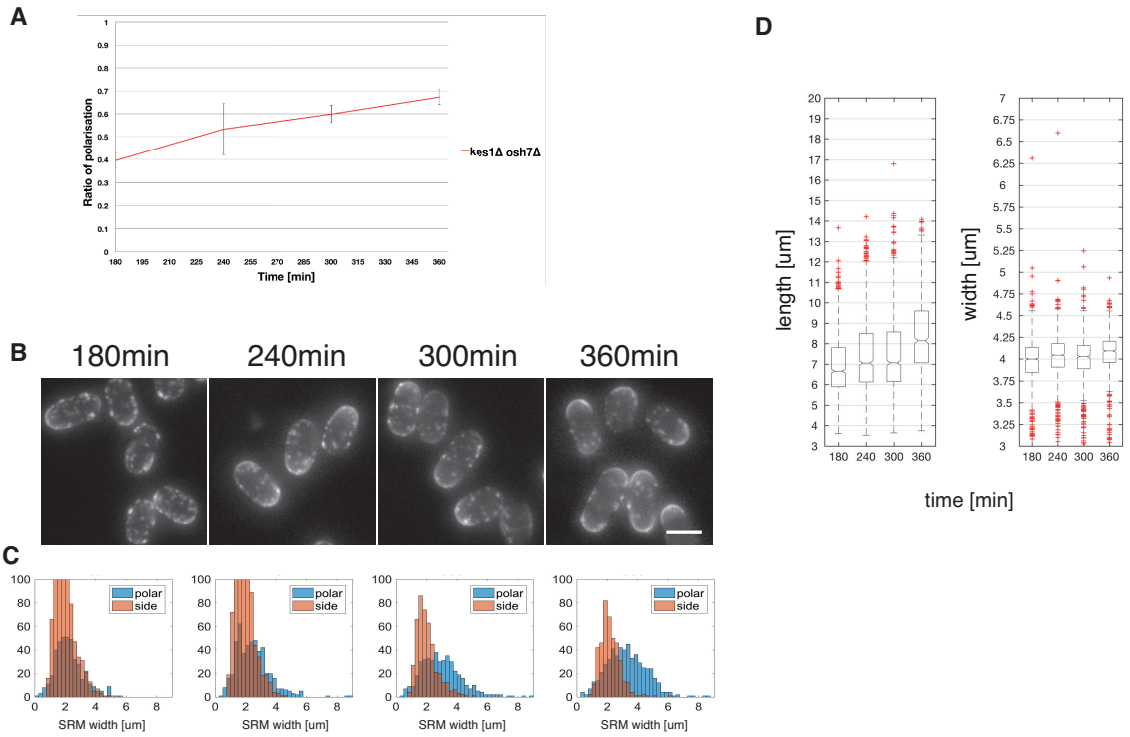

Figure 3.27: **Double mutant *kes1*Δ*osh7*Δ during later time-points of SE**

A - Time course of average rP (Ratio of Polarisation) values for *kes1*Δ*osh7*Δ mutants in SE. The average rP was measured from the mean rPs from 3 experiments (n>200 per experiment). Error bars represent the average standard deviations of mean rP values.
B - Filipin staining of *kes1*Δ*osh7*Δ cells between 180min-360min of SE. Scale bar, 5μm.
C - Classification of polar (blue) and side (orange) SRMs for different time-points of SE. Histograms showing count normalised distribution of SRM width (μm). Plots represent subsequent time-points of SE. Quantification was performed as described in Materials and methods (see, **2.2.2.2**).
D - Boxplots representing the distribution of cell length and cell width of *kes1*Δ*osh7*Δ (n>600). Notches represent 95% confidence intervals of the median.

3.2.1.6 cdc42p activity is required for P3. In the absence of kes1p, cells need the active cdc42p to stabilise SRMs at cell poles

Previously, we showed that *kes1*Δ and *osh7*Δ are delayed in P2 entry (see, **3.2.1.2**). This suggests a role for oshes in the tea1p-dependent entry into P2. MT/tealp system controls polar cdc42p activation at the onset of P2 in SE [Makushok et al., 2016b]. Previous studies on temperature-sensitive alleles of *cdc42* (*cdc42-L160S* and *cdc42-879* [Rincon et al., 2009], [Toya et al., 1999]) revealed that the MT/tealp-mediated cell polarisation pathway does not act via cdc42p [Makushok et al., 2016b]. These moderate cdc42 mutants were able to initiate P3 and P4 and even enter mitosis and perform cytokinesis [Makushok et al., 2016b]. Although, it was suggested that cdc42p activity might become central in *tea1*Δ cells, which remain in P1 for prolonged time periods [Makushok et al., 2016b]. We wondered if the delayed polarisation in *kes1*Δ and *osh7*Δ mutants was dependent on cdc42p. We studied double mutants defective both in cdc42p and kes1p/osh7p.

In order to strengthen our experiments we used *cdc42-3* mutant, which has a stronger polarity phenotype [Tatebe et al., 2008]. These cells were significantly shorter and much wider (around 1μm) in starvation than a control cells (**Figure 3.29**, A, B). It is likely that this effect is the result of hypomorphic features of the strain [Tatebe et al., 2008]. Double mutants *cdc42-3kes1*Δ and *cdc42-3 osh7*Δ were similar to the single *cdc42-3* in this term (**Figure 3.29**, A, B). As expected *cdc42-3osh7*Δ had numerous filipin dots in the PM (similar to single *osh7*Δ mutants) (**Figure 3.28**, B). Surprisingly, filipin dots in *cdc42-3kes1*Δ mutants were not as numerous as in the single *kes1*Δ cells (**Figure 3.28**, B), (**Figure 3.20**, B).

Wild-type cells and the *cdc42-3* mutant started entering P2 after 60min of SE, however on average the *cdc42-3* was visibly delayed and the rP ratio was lower than for the wild-type cells (**Figure 3.28**, A, B), (see Materials and methods, **2.2.2.2.6**). In addition SRM domains, detected at cell poles, were not significantly brighter than still present side SRMs (**Figure 3.28**, B). At this time-point *cdc42-3osh7*Δ did not

enter P1 and large number of filipin dots were present (**Figure 3.28**, B). In contrast, *cdc42-3kes1*Δ entered P1. These cells built defined and strongly fluorescent SRM domains, however they were rare and present mostly on one side of the cell (**Figure 3.28**, B). As expected the rP ratios for this mutant were significantly lower than for a wild-type and the single *cdc42-3* (**Figure 3.28**, A).

180min after the start of SE, wild-type cells were already in P3 (**Figure 3.29**, A, B). In contrast, *cdc42-3* entered P2. This is confirmed by the high rP ratio, scoring above 0.8 (**Figure 3.28**, A). Additionally, a weak signal of filipin was sometimes present at cell sides (**Figure 3.28**, B). *cdc42-3osh7*Δ behaved similar to the single *cdc42-3*, although we observed numerous additional filipin dots (**Figure 3.28**, B). The rP ratio was high and scored even higher than for the single *osh7*Δ (**Figure 3.28**, A). Similar to *osh7*Δ mutants, *cdc42-3osh7*Δ cells did not significantly elongate in either length nor or width during the first 180min of SE (**Figure 3.29**, A, B), (**Figure 3.21**, A, B). Also *cdc42-3* single mutants did not enter P3 until 180min in SE but were increasing their width (**Figure 3.29**, A, B).

*cdc42-3kes1*Δ double mutants also increased their width similar to single *cdc42-3* mutants (**Figure 3.29**, B). In these cells, strongly fluorescent side SRM domains were very prominent. Most cells contained only one big SRM at the cell side. We could not detect SRMs at cells poles. None of cells were able to polarise at cell poles (**Figure 3.28**, B). In contrast to a single *kes1*Δ mutant, filipin dots were not visible in these cells (**Figure 3.28**, B), (**Figure 3.20**, B). This phenotype was similar to that seen in a *tea1*Δ mutant. We interpret these observations as *cdc42-3kes1*Δ mutants not being able to stabilise SRMs at cell poles and initiate a second SRM at the opposite end. In contrast to *tea1*Δ, *cdc42-3kes1*Δ mutants did not visibly growth.

To evaluate if this phenotype is also present at permissive temperature, we studied *cdc42-3kes1*Δ cells at 25 °C. These cells behaved like single *cdc42-3* mutants at restrictive temperature (**Figure 3.28**, B, C). We did not observe numerous filipin dots as in the single *kes1*Δ mutant (**Figure 3.28**, C), (**Figure 3.20**, B). *cdc42-3 kes1*Δ mutants at permissive temperature entered P1 after 60min of SE. They were delayed

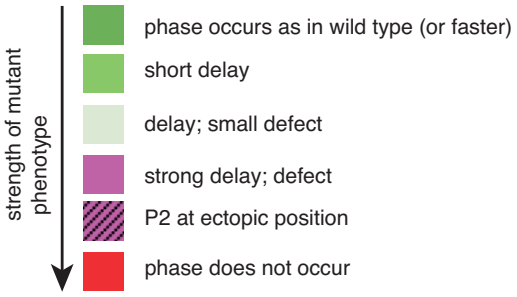

Strain name	P1	P2	P3
osh7Δ			
kes1Δ			
cdc42-3			
cdc42-3 kes1Δ			
cdc42-3 osh7Δ			

Table 11: **Table summarising phases of SE in kes1Δ osh7Δ and cdc42-3Δ mutants and in the double mutants of cdc42 and oshΔ**
The table considers data until 180min in SE (Materials and methods, 2.2.3).

in the P2 entry but were visibly polar after 180min. However, cells were clearly more elongated than single *cdc42-3* at restrictive temperature. (**Figure 3.28**, B, C) This is probably due to the increased activity of the cdc42p GTPase domain and its higher potential in determining cell width. We also made sure that the *kes1*Δ single mutants behaved in a similar way at these temperatures, therefore excluding a role for the *kes1*Δ mutation on the observed phenotypes (**Figure 3.28**, D).

We wanted to see if the *cdc42-3kes1*Δ mutant is able to polarise during later time-points of SE. We imaged these cells between 300-480min after the start of SE and observed that the mutant was still not able to accumulate strong SRMs at cells poles within this time. Strong fluorescent side SRMs were present in most of the cells. Often, these SRMs were forming invagination-like structures, similar to filipin signal during cytokinesis (**Figure 3.28**, E, F). These SRM domains were often placed in the cell middle while cells seemed to start entering division (**Figure 3.28**, E).

We propose that in the absence of kes1p, cells need the active cdc42p in order to stabilise SRMs at cell poles and to enter P3.

Summarised information about phases of SE in the described mutants of *cdc42* are presented in a **Table 11**. Width measurements of polar and side SRMs are included as a supplementary figure (see, **Figure 5.10**).

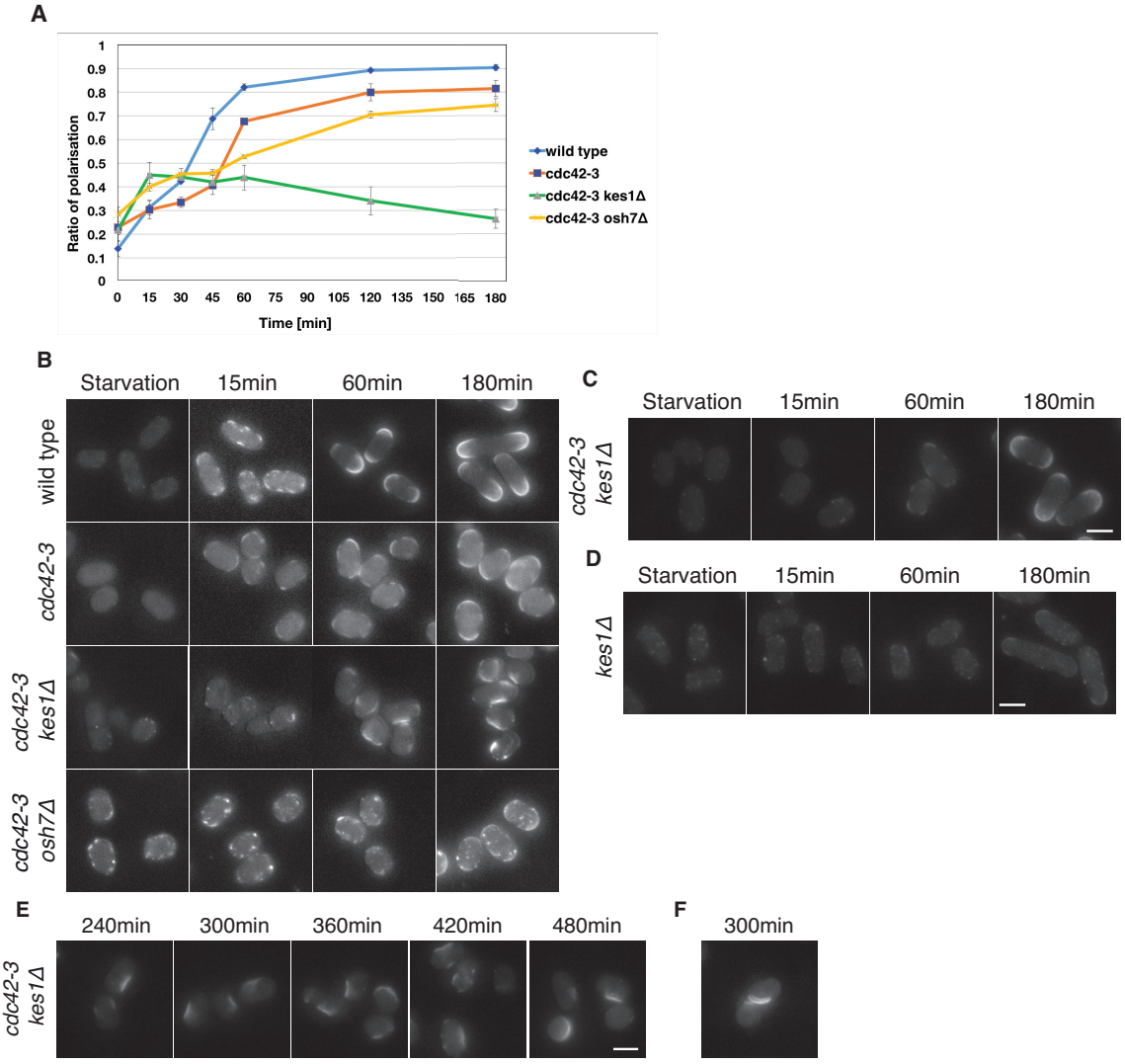

Figure 3.28: **Genetic interaction between *cdc42*, *kes1* and *osh7* during SE**

A - Time course of average rP (Ratio of Polarisation) values for cells in SE. Each average rP was measured from mean rPs from 3 experiments (n>200 per experiment). Error bars represent the average standard deviations of mean rP values. **B** - Filipin staining of wild-type, *cdc42-3*Δ, *cdc42-3kes1*Δ and *cdc42-3*Δ*osh7*Δ, cells in starvation and during SE. Scale bar, 5μm. **C** - Filipin staining of *cdc42-3kes1*Δ in starvation and during SE at permissive temperature. **D** - Filipin staining of *kes1*Δ in starvation and during SE at 36 °C. **E** - Filipin staining of *cdc42-3kes1*Δ during later time-points of SE at restrictive temperature. **F** - Filipin staining of example dividing *cdc42-3kes1*Δ mutant 300min in SE.

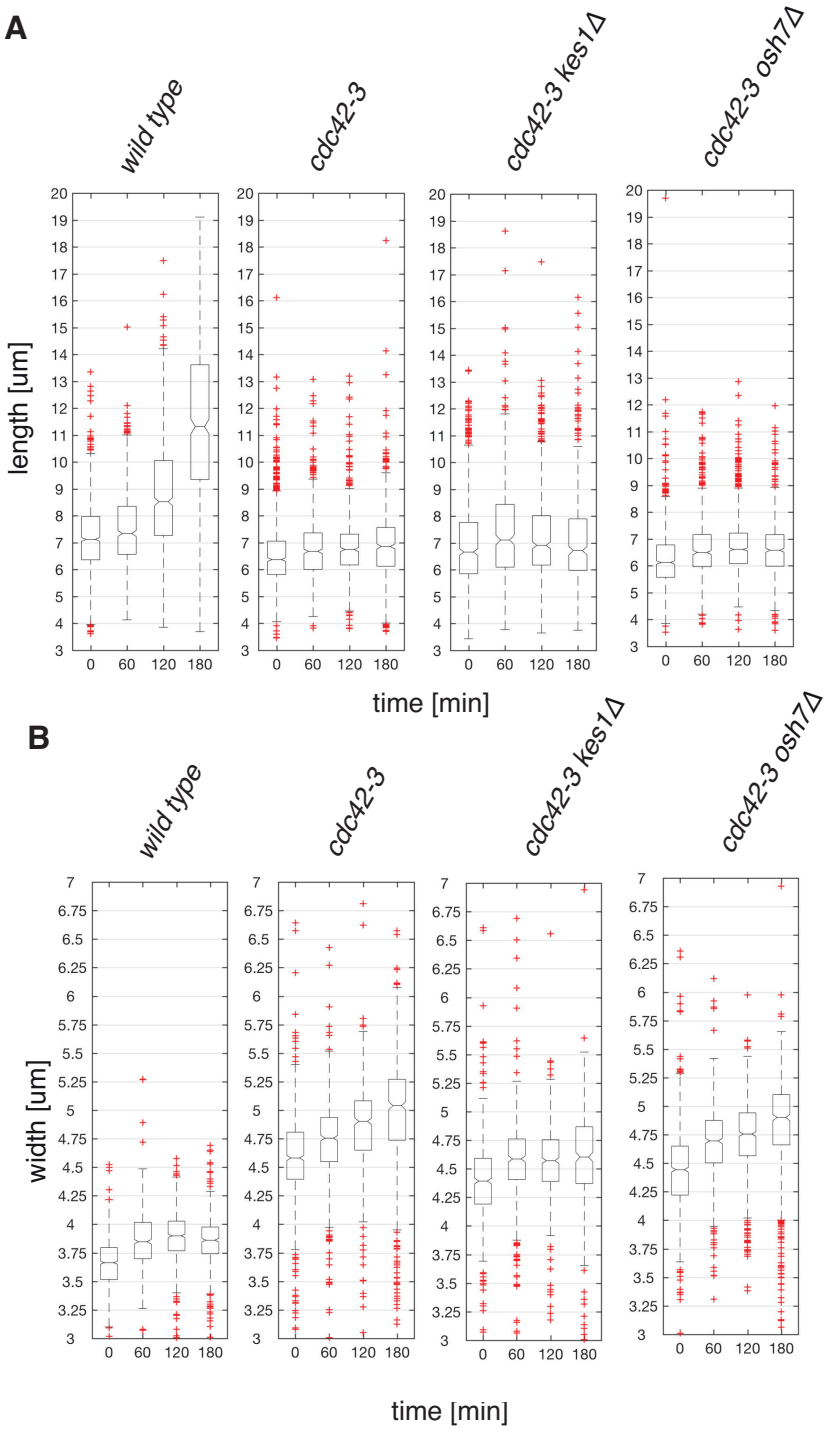

Figure 3.29: **Cell length and width during SE of double mutants between *cdc42-3*, two *osh* deletions - *kes1* and *osh7***

A - Boxplots representing the distribution of measurements of cell length. Quantification of glucose starved cells (0min) and cells during SE (n>600). Notches represent 95% confidence intervals of the median. **B** - Boxplots representing the distribution of measurements of cell width. Quantification of glucose starved cells (0min) and cells during SE (n>600). Notches represent 95% confidence intervals of the median.

3.3 Role of phosphatidylinositol kinases and ER-shaping proteins in cell polarisation

3.3.1 PI(4)P is essential for cell polarisation

We propose that in fission yeast, *de novo* formation of SRMs and their polarisation is regulated by two lipid-transfer proteins: kes1p and osh7p. Structural analysis of kes1p and osh7 protein sequence homologs in budding yeast revealed that both have a similar lipid binding motifs, however detailed analysis showed that minor sequence differences determine their specificity for either ergosterol or a phosphoserine [Im et al., 2005], [Maeda et al., 2013]. We can only speculate if such differences extend to the fission yeast orthologues as well. In addition, *in vitro* studies of oxysterol binding-proteins (both from budding yeast and mammalian cells) revealed their highly conserved property to bind Phosphatidylinositol 4-phosphate (PI(4)P) [Saint-Jean de et al., 2011b]. Oshes can bind specific lipids and PI(4)P in a mutually exclusive manner [Saint-Jean de et al., 2011b], [Drin et al., 2016]. This feature gives insight into the mechanism of regulation of the directional movement of lipids and their asymmetric distribution. A recent model proposes how kes1p exchanges ergosterol and PI(4)P between the ER and the trans-Golgi network [Filseck Moser von et al., 2015b]. A similar mechanism was proposed for the transport of phosphoserine between the ER and the PM [Filseck Moser von et al., 2015a], [Chung et al., 2015]. Both include extraction of the lipid of interest from the ER, its exchange with PI(4)P at the opposing membrane and the offloading of PI(4)P back at the ER. Maintenance of this gradient is ATP dependent and controlled by phosphatase, which controls the levels of PI(4)P in the cell [Drin et al., 2016].

PI(4)P is an essential signalling molecule at the PM and the Golgi, and controls membrane trafficking, cytoskeletal organization, lipid metabolism, signal transduction pathways and cytokinesis in different organisms [D'Angelo et al., 2008], [Matteis, Godi, 2004], [Janetopoulos et al., 2005], [Strahl, Thorner, 2007], [Strahl et al., 2005], [Walch-Solimena, Novick, 1999a], [Garcia-Bustos et al., 1994], [Brill et al., 2000]. Therefore, it is critical to keep the right balance of this lipid.

PI(4)P is a product of phosphorylation of phosphatidylinositol (PI) by the phosphatidylinositol 4-kinases [Balla, Balla, 2006]. The fission yeast genome encodes 3 putative phosphatidylinositol 4-kinases: lsb6p (SPAC343.19), sst4p (SPBC577.06c) and pik1p (SPAC22E12.16c) [Wood et al., 2011], of which only pik1 is essential [Park et al., 2009] [Wood et al., 2011]. In cycling cells pik1p is required for septation and cell separation, its absence results in accumulation of membranous and vacuolar structures [Park et al., 2009]. Since, kes1p and osh7p most probably bind PI(4)P, it was interesting whether synthesis of this lipid contributes to SE in fission yeast cells.

We studied cells containing the temperature-sensitive allele *pik1-td* [Park et al., 2009]. *pik1-td* allele leads to cell death at restrictive temperature (more in Introduction **1.2.5**). In starvation, *pik1-td* mutants retained numerous strong fluorescent filipin dots - similar to *kes1*Δ, *osh7*Δ and *kes1*Δ*osh7*Δ cells (**Figure 3.30**, B). After 15min in SE the mutant did not enter P1; filipin dots were present but their number markedly decreased (**Figure 3.30**, B). This trend of removal of filipin dots continued up to 180min in SE and is similar to what was seen in *kes1*Δ, *osh7*Δ and *kes1*Δ*osh7*Δ mutants. Up to 180min *pik1-td* cells did not enter P1. Therefore, we conclude that pik1p is essential for SRM formation and cell polarisation. Cells did increase their length and width by less than 0.5μm from the start of SE (**Figure 3.31**). We speculate that the retained filipin dots could actively contribute to attracting a portion of new cell wall material to ectopic sites on the PM. Nevertheless, *pik1-td* mutants are not building defined SRM domains and are not polarising (**Figure 3.30**, A, B).

Studies of the mutant at permissive temperature showed that cells have problems in building SRMs, and most cells showed weak filipin signal all around the PM (**Figure 3.30**, D). After 180min in SE, many cells readily polarised, however filipin signal at the sides was visible. Often, cells kept their filipin signal, which was located all around the membrane (**Figure 3.30**, D). This reveals that pik1p is involved both in SRM formation, but also in SRM removal (similar to the role of filamentous actin) (see, [Makushok et al., 2016a] and **1.4**).

We summarise that synthesis of PI(4)P is essential for SRM formation and cell polarisation during SE.

3.3.2 PIP2 is involved in cell polarisation and is required for stabilisation of SRM at the secondary pole

After synthesis of PI(4)P, it is further phosphorylated to produce another signalling lipid - PIP2, which in exponentially growing fission yeast cells is required for cell growth, organisation of the actin cytoskeleton, cell division, and membrane trafficking [Desrivieres, 1998], [Zhang et al., 2000], [He et al., 2007a], [He et al., 2007b], [Sun et al., 2007], [Zhang et al., 2008], [Yakir-Tamang, Gerst, 2009], [Bendezú et al., 2012]. Conditional mutation in *its3* - *its3-1* result in low levels of PIP2 and elevated levels of PI(4)P [Zhang et al., 2000].

its3-1 mutants built wild-type looking SRM domains after the first 15min of SE (**Figure 3.30**, B). However, after 60min in SE, cells were not polarised. Mutants showed intense SRM domain staining at both opposite lateral regions of the cell (**Figure 3.30**, B). This is reflected by the drop in the rP ratio (**Figure 3.30**, A), (see, Materials and methods **2.2.2.2.6**). We also observed many side SRMs as quantified in the corresponding histogram (Supplementary figure, (**Figure 5.11**). Sometimes, even more intensely stained SRMs were detected, which localised to bulges at cell sides (**Figure 3.30**, B), therefore we think that small subset of *its3-1* mutant cells initiate ectopic growth at the sides of the cells.

After 120min in SE, *its3-1* mutants increased their rP ratio, however it remained very low compared to wild-type cells (**Figure 3.30**, A). High number of *its3-1* cells were dead or very sensitive to filipin. This was detected through the very high filipin intensity inside the cells (**Figure 3.30**, C). Majority of viable cells had mono-polar SRMs (**Figure 3.30**, C), however there was no significant length increase between 60-120min time-points (**Figure 3.31**, A). Only occasionally did we observed cells which initiated growth projections at the sides of the cells, and those were more elongated than the bulges from the 60min time-point (**Figure 3.30**, B, C). We think that these cells continued

their ectopic growth at these sites between 60-120min.

After 180min in SE, more than many *its3-1* cells were dead after filipin staining and viable cells were strongly mono-polar (**Figure 3.30**, B). We could not detect cells with ectopic SRM positioning at this time-point. The rP ratio was therefore higher than for the previous time-point (**Figure 3.30**, A). Cells were clearly elongated from cell poles (**Figure 3.30**, B), (**Figure 3.31**, A, B), as also seen by the increase in polar SRMs in the histograms of **Figure 5.11**.

We conclude that drop in PIP2 synthesis results in delays in the P2 entry. Cells are delayed in stabilisation of the SRMs at cell poles, what results in ectopic growth site positioning in small subset of mutant cells. Eventually mutants polarise but they cannot stabilise a strongly fluorescent SRM at the secondary pole. This suggests that most probably these cells do not enter P4, what might be related to the membrane trafficking role of PIP2 and its binding to the exocyst complex [He et al., 2007a] (which also has a mono-polar pattern of SRMs after 180min in SE (**Figure 3.5**)).

Summarised information about phases of SE in the described mutants of PI synthesis are presented in a **Table 12**. Width measurements of polar and side SRMs are included as a supplementary figure (see, **Figure 5.11**).

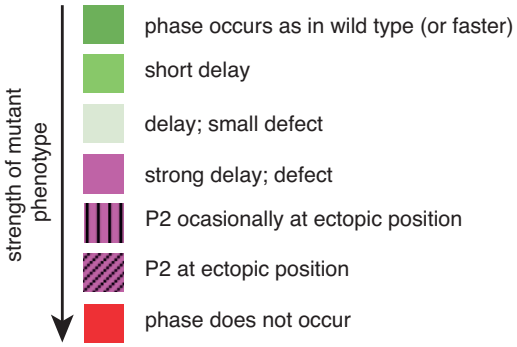

Strain name	P1	P2	P3
pik1-td			
its3-1			

Table 12: **Table summarising phases of SE in cells deficient in PI(4)P and PIP2 synthesis**

The table considers data until 180min in SE (Materials and methods, **2.2.3**).

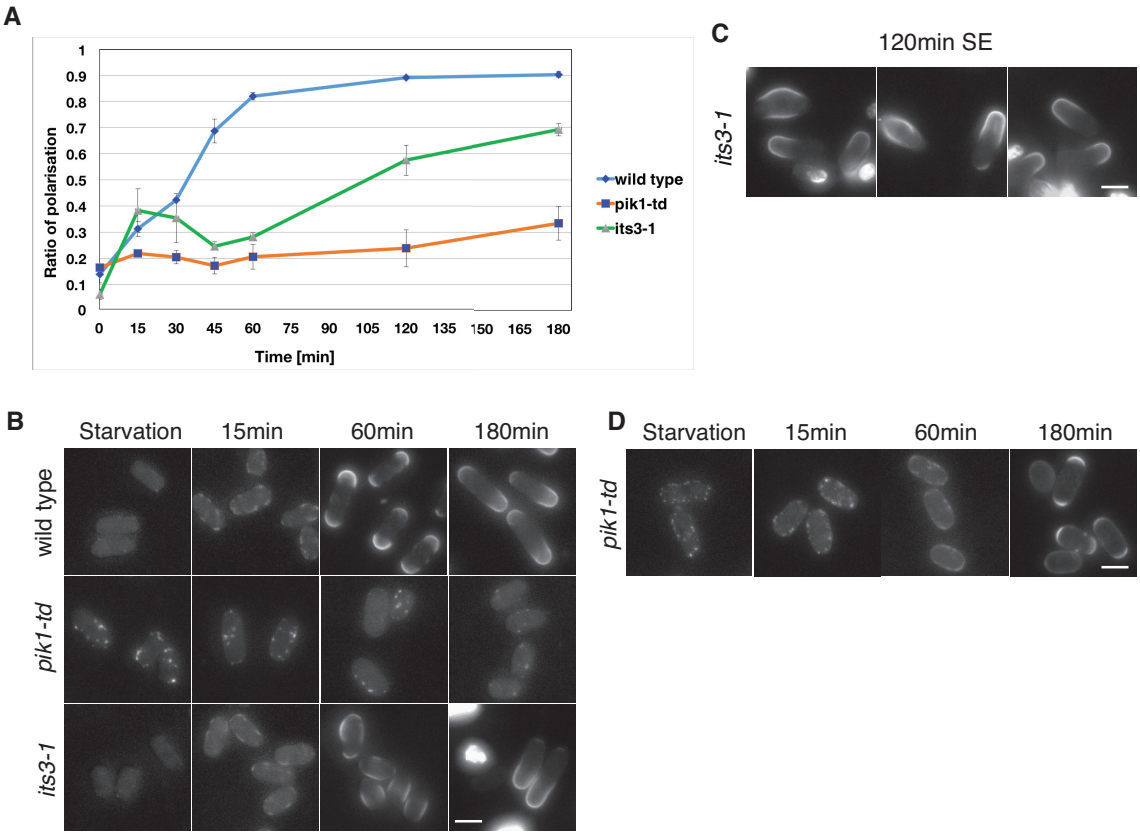

Figure 3.30: **Role of the main phosphatidylinositol kinases in *de novo* cell polarisation of *S. pombe***

A - Time course of average rP (Ratio of Polarisation) values for cells in SE. Each average rP was measured from mean rPs from 3 experiments (n>200 per experiment). Error bars represent the average standard deviations of mean rP values. *pik-td* cells were starved and recovered in continuous presence of a thiamine repressor. **B** - Filipin staining of wild-type, *pik1-td* and *its3-1*, cells in starvation and during SE. Starvation and SE of *pik-td* cells were performed in the continuous presence of thiamine-repressible conditions. **C** - Selected branching cells of *its3-1* after 120min SE. Filipin staining. **D** - Filipin staining of *pik1-td* cells in starvation and during SE at permissive temperature without a thiamine repressor.
Scale bars, 5μm.

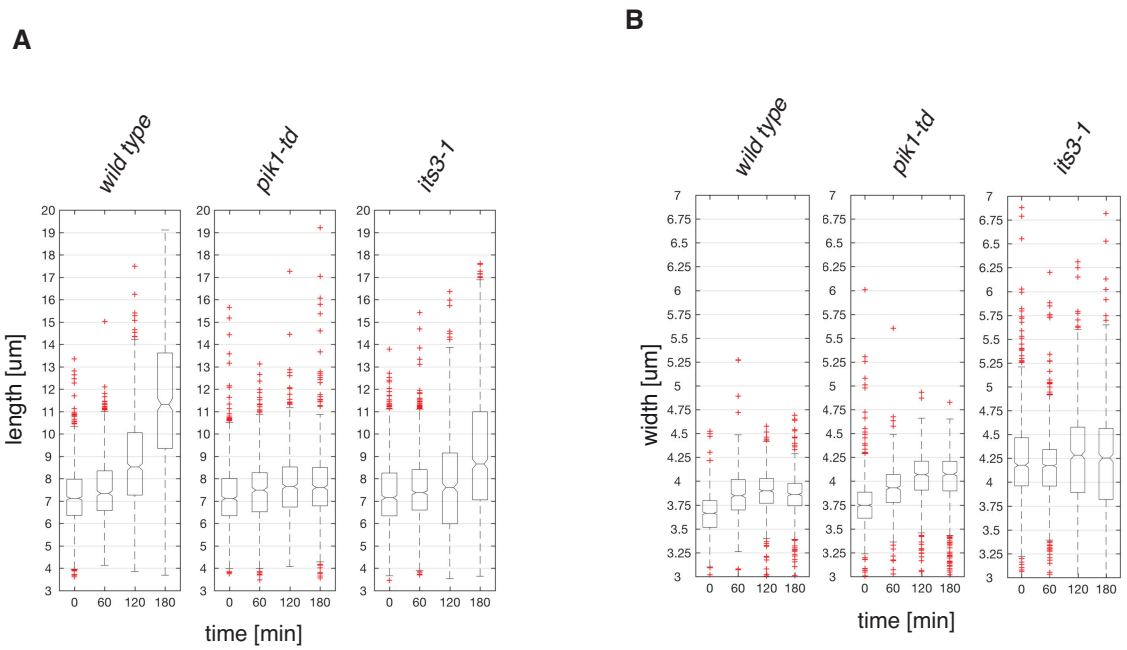

Figure 3.31: **Cell length and width during SE at restrictive temperature of main phosphatidylinositol kinases in *de novo* cell polarisation of *S. pombe***

A - Boxplots representing the distribution of measurements of cell length. Quantification of glucose starved cells (0min) and cells during SE (n>600). Notches represent 95% confidence intervals of the median. **B** - Boxplots representing the distribution of measurements of cell width. Quantification of glucose starved cells (0min) and cells during SE (n>600). Notches represent 95% confidence intervals of the median.
Starvation and SE of *pik-td* cells were performed in the continuous presence of thiamine-repressible conditions.

3.3.3 Connections between the ER and the PM play role in SRM formation and cell polarisation

We have shown that non-vesicular transport of sterol is involved in *de novo* cell polarisation (see, **3.2.1.2**). Non-vesicular transport of sterols has been mainly reported *in vitro* in the transport between the ER and the Golgi apparatus [Mesmin, Antonny, 2016], (see, Introduction **1.3.1.3**). However, our data reveal that the Golgi apparatus is not crucial for sorting of *de novo* synthesised ergosterol to the PM during SE (**Figure 3.4**). Moreover, we have shown that the oshes: kes1p and osh7p are enriched at the cell cortex where cortical ER is normally localised (**Figure 3.22**).

The cortical ER consists of interconnected tubules and cisternae, which are found at an average distance of 33nm from the PM [Pichler et al., 2001], [West et al., 2011]. Large areas of the PM are covered by ER membranes [Wolf et al., 2012]. Part of this cortical ER associates with the PM in different organims [Alison L Pidoux, 1993], [Prinz et al., 2000], [Schneider, 1994], via specialised proteins forming membrane contact sites (MCSs) [Prinz, 2014], (see, Introduction **1.3.1.2**). We hypothesised that these regions are involved in the transport of *de novo* synthesised ergosterol to the PM during SE, what leads to formation of SRMs.

ER-PM contacts in fission yeast are mediated by the vesicle-associated membrane proteins (VAP): scs2p (SPBC16G5.05c) and scs22p (SPAC17C9.12) [Zhang et al., 2012]. In budding yeast, the ER VAP proteins function at the ER-PM contact sites, controlling PI(4)P metabolism through their interaction with the PM-localised osh proteins [Stefan et al., 2011]. In fission yeast marker of one of the VAP proteins - GFP-tagged scs2p localises to the ER and is enriched at the cell sides [Zhang et al., 2012].

*scs2*Δ*scs22*Δ mutations in fission yeast result in elevated levels of the PI(4)P. scs2p and scs22p, together with ER-shaping proteins contribute to symmetric cell division [Zhang et al., 2012]. The ER in *scs2*Δ*scs22*Δ double mutants is mostly dissociated from the PM and accumulates at the cell poles, depending on active delivery by for3p and myo52p [Zhang et al., 2012].

We studied double mutant *scs2*Δ*scs22*Δ during SE. Similar to *kes1*Δ and *osh7*Δ mutant cells retained a large amount of filipin dots during starvation (**Figure 3.32**, B), (Figure 23, B). After 15min of SE, cells did not build SRMs, and similar to starvation, filipin staining was almost invisible (**Figure 3.32**, B). 60min into SE only small number of *scs2*Δ*scs22*Δ entered P1 (**Figure 3.32**, B, C). Numerous filipin dots were still present and only occasionally could a layer of large SRM domain be observed. Instead, very small patches of filipin signal were distributed all around the cell. These structures were clearly small and they looked different comparing to well-defined SRMs in control cells (**Figure 3.32**, B, C). The rP ratio for this mutant was significantly decreased, compared to the wild-type control (**Figure 3.32**, A). This indicates that filipin is predominantly localised at the cell sides, also seen in the histogram in supplementary **Figure 5.12**.

After 120min in SE the rP ratio (Materials and methods, **2.2.2.2.6**) was high suggesting that filipin signal was localised predominantly to cell poles (**Figure 3.32**, A). However, after evaluation of images corresponding to 120min time-point *scs2*Δ*scs22*Δ cells did not resemble cells in P2. Instead, intensive filipin signal was present at lateral positions and filipin was detected in random positions (**Figure 3.32**, B, D) . Often, identified domains were elongated and they seemed to expand to the whole side region of the cell. We do not know why the rP ratio showed a high score (0.7), however this might be due to higher intensity of SRMs at cell poles, which we could not notice in the unbiased way in these images (see also, Materials and methods **2.2.2.2.6**). Until 120min in SE cells did not initiate any significant growth (**Figure 3.33**, A, B).

180min after start of SE *scs2*Δ*scs22*Δ cells were generally polarised and their rP ratio was in excess of 0.8 (**Figure 3.32**, A, B), additionally reflected in the corresponding histograms (see, Supplementary **Figure 5.12**). Only occasionally we observed cells which were not properly polarised. They retained densely located lateral SRMs with lower or similar filipin intensity comparing to SRMs at cell poles (**Figure 3.32**, B). Size measurements of the mutant confirms that cells did not enter P3, however they slightly increased their length between 120-180min in SE (**Figure 3.33**, A). Similar slow growth is known for wild-type cells in P2 [Makushok et al., 2016b].

We conclude that ER-PM attachments are involved in proper formation of SRMs, speed of cell polarisation and fast growth initiation.

Summarised information about phases of SE in the described mutant are presented in a **Table 13**. Width measurements of polar and side SRMs are included as a supplementary figure (see, **Figure 5.12**).

3.3.4 ER tubules play role in cell polarisation and fast growth initiation

The ER network in fission yeast contains a specialised domain, which is sustained by three proteins: reticulon/rtn1p, DP1/yop1p, and tts1p [Zhang et al., 2010]. This domain controls the maintenance of the proper tubular morphology of the ER. The ER at the growing ends in cycling fission yeast cells is dynamically remodelled and contains more tubular regions than cisternal regions. In these cells ER cisternae are observed at lateral regions of the cell where ER-PM connections are also present [Zhang et al., 2010]. Since we observed that ER-PM connections play role in P1, P2 and P3 of SE, we wanted to know if defective ER morphology in the mutant lacking ER tubules results in phenotypes during SE. Therefore, we followed SE in mutant cells lacking reticulon/rnlp, DP1/yop1p, and tts1p (further called *try*Δ).

*try*Δ cells retained numerous filipin dots in starvation (**Figure 3.32**, B) (similar to *scs2*Δ*scs22*Δ, kes1Δ, osh7Δ and PIP(4)P mutants, (**Figure 3.32**, B), (**Figure 3.20**, B), (**Figure 3.30**, B). After 15min in SE, the filipin signal was significantly brighter than in starvation but defined SRM domains were rare (**Figure 3.32**, B). 60min into SE, *try*Δ mutants had already passed P1 and most of them had only one strongly fluorescent SRM at one of cell sides (**Figure 3.32**, B, E). Between 60-120min mutants did not increase their length but instead became slightly wider (**Figure 3.33**, A, B). After 120min many SRM domains were elongated and concentrated at cell sides, often passing through one of its lateral sides (**Figure 3.32**, B, F). Similar to *scs2*Δ*scs22*Δ, we do not understand why the rP ratio showed a high score (0.7) (**Figure 3.32**, A). This might be due to higher intensity of SRMs at cell poles, which we could notice in the unbiased way from

these images (see also, Materials and methods **2.2.2.2.6**). We conclude that *try*Δ cells are defective in P2. 180min in SE cells were mostly polarised and SRMs were present at cell poles (**Figure 3.32**, B). Between 120-180min, a length increase was detected, however it was significantly smaller than in the wild-type (**Figure 3.33**, A). We think these cells do not enter P3, but rather are slightly elongating as P2 cells described in [Makushok et al., 2016b].

Summarising, we observed that low tubulation of the ER in the *try*Δ mutant causes defects in SRM formation. We think that this phenotype is different from the phenotype of *scs2*Δ*scs22*Δ mutants because the filipin signal was significantly higher after 15min of SE in contrast to *scs2*Δ*scs22*Δ mutants (**Figure 3.32**, B). We speculate that proper ER tubulation defines zones for sterol clustering during P1. Lack of ER tabulation causes the irregular distribution of filipin staining. Often after 60 and 120min of SE intensive and well-defined SRM at lateral position of the cell is visible (similar to the *tea1*Δ and *cdc42-3kes1*Δ mutants). We speculate that *try*Δ mutants are defective in restricting the zone where single SRMs appear during P1, resulting in elongated SRMs. These cells are also defective in fast growth initiation (at least until 180min of SE). It has been proposed that the role of the peripheral ER reticulation is to allow efficient execution of surface-dependent functions, enabling positions where cortex-associated processes, and communication between the cytoplasm and the PM, can occur [Zhang et al., 2012]. We conclude that tubulation of the ER strongly contribute to the establishment of cell polarity of fission yeast cells.

Summary information about phases of SE in the described mutant are presented in a **Table 13**. Width measurements of polar and side SRMs are included as a supplementary figure (see, **Figure 5.12**).

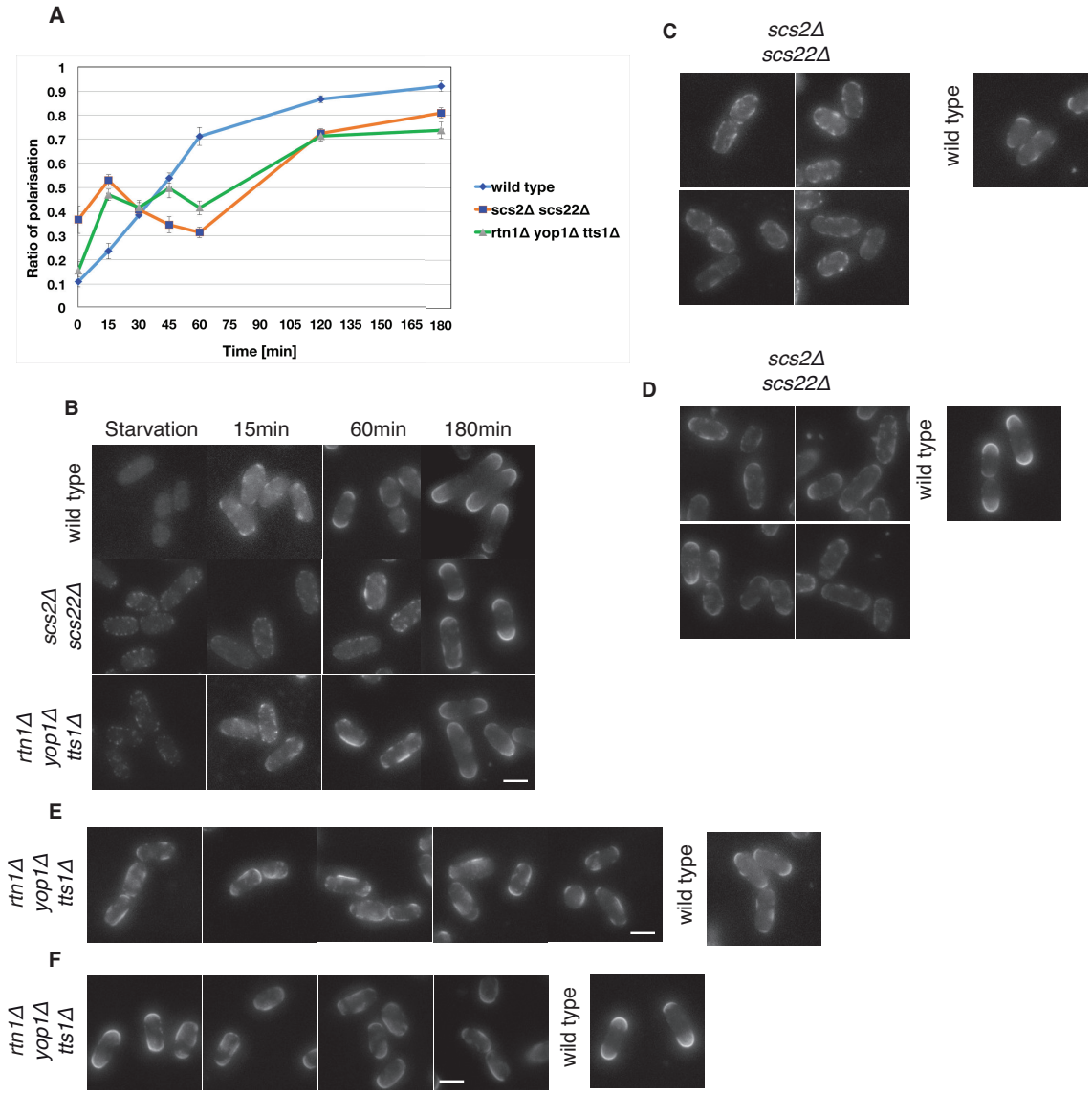

Figure 3.32: **Role of ER-shaping proteins in *de novo* cell polarisation of *S. pombe***

A - Time course of average rP (Ratio of Polarisation) values for wild type, *scs2*Δ*scs22*Δ and *rtn1*Δ*yop1*Δ*tts1*Δ in SE. Each average rP was measured from mean rPs from 3 experiments (n>200 per experiment). Error bars represent the average standard deviations of mean rP values. **B** - Filipin staining of wild-type, *scs2*Δ*scs22*Δ and *rtn1*Δ*yop1*Δ*tts1*Δ cells in starvation and during SE. **C** - Filipin staining of *scs2*Δ*scs22*Δ and wild-type 60min in SE. **D** - Filipin staining of *scs2*Δ*scs22*Δ and wild-type 120min in SE. **E** - Filipin staining of *rtn1*Δ*yop1*Δ*tts1*Δ and wild-type 60min in SE. **F** - Filipin staining of *rtn1*Δ*yop1*Δ*tts1*Δ and wild-type 120min in SE.
All strains were auxotrophs carrying: *ade6-M216*, *leu1* and *ura4-D18*. Medium was supplemented with appropriate amount of amino-acids.
Scale bars, 5μm.

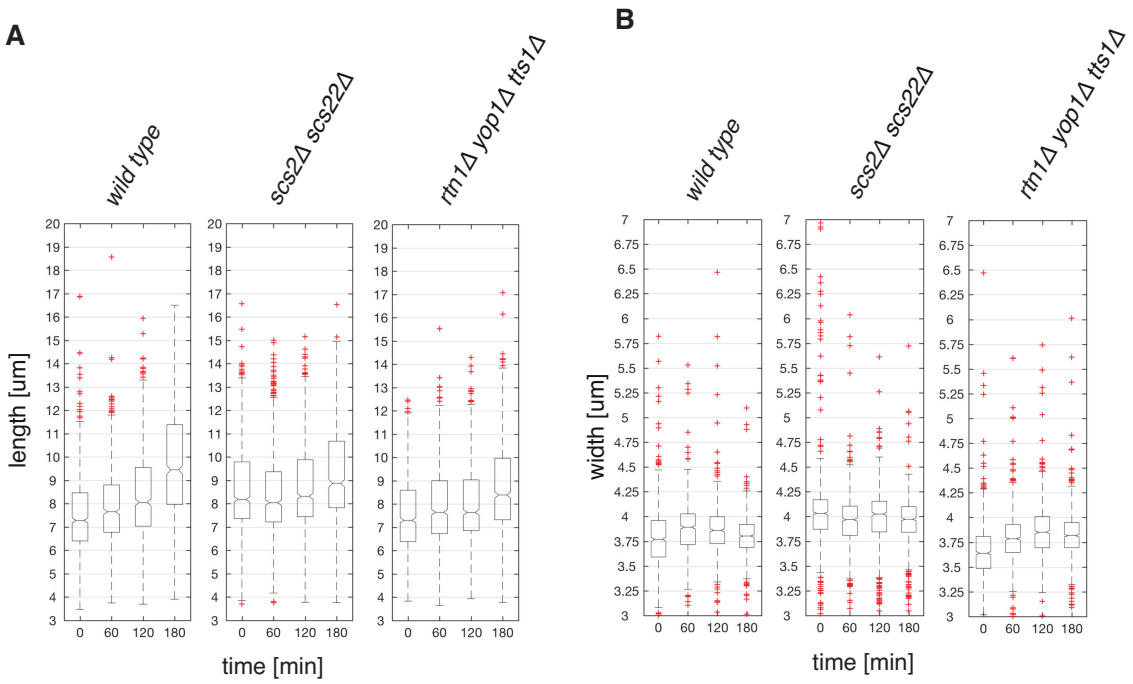

Figure 3.33: **Cell length and width of ER-shaping mutants during SE**

A - Boxplots representing the distribution of measurements of cell length. Quantification of glucose starved cells (0min) and cells during SE (n>600). Notches represent 95% confidence intervals of the median. **B** - Boxplots representing the distribution of measurements of cell width. Quantification of glucose starved cells (0min) and cells during SE (n>600). Notches represent 95% confidence intervals of the median.
All strains were auxotrophs carrying: *ade6-M216*, *leu1* and *ura4-D18*. Medium was supplemented with appropriate amount of amino acids.

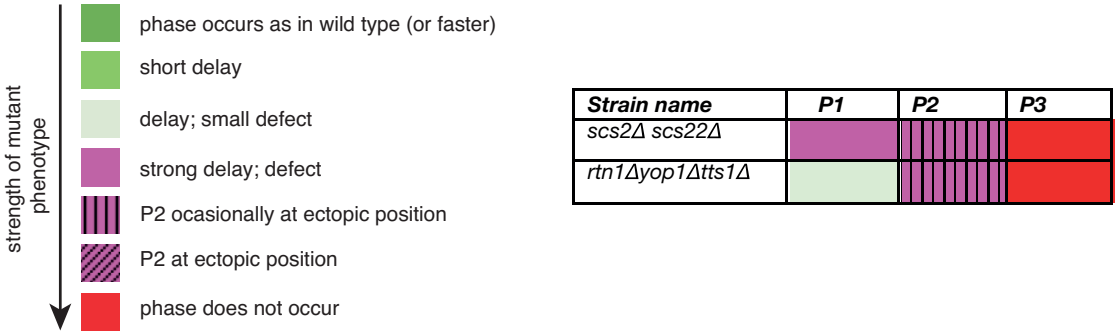

Table 13: **Table summarising phases of SE in the ER-shaping mutants**
The table considers data until 180min in SE (Materials and methods, 2.2.3).

4 Discussion

4.1 Introduction and motivation

S. pombe (fission yeast) cells are eukaryotic single cell microorganisms, which maintain their rod-shape during growth phases and divide by medial fission after reaching a critical length [Huisman, Brunner, 2011]. Fission yeast cells are commonly used as a model organism to study cell polarity control [Martin, Arkowitz, 2014] - a process which can lead to the generation of morphological diversity [Rolls et al., 2003].

The rod shape of S. pombe cells is a consequence of maintaining the growth and polarity machineries at the two opposing cell ends [Chang, Huang, 2014]. Interestingly, the growth pattern of *S. pombe* cells changes several times during the cell cycle [Huisman, Brunner, 2011], [Martin, Arkowitz, 2014]. Shortly after cell division, cells initiate mono-polar growth from their old end. Later bi-polar growth initiation occurs, a process called new end take off (NETO) [Huisman, Brunner, 2011]. After reaching the critical size, cells stop elongating and restrict their growth and polarity machineries to the cell middle in order to perform medial fission [Huisman, Brunner, 2011].

Cdc42p is a member of the Rho GTPase protein family. It is a key regulator of cell polarisation and it can spontaneously break the cell symmetry [Etienne-Manneville, 2004], [Etienne-Manneville, Hall, 2002], [Wedlich-Soldner, Li, 2008], [Bendezú et al., 2015]. Localised and active cdc42p can control different sub-cellular processes, such as actin organization, endo/exo-cytosis, and affect cellular architecture [Martin, Arkowitz, 2014].

In addition, many cells use the microtubule (MT) cytoskeleton to position internal polarity cues [Siegrist, Doe, 2007]. In *S. pombe* interphase MTs are organised in anti-parallel bundles that span the long axis of the cell. Their plus ends are directed towards the cell poles, while their minus ends are clustered around the cell centre, where they are bound to the nuclear membrane. The role of these MT bundles is to deposit the tea1p marker protein at both cell poles. This ensures proper polar growth site positioning [Mata, Nurse, 1997], [Huisman, Brunner, 2011]. As a consequence, *tea1*Δ

cells grow bent or branched [Huisman, Brunner, 2011]. In addition, growth initiation at these sites is triggered by actin-based delivery of cell wall components [Martin, Arkowitz, 2014].

The basic feature of a polarised cell is an asymmetric organization of its plasma membrane, which can be compartmentalised by specialised lipid domains (often called lipid rafts) [Rajendran, 2005]. *De novo* synthesised ergosterol, which subsequently contributes to formation of sterol-rich membrane domains (SRMs), is crucial for *de novo* cell polarisation of *S. pombe* cells [Makushok et al., 2016b]. SRMs localize to polar cell ends in exponentially growing cells and to the cell middle during cytokinesis [Wachtler et al., 2003], [Makushok et al., 2016b]. It has been proposed that SRMs appear as a consequence of the established polar growth machinery, however, based on [Makushok et al., 2016b] SRMs are central to the establishment of cell polarity. Briefly, in glucose starvation, cells lose their polar localisation of SRMs. Re-feeding, called starvation exit (SE), leads to an initial phase (P1), during which randomly distributed SRM domains appear first in the PM and serve as platforms for the growth and polarity machineries. In a second phase (P2) SRMs at cell poles are stabilised and the side SRMs are being removed. P1 and P2 are independent from fast growth initiation, however, very slow growth is detectable [Makushok et al., 2016b]. In phase 3 (P3), cells initiate fast growth from one of the cell ends, which in many cells can later switch to bi-polar growth in phase 4 (P4) (probably equivalent to NETO) [Makushok et al., 2016b].

The SE assay shows that SRM positioning is central to any detectable localisation of the growth machinery, except microtubule-delivered tea1p [Makushok et al., 2016b]. In addition, those data reveals that tea1p controls the position and growth activity of SRM domains at the PM [Makushok et al., 2016b]. Interestingly, tea1p activity is not dependent on the previously proposed biochemical links between a downstream factor of tea1p and tea4p - for3p (a nucleator of linear actin filaments) [Makushok et al., 2016b]. *tea1*Δ cells exhibit two major phenotypes during SE: defects in stabilisation of SRM domains at cell poles, resulting in branched or bent cells, and a defect in bi-polar growth site activation. Most importantly, [Makushok et al., 2016b] showed good evidence that

cell polarisation is not dependent on cdc42p, which gradually increases its activity and becomes detectable only after 1-2h hours into SE (the moment when cells are already polarised). Mechanisms driving the initial formation of SRMs during P1 are not known. In addition, tea1p interacts with SRMs, but the factors involved are unknown. We were interested in the processes leading to P1 initiation. Moreover, we were exploring the phenotypic interaction between *tea1*Δ and mutants of potential regulators of ergosterol transport.

In the course of this work we examined the formation and distribution of sterol-rich membranes (SRMs) during SE of fission yeast cells. We used a candidate based approach to identify proteins involved in P1 and P2 initiation. We stained cells with the oxysterol-binding dye - filipin [Drabikowski et al., 1973]. Moreover, we used computer software, which helped to follow our qualitative observations in a large number of cells and to quantitatively classify SRMs based on their side or cell pole localisation (Materials and methods, **2.2.2.2.3**). Moreover, the extracted ratio of polarisation (rP), allowed us to estimate the level of polarisation for the whole cell population and contributed to the general description of SE (Materials and methods, **2.2.2.2.6**).

In this chapter, we will highlight the key conclusions of our results and discuss their novelty. Moreover, we will speculate about additional roles of the identified components and will present a new working model for the process of *de novo* cell polarisation of fission yeast cells.

4.2 Membrane trafficking does not drive cell polarisation

Membrane trafficking is required for polarised growth and cell polarity maintenance in different model organisms [Mellman, Nelson, 2008], [Martin, Arkowitz, 2014], [Rodriguez-Boulan, Macara, 2014]. Multiple lines of evidence show that actin cable machinery and the exocyst in fission yeast form two autonomous morphogenetic modules (complementing groups) [Bendezu, Martin, 2011], [Snaith et al., 2011], [Bendezú et al.,

2012], [Jourdain et al., 2012]. Removal of a member from a single group results only in defects in the membrane delivery to the PM, however does not affect cell polarity. Removal of single components from both modules in the same cells result in a shape phenotype, and therefore affect cell polarity [Snaith et al., 2011] [Bendezu, Martin, 2011] (see, **3.1.3.1**). We were interested, if such double mutants could influence *de novo* cell polarisation.

It was the first time that double mutants of both complementing groups in single cells were studied in standard growth conditions, since all previous studies in fission yeast report the requirement of an osmotic stabiliser or synthetic lethality between interacting genes [Bendezu, Martin, 2011], [Snaith et al., 2011], [Bendezú et al., 2012], [Jourdain et al., 2012]. Strikingly, our data revealed that *sec8-1for3*Δ, *sec8-1 ypt2VN* and *sec3-916 exo70*Δ mutants were able to enter P1 and P2 (**Figure 3.9**). Since it is known that actin cable transport and the exocyst are both under control of cdc42p [Martin, Arkowitz, 2014] our data are in agreement with the recent report, showing that cdc42p is not involved in the establishment of the cell polarity [Makushok et al., 2016b]. Additionally, we treated the double mutants with Brefeldin A (BFA) (**Figure 3.12**). In BFA-treated cells the Golgi marker signal disappeared, which suggested that a structure of the Golgi-apparatus was sensitive to BFA treatment in SE (**Figure 3.3**, C). Wild-type cells and the double mutants treated with BFA entered P1 and P2, which supported our hypothesis that neither post-Golgi membrane delivery to the PM, nor membrane tethering are involved in cell polarisation. In line with previous studies, BFA-treated cells did not initiate fast growth (P3), showing that P2 is not dependent on fast growth initiation [Makushok et al., 2016b].

Current dogma says that transport vesicles are finally fused with their donor membrane and this event is mediated by the SNARE complexes [Jahn et al., 2003]. Therefore, we were wondering if membrane fusion, mediated by the PM-SNARE protein complex [Jahn et al., 2003], is playing this role during *de novo* cell polarisation in fission yeast cells. We studied progress of SE in single mutants of the PM-SNARE complex: *psy1-S1* (t-SNARE mutant), *syb1-sp58* (v-SNARE mutant) and *sec9-10* (SNAP25-like

component mutant), which are known to be essential at restrictive temperature [Maeda et al., 2014]), [Yamaoka et al., 2013], [Nakamura et al., 2005]. In our growth conditions *psy1-S1* and *syb1-sp58* were actually viable at 36 °C (showing only misshapen and asymmetrically dividing cells), therefore we created a double mutant strain between these two components. To our knowledge it is the first time that the effects on *de novo* cell polarisation were studied in cells mutated in both the PM-t-SNARE and the PM-v-SNARE. It was to our considerable surprise that *S. pombe* cells without fully functional PM-SNAREs (even t- and v-SNAREs), were able to polarise (**Figure 3.14**).

Subsequently, we wanted to know if the PM-SNAREs do not act redundantly with the Golgi-dependent membrane trafficking. Therefore, we treated PM-SNARE mutants with BFA and observed that the double mutant *psy1-S1 syb1-sp58* can enter P1 (**Figure 3.16**). Mutants were able to place their SRMs at cell poles (they entered P2), however these domains were slightly offset from the main polarity axis. Later, BFA-treated double mutants of the two PM-SNAREs did not maintain their polarised state and lost their SRMs, or positioned them away from the cell poles (**Figure 3.16**). We hypothesise that the membrane fusion machinery is redundant with the Golgi apparatus for the maintenance of previously acquired cell polarity.

psy1-S1, *sec9-10* and *psy1-S1 syb1-sp58* were also slightly defective in proper P1 entry. Their SRMs were weaker (*psy1-S1*, *syb1-sp58*) or misshapen (*sec9-10*), however significant change in filipin intensity was observed between starved cells and cells 15min in SE (**Figure 3.14**). This indicated that although SNARE mutants were able to deliver ergosterol to the PM, membrane fusion was involved in the shaping of SRMs (or in some other regulatory function). It is possible that the PM-SNAREs in fission yeast are involved in membrane fusion of additional regulatory components, thereby facilitating the efficiency of the membrane integration. However, thus far, we did not find evidence for this hypothesis. It is possible that hypomorphic effects of particular mutants and their cell wall defects from the pre-starvation phase could contribute to inefficient filipin binding at the beginning of SE. Moreover, BFA-treated double PM-SNARE mutants had pronounced defects in SRM formation (compared to non-treated cells), and formed

a small number of SRMs with high intensity (**Figure 3.16**). We suggest that the membrane fusion mechanism together with the Golgi apparatus are involved in the proper clustering of the ergosterol during P1, however they are not essential for the process of delivery of *de novo* synthesised ergosterol to the PM. Interestingly, all studied secretory mutants showed small delays in P2 entry (**Figure 3.11**), (**Figure 3.16**). We think this is due to defects in the removal of side SRMs (similar to LatB treated cells - see, [Makushok et al., 2016b]). After 60min in SE, many cells had polarised SRMs at their poles but additional side SRMs were also present (**Figure 3.11**), (**Figure 3.16**).

Membrane trafficking is involved in polarity maintenance [Apodaca et al., 2012], however, our data show that its essential role during *de novo* cell polarisation is unlikely. In agreement with our data, ergosterol can be transported to the PM via Golgi-independent or partially-independent pathways [Urbani, Simoni, 1990] [Heino et al., 2000]. Two pools of sterols in the PM are proposed: free sterol and the sterol condensed by the sphingolipids (forming sterol-enriched compartments in the PM - most probably lipid raft equivalents) [Baumann et al., 2005a]. An essential role for the membrane-dependent transport of the free sterol pool to the sterol-enriched compartments in the PM is ruled out. Instead, it was proposed that this process depends on non-vesicular transport, which happens via equilibration between the ER and the PM [Baumann et al., 2005a]. In contrast, it is proposed that in budding yeast the condensation of the PM-destined sterol into lipid rafts happens already at the level of the Golgi-apparatus and these newly formed vesicles are delivered to the PM via the post-Golgi machinery [Klemm et al., 2009]. Although, polarity maintenance is reported to be not critically dependent on membrane trafficking in *Drosophila* neuroblasts [Halbsgut et al., 2011], our data are most probably the first evidence showing that during *de novo* cell polarisation the Golgi apparatus and the post-Golgi membrane-transport do not play a crucial role.

4.3 Starvation exit and non-vesicular transport of sterol

As previously mentioned, we conclude that *de novo* cell polarisation of fission yeast cells is not critically dependent on membrane trafficking and membrane fusion. This is strong evidence that non-vesicular transport of ergosterol is driving SRM formation and cell polarisation. The oxysterol-binding protein family members in different organisms have the structural property to bind sterols and other lipids [Schulz et al., 2009], [Maeda et al., 2013], [Filseck von et al., 2015], [Filseck Moser von et al., 2015a], [Chung et al., 2015]. Moreover, these proteins coordinate non-vesicular sterol transport, and are involved in sterol sensing, homeostasis and organisation in the PM [Perry, 2006], [Kozminski et al., 2006], [Olkkonen, Li, 2013]. Their collective removal in budding yeast causes a range of polarity phenotypes, including mis-positioning of cdc42p and membrane trafficking machineries [Kozminski et al., 2006] (see also, **3.2**). Moreover, recent studies in *A. nidulans*, revealed a function for oshes in the maintenance of single growth positions [Bühler et al., 2015b]. All this suggests that oshes might play a role in the establishment of cell polarity in fission yeast cells. In the course of this work we studied SE in a series of mutants, carrying deletions of genes for oxysterol-binding proteins. We showed that two of them: kes1p and osh7p play important roles at different stages of SE (see, **3.2**).

4.3.1 kes1p and osh7p are involved in different stages of SE

Based on [Wood et al., 2011] and [Bühler et al., 2015b] there are 6 members of this family in *S. pombe*. We named them based on their closest protein sequence homologs (see, **3.2.1**). We have observed that during starvation *kes1*Δ and *osh7*Δ cells retain filipin signal in the form of filipin dots in the PM (**Figure 3.20**), this correlates with the role of their budding yeast orthologues in ergosterol removal from the PM [Beh et al., 2001]. Strikingly, these mutants were defective in P1, since no defined SRM domains were detected between the magnitude of filipin-stainable dots after 15min in SE (**Figure 3.20**). Moreover, no dramatic increase in the filipin signal was observed after the first 15min in SE, which suggested that sterol delivery to the PM was defective (**Figure 3.20**, B). Both mutants eventually formed SRM domains at later

time-points (between still present filipin dots). Strikingly, mutants were strongly delayed in cell polarisation, similar to *tea1*Δ mutants (**Figure 3.20**), [Makushok et al., 2016b]. However, in contrast to *tea1*Δ mutants, both *kes1*Δ and *osh7*Δ cells were able to establish SRMs at opposite cell ends after 120-180min in SE (**Figure 3.20**), [Makushok et al., 2016b]. Additionally, we observed that *kes1*Δ and *osh7*Δ mutants had defects in P3, since *kes1*Δ mutants were elongating slower than wild-type cells (**Figure 3.21**). More strikingly, *osh7*Δ cells were increasing both their length and width and were growing almost isotropically.

Removal of genes for the remaining oshes did not result in defective P1 and P2 (**Figure 3.20**), however we observed slower growth rates during P3/P4 (**Figure 3.21**).

Interestingly, the double mutant between *kes1*Δ and *osh7*Δ revealed that their phenotypes are additive, meaning that entries into particular phases of SE were significantly delayed (compared to the corresponding single deletions). Cells had a much higher number of filipin dots in the PM in starvation and during SE than corresponding single mutants (**Figure 3.23**). After 180min in SE, wild-type cells were in P3/P4, however most *kes1*Δ*osh7*Δ double mutants have still not entered P1. At this time-point we detected slow but almost completely isotropic growth (**Figure 3.24**). In another hour many cells entered P2 and switched to mostly length increase, however these cells were not in P3 (**Figure 3.27**). At this time-point we observed that the number of filipin dots was significantly lower than in the previous time-point. Later, double mutants interrupted their growth completely, however, surprisingly, they initiated it again between 300-360min in SE (**Figure 3.27**). Growth speeds during this time exceeded 0.8μm/h, the threshold for fast growth (**Figure 3.27**), (see, **3.1** and [Makushok et al., 2016b]). Incidents of growth interruption suggested instabilities in the maintenance of the polarised SRMs. This correlates with the previously observed phenotype of *bud6*Δ and *for3*Δ mutants, which have defects in the maintenance of polarity, as observed by the temporal disappearance of SRMs at the second growing end [Makushok et al., 2016b]. Further evaluation of this hypothesis requires live observation of SRM dynamics using an SRM live marker. We conclude that kes1p and osh7p are collectively involved in cell

polarisation and their removal leads to cell polarisation defects.

Combinatorial effects of double mutants between *kes1*Δ/*osh7*Δ with deletions of other oshes displayed weaker phenotypes than single *kes1*Δ or *osh7*Δ, however few mutants were similar to single *kes1*Δ or *osh7*Δ mutants (see, **3.2.1.4**). The most striking phenotype was a combinatorial effect between *osh3*Δ and *osh7*Δ, which manifested itself in the ability of these cells to completely remove filipin dots during entry to starvation (in contrast to *kes1*Δ, *osh7*Δ and *kes1*Δ*osh7*Δ cells), in the formation of wild type like SRMs (**Figure 3.25**), and in ability of these cells to enter P3 before 180min in SE (in contrast to *osh7*Δ mutants) (**Figure 3.25**). We consider the possibility that particular osh proteins might work as transcriptional regulators for the expression of other oshes. Interestingly, one of the localisations of endogenously expressed osh7p-GFP is the cell nucleus (see, **3.2.1.3**). However, the functionality of the osh7-GFP construct and its role in the expression of other *osh* genes will need to be further evaluated.

Additionally, we were not able to isolate the double mutant *kes1*Δ*osh2*Δ based on tetrad analysis (see, **3.2.1.4**). This suggests a redundant role for cell viability, however different methods to evaluate this genetic interaction should be performed. Moreover, in the course of this study we presented a double mutant *kes1-shut off osh2*Δ, where gene expression of *kes1* was repressed by the continued presence of thiamine (see, **3.2.1.4**). Data showed that these cells had bigger diameters than wild-type cells, had defects in the removal of SRMs during P2, and did not initiate P3 (at least until 180min in SE) (**Figure 3.23**), (**Figure 3.24**). We could not exclude the possibility that this effect is due to a combination between *kes1-shut off* and *osh2*Δ or that it is only the effect of shutting off *kes1* expression. The second possibility is unlikely, since the phenotype significantly differs from the one observed in *kes1* mutant cells.

Our data about delayed P2 in *kes1*Δ and *osh7*Δ mutants is in line with previous studies, showing the collective role of osh proteins in ergosterol distribution [Georgiev et al., 2011], [Mesmin et al., 2013b]. Moreover, the delay is similar to that seen in *tea1*Δ cells, which are delayed in P2, where these mutants are waiting for sufficient cdc42p activity at any of the SRMs during P1. We hypothesise that something similar happens

in *kes1*Δ*osh7*Δ mutants, however the presence of tea1p in these mutants eventually promotes the stabilisation of SRMs at cell poles. Our data suggest that kes1p and osh7p might execute one of the functions of tea1p. To our knowledge, these data are the first evidence for the role of oxysterol-binding proteins in sterol distribution during *de novo* cell polarisation in fission yeast cells.

Previous *in vitro* studies showed that osh proteins from budding yeast have the structural property to bind sterol and its transport [Schulz et al., 2009], [Mesmin et al., 2013b] [Filseck von et al., 2015], however their role in sterol transport *in vivo* is disputed [Georgiev et al., 2011] [Beh et al., 2012]. Our data show that both kes1p and osh7p are involved in SRM formation during the first phase of cell polarisation (see, **3.2**).

Summarising, our data showed that deletion of *osh* genes result in defects at different stages of SE, with kes1p and osh7p, playing important roles in P1, P2 and P3 (see, **3.2**).

4.3.2 kes1p and osh7p facilitate non-vesicular transport

As previously mentioned, the budding yeast orthologues of kes1p and osh7p are implicated in non-vesicular transport of different lipids [Im et al., 2005], [Saint-Jean de et al., 2011b], [Drin et al., 2016], [Chung et al., 2015], [Filseck Moser von et al., 2015a], however the kes1p orthologue in budding yeast is also known to bind to post-Golgi secretory vesicles and to mediate interactions between several vesicle trafficking regulators [Alfaro et al., 2011a], [Ling et al., 2014]. Kes1p from budding yeast can bind sterols on liposomes, transporting sterol from the ER to the Golgi apparatus membranes [Saint-Jean de et al., 2011b], [Mesmin et al., 2013b], [Filseck von et al., 2015] (Introduction, **1.3.1.3**). The mammalian OSBP (oxysterol-binding protein) has similar properties [Mesmin et al., 2013b]. Interestingly, *in vivo* studies of mutants of osh7p orthologues - osh6/osh7p in budding yeast [Maeda et al., 2013], [Filseck Moser von et al., 2015a], and mammalian equivalents [Chung et al., 2015], reveal their function in non-vesicular transport of phosphoserine between the ER and the PM. Moreover, both kes1p and osh7p orthologues have the property to bind PI(4)P in the same binding pocket as sterol or phosphoserine [Im et al., 2005], [Saint-Jean de et al., 2011b], [Filseck

Moser von et al., 2015a]. Both models for kes1p and osh7p orthologue function, involve the exchange of their specific lipids with PI(4)P between the ER and the opposing membrane. After transporting PI(4)P back to the ER, PI(4)P is hydrolysed by the phosphatase sac1p into PI(4)P [Mesmin et al., 2013b], [Filseck von et al., 2015], [Filseck Moser von et al., 2015a]. Therefore, the level of PI(4)P is the limiting factor of this lipid transport system [Mesmin et al., 2013b].

4.3.2.1 Cells with aberrant levels of PI(4)P resemble *kes1*Δ and *osh7*Δ mutants during early stages of SE

We studied the role of the hypothetical osh/PI(4)P counter-transport system in the execution of kes1p and osh7p functions and establishment of the sterol gradient. This system should result in SRM formation during SE. Therefore, we followed SE in cells defective in the essential 1-phosphatidylinositol 4-kinase - pik1p (see, **3.3**). This kinase phosphorylates phosphatidylinositol (PI) to yield PI(4)P [Park et al., 2009]. Strikingly, *pik1-td* conditional mutant cells were completely defective in P1 initiation and we did not observe any SRM domains in the PM (**Figure 3.30**). Therefore, PI(4)P is essential for the establishment of the cell polarity. This result supports our hypothesis that kes1p and osh7p could execute their function during SE in the counter-transport of sterol and PI(4)P.

4.3.2.2 The osh system does not act on the Golgi apparatus

We previously mentioned that the kes1p orthologue from budding yeast and mammalian OSBP are transferring sterol *in vitro* between membranes of the ER and the Golgi apparatus [Filseck Moser von et al., 2015a], [Mesmin et al., 2013b]. Moreover, kes1p in budding yeast localises to post-Golgi vesicles [Alfaro et al., 2011a], [Ling et al., 2014]. In addition, fission yeast pik1p kinase locates to the Golgi apparatus [Park et al., 2009]. However, our observations showed that cells without an intact Golgi apparatus (BFA-treated cells) are not defective in P1 and P2, therefore providing evidence that

the Golgi is not essential organelle for the newly synthesised ergosterol in fission yeast cells (**Figure 3.4**).

4.3.2.3 kes1p and osh7p concentrate at cortical regions in fission yeast cells

In agreement with our hypothesis that kes1p and osh7p execute their functions at a different location than the Golgi apparatus, we showed that in exponentially growing cells, kes1p-GFP localised to the cytoplasm and was concentrated at cell poles (and also at sites of cytokinesis during cell division) (**Figure 3.19**). We were not able to distinguish the signal of kes1-GFP from the typical auto-fluorescence in starved cells, however during SE, we observed that kes1p-GFP increasingly accumulated around the cell cortex during consecutive time-points of SE (**Figure 3.22**). Osh7-GFP also located to the cytoplasm, and had signs of cortical accumulation. In addition, osh7-GFP was strongly concentrated in the nucleus (**Figure 3.19**), (**Figure 3.22**). Since different oshes from budding yeast and mammalian cells locate to the cortical ER (or ER-PM contact sites) [Mesmin, Antonny, 2016], we presume that the cortical localisation of kes1p-GFP and osh7p-GFP during SE indicate a cortical ER localisation.

All together, these results suggest that during SE, the presumptive osh/PI(4)P module might function at the cell cortex.

4.3.2.4 ER-PM connections mutant is defective in P1 and P2

De novo cell polarisation of *S. pombe* depends on newly synthesised ergosterol [Makushok et al., 2016b]. We showed that during SE presumptive kes1p-GFP and osh7-GFP concentrated at the cell cortex (**Figure 3.22**). We also showed that kes1p and osh7p might act in a similar fashion to their orthologues, being involved in non-vesicular transport of lipids between two closely opposed lipid bilayers [Im et al., 2005], [Saint-Jean de et al., 2011b] [Drin et al., 2016], [Chung et al., 2015], [Filseck Moser von et al., 2015a]. Therefore, we were interested if the function of the presumptive osh/PI(4)P module is dependent on the distance between the ER and the PM.

These connections in fission yeast are mediated by two VAP proteins - scs2p and scs22p [Zhang et al., 2012]. Deletion of both, leads to significant loss in ER-PM connections and detachment of most of the ER from the PM [Zhang et al., 2012]. Strikingly, we observed that *scs2*Δ*scs22*Δ mutants did not form SRMs after the first 15min in SE and filipin signal was not more intense (in contrast to the wild-type control) (**Figure 3.32**). Cells behaved similar to *kes1*Δ, *osh7*Δ, and *pik1-td* mutants, which retained numerous filipin dots in starvation and during SE (**Figure 3.20**), (**Figure 3.30**). We conclude that ER-PM connections, mediated by scs2p and scs22p, are involved in P1 entry at early time-points of SE. Strikingly, *scs2*Δ*scs22*Δ mutants were strongly defective in P2 entry, since at 60min in SE mutants rarely formed wild-type looking SRMs. Moreover, we observed a high variability of phenotypes, ranging from completely unpolarised cells (with misshapen SRMs or SRMs mainly at sides of these cells) to cells which entered P2 normally (**Figure 3.32**). The cells did not enter P3, however a slow increase in cell length was observed (**Figure 3.33**). Unfortunately, we did not follow growth progression on the single cell level and did not study the changes in dynamics of SRMs in single *scs2*Δ*scs22*Δ cells. Such studies should be performed.

We conclude that ER-PM connections, mediated by scs2p and scs22p in fission yeast, are required for proper SRM formation during SE and efficient stabilisation of SRMs at cell poles. These mutants partially resembled *kes1*Δ and *osh7*Δ phenotypes during SE (**Figure 3.20**). Moreover, similar to *tea1*Δ and *kes1*Δ/*osh7*Δ, *scs2*Δ*scs22*Δ mutants were delayed in polarisation, and we think that they were waiting for cdc42p in order to activate any SRMs and to initiate P3 [Makushok et al., 2016b]. Moreover, we speculate that similar to *tea1*Δ cells, any SRM during P1 in *scs2*Δ*scs22*Δ mutants has, at least temporarily, the potential to become the future growth site, because numerous cells after 60min in SE displayed one SRM at the cell side which had significantly higher filipin intensity than other SRMs. The presence of the tea1p system explains why most of *scs2*Δ*scs22*Δ mutants eventually polarised at cell poles.

In addition, VAP proteins, which are involved in formation of ER-PM connections in fission yeast, regulate the level of the signalling lipid PIP2 , which is the phosphorylation

product of PI(4)P [Zhang et al., 2000]. It is possible that the defects which we observed in the *scs2*Δ*scs22*Δ mutants, were related to the binding of VAP proteins to PIP2. The role of this lipid in SE is discussed in paragraphs further down (see, **4.5**).

Similarities between *kes1*Δ/*osh7*Δ and VAP mutants are a strong suggestion that ER-PM contact sites control the distance between the ER and the PM for efficient functioning of the presumptive osh/PI(4)P module. Detachment of the ER from the PM in the *scs2*Δ*scs22*Δ mutants, results in elevated levels of PI(4)P in the PM [Zhang et al., 2012]. This matches our hypothesis that the osh/PI(4)P system acts at ER-PM contact sites. Loss of these connections would lead to the inability for osh proteins to deliver ergosterols to the PM. Therefore, counter-transport of PI(4)P from the PM to the ER would be ineffective, resulting in elevated levels of this lipid in the PM. The homeostatic balance of this non-vesicular transport would be disturbed, resulting in improper SRM formation and defective polarity progression during SE.

4.3.3 Roles of cdc42p in SE

4.3.3.1 cdc42p activity in wild-type fission yeast cells is not essential for P2 but is crucial for P3

We previously mentioned that the process of cell polarisation proceeds even without cdc42p activity (see, **1.4**). Cdc42 activity is detected only after 1-2h into SE [Makushok et al., 2016b]. Consistently, *cdc42-L160S* mutants were shown to enter P2 but also to enter P3 and to perform cell division [Makushok et al., 2016b]. These mutants are defective in the formation of actin cables like *for3*Δ mutants, but experience almost normal growth speeds. This poses a paradox since *for3*Δ mutants do have problems in P3 [Makushok et al., 2016b].

Here, we followed SE using another temperature-sensitive mutant of cdc42p -

cdc42-3, which we found to mediate a stronger loss of function [Tatebe et al., 2008]. Interestingly, all cells entered P1 and P2 and even displayed bi-polar SRM distribution (**Figure 3.28**). It provides more support for [Makushok et al., 2016b], who showed that the tea1p-dependent pathway does not involve cdc42p. We conclude that *cdc42-3* mutants are able to establish cell polarity and can restrict SRM domains to cell poles.

In contrast to *cdc42-L160S* [Makushok et al., 2016b], the *cdc42-3* mutants did not enter P3 (**Figure 3.29**). We explain this by the known upstream role of cdc42p in secretory trafficking [Estravís et al., 2012]. In addition, this matches the observation from [Makushok et al., 2016b], showing that *for3*Δ mutants have defects in P3 entry. Importantly, this result confirmed the data from [Makushok et al., 2016b], that P2 entry is not dependent on fast growth initiation in wild-type cells. Moreover, we think that the *cdc42-3* cells have problems in maintaining the size of the growth sites and thereby the cell width (**Figure 3.29**), [Kelly, Nurse, 2011b]. In addition, weak filipin signal could be detected at cell sides (with much weaker intensity than SRMs at cell poles) (**Figure 3.28**), which suggests that the defect in cell width maintenance in cdc42-3 cells might be due to role of cdc42p in the polymerisation of the actin filaments and removal of side SRMs [Estravís et al., 2012] (linking to LatB-treated cells showed in [Makushok et al., 2016b]).

In addition, we observed that *cdc42-3* mutants were slightly defective in P1 and delayed in P2 entry (**Figure 3.28**). It is likely that these surprising effects are the result of hypomorphic features of the strain [Tatebe et al., 2008]. It is possible that these cells had abnormal cell wall from their pre-starvation growth phase, thus filipin could have different binding properties than in the wild-type.

Nevertheless, we confirm the observations from [Makushok et al., 2016b] that cdc42p activity is not needed for *de novo* cell polarisation in wild type fission yeast cells, however we show that it is essential for P3.

4.3.3.2 kes1p is redundant with cdc42p for stabilisation of SRMs at cell poles during P2

Cdc42p in not involved in cell polarisation in wild-type fission yeast cells (**Figure 3.28**), [Makushok et al., 2016b]. Instead, tea1p is central for cell polarisation. It stabilises SRMs at cell poles and controls the polar activation of cdc42p [Makushok et al., 2016b]. It was suggested that cdc42p activity might become central in *tea1*Δ cells, which remain in P1 for prolonged time periods [Makushok et al., 2016b]. Moreover, we mentioned that functions of kes1p and osh7p in P2 might be linked to tea1p because they are strongly delayed in P2 entry (**Figure 3.20**). Therefore, we wondered if the delayed polarisation in *kes1*Δ and *osh7*Δ mutants is dependent on cdc42p. We studied double mutants *cdc42-3kes1*Δ and *cdc42-3osh7*Δ in SE (**Figure 3.28**).

Strikingly, *cdc42-3kes1*Δ mutants behaved differently than corresponding single mutants because at 60min in SE we observed SRMs mostly at cell sides (**Figure 3.20**), (**Figure 3.28**). In the following hours of SE, *cdc42-3kes1*Δ mutants contained mostly one strongly fluorescent SRM at one side of each cell. This correlates with *tea1*Δ mutants, which cannot stabilise SRM at cell poles and cannot build defined SRM at opposite cell ends [Makushok et al., 2016b]. These results showed, that similar to *tea1*Δ mutants, each SRM in *cdc42-3kes1*Δ cells can become the site of P2 initiation (**Figure 3.28**), [Makushok et al., 2016b]. In addition, similar to *tea1*Δ, *cdc42-3kes1*Δ mutants did not build defined SRMs at opposite cell ends (**Figure 3.28**).

The previously suggested essential role of cdc42p in *tea1*Δ cells is based on the fact that strongly delayed P2 initiation in these cells, is accompanied by fast growth initiation [Makushok et al., 2016b]. Therefore, the authors suggested that cdc42p might play a central role in these mutant cells to initiate P2 and P3. Our data showed that the formation of one defined side SRM (similar to *tea1*Δ) in *cdc42-3kes1*Δ mutants, which remain in P1 for a long time, did not necessary require cdc42p-dependent growth activity. Interestingly, cdc42p became crucial for the stabilisation of SRMs at cell poles in the absence of kes1p. Therefore, *kes1*Δ mutants might be an example of a special condition,

since SRM formation in these cells was strongly defective. We can only speculate that, since SRM formation was abnormal, tea1p potential to stabilise these mutant SRMs was weaker. Such cells would wait until sufficient reservoirs of ergosterol are collected in the PM and proper SRMs are formed. During the delayed P1 of *kes1*Δ mutants, cdc42p would already be active and would initiate polarisation from random SRM.

In contrast to *cdc42-3 kes1*Δ, *cdc42-3 osh7*Δ shared features of both *osh7*Δ or *cdc42-3* (**Figure 3.28**). This observation, together with the fact that a double mutant *kes1*Δ*osh7*Δ had additive phenotype and that the orthologues of osh7p in budding yeast and mammalian cells are involved in the transport of phosphoserine rather than sterol [Filseck Moser von et al., 2015a], [Chung et al., 2015], suggest that osh7p could act in a different pathway than kes1p, which could be independent of kes1p and cdc42p. It is highly interesting to evaluate the lipid binding property of both kes1p and osh7p in fission yeast.

Summarising, we conclude that in the absence of kes1p, cells need the active cdc42p in order to stabilise SRMs at cell poles and to enter P3.

4.4 ER tubularity mutant is defective in cell polarisation

The cortical ER is built of interconnected tubules and flat cisternae, which are located at an average distance of 33nm from the PM [Pichler et al., 2001], [West et al., 2011]. In *S. pombe* ER cisternae predominantly localise to non-growing parts of the cell [Zhang et al., 2010], [Zhang et al., 2012] and localisation of cisternae correlates with the presence of ER-PM contact sites. Moreover, localisation of ER tubules depends on the cell cycle stage of the cells [Zhang et al., 2010]. Elongating cell ends and sites of cytokinesis are highly enriched in ER tubules [Zhang et al., 2010]. It was shown that the tubularity of the ER is involved in restricting regions for placing growth machinery at sites of cytokinesis and assuring a symmetric cell division [Zhang et al., 2010]. We were interested if perturbed ER morphology and eventually abnormal distribution of ER-PM connections might have an effect in *de novo* cell polarisation and growth initiation.

We followed SE in a mutant strain, which lacks ER tubules (*rtn1*Δ*yop1*Δ*tts1*Δ, further called *try*Δ). Our study showed that after 60min in SE, mutants contained defined SRMs at cell sides, which looked different than wild-type SRMs, because often there was the single SRM that looked wider than typical SRM in P1 and had a stronger filipin intensity than the remaining SRMs (**Figure 3.32**). This suggested that these mutants were initiating P2 from other regions than cell poles. After 180min in SE we observed a variety of phenotypes, including wild-type looking cells (**Figure 3.32**). We did not observe bulges in locations of strongly fluorescent side SRMs, suggesting that mutants did not initiate growth from these regions. Up to 180min in SE the mutants did not initiate fast growth also from cell poles (**Figure 3.33**). All together, we hypothesise that ER tubularity is involved in SRM stabilisation at cell poles. Since, improper tubularity results in predominant cisternal regions at the cell cortex, which is known to form connections with the PM [Zhang et al., 2010], it is possible that such close connections between the ER and the PM resulted in the inhibition of cell pole regions, restricting space for the cell growth machinery and consequently delaying fast growth initiation. No P3 initiation up to 180min in SE was seen, and is in line with this hypothesis (**Figure 3.33**).

We conclude that that ER tubularity is involved in stabilisation of SRMs at cell poles during SE.

4.5 PIP2 synthesis is important for SE

PIP2 is a signalling lipid, which is a product of phosphorylation of PI(4)P by the kinase its3p in fission yeast [Zhang et al., 2000]. *its3* is an essential gene. Its product in fission yeast plays a role in the organisation of actin patches, cell separation, cell wall integrity, membrane trafficking and polarised localisation of membrane tethering complex - exocyst [Zhang et al., 2000], [Deng et al., 2005], [Li et al., 2013], [Jourdain et al., 2012], [Bendezú et al., 2012]. PIP2 production most probably impacts the level of the essential PI(4)P (which we showed to be essential for SRM formation during SE (see, **3.3.1**)). Therefore, we wanted to know whether PIP2 synthesis has an impact on

SE.

Interestingly, a conditional mutant of PIP2 synthesis - *its3-1* formed wild-type looking SRMs, however, these cells were strongly defective in cell polarisation (**Figure 3.30**). 60min in SE most of cells concentrated defined and wider SRM domains at lateral sides in the PM (**Figure 3.30**). Often, single lateral SRM had stronger filipin intensity than other SRMs, which could suggest ectopic P2 initiation (**Figure 3.30**). Therefore, we thought that subset of *its3-1* cells would have the potential for ectopic growth initiation at these sites. We did not observe defined SRMs at the opposing poles (most probably cells could not stabilise SRMs at secondary poles prior to P3 initiation), similar to *tea1*Δ cells [Makushok et al., 2016b]). Interestingly, after 120min in SE most of the cells had a clearly mono-polar SRM at one of the cell poles, although cell length measurements did not indicate that P3 had initiated yet. Very occasionally, mutants contained bulges at cell sides (**Figure 3.30**, C), at this time-point. These cells looked like *tea1*Δ mutants, which started growing from random SRM [Makushok et al., 2016b]. It would be interesting to observe live progression through SE of *its3-1* mutants in order to observe the dynamics of SRMs during SE in these cells and to correlate their size with the detailed growth pattern at particular cell ends.

Moreover, between 60-180min in SE many cells were dead (or were sensitive to filipin staining) (**Figure 3.30**, B) (observed by intensive filipin signal inside these cells, which suggested permeability of the PM). It would be interesting to understand why many *its3-1* mutants died (or were filipin-sensitive) during SE. Interestingly, all living cells at 180min in SE contained exclusively mono-polar and wide SRMs at cell poles (**Figure 3.30**). These mono-polar *its3-1* mutants initiated P3 (**Figure 3.31**). In contrast to 120min in SE, we could not detect any cells with bulges after 180min in SE (**Figure 3.30**).

We conclude that perturbations in the PIP2 synthesis play role in stabilisation of SRMs at cell poles during P2, which causes a delay in the establishment of the cell polarity in most of the cells, and results in ectopic growth site positioning in a small portion of mutant cells. Eventually, mutants (in which we could observe filipin staining

in the PM) were polarised after 180min in SE but they did not have strongly fluorescent SRMs at opposite poles. This might impact future P4 initiation and suggests correlation between PIP2 synthesis and tea1p-dependent function (**Figure 3.30**).

We have previously showed that VAP proteins (which form ER-PM contact sites) are required for SRM formation and cell polarisation (see, **3.3.3**). Interestingly, scs2p can directly bind a substrate for the PIP2 synthesis - PI(4)P in mammalian cells [Drin et al., 2016], therefore suggesting that scs2p could modulate access of signalling lipids to the cell cortex [Mesmin, Antonny, 2016]. This would additionally couple PIP2 to the osh/PI(4)P system (see, **Figure 3.30**). Interestingly, removal of scs2p in fission yeast results in increased level of PI(4)P in the PM [Zhang et al., 2000], suggesting that the level of PIP2 might also be affected. A role for PIP2 during SE at the cell cortex is very likely, since both GFP-its3p and a marker for PIP2 (PLC(PH)) mainly localise to cortical regions in exponentially growing cells [Li et al., 2013]. It is therefore interesting to study, how regulation between the levels of Pi(4)P and PIP2 contribute to the establishment of fission yeast cell polarity. Moreover, PIP2 was shown to interact with cdc42p [Martin, Arkowitz, 2014]. We previously mentioned that cdc42p activity is involved in SRM stabilisation at cell poles in the absence of kes1p (see, **4.3.3.2**). It is possible that in these special conditions, cdc42p uses PIP2 (which could be provided by the scs2p at the ER-PM contact sites), to stabilise SRMs at cell poles.

4.6 Regulation of the bi-polar SRM pattern during SE

During P2, SRMs in wild-type fission yeast cells start covering both cell poles and remaining SRMs are being removed [Makushok et al., 2016b]. Later, growth significantly increase (P3) at only one of the cell poles and SRMs at this pole become wider [Makushok et al., 2016b]. P4 starts when fast growth also initiates at the secondary end and its SRM domain also becomes more prominent [Makushok et al., 2016b]. It has been suggested that tea1p is responsible for the formation of SRMs at secondary poles prior to growth initiation, therefore *tea1*Δ mutants cannot stabilise SRMs at the non-growing ends and

further to activate a second growth site [Makushok et al., 2016b].

During cell polarisation in starvation exit, *sec8-1 for3*Δ mutants also displayed a mono-polar SRM pattern most probably before P3 was initiated (see, **3.1.5.1**). Strikingly, *sec8-1 for3*Δ mutant cells treated with BFA to prevent growth, also showed SRM at a single pole. It suggests that lack of filipin staining at the secondary pole of *sec8-1for3*Δ cells is a consequence of defective SRM formation or stabilisation, similar to the situation in *tea1*Δ cells (**Figure 3.10**). In addition, sec8p-GFP localised predominantly to cell ends, which exhibit only low or weak filipin signal (**Figure 3.7**). These observations suggest that sec8p might be controlled by tea1p in order to form and stabilise SRMs at opposing cell ends what has an impact on future growth site activation at the secondary pole. Additionally, it is possible that something similar happens in the PIP2 synthesis mutant (*its3-1*), where most cells showed a mono-polar SRM pattern (**Figure 3.30**). This finding correlates with sec8p-mediated membrane trafficking, as PIP2 is known to regulate the positioning of the exocyst complex components [Jourdain et al., 2012], [Bendezú et al., 2012]. Unfortunately, we cannot exclude that *sec8-1 for3*Δ and *its3-1* mutants are able to form prominent SRMs at opposing cell ends with a delay. Moreover, we did not analyse growth profiles for particular cell ends (in contrast to [Makushok et al., 2016b]). Additional studies will be necessary to evaluate our hypothesis further.

4.7 Working model and summary

We present a working model, in which the osh/PI(4)P module is required for the transport of *de novo* synthesised ergosterol to the PM and formation of SRM domains during P1. We hypothesise that the osh/PI(4)P module acts at ER-PM contact sites, which provide the appropriate distance for non-vesicular transport between these two organelles. Osh proteins actively transport ergosterol from the ER to the PM, where PI(4)P is synthesised. At the PM sterol is exchanged for PI(4)P, which is delivered back by osh proteins to the ER. There PI(4)P is dephosphorylated (see introduction **1.3.1.3**). In our model, PI(4)P would be rate-limiting for the proper functioning of the osh/PI(4)P

system.

Prior to and during P2, regulation of PI(4)P and PIP2 levels would be important. PI(4)P/PIP2 probably modulate the homeostasis between actin-dependent SRM removal and tea1p-dependent polarisation at the cell poles. After establishing cell polarity, cells critically depend on the redundantly acting Golgi-apparatus and membrane fusion machinery to maintain their polarised state.

Polarised wild-type cells subsequently initiate P3, which involves the Golgi and cdc42p-mediated membrane trafficking. Interestingly, non-vesicular transport, mediated by oshes, also contributes to the rate of the cell elongation. In addition, tea1p-related stabilisation of SRMs at the secondary pole depends on the membrane tethering via sec8p and PIP2 synthesis. This secretion-dependent maintenance of SRM at the secondary pole during P3, would have an impact on the future P4 initiation.

Understanding of all these interactions in space and time is crucial to dissect the process of cell polarisation.

5 Supplementary figures

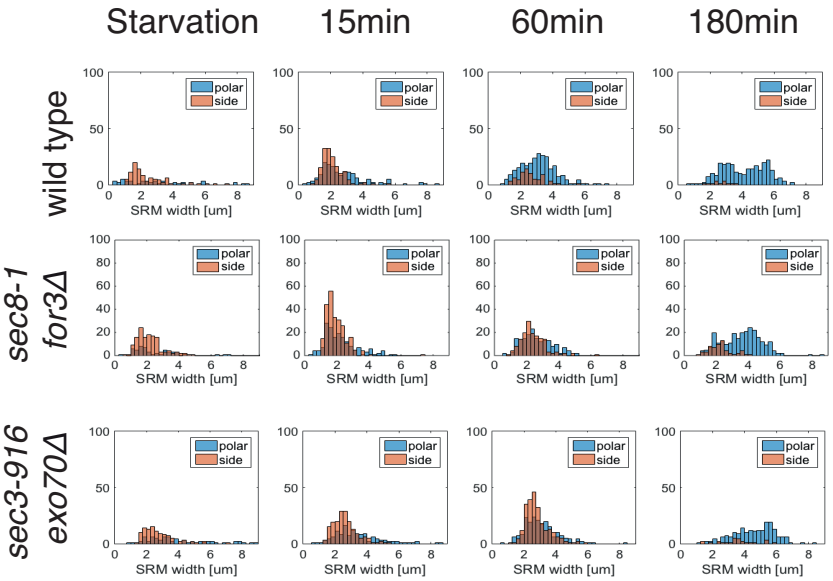

Figure 5.1: **Histograms showing count normalised distribution of SRM width and SRM classification during SE in post-Golgi trafficking mutants**

Classification of polar (blue) and side (orange) SRMs for different time-points of SE. Histograms showing count normalised distribution of SRM width (μm). Rows of plots represent subsequent time-points of SE. Quantification was performed as described in Materials and methods (see, **2.2.2.2**).

	fission yeast	**budding yeast**	***A. nidualns***
kes1p	cytoplasm, cell poles, site of cytokinesis	Golgi apparatus, exocytic vesicles, cytoplasm	cytoplasm, in some cells puncta at apical regions
kes2p	cytoplasm, nuclear envelope, ER?	Golgi apparatus, exocytic vesicles, cytoplasm	cytoplasm, puncta at apical regions
osh2p	cytoplasm, particles	bud, bud neck, nuclear-vacuolar junctions	Golgi cisternae
osh3p	-	cortical ER (ER cisternae)	cortical puncta adjustment to ER tubules
oshEp	cytoplasm, cell periphery	-	puncta at peripheral ER
osh7p	cytoplasm, nucleus, cell periphery	cytoplasm, cell periphery	cytoplasm, cortical ER

Table 14: **Localisations of fission yeast oxysterol-binding proteins and their orthologues**

Localisations of oshes from fission yeast are based on our studies (they do not include information from *S. pombe* Postgenome Database).

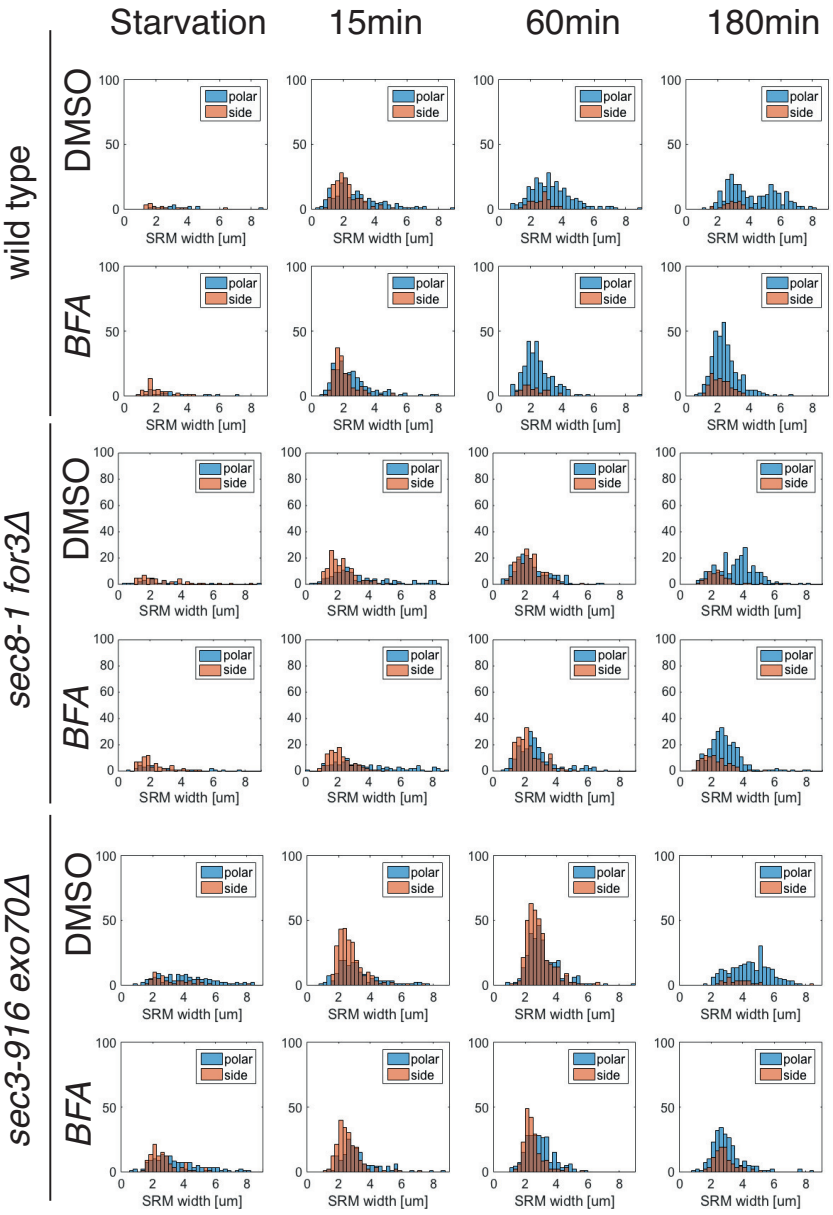

Figure 5.2: **Histograms showing count normalised distribution of SRM width and SRM classification during SE in post-Golgi trafficking mutants treated with BFA**

Classification of polar (blue) and side (orange) SRMs for different time-points of SE. Histograms showing count normalised distribution of SRM width (μm). Rows of plots represent subsequent time-points of SE. Quantification was performed as described in Materials and methods (see, 2.2.2.2).

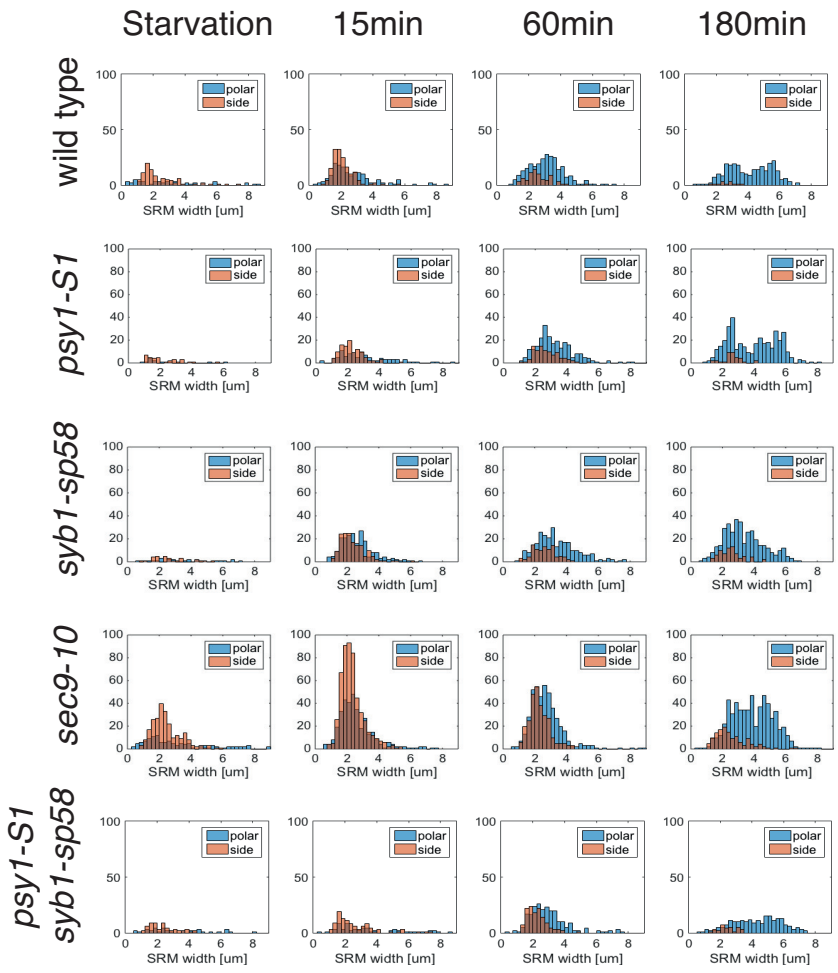

Figure 5.3: **Histograms showing count normalised distribution of SRM width and SRM classification during SE in PM-SNARE mutants**

Classification of polar (blue) and side (orange) SRMs for different time-points of SE. Histograms showing count normalised distribution of SRM width (μm). Rows of plots represent subsequent time-points of SE. Quantification was performed as described in Materials and methods (see, **2.2.2.2**).

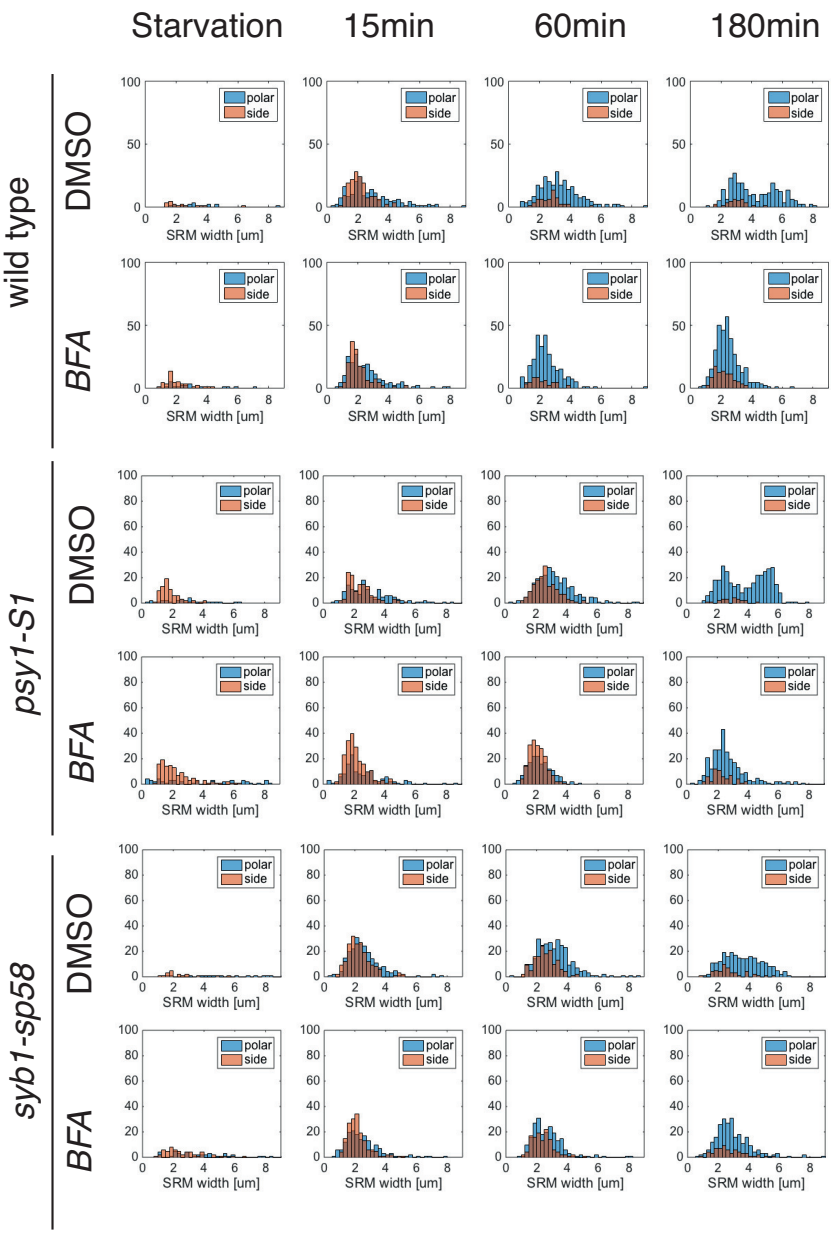

Figure 5.4: **Histograms showing count normalised distribution of SRM width and SRM classification during SE in *psy1-S1* and *syb1-sp58* treated with BFA**

Classification of polar (blue) and side (orange) SRMs for different time-points of SE. Histograms showing count normalised distribution of SRM width (μm). Rows of plots represent subsequent time-points of SE. Quantification was performed as described in Materials and methods (see, **2.2.2.2**).

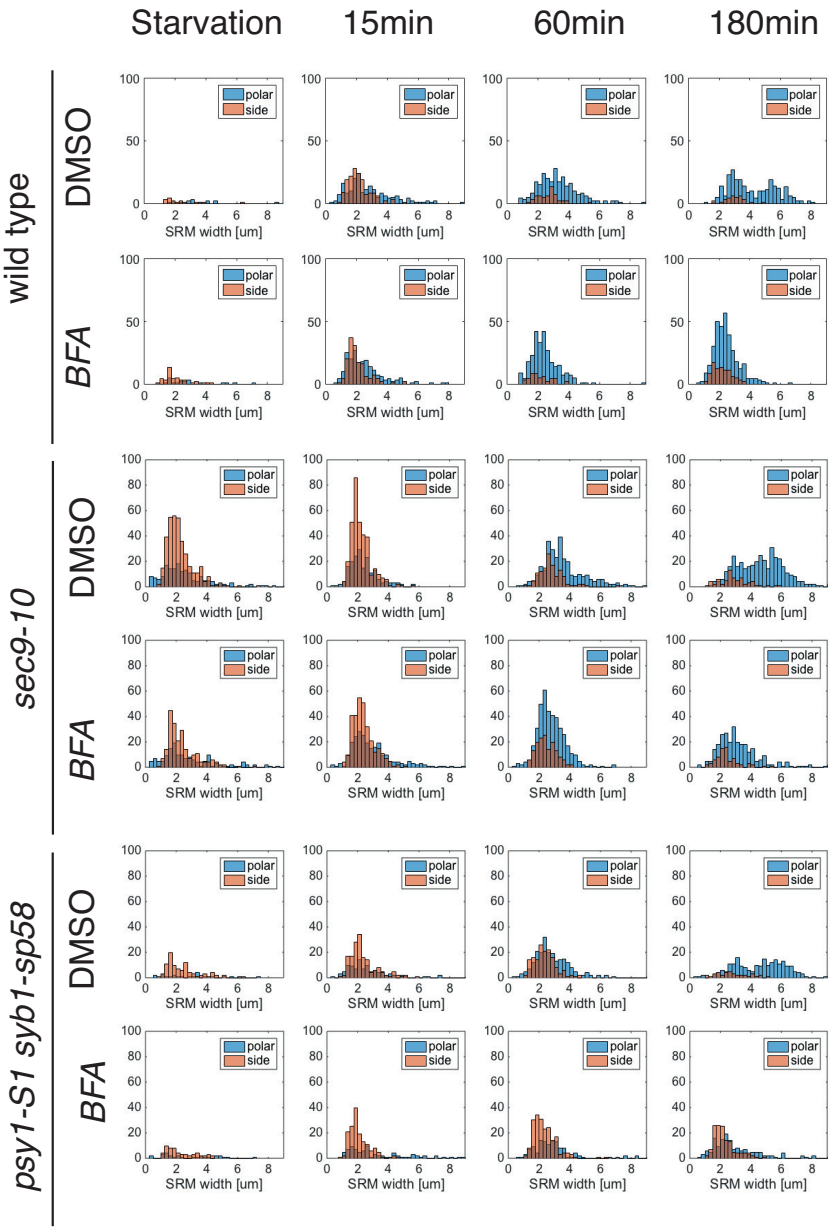

Figure 5.5: **Histograms showing count normalised distribution of SRM width and SRM classification during SE in *sec9-10* and *psy-S1 syb1-sp58* treated with BFA**

Classification of polar (blue) and side (orange) SRMs for different time-points of SE. Histograms showing count normalised distribution of SRM width (μm). Rows of plots represent subsequent time-points of SE. Quantification was performed as described in Materials and methods (see, **2.2.2.2**).

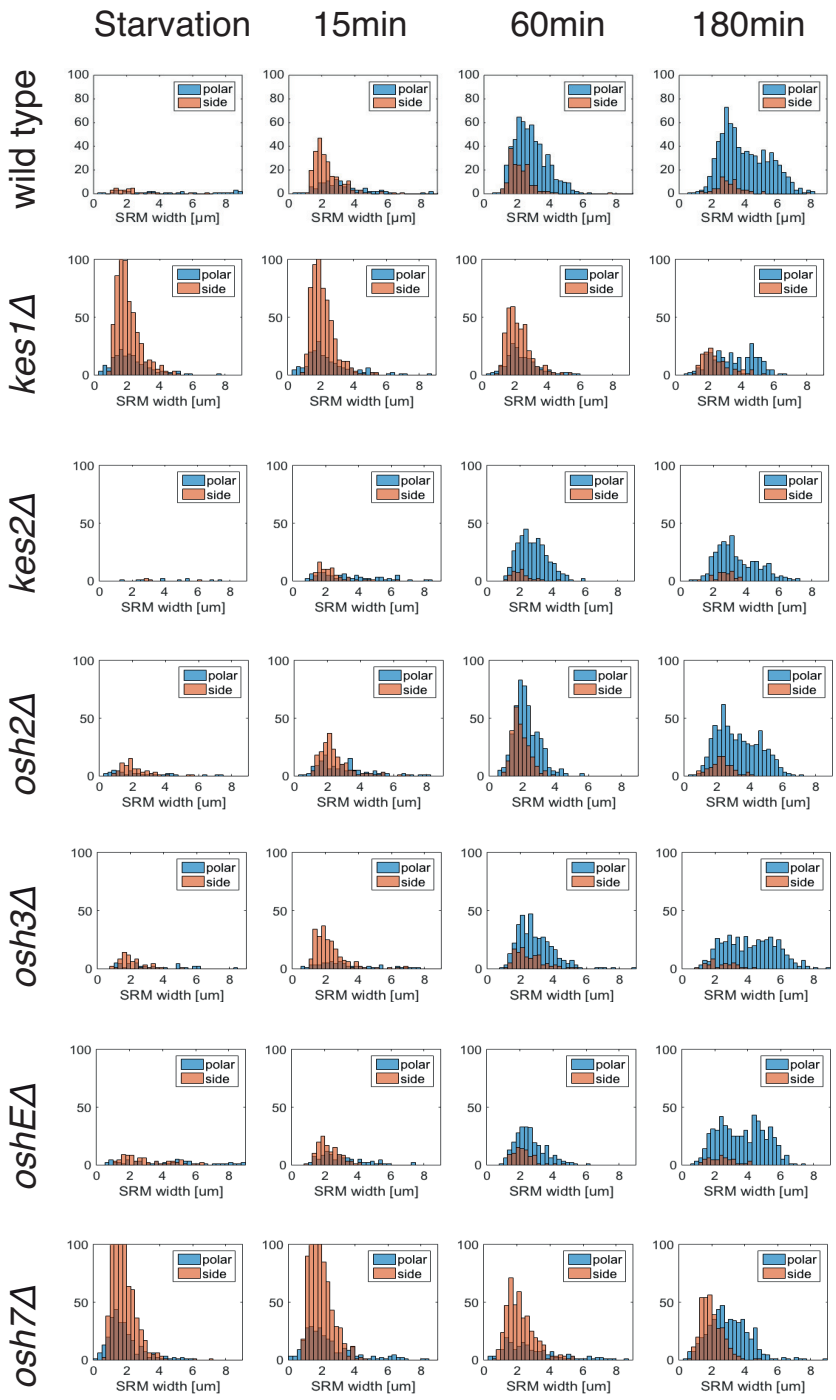

Figure 5.6: **Histograms showing count normalised distribution of SRM width and SRM classification during SE in *osh*Δ mutants**

Classification of polar (blue) and side (orange) SRMs for different time-points of SE. Histograms showing count normalised distribution of SRM width (μm). Rows of plots represent subsequent time-points of SE. Quantification was performed as described in Materials and methods (see, 2.2.2.2).

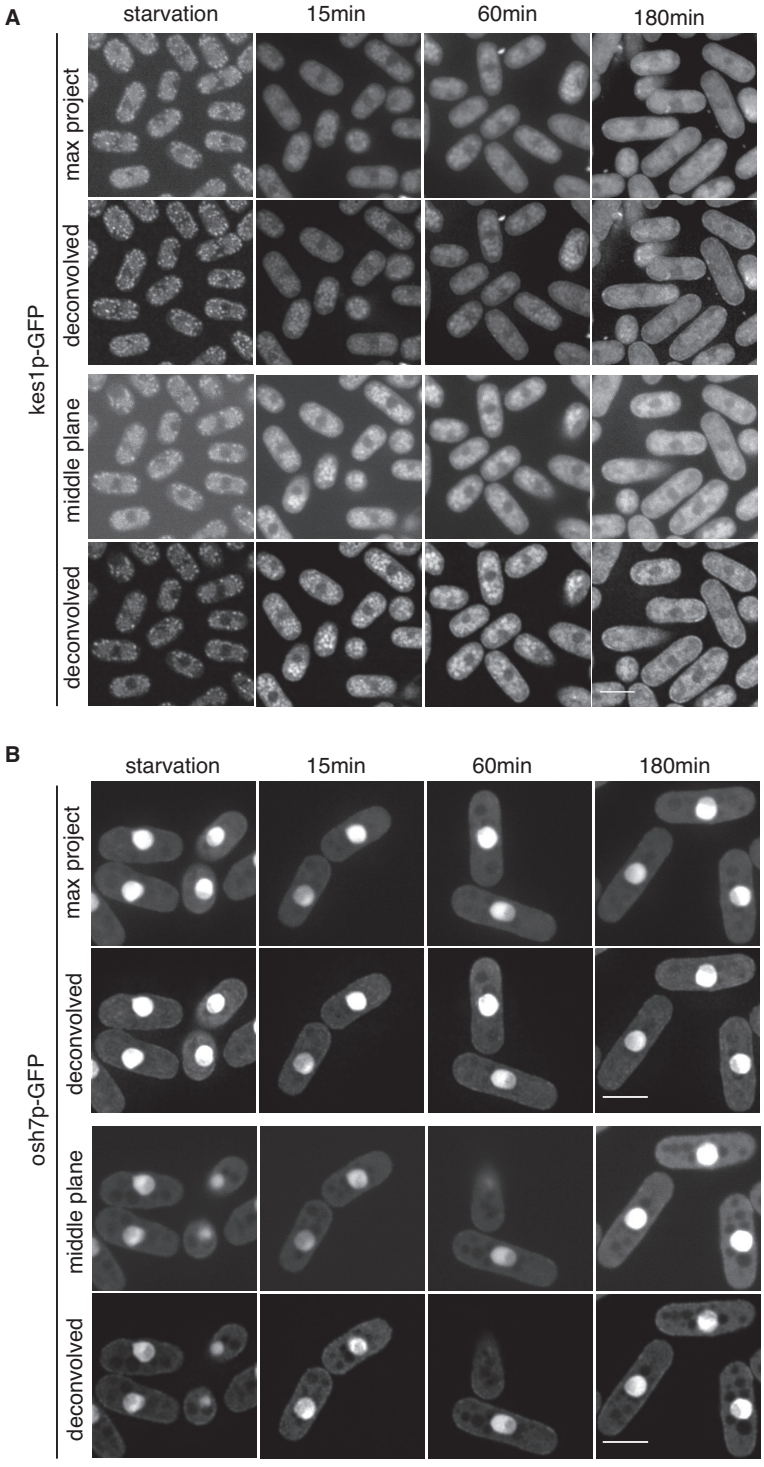

Figure 5.7: **Localization of kes1p-GFP and osh7p-GFP during SE**

A - Localisation of kes1p-GFP under its endogenous promoter during SE. First two rows present max-projected images and their deconvolved equivalents (below). Third and fourth row show middle z-sections from the stack and their corresponding deconvolved images (fourth row). Time-scale presents time in SE. **B** - Localisation of osh7p-GFP under its endogenous promoter during SE. First two rows present max-projected pictures and their deconvolved equivalents (below). Third and fourth row show middle z-sections from the stack and their corresponding deconvolved images (fourth row). Time-scale presents time into SE. Max-projections of 11 z-sections (acquired in 0.5μm distance). Scale bars: 5μm.

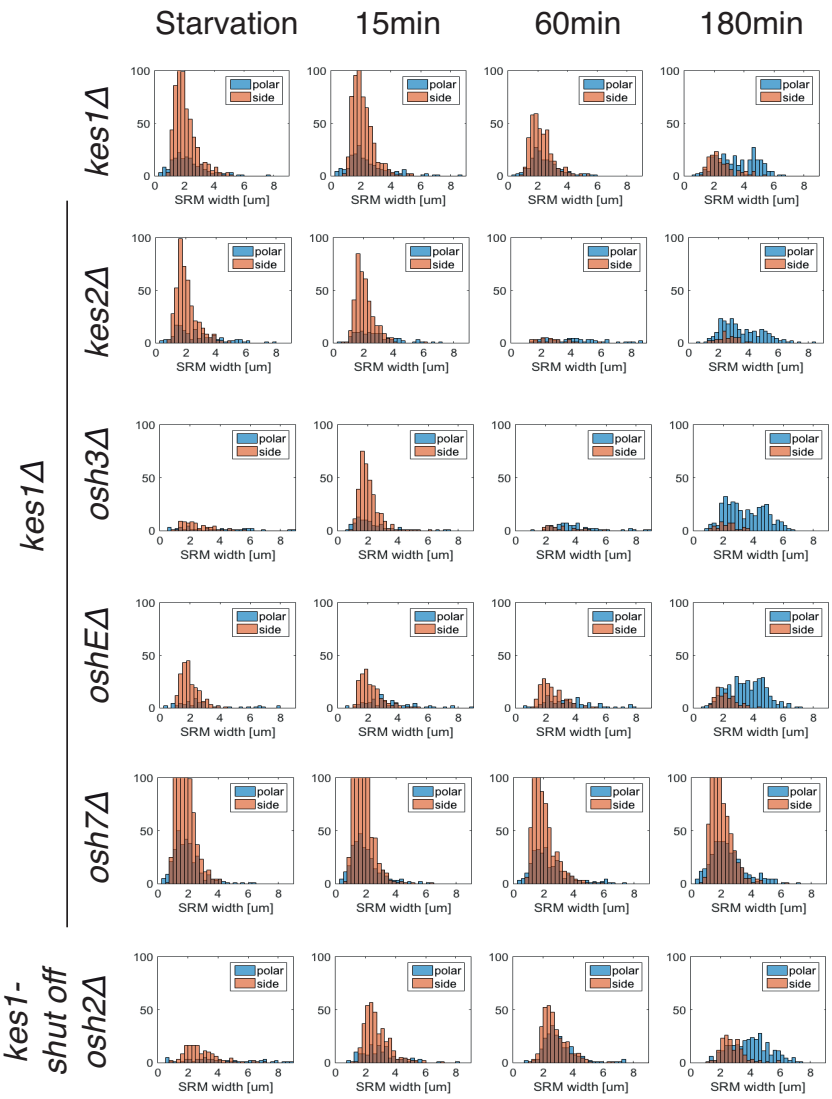

Figure 5.8: **Histograms showing count normalised distribution of SRM width and SRM classification during SE in mutants between *kes1*Δ and other *osh*Δ mutants**

Classification of polar (blue) and side (orange) SRMs for different time-points of SE in *kes1*Δ and double mutants between *kes1*Δ and other *osh*Δ. Histograms showing count normalised distribution of SRM width (μm). Rows of plots represent subsequent time-points of SE. Quantification was performed as described in Materials and methods (see, **2.2.2.2**).

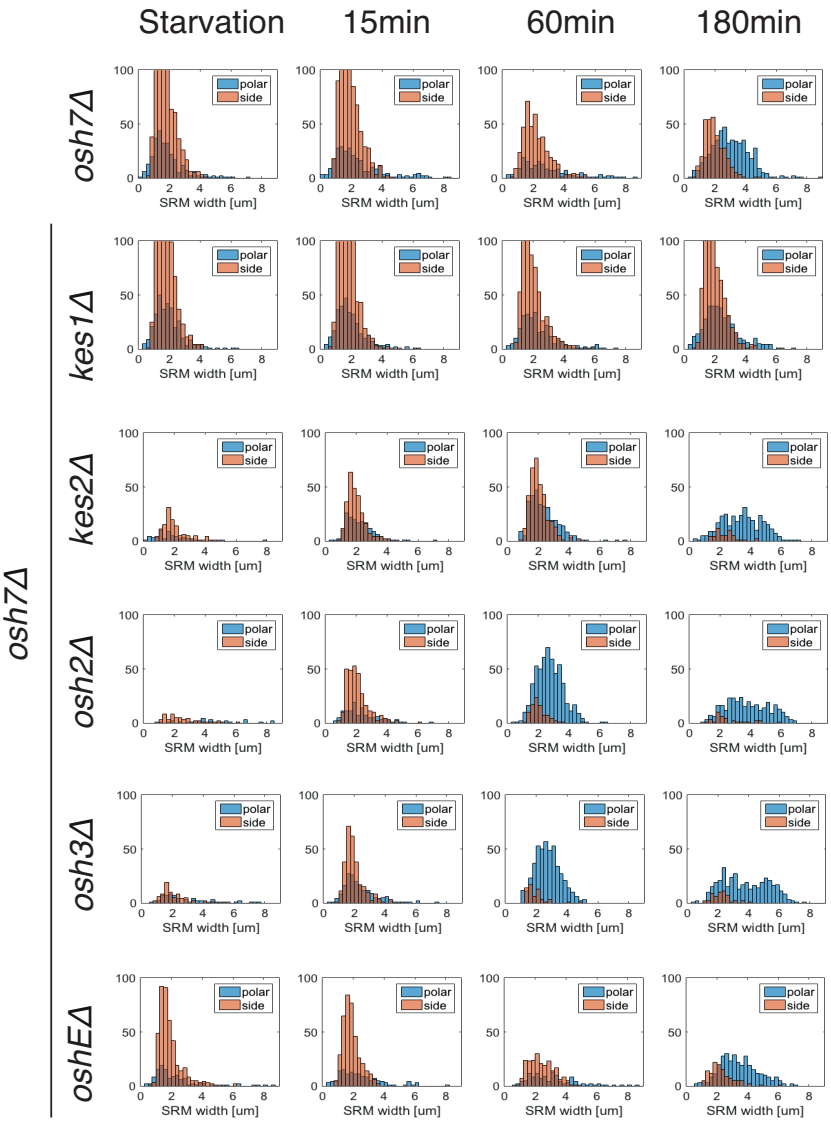

Figure 5.9: **Histograms showing count normalised distribution of SRM width and SRM classification during SE in mutants between *osh7*Δ and other *osh*Δ mutants**

Classification of polar (blue) and side (orange) SRMs for different time-points of SE in *osh7*Δ and double mutants between *osh7*Δ mutants and other *osh*Δ. Histograms showing count normalised distribution of SRM width (μm). Rows of plots represent subsequent time-points of SE. Quantification was performed as described in Materials and methods (see, **2.2.2.2**).

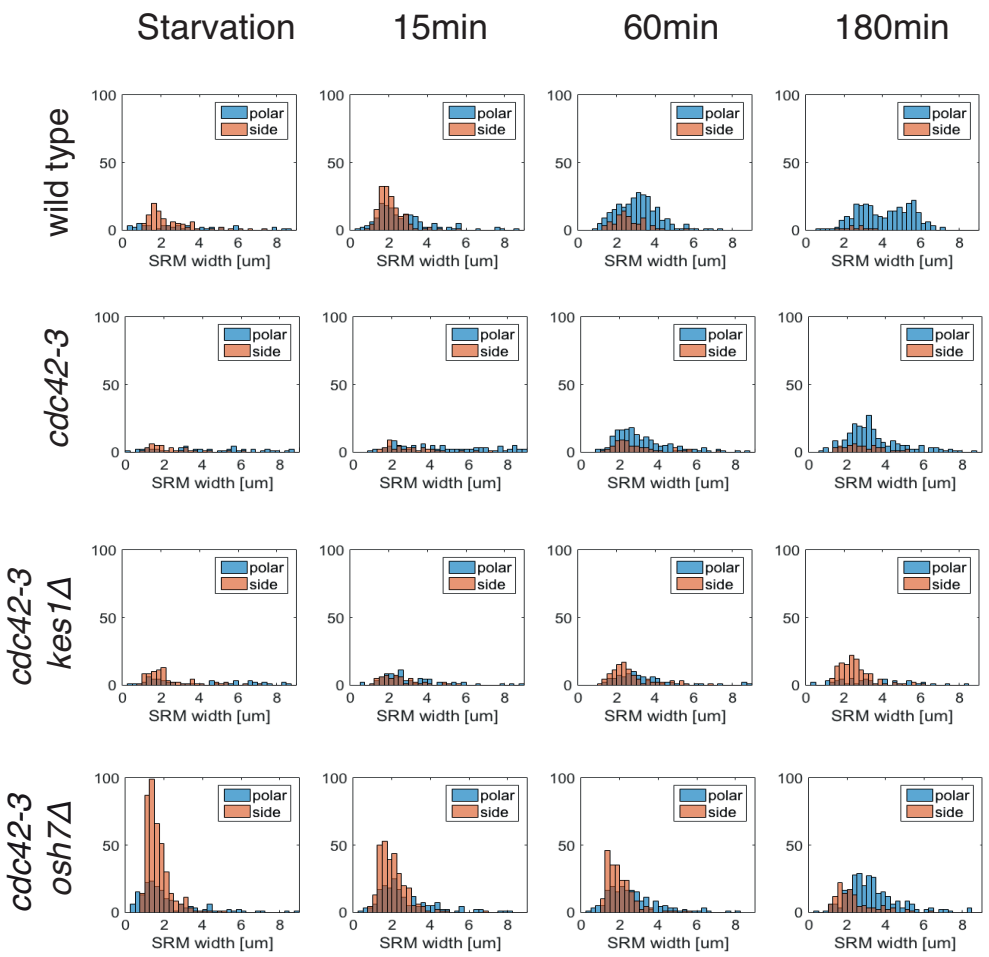

Figure 5.10: **Histograms showing count normalised distribution of SRM width and SRM classification during SE in mutants between *cdc42-3* and two *osh* deletions - *kes1* and *osh7***

Classification of polar (blue) and side (orange) SRMs for different time-points of SE in cells defective in cdc42p and double mutants defective both in cdc42p and kes1p/osh7p. Histograms showing count normalised distribution of SRM width (μm). Rows of plots represent subsequent time-points of SE. Quantification was performed as described in Materials and methods (see, 2.2.2.2).

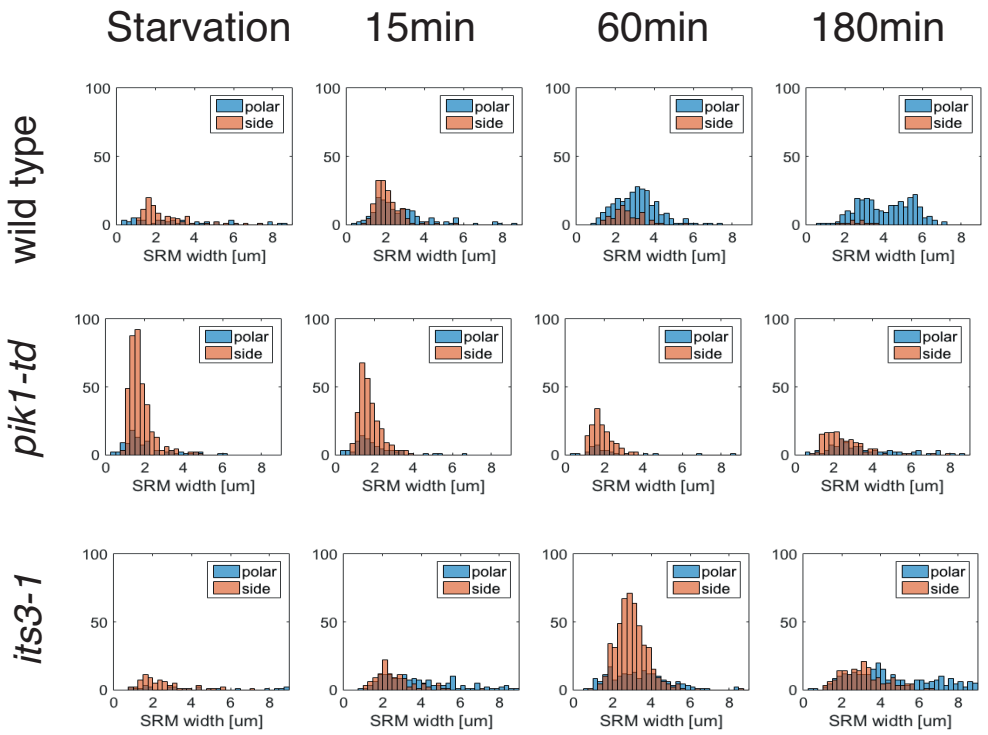

Figure 5.11: **Role of the main phosphatidylinositol kinases in *de novo* cell polarisation of *S. pombe***

Classification of polar (blue) and side (orange) SRMs for different time-points of SE in cells. Histograms showing count normalised distribution of SRM width (μm). Rows of plots represent subsequent time-points of SE. Quantification was performed as described in Materials and methods (see, **2.2.2.2**).
Starvation and SE in *pik-td* cells were performed in the continuous presence of thiamine-repressible conditions.

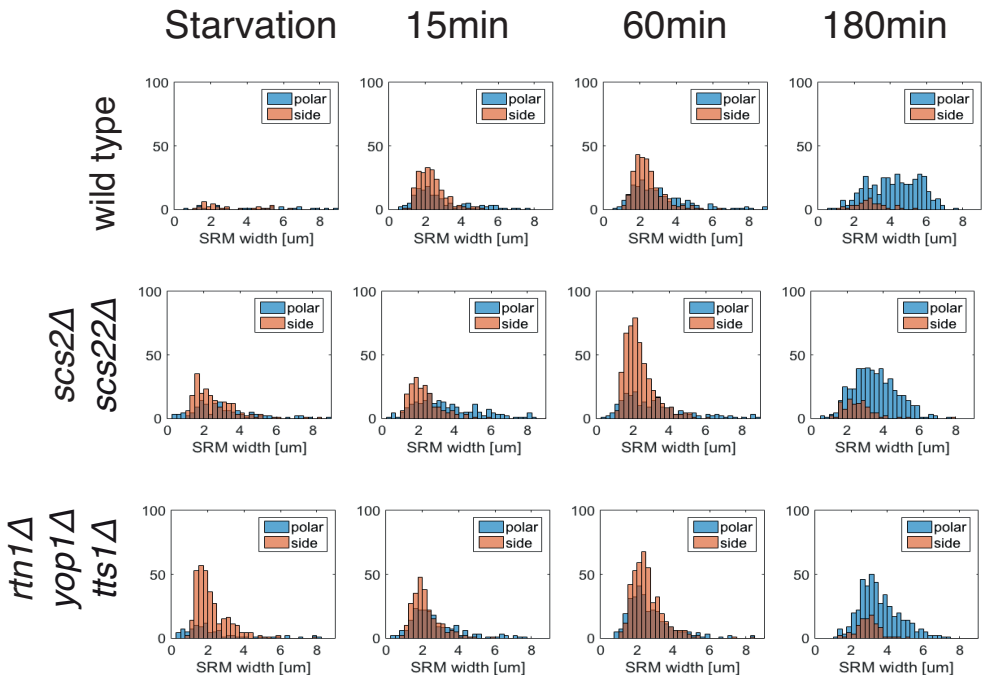

Figure 5.12: **Role of ER-shaping proteins in *de novo* cell polarisation of *S. pombe***

Classification of polar (blue) and side (orange) SRMs for different time-points of SE in cells. Histograms showing count normalised distribution of SRM width (μm). Rows of plots represent subsequent time-points of SE. Quantification was performed as described in Materials and methods (see, 2.2.2.2).
All strains were auxotrophs carrying: *ade6-M216*, *leu1* and *ura4-D18*. Medium was supplemented with appropriate amount of amino-acids.

6 References

Abenza Juan F, Couturier Etienne, Dodgson James, Dickmann Johanna, Chessel Anatole, Dumais Jacques, Salas Rafael E Carazo. Wall mechanics and exocytosis define the shape of growth domains in fission yeast // Nature communications. X 2015. 6. 8400.

Alberts Bruce, johnson Alexander, Lewis Julian, Morgan David, Raff Martin, Roberts Keith, Walter Peter. Molecular Biology of the Cell, Sixth Edition. XI 2014.

Alfaro Gabriel, Johansen Jesper, Dighe Shubha A, Duamel Giselle, Kozminski Keith G, Beh Christopher T. The Sterol-Binding Protein Kes1/Osh4p Is a Regulator of Polarized Exocytosis // Traffic (Copenhagen, Denmark). IX 2011a. 12, 11. 1521–1536.

Alfaro Gabriel, Johansen Jesper, Dighe Shubha A, Duamel Giselle, Kozminski Keith G, Beh Christopher T. The Sterol-Binding Protein Kes1/Osh4p Is a Regulator of Polarized Exocytosis // Traffic (Copenhagen, Denmark). IX 2011b. 12, 11. 1521–1536.

Alison L Pidoux John Armstrong. The BiP protein and the endoplasmic reticulum of *Schizosaccharomyces pombe*: fate of the nuclear envelope during cell division // Journal of cell science. 1993. 105. 1115–1120.

Altschul Stephen F, Gish Warren, Miller Webb, Myers Eugene W, Lipman David J. Basic local alignment search tool // Journal of Molecular Biology. X 1990. 215, 3. 403–410.

Alvarez F J, Douglas L M, Konopka J B. Sterol-Rich Plasma Membrane Domains in Fungi // Eukaryotic cell. V 2007. 6, 5. 755–763.

Alvarez-Tabares I, Grallert A, Ortiz J M, Hagan I M. Schizosaccharomyces pombe protein phosphatase 1 in mitosis, endocytosis and a partnership with Wsh3/Tea4 to control polarised growth // Journal of cell science. X 2007. 120, 20. 3589–3601.

Anderson J M, Van Itallie C M. Physiology and Function of the Tight Junction // Cold Spring Harbor Perspectives in Biology. VIII 2009. 1, 2. a002584–a002584.

Ang Agnes Lee, Taguchi Tomohiko, Francis Stephen, Fölsch Heike, Murrells Lindsay J, Pypaert Marc, Warren Graham, Mellman Ira. Recycling endosomes can serve as intermediates during transport from the Golgi to the plasma membrane of MDCK cells // The Journal of cell biology. XI 2004. 167, 3. 531–543.

Apodaca Gerard, Gallo Luciana I, Bryant David M. Role of membrane traffic in the generation of epithelial cell asymmetry // Nature cell biology. XII 2012. 14, 12. 1235–1243.

Arellano Manuel, Niccoli Teresa, Nurse Paul. Tea3p Is a Cell End Marker Activating Polarized Growth in Schizosaccharomyces pombe // Current Biology. IV 2002. 12, 9. 751–756.

Arioka M, Hirata A, Takatsuki A, Yamasaki M. Brefeldin A blocks an early stage of protein transport in Candida albicans // Journal of General Microbiology. VI 1991. 137, 6. 1253–1262.

Atilgan Erdinc, Magidson Valentin, Khodjakov Alexey, Chang Fred. Morphogenesis of the Fission Yeast Cell through Cell Wall Expansion // Current Biology. VIII 2015. 25, 16. 2150–2157.

Audhya A, Foti M, Emr S D. Distinct Roles for the Yeast Phosphatidylinositol 4-Kinases, Stt4p and Pik1p, in Secretion, Cell Growth, and Organelle Membrane Dynamics // Molecular biology of the cell. VIII 2000. 11, 8. 2673–2689.

Audhya Anjon, Loewith Robbie, Parsons Ainslie B, Gao Lu, Tabuchi Mitsuaki, Zhou Huilin, Boone Charles, Hall Michael N, Emr Scott D. Genome-wide lethality screen identifies new PI4,5P2 effectors that regulate the actin cytoskeleton // The EMBO journal. IX 2004. 23, 19. 3747–3757.

Ayscough Kathryn, Hajibagheri Nasser M A, Watson Rose, Warren Graham. Stacking of Golgi cisternae in Schizosaccharomyces pombe requires intact microtubules // Journal of cell science. 1993a. 106. 1227–1237.

Ayscough Kathryn, Hajibagheri Nasser M A, Watson Rose, Warren Graham. Stacking of Golgi cisternae in Schizosaccharomyces pombe requires intact microtubules // Journal of cell science. 1993b. 106. 1227–1237.

Ayscough Kathryn, Warren Graham. Inhibition of protein synthesis disrupts the golgi apparatus in the fission yeast,Schizosaccharomyces pombe // Yeast. I 1994. 10, 1. 1–11.

Bagnat M. Lipid rafts function in biosynthetic delivery of proteins to the cell surface in yeast // Proceedings of the National Academy of Sciences. III 2000. 97, 7. 3254–3259.

Bagnat M, Simons K. Cell surface polarization during yeast mating // Proceedings of the National Academy of Sciences of the United States of America. X 2002a. 99, 22. 14183–14188.

Bagnat M, Simons K. Lipid Rafts in Protein Sorting and Cell Polarity in Budding Yeast Saccharomyces cerevisiae // Biological chemistry. 2002b. 383, 10.

Bähler J, Pringle J R. Pom1p, a fission yeast protein kinase that provides positional information for both polarized growth and cytokinesis // Genes & Development. V 1998. 12, 9. 1356–1370.

Bähler Jürg, Wu Jian-Qiu, Longtine Mark S, Shah Nirav G, Mckenzie III Amos, Steever Alexander B, Wach Achim, Philippsen Peter, Pringle John R. Heterologous modules for efficient and versatile PCR-based gene targeting inSchizosaccharomyces pombe // Yeast. VII 1998. 14, 10. 943–951.

Balla Andras, Balla Tamas. Phosphatidylinositol 4-kinases: old enzymes with emerging functions // Trends in cell biology. VII 2006. 16, 7. 351–361.

Basu Roshni, Munteanu Emilia Laura, Chang Fred. Role of turgor pressure in endocytosis in fission yeast. // Molecular biology of the cell. III 2014. 25, 5. 679–687.

Baumann Nikola A, Sullivan David P, Ohvo-Rekilä Henna, Simonot Cedric, Pottekat Anita, Klaassen Zachary, Beh Christopher T, Menon Anant K. Transport of Newly Synthesized Sterol to the Sterol-Enriched Plasma Membrane Occurs via Nonvesicular Equilibration † // Biochemistry. 2005a. 44, 15. 5816–5826.

Baumann Nikola A, Sullivan David P, Ohvo-Rekilä Henna, Simonot Cedric, Pottekat Anita, Klaassen Zachary, Beh Christopher T, Menon Anant K. Transport of Newly Synthesized Sterol to the Sterol-Enriched Plasma Membrane Occurs via Nonvesicular Equilibration † // Biochemistry. IV 2005b. 44, 15. 5816–5826.

Beh C T. A role for yeast oxysterol-binding protein homologs in endocytosis and in the maintenance of intracellular sterol-lipid distribution // Journal of cell science. VI 2004. 117, 14. 2983–2996.

Beh C T, McMaster C R, Kozminski K G, Menon A K. A Detour for Yeast Oxysterol Binding Proteins // The Journal of biological chemistry. III 2012. 287, 14. 11481–11488.

Beh Christopher T, Cool Laurence, Phillips John, Rine Jasper. Overlapping Functions of the Yeast Oxysterol-Binding Protein Homologues // Genetics. III 2001. 157. 1117–1140.

Bendezu F O, Martin S G. Actin cables and the exocyst form two independent morphogenesis pathways in the fission yeast // Molecular biology of the cell. I 2011. 22, 1. 44–53.

Bendezú Felipe O, Vincenzetti Vincent, Martin Sophie G. Fission Yeast Sec3 and Exo70 Are Transported on Actin Cables and Localize the Exocyst Complex to Cell Poles // PloS one. VI 2012. 7, 6. e40248.

Bendezú Felipe O, Vincenzetti Vincent, Vavylonis Dimitrios, Wyss Romain, Vogel Horst, Martin Sophie G. Spontaneous Cdc42 Polarization Independent of GDI-Mediated Extraction and Actin-Based Trafficking // PLOS Biology. IV 2015. 13, 4. e1002097.

Benli Mustafa, Doring Frank, Robinson David G, Yang Xiaoping, DieterGallwitz . Two GTPase isoforms, Ypt31p and Ypt32p, are essential for Golgi function in yeast // The EMBO journal. 1996. 115. 6460–6475.

Berridge Michael J, Irvine Robin F. Inositol trisphosphate, a novel second messenger in cellular signal transduction // Nature. XI 1984. 312, 5992. 315–321.

Bicho Claudia C, Kelly David A, Snaith Hilary A, Goryachev Andrew B, Sawin Kenneth E. A Catalytic Role for Mod5 in the Formation of the Tea1 Cell Polarity Landmark // Current Biology. X 2010. 20, 19. 1752–1757.

Blagoveshchenskaya Anastasia, Cheong Fei Ying, Rohde Holger M, Glover Greta, Knödler Andreas, Nicolson Teresa, Boehmelt Guido, Mayinger Peter. Integration of Golgi trafficking and growth factor signaling by the lipid phosphatase SAC1 // The Journal of cell biology. II 2008. 180, 4. 803–812.

Bonifacino Juan S, Glick Benjamin S. The Mechanisms of Vesicle Budding and Fusion // Cell. I 2004. 116, 2. 153–166.

Bradley M P, Rayns D G, Forrester I T. Effects of Filipin, Digitonin, and Polymyxin B on Plasma Membrane of Ram Spermatozoa—An EM Study // Archives of Andrology. 1980. 4, 3. 195–204.

Brazer S C, Williams H P, Chappell T G, Cande W Z. A fission yeast kinesin affects Golgi membrane recycling. // Yeast. I 2000. 16, 2. 149–166.

Brill Julie A, Hime Gary R, Scharer-Schuksz Manuela, Fuller Margaret T. A phospholipid kinase regulates actin organization and intercellular bridge formation during germline cytokinesis // Development. VIII 2000. 127. 3855–3864.

Bühler Nicole, Hagiwara Daisuke, Takeshita Norio. Functional Analysis of Sterol Transporter Orthologues in the Filamentous Fungus Aspergillus nidulans // Eukaryotic cell. IX 2015a. 14, 9. 908–921.

Bühler Nicole, Hagiwara Daisuke, Takeshita Norio. Functional Analysis of Sterol Transporter Orthologues in the Filamentous Fungus Aspergillus nidulans. // Eukaryotic cell. IX 2015b. 14, 9. 908–921.

Cadou Angela, Couturier Anne, Le Goff Cathy, Soto Teresa, Miklos Ida, Sipiczki Matthias, Xie Linfeng, Paulson James R, Cansado Jose, Le Goff Xavier. Kin1 is a plasma membrane-associated kinase that regulates the cell surface in fission yeast // Molecular microbiology. VIII 2010. 77, 5. 1186–1202.

Cai Huaqing, Reinisch Karin, Ferro-Novick Susan. Coats, Tethers, Rabs, and SNAREs Work Together to Mediate the Intracellular Destination of a Transport Vesicle // Developmental cell. V 2007. 12, 5. 671–682.

Casavola Elena Caroli, Catucci Alessandro, Bielli Pamela, Di Pentima Alessio, Porcu Giampiero, Pennestri Matteo, Cicero Daniel O, Ragnini-Wilson Antonella. Ypt32p and Mlc1p bind within the vesicle binding region of the class V myosin Myo2p globular tail domain // Molecular microbiology. III 2008. 67, 5. 1051–1066.

Casey P. Protein lipidation in cell signaling // Science (New York, N.Y.). IV 1995. 268, 5208. 221–225.

Castagnetti Stefania, Behrens Ralf, Nurse Paul. End4/Sla2 is involved in establishment of a new growth zone in Schizosaccharomyces pombe. // Journal of cell science. V 2005. 118, Pt 9. 1843–1850.

Caviston J P, Tcheperegine S E, Bi E. Singularity in budding: A role for the evolutionarily conserved small GTPase Cdc42p // Proceedings of the National Academy of Sciences of the United States of America. IX 2002. 99, 19. 12185–12190.

Chang F, Martin S G. Shaping Fission Yeast with Microtubules // Cold Spring Harbor Perspectives in Biology. VII 2009. 1, 1. a001347–a001347.

Chang Fanny S, Han Gil-Soo, Carman George M, Blumer Kendall J. A WASp-binding type II phosphatidylinositol 4-kinase required for actin polymerization-driven endosome motility // The Journal of cell biology. X 2005. 171, 1. 133–142.

Chang Fred, Huang Kerwyn Casey. How and why cells grow as rods // BMC Biology. VIII 2014. 12, 1. 2102.

Cheng Hong, Sugiura Reiko, Wu Wenlian, Fujita Masaaki, Lu Yabin, Sio Susie O, Kawai Rena, Takegawa Kaoru, Shuntoh Hisato, Kuno Takayoshi. Role of the Rab GTP-binding protein Ypt3 in the fission yeast exocytic pathway and its connection to calcineurin function. // Molecular biology of the cell. VIII 2002. 13, 8. 2963–2976.

Chung Jeeyun, Torta Federico, Masai Kaori, Lucast Louise, Czapla Heather, Tanner Lukas B, Narayanaswamy Pradeep, Wenk Markus R, Nakatsu Fubito, De Camilli Pietro. INTRACELLULAR TRANSPORT. PI4P/phosphatidylserine countertransport at ORP5- and ORP8-mediated ER-plasma membrane contacts. // Science (New York, N.Y.). VII 2015. 349, 6246. 428–432.

Codlin Sandra, Haines Rebecca L, Mole Sara E. btn1 Affects Endocytosis, Polarization of Sterol-Rich Membrane Domains and Polarized Growth in Schizosaccharomyces pombe // Traffic (Copenhagen, Denmark). VI 2008. 9, 6. 936–950.

Coll P M. Gef1p, a New Guanine Nucleotide Exchange Factor for Cdc42p, Regulates Polarity in Schizosaccharomyces pombe // Molecular biology of the cell. XI 2002. 14, 1. 313–323.

Coskun Ünal, Simons Kai. Membrane rafting: From apical sorting to phase segregation // FEBS Letters. XII 2009. 584, 9. 1685–1693.

Craighead M W, Bowden S, Watson R, Armstrong J. Function of the ypt2 gene in the exocytic pathway of Schizosaccharomyces pombe. // Molecular biology of the cell. X 1993. 4, 10. 1069–1076.

D'Angelo G, Vicinanza M, Di Campli A, De Matteis M A. The multiple roles of PtdIns(4)P - not just the precursor of PtdIns(4,5)P2 // Journal of cell science. VI 2008. 121, 12. 1955–1963.

Danielsen E M. A transferrin-like GPI-linked iron-binding protein in detergent- insoluble noncaveolar microdomains at the apical surface of fetal intestinal epithelial cells // The Journal of cell biology. XI 1995. 131, 4. 939–950.

Das M, Drake T, Wiley D J, Buchwald P, Vavylonis D, Verde F. Oscillatory Dynamics of Cdc42 GTPase in the Control of Polarized Growth // Science (New York, N.Y.). VII 2012. 337, 6091. 239–243.

Das Maitreyi, Chiron Stéphane, Verde Fulvia. Microtubule-Dependent Spatial Organization of Mitochondria in Fission Yeast // Microtubules: in vivo. 2010. 203–221.

Das Maitreyi, Wiley David J, Chen Xi, Shah Kavita, Verde Fulvia. The Conserved NDR Kinase Orb6 Controls Polarized Cell Growth by Spatial Regulation of the Small GTPase Cdc42 // Current Biology. VIII 2009. 19, 15. 1314–1319.

Day Kasey J, Staehelin L Andrew, Glick Benjamin S. A three-stage model of Golgi structure and function // Histochemistry and Cell Biology. VII 2013. 140, 3. 239–249.

Deng L, Sugiura R, Ohta K, Tada K, Suzuki M, Hirata M, Nakamura S i, Shuntoh H, Kuno T. Phosphatidylinositol-4-phosphate 5-Kinase Regulates Fission Yeast Cell Integrity through a Phospholipase C-mediated Protein Kinase C-independent Pathway // The Journal of biological chemistry. VII 2005. 280, 30. 27561–27568.

Desrivieres S. MSS4, a Phosphatidylinositol-4-phosphate 5-Kinase Required for Organization of the Actin Cytoskeleton in Saccharomyces cerevisiae // Journal of Biological Chemistry. VI 1998. 273, 25. 15787–15793.

Dimopoulos Sotiris, Mayer Christian E, Rudolf Fabian, Stelling Joerg. Accurate cell segmentation in microscopy images using membrane patterns. // Bioinformatics (Oxford, England). V 2014. 30, 18. btu302–2651.

Dodgson James, Chessel Anatole, Yamamoto Miki, Vaggi Federico, Cox Susan, Rosten Edward, Albrecht David, Geymonat Marco, Csikasz-Nagy Attila, Sato Masamitsu, Carazo-Salas Rafael E. Spatial segregation of polarity factors into distinct cortical clusters is required for cell polarity control // Nature communications. V 2013. 4. 1834.

Drabikowski W, Łagwińska E, Sarzała M G. Filipin as a fluorescent probe for the location of cholesterol in the membranes of fragmented sarcoplasmic reticulum // Biochimica et Biophysica Acta (BBA) - Biomembranes. I 1973. 291, 1. 61–70.

Drin G, Filseck J M von, opi A. New molecular mechanisms of inter-organelle lipid transport // Biochemical Society Transactions. IV 2016. 44, 2. 486–492.

Driouich A. Effect of brefeldin A on the structure of the Golgi apparatus and on the synthesis and secretion of proteins and polysaccharides in sycamore maple (Acer pseudoplatanus) suspension-cultured cells // PLANT PHYSIOLOGY. IV 1993. 101, 4. 1363–1373.

Duran Juan M, Campelo Felix, Galen Josse van, Sachsenheimer Timo, Sot Jesús, Egorov Mikhail V, Rentero Carles, Enrich Carlos, Polishchuk Roman S, Goñi Félix M, Brügger Britta, Wieland Felix, Malhotra Vivek. Sphingomyelin organization is required for vesicle biogenesis at the Golgi complex // The EMBO journal. XI 2012. 31, 24. 4535–4546.

Edamatsu Masaki, Toyoshima Yoko Y. Fission yeast synaptobrevin is involved in cytokinesis and cell elongation // Biochemical and biophysical research communications. II 2003. 301, 3. 641–645.

Engelman Donald M. Membranes are more mosaic than fluid // Nature. XII 2005. 438, 7068. 578–580.

Enrich C, Rentero C, Hierro A, Grewal T. Role of cholesterol in SNARE-mediated trafficking on intracellular membranes // Journal of cell science. III 2015. 128, 6. 1071–1081.

Estravís Miguel, Rincon Sergio, Pérez Pilar. Cdc42 regulation of polarized traffic in fission yeast // Communicative & Integrative Biology. 2012. 5, 4. 370–373.

Estravís Miguel, Rincón Sergio A, Santos Beatriz, Pérez Pilar. Cdc42 regulates multiple membrane traffic events in fission yeast. // Traffic (Copenhagen, Denmark). XII 2011. 12, 12. 1744–1758.

Etienne-Manneville S. Cdc42 - the centre of polarity // Journal of cell science. III 2004. 117, 8. 1291–1300.

Etienne-Manneville Sandrine, Hall Alan. Rho GTPases in cell biology // Nature. XII 2002. 420, 6916. 629–635.

Fang Yue, Jaiseng Wurentuya, Ma Yan, Hu Lingling, Yamazaki Shizuka, Zhang Xibo, Hayafuji Tsutomu, Shi Lin, Kuno Takayoshi. E3 Ubiquitin Ligase Pub1 Is implicated in Endocytosis of a GPI-Anchored Protein Ecm33 in Fission Yeast // PloS one. I 2014. 9, 1. e85238–11.

Fang Yue, Sugiura Reiko, Ma Yan, Yada-Matsushima Tomoko, Umeno Hirotatsu, Kuno Takayoshi. Cation diffusion facilitator Cis4 is implicated in Golgi membrane trafficking via regulating zinc homeostasis in fission yeast. // Molecular biology of the cell. IV 2008. 19, 4. 1295–1303.

Feierbach Becket, Chang Fred. Roles of the fission yeast formin for3p in cell polarity, actin cable formation and symmetric cell division // Current Biology. X 2001. 11, 21. 1656–1665.

Filseck Joachim Moser von, Čopič Alenka, Delfosse Vanessa, Vanni Stefano, Jackson Catherine L, Bourguet William, Drin Guillaume. INTRACELLULAR TRANSPORT. Phosphatidylserine transport by ORP/Osh proteins is driven by phosphatidylinositol 4-phosphate. // Science (New York, N.Y.). VII 2015a. 349, 6246. 432–436.

Filseck Joachim Moser von, Vanni Stefano, Mesmin Bruno, Antonny Bruno, Drin Guillaume. A phosphatidylinositol-4-phosphate powered exchange mechanism to create a lipid gradient between membranes. // Nature communications. 2015b. 6. 6671.

Filseck Joachim Moser von, Vanni Stefano, Mesmin Bruno, Antonny Bruno, Drin Guillaume. A phosphatidylinositol-4-phosphate powered exchange mechanism to create a lipid gradient between membranes // Nature communications. III 2015. 1–12.

Fischer Reinhard, Zekert Nadine, Takeshita Norio. Polarized growth in fungi–interplay between the cytoskeleton, positional markers and membrane domains. // Molecular microbiology. V 2008. 68, 4. 813–826.

Forsburg Susan L, Rhind Nicholas. Basic methods for fission yeast // Yeast. 2006. 23, 3. 173–183.

Frechin Mathieu, Stoeger Thomas, Daetwyler Stephan, Gehin Charlotte, Battich Nico, Damm Eva-Maria, Stergiou Lilli, Riezman Howard, Pelkmans Lucas. Cell-intrinsic adaptation of lipid composition to local crowding drives social behaviour // Nature. V 2015. 523, 7558. 88–91.

Fruman David A, Meyers Rachel E, Cantley Lewis C. PHOSPHOINOSITIDE KINASES // Annual Review of Biochemistry. VI 1998. 67, 1. 481–507.

Fukui Yasuhisa, Kozasa Tohru, Kaziro Yoshito, Takeda Tadayukl, Yamamoto Masayukl. Role of a ras homolog in the life cycle of schizosaccharomyces pombe // Cell. I 1986. 44, 2. 329–336.

Gagescu R, Demaurex N, Parton R G, Hunziker W, Huber L A, Gruenberg J. The Recycling Endosome of Madin-Darby Canine Kidney Cells Is a Mildly Acidic Compartment Rich in Raft Components // Molecular biology of the cell. VIII 2000. 11, 8. 2775–2791.

Garcia-Bustos Jose F, Marini Federica, Stevenson Isabelle, Frei Christian, Hall Michael N. PIK1, an essential phosphatidylinositol 4-kinase associated with the yeast nucleus // The EMBO journal. 1994. 13. 2353–2361.

Georgiev Alexander G, Sullivan David P, Kersting Michael C, Dittman Jeremy S, Beh Christopher T, Menon Anant K. Osh Proteins Regulate Membrane Sterol Organization but Are Not Required for Sterol Movement Between the ER and PM // Traffic (Copenhagen, Denmark). VII 2011. 12, 10. 1341–1355.

Gierer A, Meinhardt H. A theory of biological pattern formation // Kybernetik. XII 1972. 12, 1. 30–39.

Graham T R, Scott P A, Emr S D. Brefeldin A reversibly blocks early but not late protein transport steps in the yeast secretory pathway // The EMBO journal. V 2004. 1–9.

Hachet Olivier, Berthelot-Grosjean Martine, Kokkoris Kyriakos, Vincenzetti Vincent, Moosbrugger Josselin, Martin Sophie G. A phosphorylation cycle shapes gradients of the DYRK family kinase Pom1 at the plasma membrane. // Cell. VI 2011. 145, 7. 1116–1128.

Halbsgut N, Linnemannstons K, Zimmermann L I, Wodarz A. Apical-basal polarity in Drosophila neuroblasts is independent of vesicular trafficking // Molecular biology of the cell. XI 2011. 22, 22. 4373–4379.

Hao M. Effects of Cholesterol Depletion and Increased Lipid Unsaturation on the Properties of Endocytic Membranes // The Journal of biological chemistry. II 2004. 279, 14. 14171–14178.

Hayles Jacqueline, Nurse Paul. A JOURNEY INTO SPACE // Nature reviews. Molecular cell biology. IX 2001. 2.

He Bing, Xi Fengong, Zhang Xiaoyu, Zhang Jian, Guo Wei. Exo70 interacts with phospholipids and mediates the targeting of the exocyst to the plasma membrane // The EMBO journal. XII 2007a. 26, 24. 5167–5167.

He Bing, Xi Fengong, Zhang Xiaoyu, Zhang Jian, Guo Wei. Exo70 interacts with phospholipids and mediates the targeting of the exocyst to the plasma membrane // The EMBO journal. VIII 2007b. 26, 18. 4053–4065.

He Yi, Sugiura Reiko, Ma Yan, Kita Ayako, Deng Lu, Takegawa Kaoru, Matsuoka Ken, Shuntoh Hisato, Kuno Takayoshi. Genetic and functional interaction between Ryh1 and Ypt3: two Rab GTPases that function in S. pombe secretory pathway. // Genes to cells : devoted to molecular & cellular mechanisms. III 2006. 11, 3. 207–221.

Heino S, Lusa S, Somerharju P, Ehnholm C, Olkkonen V M, Ikonen E. Dissecting the role of the Golgi complex and lipid rafts in biosynthetic transport of cholesterol to the cell surface // Proceedings of the National Academy of Sciences. 2000. 97, 15. 8375–8380.

Herevard F V. ROUGH MEMBRANES IN SCHIZOSACCHAROMYCES POMBE PROTOPLASTS // Experimental Cell Research. 1974. 87. 213–218.

Hirota K. Gef1p and Scd1p, the Two GDP-GTP Exchange Factors for Cdc42p, Form a Ring Structure that Shrinks during Cytokinesis in Schizosaccharomyces pombe // Molecular biology of the cell. VII 2003. 14, 9. 3617–3627.

Holthuis Joost C M, Menon Anant K. Lipid landscapes and pipelines in membrane homeostasis. // Nature. VI 2014. 510, 7503. 48–57.

Höög Johanna L, Huisman Stephen M, Brunner Damian, Antony Claude. Electron Tomography Reveals Novel Microtubule Lattice and Microtubule Organizing Centre Defects in +TIP Mutants // PloS one. IV 2013. 8, 4. e61698.

Höög Johanna L, Schwartz Cindi, Noon Angela T, O'Toole Eileen T, Mastronarde David N, McIntosh J Richard, Antony Claude. Organization of interphase microtubules in fission yeast analyzed by electron tomography. // Developmental cell. III 2007. 12, 3. 349–361.

Huh Won-Ki, Falvo James V, Gerke Luke C, Carroll Adam S, Howson Russell W, Weissman Jonathan S, O'Shea Erin K. Global analysis of protein localization in budding yeast // Nature. X 2003. 425, 6959. 686–691.

Huisman Stephen M, Brunner Damian. Cell polarity in fission yeast: A matter of confining, positioning, and switching growth zones // Seminars in Cell & Developmental Biology. X 2011. 22, 8. 799–805.

Ikenouchi J, Suzuki M, Umeda K, Ikeda K, Taguchi R, Kobayashi T, Sato S B, Stolz D B, Umeda M. Lipid Polarity Is Maintained in Absence of Tight Junctions // The Journal of biological chemistry. III 2012. 287, 12. 9525–9533.

Im Young Jun, Raychaudhuri Sumana, Prinz William A, Hurley James H. Structural mechanism for sterol sensing and transport by OSBP-related proteins // Nature. IX 2005. 437, 7055. 154–158.

Iwaki Tomoko, Iefuji Haruyuki, Hiraga Yoshikazu, Hosomi Akira, Morita Tomotake, Giga-Hama Yuko, Takegawa Kaoru. Multiple functions of ergosterol in the fission yeast Schizosaccharomyces pombe. // Microbiology (Reading, England). III 2008. 154, Pt 3. 830–841.

Iwaki Tomoko, Osawa Fumi, Onishi Masayuki, Koga Takako, Fujita Yasuko, Hosomi Akira, Tanaka Naotaka, Fukui Yasuhisa, Takegawa Kaoru. Characterization ofvps33+, a gene required for vacuolar biogenesis and protein sorting inSchizosaccharomyces pombe // Yeast. 2003. 20, 10. 845–855.

Jacobson Ken, Mouritsen Ole G, Anderson Richard G W. Lipid rafts: at a crossroad between cell biology and physics // Nature cell biology. I 2007. 9, 1. 7–14.

Jahn Reinhard, Fasshauer Dirk. Molecular machines governing exocytosis of synaptic vesicles // Nature. X 2012. 490, 7419. 201–207.

Jahn Reinhard, Lang Thorsten, Südhof Thomas C. Membrane Fusion // Cell. II 2003. 112, 4. 519–533.

Jaiseng Wurentuya, Fang Yue, Ma Yan, Sugiura Reiko, Kuno Takayoshi. Studies on the roles of clathrin-mediated membrane trafficking and zinc transporter Cis4 in the transport of GPI-anchored proteins in fission yeast. // PloS one. 2012. 7, 7. e41946.

Janetopoulos Chris, Borleis Jane, Vazquez Francisca, Iijima Miho, Devreotes Peter. Temporal and Spatial Regulation of Phosphoinositide Signaling Mediates Cytokinesis // Developmental cell. IV 2005. 8, 4. 467–477.

Jedd Gregory, Mulholland Jon, Segev Nava. Two New Ypt GTPases Are Required for Exit From the Yeast trans-Golgi Compartment // The Journal of cell biology. V 1997. 137, 3. 563–580.

Jena Bhanu P. Role of SNAREs in Membrane Fusion // Cell Fusion in Health and Disease. Dordrecht: Springer Netherlands, 2011. 13–32.

Jin Yui, Sultana Azmiri, Gandhi Pallavi, Franklin Edward, Hamamoto Susan, Khan Amir R, Munson Mary, Schekman Randy, Weisman Lois S. Myosin V Transports Secretory Vesicles via a Rab GTPase Cascade and Interaction with the Exocyst Complex // Developmental cell. XII 2011. 21, 6. 1156–1170.

Jourdain Isabelle, Dooley Hannah C, Toda Takashi. Fission yeast sec3 bridges the exocyst complex to the actin cytoskeleton. // Traffic (Copenhagen, Denmark). XI 2012. 13, 11. 1481–1495.

Jourdain Isabelle, Sontam Dharani, Johnson Chad, Dillies Clément, Hyams Jeremy S. Dynamin-Dependent Biogenesis, Cell Cycle Regulation and Mitochondrial Association of Peroxisomes in Fission Yeast // Traffic (Copenhagen, Denmark). III 2008. 9, 3. 353–365.

Kälin Nanette, Meer Gerrit van. Tight Junctions and Cell Surface Lipid Polarity // Tight Junctions. XII 2009.

Kashiwazaki J, Yamasaki Y, Itadani A, Teraguchi E, Maeda Y, Shimoda C, Nakamura T. Endocytosis is essential for dynamic translocation of a syntaxin 1 orthologue during fission yeast meiosis // Molecular biology of the cell. IX 2011. 22, 19. 3658–3670.

Kelly F D, Nurse P. Spatial control of Cdc42 activation determines cell width in fission yeast // Molecular biology of the cell. X 2011a. 22, 20. 3801–3811.

Kelly Felice D, Nurse Paul. De Novo Growth Zone Formation from Fission Yeast Spheroplasts // PloS one. XII 2011b. 6, 12. e27977.

Kita Ayako, Li Cuifang, Yu Yang, Umeda Nanae, Doi Akira, Yasuda Mitsuko, Ishiwata Shunji, Taga Atsushi, Horiuchi Yoshitaka, Sugiura Reiko. Role of the Small GTPase Rho3 in Golgi/Endosome trafficking through functional interaction with adaptin in Fission Yeast. // PloS one. 2011. 6, 2. e16842.

Kita Ayako, Sugiura Reiko, Shoji Hiromi, He Yi, Deng Lu, Lu Yabin, Sio Susie O, Takegawa Kaoru, Sakaue Motoyoshi, Shuntoh Hisato, Kuno Takayoshi. Loss of Apm1, the micro1 subunit of the clathrin-associated adaptor-protein-1 complex, causes distinct phenotypes and synthetic lethality with calcineurin deletion in fission yeast. // Molecular biology of the cell. VI 2004. 15, 6. 2920–2931.

Klemm Robin W, Ejsing Christer S, Surma Michal A, Kaiser Hermann-Josef, Gerl Mathias J, Sampaio Julio L, Robillard Quentin de, Ferguson Charles, Proszynski Tomasz J, Shevchenko Andrej, Simons Kai. Segregation of sphingolipids and sterols during formation of secretory vesicles at the trans-Golgi network // The Journal of cell biology. V 2009. 185, 4. 601–612.

Klose C, Ejsing C S, Garcia-Saez A J, Kaiser H J, Sampaio J L, Surma M A, Shevchenko A, Schwille P, Simons K. Yeast Lipids Can Phase-separate into Micrometer-scale Membrane Domains // The Journal of biological chemistry. IX 2010. 285, 39. 30224–30232.

Kokkoris Kyriakos, Gallo Castro Daniela, Martin Sophie G. The Tea4-PP1 landmark promotes local growth by dual Cdc42 GEF recruitment and GAP exclusion. // Journal of cell science. V 2014. 127, Pt 9. 2005–2016.

Kowalczyk Katarzyna M, Petersen Janni. Fission Yeast SCYL1/2 Homologue Ppk32: A Novel Regulator of TOR Signalling That Governs Survival during Brefeldin A Induced Stress to Protein Trafficking // PLoS Genetics. V 2016. 12, 5. e1006041.

Kozminski Keith G, Alfaro Gabriel, Dighe Shubha, Beh Christopher T. Homologues of Oxysterol-Binding Proteins Affect Cdc42p- and Rho1p-Mediated Cell Polarization in Saccharomyces cerevisiae // Traffic (Copenhagen, Denmark). VIII 2006. 7, 9. 1224–1242.

Kvam E. Nvj1p is the outer-nuclear-membrane receptor for oxysterol-binding protein homolog Osh1p in Saccharomyces cerevisiae // Journal of cell science. X 2004. 117, 21. 4959–4968.

La Carbona Stéphanie, Le Goff Xavier. Spatial regulation of cytokinesis by the Kin1 and Pom1 kinases in fission yeast // Current genetics. IX 2006. 50, 6. 377–391.

Laporte Damien, Courtout Fabien, Pinson Benoît, Dompierre Jim, Salin Bénédicte, Brocard Lysiane, Sagot Isabelle. A stable microtubule array drives fission yeast polarity reestablishment upon quiescence exit // The Journal of cell biology. VII 2015. 210, 1. 99–113.

León Nagore de, Hoya Marta, Curto M Angeles, Moro Sandra, Yanguas Francisco, Doncel Cristina, Valdivieso M Henar. The AP-2 complex is required for proper temporal and spatial dynamics of endocytic patches in fission yeast // Molecular microbiology. I 2016. n/a–n/a.

Levine T P, Munro S. Dual Targeting of Osh1p, a Yeast Homologue of Oxysterol-binding Protein, to both the Golgi and the Nucleus-Vacuole Junction // Molecular biology of the cell. VI 2001. 12, 6. 1633–1644.

Li Cuifang, Kita Ayako, Hashimoto Yuuka, Ihara Misako, Kato Ayaka, Ogura Naoya, Doi Akira, Oku Masahide, Itoh Toshiki, Sakai Yasuyoshi, Sugiura Reiko. Functional link between Rab GTPase-mediated membrane trafficking and PI4,5P 2signaling // Genes to cells : devoted to molecular & cellular mechanisms. XII 2013. 19, 3. 177–197.

Li Tianpeng, Zheng Fan, Cheung Martin, Wang Fengsong, Fu Chuanhai. Fission yeast mitochondria are distributed by dynamic microtubules in a motor-independent manner // Scientific Reports. VI 2015. 5. 11023.

Li Xinmin, Rivas Marcos P, Fang Min, Marchena Jennifer, Mehrotra Bharat, Chaudhary Anu, Feng Li, Prestwich Glenn D, Bankaitis Vytas A. Analysis of oxysterol binding protein homologue Kes1p function in regulation of Sec14p-dependent protein transport from the yeast Golgi complex // The Journal of cell biology. IV 2002. 157, 1. 63–78.

Ling Y, Hayano S, Novick P. Osh4p is needed to reduce the level of phosphatidylinositol-4-phosphate on secretory vesicles as they mature // Molecular biology of the cell. X 2014. 25, 21. 3389–3400.

Lingwood Daniel, Kaiser Hermann-Josef, Levental Ilya, Simons Kai. Lipid rafts as functional heterogeneity in cell membranes // Biochemical Society Transactions. X 2009. 37, 5. 955–960.

Lipatova Z, Tokarev A A, Jin Y, Mulholland J, Weisman L S, Segev N. Direct Interaction between a Myosin V Motor and the Rab GTPases Ypt31/32 Is Required for Polarized Secretion // Molecular biology of the cell. IX 2008. 19, 10. 4177–4187.

Lippincott-Schwartz Jennifer, Yuan Lydia, Tipper Christopher, Amherdt Myléne, Orci Lelio, Klausner Richard D. Brefeldin A's effects on endosomes, lysosomes, and the TGN suggest a general mechanism for regulating organelle structure and membrane traffic // Cell. XI 1991. 67, 3. 601–616.

Liu Xiao-Man, Sun Ling-Ling, Hu Wen, Ding Yue-He, Dong Meng-Qiu, Du Li-Lin. ESCRTs Cooperate with a Selective Autophagy Receptor to Mediate Vacuolar Targeting of Soluble Cargos // Molecular Cell. IX 2015. 59, 6. 1035–1042.

Lo Presti L, Chang F, Martin S G. Myosin Vs organize actin cables in fission yeast // Molecular biology of the cell. XI 2012. 23, 23. 4579–4591.

Lo Presti Libera, Martin Sophie G. Shaping fission yeast cells by rerouting actin-based transport on microtubules. // Current biology : CB. XII 2011. 21, 24. 2064–2069.

Low S H, Miura M, Roche P A, Valdez A C, Mostov K E, Weimbs T. Intracellular Redirection of Plasma Membrane Trafficking after Loss of Epithelial Cell Polarity // Molecular biology of the cell. IX 2000. 11, 9. 3045–3060.

Ma Yan, Takeuchi Mai, Sugiura Reiko, Sio Susie O, Kuno Takayoshi. Deletion mutants of AP-1 adaptin subunits display distinct phenotypes in fission yeast. // Genes to cells : devoted to molecular & cellular mechanisms. VIII 2009. 14, 8. 1015–1028.

Maeda Kenji, Anand Kanchan, Chiapparino Antonella, Kumar Arun, Poletto Mattia, Kaksonen Marko, Gavin Anne-Claude. Interactome map uncovers phosphatidylserine transport by oxysterol-binding proteins // Nature. VIII 2013. 501, 7466. 257–261.

Maeda Yukari, Kashiwazaki Jun, Shimoda Chikashi, Nakamura Taro. The Schizosaccharomyces pombeSyntaxin 1 Homolog, Psy1, Is Essential in the Development of the Forespore Membrane // Bioscience, Biotechnology and Biochemistry. V 2014. 73, 2. 339–345.

Makushok Tatyana, Alves Paulo, Huisman Stephen, Kijowski Adam Rafal, Brunner Damian. Sterol-rich membrane domains define fission yeast cell polarity // Cell. VI 2016a. 1–93.

Makushok Tatyana, Alves Paulo, Huisman Stephen Michiel, Kijowski Adam Rafal, Brunner Damian. Sterol-Rich Membrane Domains Define Fission Yeast Cell Polarity // Cell. V 2016b. 1–37.

Manford Andrew G, Stefan Christopher J, Yuan Helen L, MacGurn Jason A, Emr Scott D. ER-to-Plasma Membrane Tethering Proteins Regulate Cell Signaling and ER Morphology // Developmental cell. XII 2012. 23, 6. 1129–1140.

Marco Eugenio, Wedlich-Soldner Roland, Li Rong, Altschuler Steven J, Wu Lani F. Endocytosis Optimizes the Dynamic Localization of Membrane Proteins that Regulate Cortical Polarity // Cell. IV 2007. 129, 2. 411–422.

Martin Sophie G, Arkowitz Robert A. Cell polarization in budding and fission yeasts // FEMS Microbiology Reviews. III 2014. 38, 2. 228–253.

Mata Juan, Nurse Paul. tea1 and the Microtubular Cytoskeleton Are Important for Generating Global Spatial Order within the Fission Yeast Cell // Cell. VI 1997. 89, 6. 939–949.

Matsuyama Akihisa, Arai Ritsuko, Yashiroda Yoko, Shirai Atsuko, Kamata Ayako, Sekido Shigeko, Kobayashi Yumiko, Hashimoto Atsushi, Hamamoto Makiko, Hiraoka Yasushi, Horinouchi Sueharu, Yoshida Minoru. ORFeome cloning and global analysis of protein localization in the fission yeast Schizosaccharomyces pombe // Nature Biotechnology. VI 2006. 24, 7. 841–847.

Matteis Maria Antonietta De, Godi Anna. PI-loting membrane traffic // Nature cell biology. VI 2004. 6, 6. 487–492.

Maundrell Kinsey. nmt1 of Fission Yeast. A highly transcribed gene completely repressed by thiamine // The Journal of biological chemistry. VII 1990. 265. 10857–10864.

Maxfield Frederick R, McGraw Timothy E. Endocytic recycling // Nature reviews. Molecular cell biology. II 2004. 5, 2. 121–132.

Maxfield Frederick R, Menon Anant K. Intracellular sterol transport and distribution // Current opinion in cell biology. VIII 2006. 18, 4. 379–385.

McCollum D. Schizosaccharomyces pombe cdc4+ gene encodes a novel EF-hand protein essential for cytokinesis // The Journal of cell biology. VIII 1995. 130, 3. 651–660.

Meder Doris, Shevchenko Anna, Simons Kai, Füllekrug Joachim. Gp135/podocalyxin and NHERF-2 participate in the formation of a preapical domain during polarization of MDCK cells // The Journal of cell biology. I 2005. 168, 2. 303–313.

Meer Gerrit van, Simons Kai. Lipid polarity and sorting in epithelial cells // Journal of Cellular Biochemistry. I 1988. 36, 1. 51–58.

Meinhardt Hans, Gierer Alfred. Pattern formation by local self-activation and lateral inhibition // BioEssays. VII 2000. 22, 8. 753–760.

Mellman Ira, Nelson W James. Coordinated protein sorting, targeting and distribution in polarized cells // Nature reviews. Molecular cell biology. XI 2008. 9, 11. 833–845.

Mellman Ira, Warren Graham. The Road Taken: Past and Future Review Foundations of Membrane Traffic // Cell. I 2000. 100. 99–112.

Mesmin B, Pipalia N H, Lund F W, Ramlall T F, Sokolov A, Eliezer D, Maxfield F R. STARD4 abundance regulates sterol transport and sensing // Molecular biology of the cell. X 2011. 22, 21. 4004–4015.

Mesmin Bruno, Antonny Bruno. The counterflow transport of sterols and PI4P // Biochimica et Biophysica Acta (BBA) - Molecular and Cell Biology of Lipids. VIII 2016. 1861, 8. 940–951.

Mesmin Bruno, Antonny Bruno, Drin Guillaume. Insights into the mechanisms of sterol transport between organelles // Cellular and Molecular Life Sciences. I 2013a. 70, 18. 3405–3421.

Mesmin Bruno, Bigay Joëlle, Filseck Joachim Moser von, Lacas-Gervais Sandra, Drin Guillaume, Antonny Bruno. A four-step cycle driven by PI(4)P hydrolysis directs sterol/PI(4)P exchange by the ER-Golgi tether OSBP. // Cell. XI 2013b. 155, 4. 830–843.

Lipid droplets form from distinct regions of the cell in the fission yeast Schizosaccharomyces pombe. // . III 2016. n–a–n–a.

Michel Vera, Bakovic Marica. Lipid rafts in health and disease // Biology of the Cell. I 2012. 99, 3. 129–140.

Miller P J, Johnson D I. Cdc42p GTPase is involved in controlling polarized cell growth in Schizosaccharomyces pombe. // Molecular and Cellular Biology. II 1994. 14, 2. 1075–1083.

Minc Nicolas, Bratman Scott V, Basu Roshni, Chang Fred. Establishing New Sites of Polarization by Microtubules // Current Biology. I 2009. 19, 2. 83–94.

Mitchell Alex, Chang Hsin-Yu, Daugherty Louise, Fraser Matthew, Hunter Sarah, Lopez Rodrigo, McAnulla Craig, McMenamin Conor, Nuka Gift, Pesseat Sebastien, Sangrador-Vegas Amaia, Scheremetjew Maxim, Rato Claudia, Yong Siew-Yit, Bateman Alex, Punta Marco, Attwood Teresa K, Sigrist Christian J A, Redaschi Nicole, Rivoire Catherine, Xenarios Ioannis, Kahn Daniel, Guyot Dominique, Bork Peer, Letunic Ivica, Gough Julian, Oates Matt, Haft Daniel, Huang Hongzhan, Natale Darren A, Wu Cathy H, Orengo Christine, Sillitoe Ian, Mi Huaiyu, Thomas Paul D, Finn Robert D. The InterPro protein families database: the classification resource after 15 years // Nucleic Acids Research. I 2015. 43, D1. D213–D221.

Mitchison J M, Nurse P. Growth in cell length in the fission yeast Schizosaccharomyces pombe. // Journal of cell science. IV 1985. 75. 357–376.

Moreno Sergio, Klar Amar, Nurse Paul. [56] Molecular genetic analysis of fission yeast Schizosaccharomyces pombe // Guide to Yeast Genetics and Molecular Biology. 1991. 795–823.

Motegi F, Arai R, Mabuchi I. Identification of Two Type V Myosins in Fission Yeast, One of Which Functions in Polarized Cell Growth and Moves Rapidly in the Cell // Molecular biology of the cell. V 2001. 12, 5. 1367–1380.

Mukherjee Sushmita, Soe Thwe Thwe, Maxfield Frederick R. Endocytic Sorting of Lipid Analogues Differing Solely in the Chemistry of Their Hydrophobic Tails // The Journal of cell biology. III 1999. 144, 6. 1271–1284.

Mukherjee Sushmita, Zha Xiaohui, Tabas Ira, Maxfield Frederick R. Cholesterol Distribution in Living Cells: Fluorescence Imaging Using Dehydroergosterol as a Fluorescent Cholesterol Analog // Biophysical journal. X 1998. 75, 4. 1915–1925.

Mulvihill Daniel P, Edwards Suzanne R, Hyams Jeremy S. A critical role for the type V myosin, Myo52, in septum deposition and cell fission during cytokinesis inSchizosaccharomyces pombe // Cell Motility and the Cytoskeleton. 2006. 63, 3. 149–161.

Munder Matthias Christoph, Midtvedt Daniel, Franzmann Titus, Nüske Elisabeth, Otto Oliver, Herbig Maik, Ulbricht Elke, Müller Paul, Taubenberger Anna, Maharana Shovamayee, Malinovska Liliana, Richter Doris, Guck Jochen, Zaburdaev Vasily, Alberti Simon. A pH-driven transition of the cytoplasm from a fluid- to a solid-like state promotes entry into dormancy // eLife. III 2016. 5. 59.

Nakamura Taro, Kashiwazaki Jun, Shimoda Chikashi. A Fission Yeast SNAP-25 Homologue, SpSec9, Is Essential for Cytokinesis and Sporulation // Cell structure and function. X 2005. 1–10.

Nakano K. The small GTPase Rho3 and the diaphanous/formin For3 function in polarized cell growth in fission yeast // Journal of cell science. XII 2002. 115, 23. 4629–4639.

Nakano Kentaro, Arai Ritsuko, Mabuchi Issei. The small GTP-binding protein Rho1 is a multifunctional protein that regulates actin localization, cell polarity, and septum formation in the fission yeast Schizosaccharomyces pombe // Genes to cells : devoted to molecular & cellular mechanisms. XI 1997. 2, 11. 679–694.

Nakase Mai, Tani Motohiro, Morita Tomotake, Kitamoto Hiroko K, Kashiwazaki Jun, Nakamura Taro, Hosomi Akira, Tanaka Naotaka, Takegawa Kaoru. Mannosylinositol phosphorylceramide is a major sphingolipid component and is required for proper localization of plasma-membrane proteins in Schizosaccharomyces pombe. // Journal of cell science. V 2010. 123, Pt 9. 1578–1587.

Neumann Frank R, Nurse Paul. Nuclear size control in fission yeast // The Journal of cell biology. XI 2007. 179, 4. 593–600.

Nichols C B. PAK Kinases Ste20 and Pak1 Govern Cell Polarity at Different Stages of Mating in Cryptococcus neoformans // Molecular biology of the cell. VII 2004. 15, 10. 4476–4489.

Nickel Walter. The mystery of nonclassical protein secretion // European Journal of Biochemistry. IV 2003. 270, 10. 2109–2119.

Nicolson Garth L. The Fluid—Mosaic Model of Membrane Structure: Still relevant to understanding the structure, function and dynamics of biological membranes after more than 40years // Biochimica et Biophysica Acta (BBA) - Biomembranes. VI 2014. 1838, 6. 1451–1466.

Nurse Paul, Snell Valery. Genetic analysis of cell morphogenesis in fission yeast - a role for casein kinase II in the establishment of polarized growth // The EMBO journal. 1994. 13. 1066–2074.

OSUMI MASAKO. The Ultrastructure of Yeast: Cell Wall Structure and Formation // Micron. 1998. 29. 207–233.

Ohno H. Physiological Roles of Clathrin Adaptor AP Complexes: Lessons from Mutant Animals // Journal of Biochemistry. VI 2006. 139, 6. 943–948.

Olkkonen Vesa M, Li Shiqian. Oxysterol-binding proteins: Sterol and phosphoinositide sensors coordinating transport, signaling and metabolism // Progress in Lipid Research. X 2013. 52, 4. 529–538.

Onken B, Wiener H, Philips M R, Chang E C. Compartmentalized signaling of Ras in fission yeast // Proceedings of the National Academy of Sciences of the United States of America. VI 2006. 103, 24. 9045–9050.

Ortiz Darinel, Medkova Martina, Walch-Solimena Christiane, Novick Peter. Ypt32 recruits the Sec4p guanine nucleotide exchange factor, Sec2p, to secretory vesicles; evidence for a Rab cascade in yeast // The Journal of cell biology. VI 2002. 157, 6. 1005–1016.

Owen Dylan M, Magenau Astrid, Williamson David, Gaus Katharina. The lipid raft hypothesis revisited - New insights on raft composition and function from super-resolution fluorescence microscopy // BioEssays. VI 2012. 34, 9. 739–747.

Padte Neal N, Martin Sophie G, Howard Martin, Chang Fred. The Cell-End Factor Pom1p Inhibits Mid1p in Specification of the Cell Division Plane in Fission Yeast // Current Biology. XII 2006. 16, 24. 2480–2487.

Paladino S, Lebreton S, Tivodar S, Campana V, Tempre R, Zurzolo C. Different GPI-attachment signals affect the oligomerisation of GPI-anchored proteins and their apical sorting // Journal of cell science. XII 2008. 121, 24. 4001–4007.

Park Jae-Sook, Steinbach Sarah K, Desautels Michel, Hemmingsen Sean M. Essential Role for Schizosaccharomyces pombe pik1 in Septation // PloS one. VII 2009. 4, 7. e6179.

Pelham Hugh R B. Multiple targets for brefeldin A // Cell. XI 1991. 67, 3. 449–451.

Pérez Pilar, Rincón Sergio A. Rho GTPases: regulation of cell polarity and growth in yeasts // Biochemical Journal. III 2010. 426, 3. 243–253.

Perry R J. Oxysterol-binding Protein and Vesicle-associated Membrane Protein-associated Protein Are Required for Sterol-dependent Activation of the Ceramide Transport Protein // Molecular biology of the cell. III 2006. 17, 6. 2604–2616.

Pichler Harald, Gaigg Barbara, Hrastnik Claudia, Achleitner Georg, Kohlwein Sepp D, Zellnig Günther, Perktold Andreas, Daum Günther. A subfraction of the yeast endoplasmic reticulum associates with the plasma membrane and has a high capacity to synthesize lipids // European Journal of Biochemistry. XII 2001. 268, 8. 2351–2361.

Prinz William A. Bridging the gap: Membrane contact sites in signaling, metabolism, and organelle dynamics // The Journal of cell biology. VI 2014. 205, 6. 759–769.

Prinz William A, Grzyb Lara, Veenhuis Marten, Kahana Jason A, Silver Pamela A, Rapoport Tom A. Mutants Affecting the Structure of the Cortical Endoplasmic Reticulum in Saccharomyces cerevisiae // The Journal of cell biology. VIII 2000. 150, 3. 461–474.

Proszynski T J, Klemm R W, Gravert M, Hsu P P, Gloor Y, Wagner J, Kozak K, Grabner H, Walzer K, Bagnat M, Simons K, Walch-Solimena C. A genome-wide visual screen reveals a role for sphingolipids and ergosterol in cell surface delivery in yeast // Proceedings of the National Academy of Sciences of the United States of America. XII 2005. 102, 50. 17981–17986.

Qadota H, Python C P, Inoue S B, Arisawa M, Anraku Y, Zheng Y, Watanabe T, Levin D E, Ohya Y. Identification of Yeast Rho1p GTPase as a Regulatory Subunit of 1,3-beta -Glucan Synthase // Science (New York, N.Y.). IV 1996. 272, 5259. 279–281.

Rajendran L. Lipid rafts and membrane dynamics // Journal of cell science. II 2005. 118, 6. 1099–1102.

Rella Antonella, Farnoud Amir M, Del Poeta Maurizio. Plasma membrane lipids and their role in fungal virulence // Progress in Lipid Research. I 2016. 61. 63–72.

Reverter Meritxell, Rentero Carles, Garcia-Melero Ana, Hoque Monira, Muga Sandra Vilà de, Álvarez-Guaita Anna, Conway James R W, Wood Peta, Cairns Rose, Lykopoulou Lilia, Grinberg Daniel, Vilageliu Lluïsa, Bosch Marta, Heeren Joerg, Blasi Juan, Timpson Paul, Pol Albert, Tebar Francesc, Murray Rachael Z, Grewal Thomas, Enrich Carlos. Cholesterol Regulates Syntaxin 6 Trafficking at trans-Golgi Network Endosomal Boundaries // Cell reports. V 2014. 7, 3. 883–897.

Revilla-Guarinos M T, Martin-Garcia R, Villar-Tajadura M A, Estravis M, Coll P M, Perez P. Rga6 is a fission yeast Rho GAP involved in Cdc42 regulation of polarized growth // Molecular biology of the cell. IV 2016. 27, 9. 1524–1535.

Rincon S A, Ye Y, Villar-Tajadura M A, Santos B, Martin S G, Perez P. Pob1 Participates in the Cdc42 Regulation of Fission Yeast Actin Cytoskeleton // Molecular biology of the cell. X 2009. 20, 20. 4390–4399.

Rodriguez-Boulan Enrique, Macara Ian G. Organization and execution of the epithelial polarity programme // Nature reviews. Molecular cell biology. III 2014. 15, 4. 225–242.

Rolls Melissa M, Albertson Roger, Shih Hsin-Pei, Lee Cheng-Yu, Doe Chris Q. DrosophilaaPKC regulates cell polarity and cell proliferation in neuroblasts and epithelia // The Journal of cell biology. XII 2003. 163, 5. 1089–1098.

Roth M G. Phosphoinositides in Constitutive Membrane Traffic // Physiological Reviews. VII 2004. 84, 3. 699–730.

Roy Anjana, Levine Timothy P. Multiple Pools of Phosphatidylinositol 4-Phosphate Detected Using the Pleckstrin Homology Domain of Osh2p // The Journal of biological chemistry. X 2004. 279, 43. 44683–44689.

Saint-Jean Maud de, Delfosse Vanessa, Douguet Dominique, Chicanne Gaëtan, Payrastre Bernard, Bourguet William, Antonny Bruno, Drin Guillaume. Osh4p exchanges sterols for phosphatidylinositol 4-phosphate between lipid bilayers // The Journal of cell biology. XII 2011a. 195, 6. 965–978.

Saint-Jean Maud de, Delfosse Vanessa, Douguet Dominique, Chicanne Gaëtan, Payrastre Bernard, Bourguet William, Antonny Bruno, Drin Guillaume. Osh4p exchanges sterols for phosphatidylinositol 4-phosphate between lipid bilayers // The Journal of cell biology. XII 2011b. 195, 6. 965–978.

Saito Kota, Katada Toshiaki. Mechanisms for exporting large-sized cargoes from the endoplasmic reticulum // Cellular and Molecular Life Sciences. VI 2015. 72, 19. 3709–3720.

Sajiki Kenichi, Hatanaka Mitsuko, Nakamura Takahiro, Takeda Kojiro, Shimanuki Mizuki, Yoshida Tomoko, Hanyu Yuichiro, Hayashi Takeshi, Nakaseko Yukinobu, Yanagida Mitsuhiro. Genetic control of cellular quiescence in S. pombe. // Journal of cell science. V 2009. 122, Pt 9. 1418–1429.

Sampaio Julio L, Gerl Mathias J, Klose Christian, Ejsing Christer S, Beug Hartmut, Simons Kai, Shevchenko Andrej. Membrane lipidome of an epithelial cell line // Proceedings of the National Academy of Sciences of the United States of America. II 2011. 108, 5. 1903–1907.

Santiago-Tirado Felipe H, Legesse-Miller Aster, Schott Daniel, Bretscher Anthony. PI4P and Rab Inputs Collaborate in Myosin-V-Dependent Transport of Secretory Compartments in Yeast // Developmental cell. I 2011. 20, 1. 47–59.

Sawin Kenneth E, Nurse Paul. Regulation of Cell Polarity by Microtubules in Fission Yeast // The Journal of cell biology. VII 1998. 142, 2. 457–471.

Sawin Kenneth E, Tran P T. Cytoplasmic microtubule organization in fission yeast // Yeast. 2006. 23, 13. 1001–1014.

Schneider M F. Control of Calcium Release in Functioning Skeletal Muscle Fibers // Annual Review of Physiology. X 1994. 56, 1. 463–484.

Schuck S. Polarized sorting in epithelial cells: raft clustering and the biogenesis of the apical membrane // Journal of cell science. XII 2004. 117, 25. 5955–5964.

Schulz Timothy A, Choi Mal-Gi, Raychaudhuri Sumana, Mears Jason A, Ghirlando Rodolfo, Hinshaw Jenny E, Prinz William A. Lipid-regulated sterol transfer between closely apposed membranes by oxysterol-binding protein homologues // The Journal of cell biology. XII 2009. 187, 6. 889–903.

Shivanandan Arun, Radenovic Aleksandra, Sbalzarini Ivo F. MosaicIA: an ImageJ/Fiji plugin for spatial pattern and interaction analysis // BMC Bioinformatics. 2013. 14, 1. 349.

Siegrist S E, Doe C Q. Microtubule-induced cortical cell polarity // Genes & Development. III 2007. 21, 5. 483–496.

Simons K, Sampaio J L. Membrane Organization and Lipid Rafts // Cold Spring Harbor Perspectives in Biology. X 2011. 3, 10. a004697–a004697.

Simons Kai, Gerl Mathias J. Revitalizing membrane rafts: new tools and insights // Nature reviews. Molecular cell biology. X 2010. 11, 10. 688–699.

Simons Kai, Ikonen Elina. Functional rafts in cell membranes // Nature. VI 1997. 387. 1–4.

Simons Kai, Meer Gerrit van. Lipid sorting in epithelial cells // Biochemistry. VIII 1988. 27, 17. 6197–6202.

Simons Kai, Toomre Darek. Lipid rafts and signal transduction // Nature reviews. Molecular cell biology. X 2000. 1. 1–11.

Simonsen Anne, Wurmser Andrew E, Emr Scott D, Stenmark Harald. The role of phosphoinositides in membrane transport // Current opinion in cell biology. VIII 2001. 13, 4. 485–492.

Singer S J, Nicolson G L. The Fluid Mosaic Model of the Structure of Cell Membranes // Science (New York, N.Y.). II 1972. 175, 4023. 720–731.

Sirotkin Vladimir, Berro Julien, Macmillan Keely, Zhao Lindsey, Pollard Thomas D. Quantitative analysis of the mechanism of endocytic actin patch assembly and disassembly in fission yeast. // Molecular biology of the cell. VIII 2010. 21, 16. 2894–2904.

Slaughter Brian, Li Rong. Toward a molecular interpretation of the surface stress theory for yeast morphogenesis // Current opinion in cell biology. II 2006. 18, 1. 47–53.

Slaughter Brian D, Das Arupratan, Schwartz Joel W, Rubinstein Boris, Li Rong. Dual Modes of Cdc42 Recycling Fine-Tune Polarized Morphogenesis // Developmental cell. XII 2009. 17, 6. 823–835.

Snaith H A, Thompson J, Yates J R, Sawin K E. Characterization of Mug33 reveals complementary roles for actin cable-dependent transport and exocyst regulators in fission yeast exocytosis // Journal of cell science. VI 2011. 124, 13. 2187–2199.

Snaith Hilary A, Samejima Itaru, Sawin Kenneth E. Multistep and multimode cortical anchoring of tea1p at cell tips in fission yeast // The EMBO journal. X 2005. 24, 21. 3690–3699.

Sohrmann M. Polarizing without a C(l)ue // Trends in cell biology. X 2003. 13, 10. 526–533.

Sommer Christoph, Straehle Christoph, Kothe Ullrich, Hamprecht Fred A. Ilastik: Interactive learning and segmentation toolkit // 2011 8th IEEE International Symposium on Biomedical Imaging (ISBI 2011). 2011. 230–233.

Souto-Padron Thais, Souza Wanderley de. Freeze-Fracture Localization of Filipin-Cholesterol Complexes in the Plasma Membrane of Trypanosoma cruzi // The Journal of Parasitology. II 1983. 69, 1. 129.

Stefan Christopher J, Manford Andrew G, Baird Daniel, Yamada-Hanff Jason, Mao Yuxin, Emr Scott D. Osh proteins regulate phosphoinositide metabolism at ER-plasma membrane contact sites. // Cell. II 2011. 144, 3. 389–401.

Strahl Thomas, Hama Hiroko, DeWald Daryll B, Thorner Jeremy. Yeast phosphatidylinositol 4-kinase, Pik1, has essential roles at the Golgi and in the nucleus // The Journal of cell biology. XII 2005. 171, 6. 967–979.

Strahl Thomas, Thorner Jeremy. Synthesis and function of membrane phosphoinositides in budding yeast, Saccharomyces cerevisiae // Biochimica et Biophysica Acta (BBA) - Molecular and Cell Biology of Lipids. III 2007. 1771, 3. 353–404.

Suda Yasuyuki, Nakano Akihiko. The Yeast Golgi Apparatus // Traffic (Copenhagen, Denmark). XII 2011. 13, 4. 505–510.

Sun Yidi, Carroll Susheela, Kaksonen Marko, Toshima Junko Y, Drubin David G. PtdIns(4,5)P 2turnover is required for multiple stages during clathrin- and actin-dependent endocytic internalization // The Journal of cell biology. IV 2007. 177, 2. 355–367.

Taguchi T. Emerging roles of recycling endosomes // Journal of Biochemistry. V 2013. 153, 6. 505–510.

Takeda Tetsuya, Chang Fred. Role of Fission Yeast Myosin I in Organization of Sterol-Rich Membrane Domains // Current Biology. VII 2005. 15, 14. 1331–1336.

Takeda Tetsuya, Kawate Toshimitsu, Chang Fred. Organization of a sterol-rich membrane domain by cdc15p during cytokinesis in fission yeast // Nature cell biology. XI 2004. 6, 11. 1142–1144.

Takenawa Tadaomi, Itoh Toshiki. Phosphoinositides, key molecules for regulation of actin cytoskeletal organization and membrane traffic from the plasma membrane // Biochimica et Biophysica Acta (BBA) - Molecular and Cell Biology of Lipids. X 2001. 1533, 3. 190–206.

Takeo K. A Correlation between Mode of Growth and Regional Ultrastructure of the Plasma Membrane of Schizosaccharomyces pombe as Revealed by Freeze-fracturing before and after Filipin Treatment // Microbiology (Reading, England). II 1985. 131, 2. 309–316.

Takeshita N, Higashitsuji Y, Konzack S, Fischer R. Apical Sterol-rich Membranes Are Essential for Localizing Cell End Markers That Determine Growth Directionality in the Filamentous Fungus Aspergillus nidulans // Molecular biology of the cell. I 2008. 19, 1. 339–351.

Tatebe Hisashi, Nakano Kentaro, Maximo Rachel, Shiozaki Kazuhiro. Pom1 DYRK Regulates Localization of the Rga4 GAP to Ensure Bipolar Activation of Cdc42 in Fission Yeast // Current Biology. III 2008. 18, 5. 322–330.

TerBush Daniel R, Maurice Trina, Roth Dagmar, Novick Peter. The Exocyst is a multiprotein complex required for exocytosis in Saccharomyces cerevisiae // The EMBO journal. 1996. 15. 6483–6494.

Terenna Courtney R, Makushok Tatyana, Velve-Casquillas Guilhem, Baigl Damien, Chen Yong, Bornens Michel, Paoletti Anne, Piel Matthieu, Tran Phong T. Physical Mechanisms Redirecting Cell Polarity and Cell Shape in Fission Yeast // Current Biology. XI 2008. 18, 22. 1748–1753.

Toker Alex, Cantley Lewis C. Signalling through the lipid products of phosphoinositide-3-OH kinase // Nature. VI 1997. 387, 6634. 673–676.

Tong Junsen, Manik Mohammad Kawsar, Yang Huiseon, Im Young Jun. Structural insights into nonvesicular lipid transport by the oxysterol binding protein homologue family // Biochimica et Biophysica Acta (BBA) - Molecular and Cell Biology of Lipids. VIII 2016. 1861, 8. 928–939.

Toya M, Iino Y, Yamamoto M. Fission Yeast Pob1p, Which Is Homologous to Budding Yeast Boi Proteins and Exhibits Subcellular Localization Close to Actin Patches, Is Essential for Cell Elongation and Separation // Molecular biology of the cell. VIII 1999. 10, 8. 2745–2757.

Treuner-Lange Anke, Søgaard-Andersen Lotte. Regulation of cell polarity in bacteria // The Journal of cell biology. VII 2014. 206, 1. 7–17.

Truong-Quang Binh-An, Lenne Pierre-François. Membrane microdomains: from seeing to understanding. // Frontiers in plant science. 2014. 5.

Turi T G, Webster Paul, Rose John K. Brefeldin A sensitivity and resistance in Schizosaccharomyces pombe // The Journal of biological chemistry. VI 2001. 1–8.

Turing A M. The Chemical Basis of Morphogenesis // Philosophical Transactions of the Royal Society B: Biological Sciences. VIII 1952. 237, 641. 37–72.

Urbani Lenore, Simoni Robert D. Cholesterol and Vesicular Stomatitis Virus G Protein Take Separate Routes from the Endoplasmic Reticulum to the Plasma Membrane* // The Journal of biological chemistry. II 1990. 265. 1–6.

Verde F. Fission yeast cell morphogenesis: identification of new genes and analysis of their role during the cell cycle // The Journal of cell biology. XII 1995. 131, 6. 1529–1538.

Villar-Tajadura Ma Antonia, Coll Pedro M, Madrid Marisa, Cansado Jose, Santos Beatriz, Pérez Pilar. Rga2 is a Rho2 GAP that regulates morphogenesis and cell integrity in S.pombe // Molecular microbiology. XI 2008. 70, 4. 867–881.

Vjestica A, Tang X Z, Oliferenko S. The Actomyosin Ring Recruits Early Secretory Compartments to the Division Site in Fission Yeast // Molecular biology of the cell. XII 2007. 19, 3. 1125–1138.

Wachtler V, Rajagopalan S, Balasubramanian M K. Sterol-rich plasma membrane domains in the fission yeast Schizosaccharomyces pombe // Journal of cell science. 2003. 116, 5. 867–874.

Walch-Solimena Christiane, Novick Peter. The yeast phosphatidylinositol-4-OH kinase Pik1 regulates secretion at the Golgi // Nature cell biology. XI 1999a. 1–3.

Walch-Solimena Christiane, Novick Peter. The yeast phosphatidylinositol-4-OH kinase Pik1 regulates secretion at the Golgi // Nature cell biology. XI 1999b. 1, 8. 523–525.

Wang Hongyan, Tang Xie, Liu Jianhua, Trautmann Susanne, Balasundaram David, McCollum Dannel, Balasubramanian M K. The multiprotein exocyst complex is essential for cell separation in Schizosaccharomyces pombe. // Molecular biology of the cell. II 2002. 13, 2. 515–529.

Wang Ning, Lee I-Ju, Rask Galen, Wu Jian-Qiu. Roles of the TRAPP-II Complex and the Exocyst in Membrane Deposition during Fission Yeast Cytokinesis // PLOS Biology. IV 2016. 14, 4. e1002437.

Wang Penghua, Zhang Yong, Li Hongzhe, Chieu Hai Kee, Munn Alan L, Yang Hongyuan. AAA ATPases regulate membrane association of yeast oxysterol binding proteins and sterol metabolism // The EMBO journal. VIII 2005. 24, 17. 2989–2999.

Wang Y, Xu H P, Riggs M, Rodgers L, Wigler M. byr2, a Schizosaccharomyces pombe gene encoding a protein kinase capable of partial suppression of the ras1 mutant phenotype. // Molecular and Cellular Biology. VII 1991. 11, 7. 3554–3563.

Wang Yanzhuang, Thiele Christoph, Huttner Wieland B. Cholesterol is Required for the Formation of Regulated and Constitutive Secretory Vesicles from the trans-Golgi Network // Traffic (Copenhagen, Denmark). 2000. 1. 952–962.

Watson Peter, Stephens David J. ER-to-Golgi transport: Form and formation of vesicular and tubular carriers // Biochimica et Biophysica Acta (BBA) - Molecular Cell Research. VII 2005. 1744, 3. 304–315.

Wedlich-Soldner R. Spontaneous Cell Polarization Through Actomyosin-Based Delivery of the Cdc42 GTPase // Science (New York, N.Y.). I 2003. 299, 5610. 1231–1235.

Wedlich-Soldner Roland, Li Rong. Yeast and fungal morphogenesis from an evolutionary perspective // Seminars in Cell & Developmental Biology. VI 2008. 19, 3. 224–233.

West Matt, Zurek Nesia, Hoenger Andreas, Voeltz Gia K. A 3D analysis of yeast ER structure reveals how ER domains are organized by membrane curvature // The Journal of cell biology. IV 2011. 193, 2. 333–346.

Wilhelm Brian T, Marguerat Samuel, Watt Stephen, Schubert Falk, Wood Valerie, Goodhead Ian, Penkett Christopher J, Rogers Jane, Bähler Jürg. Dynamic repertoire of a eukaryotic transcriptome surveyed at single-nucleotide resolution // Nature. V 2008. 453, 7199. 1239–1243.

Win Thein Z, Gachet Yannick, Mulvihill Daniel P, May Karen M, Hyams Jeremy S. Two type V myosins with non-overlapping functions in the fission yeast Schizosaccharomyces pombe: Myo52 is concerned with growth polarity and cytokinesis, Myo51 is a component of the cytokinetic actin ring // Journal of cell science. XII 2000. 114. 69–79.

Wixon Jo. Featured Organism: Schizosaccharomyces pombe, The Fission Yeast // Comparative and Functional Genomics. 2002. 3, 2. 194–204.

Wolf Wendelin, Kilic Annett, Schrul Bianca, Lorenz Holger, Schwappach Blanche, Seedorf Matthias. Yeast Ist2 Recruits the Endoplasmic Reticulum to the Plasma Membrane and Creates a Ribosome-Free Membrane Microcompartment // PloS one. VII 2012. 7, 7. e39703.

Wood Elizabeth, Nurse Paul. Pom1 and cell size homeostasis in fission yeast. // Cell cycle (Georgetown, Tex.). IX 2013. 12, 19.

Wood V, Harris M A, McDowall M D, Rutherford K, Vaughan B W, Staines D M, Aslett M, Lock A, Bähler J, Kersey P J, Oliver S G. PomBase: a comprehensive online resource for fission yeast // Nucleic Acids Research. XII 2011. 40, D1. D695–D699.

Wood V, R Gwilliam, MA Rajandream, M Lyne, R Lyne, A Stewart, J Sgouros, N Peat, J Hayles, S Baker, D Basham, S Bowman, K Brooks, D Brown, S Brown, T Chillingworth, C Churcher, M Collins, R Connor, A Cronin, P Davis, T Feltwell, A Fraser, S Gentles, A Goble, N Hamlin, D Harris, J Hidalgo, G Hodgson, S Holroyd, T Hornsby, S Howarth, EJ Huckle, S Hunt, K Jagels, K James, L Jones, M Jones, S Leather, S McDonald, J McLean, P Mooney, S Moule, K Mungall, L Murphy, D Niblett, C Odell, K Oliver, S ONeil, D Pearson, MA Quail, E Rabbinowitsch, K Rutherford, S Rutter, D Saunders, K Seeger, S Sharp, J Skelton, M Simmonds, R Squares, S Squares, K Stevens, K Taylor, RG Taylor, A Tivey, S Walsh, T Warren, S Whitehead, J Woodward, G Volckaert, R Aert, J Robben, B Grymonprez, I Weltjens, E Vanstreels, M Rieger, M Schäfer, S Müller-Auer, C Gabel, M Fuchs, A Düsterhöft, C Fritzc, E Holzer, D Moestl, H Hilbert, K Borzym, I Langer, A Beck, H Lehrach, R Reinhardt, TM Pohl, P Eger, W Zimmermann, H Wedler, R Wambutt, B Purnelle, A Goffeau, E Cadieu, S Dréano, S Gloux, Lelaure V , S Mottier, F Galibert, SJ Aves, Z Xiang, C Hunt, K Moore, SM Hurst, M Lucas, M Rochet, C Gaillardin, VA Tallada, A Garzon, G Thode, RR Daga, L Cruzado, J Jimenez, M Sánchez, Rey F del, J Benito, A Domínguez, JL Revuelta, S Moreno, J Armstrong, SL Forsburg, L Cerutti, T Lowe, WR McCombie, I Paulsen, J Potashkin, GV Shpakovski, D Ussery, BG Barrell, P Nurse. The genome sequence of Schizosaccharomyces pombe // Nature. II 2002. 415.

Wu Bin, Guo Wei. The Exocyst at a Glance. // Journal of cell science. VIII 2015. 128, 16. 2957–2964.

Wustner D, Herrmann A, Hao M, Maxfield F R. Rapid Nonvesicular Transport of Sterol between the Plasma Membrane Domains of Polarized Hepatic Cells // The Journal of biological chemistry. VI 2002. 277, 33. 30325–30336.

Yaffe M P, Stuurman N, Vale R D. Mitochondrial positioning in fission yeast is driven by association with dynamic microtubules and mitotic spindle poles // Proceedings of the National Academy of Sciences of the United States of America. V 2011. 100, 20. 11424–11428.

Yakir-Tamang L, Gerst J E. A Phosphatidylinositol-Transfer Protein and Phosphatidylinositol-4-phosphate 5-Kinase Control Cdc42 to Regulate the Actin Cytoskeleton and Secretory Pathway in Yeast // Molecular biology of the cell. VII 2009. 20, 15. 3583–3597.

Yamaoka T, Imada K, Fukunishi K, Yamasaki Y, Shimoda C, Nakamura T. The Fission Yeast Synaptobrevin Ortholog Syb1 Plays an Important Role in Forespore Membrane Formation and Spore Maturation // Eukaryotic cell. VIII 2013. 12, 9. 1162–1170.

Yanagida Mitsuhiro. The model unicellular eukaryote, Schizosaccharomyces pombe // Genome biology. II 2002. 3.

Yin Helen L, Janmey Paul A. Phosphoinositide Regulation of the Actin Cytoskeleton // Annual Review of Physiology. III 2003. 65, 1. 761–789.

Yu Yang, Kita Ayako, Udo Masako, Katayama Yuta, Shintani Mami, Park Kwihwa, Hagihara Kanako, Umeda Nanae, Sugiura Reiko. Sip1, a conserved AP-1 accessory protein, is important for Golgi/endosome trafficking in fission yeast. // PloS one. 2012. 7, 9. e45324.

Zaitsevskaya-Carter T. Spm1, a stress-activated MAP kinase that regulates morphogenesis in S.pombe // The EMBO journal. III 1997. 16, 6. 1318–1331.

Zegman Yonatan, Bonazzi Daria, Minc Nicolas. Measurement and manipulation of cell size parameters in fission yeast // Biophysical Methods in Cell Biology. 2015. 423–436.

Zhang Dan, Bidone Tamara C, Vavylonis Dimitrios. ER-PM Contacts Define Actomyosin Kinetics for Proper Contractile Ring Assembly // Current Biology. III 2016. 26, 5. 647–653.

Zhang Dan, Oliferenko Snezhana. Remodeling the nuclear membrane during closed mitosis // Current opinion in cell biology. II 2013. 25, 1. 142–148.

Zhang Dan, Vjestica Aleksandar, Oliferenko Snezhana. The cortical ER network limits the permissive zone for actomyosin ring assembly. // Current biology : CB. VI 2010. 20, 11. 1029–1034.

Zhang Dan, Vjestica Aleksandar, Oliferenko Snezhana. Plasma membrane tethering of the cortical ER necessitates its finely reticulated architecture. // Current biology : CB. XI 2012. 22, 21. 2048–2052.

Zhang Xiaoyu, Orlando Kelly, He Bing, Xi Fengong, Zhang Jian, Zajac Allison, Guo Wei. Membrane association and functional regulation of Sec3 by phospholipids and Cdc42 // The Journal of cell biology. I 2008. 180, 1. 145–158.

Zhang Y, Sugiura R, Lu Y, Asami M, Maeda T, Itoh T, Takenawa T, Shuntoh H, Kuno T. Phosphatidylinositol 4-Phosphate 5-Kinase Its3 and Calcineurin Ppb1 Coordinately Regulate Cytokinesis in Fission Yeast // The Journal of biological chemistry. XI 2000. 275, 45. 35600–35606.